ILSB Report / ILSB-Arbeitsbericht 206
(supersedes CDL–FMD Report 3–1998)

A SHORT INTRODUCTION TO BASIC ASPECTS OF CONTINUUM MICROMECHANICS

Helmut J. Böhm

Institute of Lightweight Design and Structural Biomechanics (ILSB)
Vienna University of Technology

updated: November 13, 2010

Contents

Notes on this Document

The present document is an expanded and modified version of the CDL–FMD report 3–1998, "A Short Introduction to Basic Aspects of Continuum Micromechanics", which is based on lecture notes prepared for the European Advanced Summer Schools *Frontiers of Computational Micromechanics in Industrial and Engineering Materials* held in Galway, Ireland, in July 1998 and in August 2000. Related lecture notes were used for graduate courses in a Summer School held at Ameland, the Netherlands, in October 2000 and during the COMMAS Summer School held in September 2002 at Stuttgart, Germany. All of the above documents, in turn, are based on the micromechanics section of the lecture notes for the course "Composite Engineering" (317.003) offered regularly at the Vienna University of Technology.

The course notes "A Short Introduction to Continuum Micromechanics" (Böhm, 2004a) for the CISM Course on *Mechanics of Microstructured Materials* held in July 2003 in Udine, Italy, may be regarded as a compact version of the present report that employs a somewhat different notation. The course notes "Analytical and Numerical Methods for Modeling the Thermomechanical and Thermophysical Behavior of Microstructured Materials" for the CISM Course on *Computational and Experimental Mechanics of Advanced Materials* (held in September 2008) are related to the present report, but emphasize different aspects of continuum micromechanics.

The present report is being updated continuously to reflect current developments in continuum micromechanics as seen by the author.

Nye notation is used for the mechanical variables in chapters 1 to 3. Tensors of order 4, such as elasticity, compliance, concentration and Eshelby tensors, are written as 6×6 quasi-matrices, and stress- as well as strain-like tensors of order 2 as 6-(quasi-)vectors. These 6-vectors are connected to index notation by the relations

$$\boldsymbol{\sigma} = \begin{pmatrix} \sigma(1) \\ \sigma(2) \\ \sigma(3) \\ \sigma(4) \\ \sigma(5) \\ \sigma(6) \end{pmatrix} = \begin{pmatrix} \sigma_{11} \\ \sigma_{22} \\ \sigma_{33} \\ \sigma_{12} \\ \sigma_{13} \\ \sigma_{23} \end{pmatrix} \qquad \boldsymbol{\varepsilon} = \begin{pmatrix} \varepsilon(1) \\ \varepsilon(2) \\ \varepsilon(3) \\ \varepsilon(4) \\ \varepsilon(5) \\ \varepsilon(6) \end{pmatrix} = \begin{pmatrix} \varepsilon_{11} \\ \varepsilon_{22} \\ \varepsilon_{33} \\ \gamma_{12} \\ \gamma_{13} \\ \gamma_{23} \end{pmatrix} \quad ,$$

where $\gamma_{ij} = 2\varepsilon_{ij}$ are the shear angles[1]. Tensors of order 4 are denoted by bold upper case letters, stress- and strain-like tensors of order 2 by bold lower case Greek letters, and

[1]This notation allows strain energy densities to be obtained as $U = \frac{1}{2}\boldsymbol{\sigma}\boldsymbol{\varepsilon}$. Furthermore, the stress and strain "rotation tensors" $\mathbf{T}_\sigma^\angle$ and $\mathbf{T}_\varepsilon^\angle$ follow the relationship $\mathbf{T}_\varepsilon^\angle = [(\mathbf{T}_\sigma^\angle)^{-1}]^T$.

3-vectors by bold lower case letters. Conductivity-like tensors of order 2 are treated as 3×3 matrices and denoted by calligraphic upper case letters. All other variables are taken to be scalars.

The use of Nye notation requires that the 4th order tensors show orthotropic or higher symmetry and that the coefficients of Eshelby and concentration tensors may differ compared to index notation. The tensorial product between two tensors of order 2 is denoted by the symbol "$\otimes$", where $[\boldsymbol{\eta} \otimes \boldsymbol{\zeta}]_{ijkl} = \eta_{ij}\zeta_{kl}$, and the contraction between a tensor of order 2 and a 3-vector is denoted by the symbol "$*$", where $[\boldsymbol{\zeta} * \mathbf{n}]_i = \zeta_{ij}n_j$. A superscript $^{\mathrm{T}}$ denotes the transpose of a tensor or vector.

Constituents (phases) are denoted by superscripts, with $^{(\mathrm{p})}$ standing for a general phase, $^{(\mathrm{m})}$ for a matrix, $^{(\mathrm{i})}$ for inhomogeneities, and $^{(\mathrm{f})}$ for fibers. Axial and transverse properties of transversely isotropic materials are marked by subscripts $_A$ and $_T$, respectively, and effective properties are denoted by a superscript asterisk *.

Chapter 1

Introduction

In the present report some basic issues and some important modeling approaches in the field of continuum micromechanics of materials are discussed. The main emphasis lies on application related (or "engineering") aspects, and neither a comprehensive theoretical treatment nor a review of the pertinent literature are attempted. For more formal treatments of many of the concepts and methods discussed in the present work see, e.g., Mura (1987), Aboudi (1991), Nemat-Nasser and Hori (1993), Suquet (1997), Markov (2000), Bornert et al. (2001), Torquato (2002), Milton (2002), Qu and Cherkaoui (2006) as well as Buryachenko (2007). Short overviews of continuum micromechanics were given, e.g., by Hashin (1983) and Zaoui (2002). Discussions of the history of the development of the field can be found in Markov (2000) and Zaoui (2002).

Due to the author's research interests, more room is given to the thermomechanical behavior of two-phase materials showing a matrix–inclusion topology and especially to metal matrix composites (MMCs), than to materials with other phase topologies or phase geometries or to multi-phase materials. Extending the methods presented here to other types of inhomogeneous materials, however, in general does not cause principal difficulties.

1.1 Inhomogeneous Materials

Many industrial and engineering materials as well as the majority of biological materials are inhomogeneous, i.e., they consist of dissimilar constituents (or "phases") that are distinguishable at some (small) length scale. Each constituent shows different material properties and/or material orientations and may itself be inhomogeneous at some smaller length scale(s). Inhomogeneous materials (also referred to as microstructured, heterogeneous or complex materials) play important roles in materials science and technology. Well-known examples of such materials are composites, concrete, polycrystalline materials, porous and cellular materials, functionally graded materials, wood, and bone.

The behavior of inhomogeneous materials is determined, on the one hand, by the relevant materials properties of the constituents and, on the other hand, by their geometry and topology (the "phase arrangement"). Obviously, the availability of information on these two counts determines the accuracy of any model or theoretical description. The behavior of inhomogeneous materials can be studied at a number of length scales ranging

from sub-atomic scales, which are dominated by quantum effects, to scales for which continuum descriptions are best suited. The present report concentrates on continuum models for heterogeneous materials, the pertinent research field being customarily referred to as continuum micromechanics of materials.

As will be discussed in section 1.2, an important aim of theoretical studies of multi-phase materials lies in deducing their overall ("effective" or "apparent") behavior[2], (e.g., stiffness, thermal expansion and strength properties, heat conduction and related transport properties, electrical and magnetic properties, electromechanical properties, etc.) from the corresponding material behavior of the constituents (and of the interfaces between them) and from the geometrical arrangement of the phases. Such scale transitions from lower to higher length scales aim at achieving a marked reduction in the number of degrees of freedom describing the system. The continuum methods discussed in the following are suitable for handling scale transitions from length scales in the low micrometer range to macroscopic samples, components or structures with sizes of millimeters to meters.

In what follows, the main focus will lie on describing the thermomechanical behavior of inhomogeneous two-phase materials by methods of continuum micromechanics. Most of the discussed modeling approaches can, however, be extended to multi-phase materials in a straightforward way and there is a large body of literature applying analogous or related continuum methods to other physical properties of inhomogeneous materials, compare, e.g., Hashin (1983), Torquato (2002) as well as Milton (2002) and see sections 2.9 and 5.9 of the present report.

The most basic classification criterion for inhomogeneous materials is based on the microscopic phase topology. In matrix–inclusion arrangements (as found in particulate and fibrous materials, such as most composite materials, in porous materials, and in closed cell foams[3]) only the matrix shows a connected topology and the constituents play clearly distinct roles. In interpenetrating (interwoven) phase arrangements (as found, e.g., in functionally graded materials or in open cell foams) and in many polycrystals ("granular materials"), in contrast, the phases cannot be readily distinguished topologically.

Length Scales

In the present context the lowest length scale described by a model is termed the microscale, the largest one the macroscale and intermediate ones are called mesoscales[4]. The fields describing the behavior of an inhomogeneous material, i.e., in mechanics the stresses $\boldsymbol{\sigma}(\mathbf{x})$, strains $\boldsymbol{\varepsilon}(\mathbf{x})$ and displacements $\mathbf{u}(\mathbf{x})$, are split into contributions corresponding to the different length scales, which are referred to as micro-, macro- and mesofields, respectively.

[2]The designation "effective material properties" is typically employed for describing the macroscopic responses of bulk materials, whereas the term "apparent material properties" is used for the properties of samples (Huet, 1990).

[3]With respect to their thermomechanical behavior, porous and cellular materials can usually be treated as inhomogeneous materials in which one constituent shows vanishing stiffness, thermal expansion, conductivity etc., compare section 5.7.

[4]This nomenclature is far from universal, the naming of the length scales of inhomogeneous materials being notoriously inconsistent in the literature.

The phase geometries on the meso- and microscales are denoted as meso- and microgeometries.

Most micromechanical models are based on the assumption that the length scales in a given material differ substantially. This is understood to imply that for each pair of them, on the one hand, the fluctuating contributions to the fields at the smaller length scale ("fast variables") influence the behavior at the larger length scale only via their volume averages. On the other hand, gradients of the fields as well as compositional gradients at the larger length scale ("slow variables") are not significant at the smaller length scale, where these fields appear to be locally constant and can be described in terms of uniform "applied fields" or "far fields". Formally, this splitting of the strain and stress fields into slow and fast contributions can be written as

$$\boldsymbol{\varepsilon}(\mathbf{x}) = \langle \boldsymbol{\varepsilon} \rangle + \boldsymbol{\varepsilon}'(\mathbf{x}) \qquad \text{and} \qquad \boldsymbol{\sigma}(\mathbf{x}) = \langle \boldsymbol{\sigma} \rangle + \boldsymbol{\sigma}'(\mathbf{x}) \qquad , \tag{1.1}$$

where $\langle \boldsymbol{\varepsilon} \rangle$ and $\langle \boldsymbol{\sigma} \rangle$ are the macroscopic (slow) fields, whereas $\boldsymbol{\varepsilon}'$ and $\boldsymbol{\sigma}'$ stand for the microscopic fluctuations.

Unless specifically stated otherwise, in the present report the above conditions on the slow and fast variables are assumed to be met. If this is not the case to sufficient degree (e.g., in the cases of insufficiently separated length scales, of the presence of marked compositional or load gradients or of regions in the vicinity of free surfaces of inhomogeneous materials, or of macroscopic interfaces adjoined by at least one inhomogeneous material), embedding schemes, compare chapter 6, or special analysis methods must be applied. The latter take the form of second-order schemes that explicitly account for deformation gradients on the microscale (Kouznetsova et al., 2002) and result in nonlocal homogenized media, see, e.g., Feyel (2003).

Smaller length scales than the ones considered in a given model may or may not be amenable to continuum mechanical descriptions. For an overview of methods applicable below the continuum range see, e.g., Raabe (1998).

1.2 Homogenization and Localization

The "bridging of length scales", which constitutes the central issue of continuum micromechanics, involves two main tasks. On the one hand, the behavior at some larger length scale must be estimated or bounded by using information from a smaller length scale, i.e., homogenization problems must be solved. The most important applications of homogenization are materials characterization, i.e., simulating the overall material response under simple loading conditions such as uniaxial tensile tests, and constitutive modeling, where the responses to general loads, load paths and loading sequences must be described. Homogenization may be interpreted as describing the the behavior of a material that is inhomogeneous at some lower length scale in terms of a (fictitious) energetically equivalent, homogeneous reference material at some higher length scale. On the other hand, the local responses at the smaller length scale must be deduced from the loading conditions (and, where appropriate, from the load histories) on the larger length scale. This task, which

corresponds to "zooming in" on the local fields in an inhomogeneous material, is referred to as localization. In either case the main inputs are the geometrical arrangement and the material behaviors of the constituents at the microscale. In many continuum micromechanical methods, homogenization is less demanding than localization because the local fields tend to show a marked dependence on details of the local geometry of the constituents.

For any volume element Ω_s of an inhomogeneous material that is sufficiently large and contains no significant gradients of composition or applied loads, homogenization relations take the form of volume averages of some variable $f(\mathbf{x})$,

$$\langle f \rangle = \frac{1}{\Omega_s} \int_{\Omega_s} f(\mathbf{x}) \, \mathrm{d}\Omega \qquad . \tag{1.2}$$

Accordingly, the homogenization relations for the stress and strain tensors can be given as

$$\begin{aligned} \langle \boldsymbol{\varepsilon} \rangle &= \frac{1}{\Omega_s} \int_{\Omega_s} \boldsymbol{\varepsilon}(\mathbf{x}) \, \mathrm{d}\Omega = \frac{1}{2\Omega_s} \int_{\Gamma_s} [\mathbf{u}(\mathbf{x}) \otimes \mathbf{n}_\Gamma(\mathbf{x}) + \mathbf{n}_\Gamma(\mathbf{x}) \otimes \mathbf{u}(\mathbf{x})] \, \mathrm{d}\Gamma \\ \langle \boldsymbol{\sigma} \rangle &= \frac{1}{\Omega_s} \int_{\Omega_s} \boldsymbol{\sigma}(\mathbf{x}) \, \mathrm{d}\Omega = \frac{1}{\Omega_s} \int_{\Gamma_s} \mathbf{t}(\mathbf{x}) \otimes \mathbf{x} \, \mathrm{d}\Gamma \qquad , \end{aligned} \tag{1.3}$$

where Γ_s stands for surface of the volume element Ω_s, $\mathbf{u}(\mathbf{x})$ is the deformation vector, $\mathbf{t}(\mathbf{x}) = \boldsymbol{\sigma}(\mathbf{x}) * \mathbf{n}_\Gamma(\mathbf{x})$ is the surface traction vector, and $\mathbf{n}_\Gamma(\mathbf{x})$ is the surface normal vector. Equations (1.3) are known as the average strain and average stress theorems, and the surface integral formulation for $\boldsymbol{\varepsilon}$ given above pertains to the small strain regime and for continuous displacements. Under the latter condition the mean strains and stresses in a control volume, $\langle \boldsymbol{\varepsilon} \rangle$ and $\langle \boldsymbol{\sigma} \rangle$, are fully determined by the surface displacements and tractions. If the displacements show discontinuities, e.g., for imperfect interfaces between the constituents or in the presence of (micro) cracks, correction terms involving the displacement jumps across imperfect interfaces or cracks must be introduced, compare Nemat-Nasser and Hori (1993). In the absence of body forces the microstresses $\boldsymbol{\sigma}(\mathbf{x})$ are self-equilibrated (but not necessarily zero). In the above form, eqn. (1.3) applies to linear elastic behavior, but it can be modified to cover thermoelastic behavior and extended to the nonlinear range, e.g., to elastoplastic materials described by secant or incremental plasticity models, compare section 2.6. For a discussion of homogenization at finite deformations see, e.g., Nemat-Nasser (1999).

The microscopic strain and stress fields, $\boldsymbol{\varepsilon}(\mathbf{x})$ and $\boldsymbol{\sigma}(\mathbf{x})$, in a given volume element Ω_s are formally linked to the corresponding macroscopic responses, $\langle \boldsymbol{\varepsilon} \rangle$ and $\langle \boldsymbol{\sigma} \rangle$, by localization (or projection) relations of the type

$$\boldsymbol{\varepsilon}(\mathbf{x}) = \mathbf{A}(\mathbf{x}) \langle \boldsymbol{\varepsilon} \rangle \qquad \text{and} \qquad \boldsymbol{\sigma}(\mathbf{x}) = \mathbf{B}(\mathbf{x}) \langle \boldsymbol{\sigma} \rangle \qquad . \tag{1.4}$$

$\mathbf{A}(\mathbf{x})$ and $\mathbf{B}(\mathbf{x})$ are known as mechanical strain and stress concentration tensors (or influence functions; Hill (1963)), respectively. When they are known, localization tasks can obviously be carried out.

Equations (1.1) and (1.3) imply that the volume averages of fluctuations vanish for sufficiently large integration volumes,

$$\frac{1}{\Omega_s} \int_{\Omega_s} \boldsymbol{\varepsilon}'(\mathbf{x}) \, \mathrm{d}\Omega = 0 = \frac{1}{\Omega_s} \int_{\Omega_s} \boldsymbol{\sigma}'(\mathbf{x}) \, \mathrm{d}\Omega \qquad . \tag{1.5}$$

Similarly, surface integrals over the microscopic fluctuations of appropriate variables tend to zero[5].

For suitable volume elements of inhomogeneous materials that show sufficient separation between the length scales and for suitable boundary conditions the relation

$$\frac{1}{2}\langle\widetilde{\boldsymbol{\sigma}}^{\mathrm{T}}\,\widetilde{\boldsymbol{\varepsilon}}\rangle = \frac{1}{2\Omega}\int_{\Omega}\widetilde{\boldsymbol{\sigma}}^{\mathrm{T}}(\mathbf{x})\;\widetilde{\boldsymbol{\varepsilon}}(\mathbf{x})\,\mathrm{d}\Omega = \frac{1}{2}\langle\widetilde{\boldsymbol{\sigma}}\rangle^{\mathrm{T}}\,\langle\widetilde{\boldsymbol{\varepsilon}}\rangle \tag{1.6}$$

can be shown to hold for general statically admissible stress fields $\widetilde{\boldsymbol{\sigma}}$ and kinematically admissible strain fields $\widetilde{\boldsymbol{\varepsilon}}$, compare Hill (1967). This equation is known as Hill's macrohomogeneity condition, the Mandel–Hill condition or the energy equivalence condition, compare Bornert (2001) and Zaoui (2001). When it is fulfilled the volume average of the strain energy density of the microfields equals the strain energy density of the macrofields, making the microscopic and macroscopic descriptions energetically equivalent. The Mandel–Hill condition forms the basis of the interpretation of homogenization procedures in the thermoelastic regime[6] in terms of a homogeneous comparison material (or "reference medium") that is energetically equivalent to a given inhomogeneous material.

1.3 Volume Elements

The microgeometries of real inhomogeneous materials are at least to some extent random and, in the majority of cases of practically relevance, their detailed phase arrangements are highly complex. As a consequence, exact expressions for $\mathbf{A}(\mathbf{x})$, $\mathbf{B}(\mathbf{x})$, $\boldsymbol{\varepsilon}(\mathbf{x})$, $\boldsymbol{\sigma}(\mathbf{x})$, etc., in general cannot be given with reasonable effort and approximations have to be introduced. Typically, these approximations are based on the ergodic hypothesis, i.e., the heterogeneous material is assumed to be statistically homogeneous. This implies that sufficiently large volume elements selected at random positions within the sample have statistically equivalent phase arrangements and give rise to the same averaged material properties[7]. As mentioned above, these material properties are referred to as the overall or effective material properties of the inhomogeneous material.

Ideally, the homogenization volume should be chosen to be a proper representative volume element (RVE), i.e., a subvolume of Ω_{s} that is sufficiently large to be statistically representative of the inhomogeneous material. Representative volume elements can be defined, on the one hand, by requiring them to be statistically representative of the microgeometry. Such "geometrical RVEs" are independent of the physical property studied

[5]Whereas volume and surface integrals over products of slow and fast variables vanish, integrals over products of fluctuating variables ("correlations"), e.g., $\langle\boldsymbol{\varepsilon}'^{2}\rangle$, do not vanish in general.

[6]For a discussion of the Mandel–Hill condition for finite deformations and related issues see, e.g., Khisaeva and Ostoja-Starzewski (2006).

[7]Some inhomogeneous materials are not statistically homogeneous by design, e.g., functionally graded materials in the direction(s) of the gradient(s), and, consequently, may require nonstandard treatment. For such materials it is not possible to define effective material properties in the sense of eqn. (1.7) and representative volume elements do not exist. Deviation from statistical homogeneity may also be introduced into inhomogeneous materials by manufacturing processes.

for the inhomogeneous material. On the other hand, the definition can be based on the requirement that the overall responses with respect to some given physical behavior are independent of the actual position and orientation of the RVE and of the boundary conditions applied to it (Hill, 1963). The size of the resulting "physical RVEs" depends on the physical property considered, and it fulfills the Mandel–Hill condition, eqn. (1.6), by design.

An RVE must be sufficiently large to allow a meaningful sampling of the microfields and sufficiently small for the influence of macroscopic gradients to be negligible and for an analysis of the microfields to be possible[8]. For a discussion of microgeometries and homogenization volumes see section 4.1.

1.4 Overall Behavior, Material Symmetries

The homogenized strain and stress fields of an elastic inhomogeneous material as obtained by eqn. (1.3), $\langle\boldsymbol{\varepsilon}\rangle$ and $\langle\boldsymbol{\sigma}\rangle$, can be linked by effective elastic tensors $\mathbf{E}^*$ and $\mathbf{C}^*$ as

$$\langle\boldsymbol{\sigma}\rangle = \mathbf{E}^*\langle\boldsymbol{\varepsilon}\rangle \qquad \text{and} \qquad \langle\boldsymbol{\varepsilon}\rangle = \mathbf{C}^*\langle\boldsymbol{\sigma}\rangle \qquad , \tag{1.7}$$

respectively, which may be viewed as the elastic tensors of an appropriate equivalent homogeneous material. Using eqns. (1.3) and (1.4) these effective elastic tensors can be obtained from the local elastic tensors, $\mathbf{E}(\mathbf{x})$ and $\mathbf{C}(\mathbf{x})$, and the concentration tensors, $\mathbf{A}(\mathbf{x})$ and $\mathbf{B}(\mathbf{x})$, as volume averages

$$\begin{aligned} \mathbf{E}^* &= \frac{1}{\Omega_s}\int_{\Omega_s} \mathbf{E}(\mathbf{x})\mathbf{A}(\mathbf{x})\mathrm{d}\Omega \\ \mathbf{C}^* &= \frac{1}{\Omega_s}\int_{\Omega_s} \mathbf{C}(\mathbf{x})\mathbf{B}(\mathbf{x})\mathrm{d}\Omega \end{aligned} \tag{1.8}$$

Other effective properties of inhomogeneous materials, e.g., tensors describing their thermophysical behavior, can be evaluated in an analogous way.

The resulting homogenized behavior of many multi-phase materials can be idealized as being statistically isotropic or quasi-isotropic (e.g., for composites reinforced with spherical particles, randomly oriented particles of general shape or randomly oriented fibers, many polycrystals, many porous and cellular materials, random mixtures of two phases) or statistically transversely isotropic (e.g., for composites reinforced with aligned fibers or platelets, composites reinforced with nonaligned reinforcements showing a planar random or other axisymmetric orientation distribution function, etc.), compare (Hashin, 1983). Of course, lower material symmetries of the homogenized response may also be found, e.g., in textured polycrystals or in composites containing reinforcements with orientation distributions of low symmetry, compare Allen and Lee (1990).

Statistically isotropic multi-phase materials show the same overall behavior in all directions, and their effective elasticity tensors and thermal expansion tensors take the form

[8]This requirement was symbolically denoted as MICRO$\ll$MESO$\ll$MACRO by Hashin (1983), where MICRO and MACRO have their "usual" meanings and MESO stands for the length scale of the homogenization volume. As noted by Nemat-Nasser (1999) it is the dimension relative to the microstructure relevant for a given problem that is important for the size of an RVE.

$$\mathbf{E} = \begin{pmatrix} E_{11} & E_{12} & E_{12} & 0 & 0 & 0 \\ E_{12} & E_{11} & E_{12} & 0 & 0 & 0 \\ E_{12} & E_{12} & E_{11} & 0 & 0 & 0 \\ 0 & 0 & 0 & E_{44} & 0 & 0 \\ 0 & 0 & 0 & 0 & E_{44} & 0 \\ 0 & 0 & 0 & 0 & 0 & E_{44} = \frac{1}{2}(E_{11} - E_{12}) \end{pmatrix} \qquad \boldsymbol{\alpha} = \begin{pmatrix} \alpha \\ \alpha \\ \alpha \\ 0 \\ 0 \\ 0 \end{pmatrix} \tag{1.9}$$

in Nye notation. Two independent parameters are sufficient for describing such an overall linear elastic behavior (e.g., the effective Young's modulus $E^* = E^*_{11} - 2{E^*_{12}}^2/(E^*_{11} + E^*_{12})$, the effective Poisson number $\nu^* = E^*_{12}/(E^*_{11} + E^*_{12})$, the effective shear modulus $G^* = E^*_{44} = E^*/2(1+\nu^*)$, the effective bulk modulus $K^* = E^*/3(1-2\nu^*)$, or the effective Lamé constants) and one is required for the effective thermal expansion behavior in the linear range (the effective coefficient of thermal expansion $\alpha^* = \alpha^*_{11}$). In many cases deviations from isotropic symmetry can be assessed by the Zener parameter, $Z = 2E^*_{11}/(E^*_{11} - E^*_{12})$.

The effective elasticity and thermal expansion tensors for statistically transversely isotropic materials have the structure

$$\mathbf{E} = \begin{pmatrix} E_{11} & E_{12} & E_{12} & 0 & 0 & 0 \\ E_{12} & E_{22} & E_{23} & 0 & 0 & 0 \\ E_{12} & E_{23} & E_{22} & 0 & 0 & 0 \\ 0 & 0 & 0 & E_{44} & 0 & 0 \\ 0 & 0 & 0 & 0 & E_{44} & 0 \\ 0 & 0 & 0 & 0 & 0 & E_{66} = \frac{1}{2}(E_{22} - E_{23}) \end{pmatrix} \qquad \boldsymbol{\alpha} = \begin{pmatrix} \alpha_{\mathrm{A}} \\ \alpha_{\mathrm{T}} \\ \alpha_{\mathrm{T}} \\ 0 \\ 0 \\ 0 \end{pmatrix} \quad , \tag{1.10}$$

where 1 is the axial direction and 2–3 is the transverse plane of isotropy. Generally, the thermoelastic behavior of transversely isotropic materials is described by five independent elastic constants and two independent coefficients of thermal expansion. Appropriate elastic parameters in this context are, e.g., the axial and transverse effective Young's moduli, $E^*_{\mathrm{A}} = E^*_{11} - \frac{2E^{*2}_{12}}{E^*_{22}+E^*_{23}}$ and $E^*_{\mathrm{T}} = E^*_{22} - \frac{E^*_{11}E^{*2}_{23}+E^*_{22}E^{*2}_{12}-2E^*_{23}E^{*2}_{12}}{E^*_{11}E^*_{22}-E^{*2}_{12}}$, the axial and transverse effective shear moduli, $G^*_{\mathrm{A}} = E^*_{44}$ and $G^*_{\mathrm{T}} = E^*_{66}$, the axial and transverse effective Poisson numbers, $\nu^*_{\mathrm{A}} = \frac{E^*_{12}}{E^*_{22}+E^*_{23}}$ and $\nu^*_{\mathrm{T}} = \frac{E^*_{11}E^*_{23}-E^{*2}_{12}}{E^*_{11}E^*_{22}-E^{*2}_{12}}$, as well as the effective transverse (plane strain) bulk modulus $K^*_{\mathrm{T}} = E^*_{\mathrm{A}}/2[(1-\nu^*_{\mathrm{T}})(E^*_{\mathrm{A}}/E^*_{\mathrm{T}}) - 2{\nu^*_{\mathrm{A}}}^2]$. The transverse ("in-plane") properties are related via $G^*_{\mathrm{T}} = E^*_{\mathrm{T}}/2(1+\nu^*_{\mathrm{T}})$, but there is no general linkage between the axial properties E^*_{A}, G^*_{A} and ν^*_{A} beyond the above definition of K^*_{T}. For the special case of materials reinforced by aligned continuous fibers, however, Hill (1964) derived the relations

$$\begin{aligned} E_{\mathrm{A}} &= \xi E^{(\mathrm{f})}_{\mathrm{A}} + (1-\xi)E^{(\mathrm{m})} + \frac{4(\nu^{(\mathrm{f})}_{\mathrm{A}} - \nu^{(\mathrm{m})})^2}{(1/K^{(\mathrm{f})}_{\mathrm{T}} - 1/K^{(\mathrm{m})}_{\mathrm{T}})^2}\left(\frac{\xi}{K^{(\mathrm{f})}_{\mathrm{T}}} + \frac{1-\xi}{K^{(\mathrm{m})}_{\mathrm{T}}} - \frac{1}{K_{\mathrm{T}}}\right) \\ \nu_{\mathrm{A}} &= \xi\nu^{(\mathrm{f})}_{\mathrm{A}} + (1-\xi)\nu^{(\mathrm{m})} + \frac{\nu^{(\mathrm{f})}_{\mathrm{A}} - \nu^{(\mathrm{m})}}{1/K^{(\mathrm{f})}_{\mathrm{T}} - 1/K^{(\mathrm{m})}_{\mathrm{T}}}\left(\frac{\xi}{K^{(\mathrm{f})}_{\mathrm{T}}} + \frac{1-\xi}{K^{(\mathrm{m})}_{\mathrm{T}}} - \frac{1}{K_{\mathrm{T}}}\right) \end{aligned} \tag{1.11}$$

which allow the effective moduli E^*_{A} and ν^*_{A} to be expressed by K^*_{T}, some constituent properties, and the fiber volume fraction ξ. Equations (1.11) can be used to reduce the number of independent effective elastic parameters required for describing the behavior of unidirectional continuously reinforced composites to three. Both an axial and a transverse

effective coefficient of thermal expansion, $\alpha_A^* = \alpha_{11}^*$ and $\alpha_T^* = \alpha_{22}^*$, are required for transversely isotropic materials.

The overall material symmetries of inhomogeneous materials and their effect on various physical properties can be treated in full analogy to the symmetries of crystals as discussed, e.g., by Nye (1957). The influence of the overall symmetry of the phase arrangement on the overall mechanical behavior of inhomogeneous materials can be marked[9], especially on the nonlinear responses to mechanical loads. Accordingly, it is good practice to aim at approaching the symmetry of the actual material as closely as possible in any modeling effort.

1.5 Major Modeling Strategies in Continuum Micromechanics of Materials

All micromechanical methods described in the present report can be used to do materials characterization, i.e., simulating the overall material response under simple loading conditions such as uniaxial tensile tests. Many homogenization procedures can also be employed directly as micromechanically based constitutive material models at higher length scales. This implies that they can provide the full homogenized stress and strain tensors for any pertinent loading condition and for any pertinent loading history[10]. This task is obviously much more demanding than materials characterization. Compared to semiempirical constitutive laws, as proposed, e.g., by Davis (1996), micromechanically based constitutive models have both a clear physical basis and an inherent capability for "zooming in" on the local phase stresses and strains by using localization procedures.

The evaluation of the local responses of the constituents (in the ideal case, at any material point) for a given macroscopic state of a sample or structure is referred to as localization. It is especially important for studying and evaluating local strength relevant behavior, such as the onset and progress of plastic yielding or damage, which, of course, can have major repercussions on the macroscopic behavior. For valid descriptions of local strength relevant responses details of the microgeometry tend to be of major importance and may, in fact, determine the macroscopic response, an extreme case being the mechanical strength of brittle inhomogeneous materials.

Because for realistic phase distributions the analysis of the spatial variations of the microfields in sufficiently large volume elements tends to be beyond present capabilities, approximations have to be used. For convenience, the majority of the resulting modeling approaches may be treated as falling into two groups. The first of these comprises methods

[9]Overall properties described by tensors or lower rank, e.g., the thermal expansion and thermal conduction responses, are less sensitive to symmetry effects, compare Nye (1957).

[10]The overall thermomechanical behavior of homogenized materials is typically richer than that of the constituents, i.e., the effects of the interaction of the constituents in many cases cannot be satisfactorily described by simply adapting material parameters without changing the functional relationships in the constitutive laws of the constituents. For example, a composite consisting of a matrix that follows J_2 plasticity and elastic reinforcements shows some pressure dependence in its macroscopic plastic behavior, and two dissimilar constituents following Maxwell-type linear viscoelastic behavior in general do not give rise to a macroscopic Maxwell behavior (Barello and Lévesque, 2008).

that describe interactions, e.g., between phases or between individual reinforcements, in a collective way in terms of phase-wise uniform fields and comprises

- Mean Field Approaches (MFAs) and related methods (see chapter 2): The microfields within each constituent of an inhomogeneous material are approximated by their phase averages $\langle\boldsymbol{\varepsilon}\rangle^{(\mathrm{p})}$ and $\langle\boldsymbol{\sigma}\rangle^{(\mathrm{p})}$, i.e., piecewise (phase-wise) uniform stress and strain fields are employed. The phase geometry enters these models via statistical descriptors[11], such as volume fractions, phase topology, reinforcement aspect ratio distributions, etc. In MFAs the localization relations take the form

$$\begin{aligned} \langle\boldsymbol{\varepsilon}\rangle^{(\mathrm{p})} &= \bar{\mathbf{A}}^{(\mathrm{p})}\langle\boldsymbol{\varepsilon}\rangle \\ \langle\boldsymbol{\sigma}\rangle^{(\mathrm{p})} &= \bar{\mathbf{B}}^{(\mathrm{p})}\langle\boldsymbol{\sigma}\rangle \end{aligned} \tag{1.12}$$

  and the homogenization relations can be written as

$$\begin{aligned} \langle\boldsymbol{\varepsilon}\rangle^{(\mathrm{p})} &= \frac{1}{\Omega^{(\mathrm{p})}}\int_{\Omega^{(\mathrm{p})}} \boldsymbol{\varepsilon}(\mathbf{x})\,\mathrm{d}\Omega \qquad \text{with} \qquad \langle\boldsymbol{\varepsilon}\rangle = \sum\nolimits_{\mathrm{p}} V^{(\mathrm{p})}\langle\boldsymbol{\varepsilon}\rangle^{(\mathrm{p})} \\ \langle\boldsymbol{\sigma}\rangle^{(\mathrm{p})} &= \frac{1}{\Omega^{(\mathrm{p})}}\int_{\Omega^{(\mathrm{p})}} \boldsymbol{\sigma}(\mathbf{x})\,\mathrm{d}\Omega \qquad \text{with} \qquad \langle\boldsymbol{\sigma}\rangle = \sum\nolimits_{\mathrm{p}} V^{(\mathrm{p})}\langle\boldsymbol{\sigma}\rangle^{(\mathrm{p})} \end{aligned} \tag{1.13}$$

  where $^{(\mathrm{p})}$ denotes a given phase of the material, $\Omega^{(\mathrm{p})}$ is the volume occupied by this phase, and $V^{(\mathrm{p})}{=}\Omega^{(\mathrm{p})}/\sum_{\mathrm{k}}\Omega^{(\mathrm{k})}$ is the volume fraction of the phase. In contrast to eqn. (1.4) the phase concentration tensors $\bar{\mathbf{A}}$ and $\bar{\mathbf{B}}$ used in MFAs are not functions of the spatial coordinates.
  Mean field approaches tend to be formulated in terms of the phase concentration tensors, they pose low computational requirements, and they have been highly successful in describing the thermoelastic response of inhomogeneous materials. Their use for modeling nonlinear composites is a subject of active research. Their most important representatives are effective field and effective medium approximations.

- Variational Bounding Methods (see chapter 3): Variational principles are used to obtain upper and (in many cases) lower bounds on the overall elastic tensors, elastic moduli, secant moduli, and other physical properties of inhomogeneous materials the microgeometries of which are described by statistical parameters. Many analytical bounds are obtained on the basis of phase-wise constant stress (polarization) fields. Bounds — in addition to their intrinsic value — are important tools for assessing other models of inhomogeneous materials. Furthermore, in many cases one of the bounds provides good estimates for the physical property under consideration, even if the bounds are rather slack (Torquato, 1991). Many bounding methods are closely related to MFAs.

Because they do not explicitly account for n-particle interactions Mean Field Approaches are sometimes referred to as "noninteracting approximations" in the literature. They postulate the existence of an RVE and typically assume some idealized statistics of the phase arrangement at the microscale.

[11] Phase arrangements can be probed by n-point correlation functions (or n-point phase probability functions) that give the probability that some configuration of n points with coordinates $\mathbf{x}_1 \ldots \mathbf{x}_n$ lies within a prescribed phase. For statistically homogeneous materials 1-point correlations provide the volume fractions, 2-point correlations contain information on the macroscopic isotropy or anisotropy, and higher correlations contain details on the shapes and arrangements of the phases.

The second group of approximations is based on studying discrete microgeometries, for which they aim at fully accounting for the interactions between phases. It includes

- Periodic Microfield Approaches (PMAs), also referred to as periodic homogenization schemes or unit cell methods, see chapter 5. In these methods the inhomogeneous material is approximated by an infinitely extended model material with a periodic phase arrangement[12]. The resulting periodic microfields are usually evaluated by analyzing unit cells (which may describe microgeometries ranging from rather simplistic to highly complex ones) via analytical or numerical methods. Unit cell methods are often used for performing materials characterization of inhomogeneous materials in the nonlinear range, but they can also be employed as micromechanically based constitutive models. The high resolution of the microfields provided by PMAs can be very useful for studying the initiation of damage at the microscale. However, because they inherently give rise to periodic configurations of damage, PMAs are not suited to investigating phenomena such as the interaction of the microgeometry with macroscopic cracks.
  Periodic microfield approaches can give detailed information on the local stress and strain fields within a given unit cell, but they tend to be computationally expensive.

- Embedded Cell or Embedding Approaches (ECAs; see chapter 6): The inhomogeneous material is approximated by a model material consisting of a "core" containing a discrete phase arrangement that is embedded within some outer region to which far field loads are applied. The material properties of this outer region may be described by some macroscopic constitutive law, they can be determined self-consistently or quasi-self-consistently from the behavior of the core, or the embedding region may take the form of a coarse description and/or discretization of the phase arrangement. ECAs can be used for materials characterization, and they are usually the best choice for studying regions of special interest in inhomogeneous materials, such as the tips of macroscopic cracks and their surroundings. Like PMAs, embedded cell approaches can resolve local stress and strain fields in the core region at high detail, but tend to be computationally expensive.

- Windowing Approaches (see chapter 7): Subregions ("windows") — typically of rectangular or hexahedral shape — are randomly chosen from a given phase arrangement and subjected to boundary conditions that guarantee energy equivalence between the micro- and macroscales. Accordingly, windowing methods describe the behavior of individual inhomogeneous samples rather than of inhomogeneous materials and give rise to apparent rather than effective macroscopic responses. For the special cases of macrohomogeneous stress and strain boundary conditions, respectively, lower and upper estimates for and bounds on the overall behavior of the inhomogeneous material can be obtained[13]. In addition, mixed homogeneous boundary conditions can be applied to obtain estimates.

- Other homogenization approaches employing discrete microgeometries, such as the statistics-based non-periodic homogenization scheme of Cui et al. (Li and Cui, 2005).

[12]Whereas most mean field methods make the implicit assumption that there is no long range order in the inhomogeneous material, periodic phase arrangements imply the existence of just such an order.

[13]For samples that are sufficiently big to be proper representative volume elements the lower and upper estimates and bounds coincide, and the effective properties are identical to the apparent ones.

Because this group of methods explicitly study mesodomains as defined by Hashin (1983) they are sometimes referred to as "mesoscale approaches". Figure 1 shows a sketch of a microgeometry as well as PMA, ECA and windowing approaches applied to it.

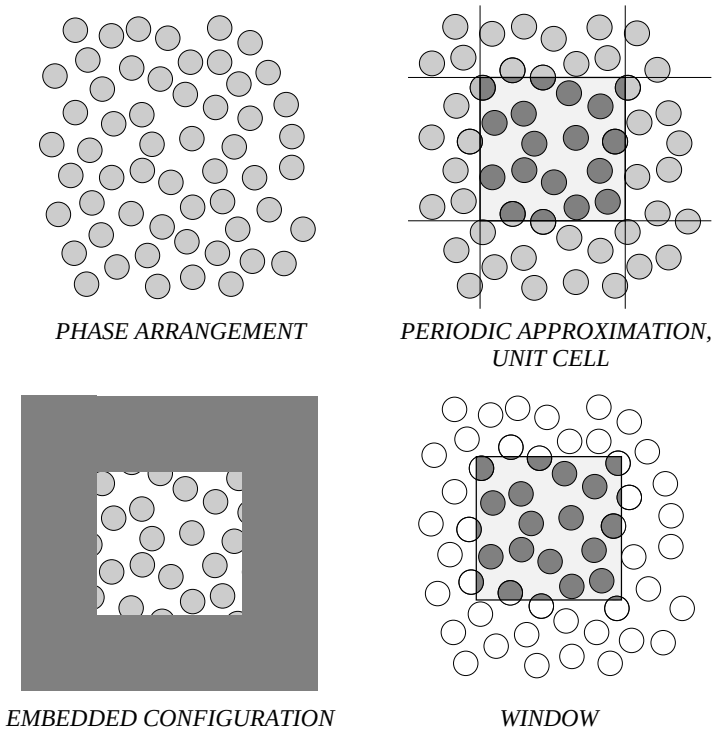

Figure 1.1: Schematic sketch of a random matrix–inclusion microstructure and of the volume elements used by a periodic microfield method (which employs a slightly different periodic "model" microstructure), an embedding scheme and a windowing approach for studying this inhomogeneous material.

For small inhomogeneous samples (i.e., samples the size of which exceeds the microscale by not more than, say, an order of magnitude) the full microgeometry can be modeled and studied, see, e.g., Papka and Kyriakides (1994), Silberschmidt and Werner (2001) or Luxner et al. (2005). In such models boundary effects (and thus the boundary conditions applied to the sample as well as the sample's size in terms of the characteristic length of the inhomogeneities) typically play a prominent role in the mechanical behavior.

Further descriptions of inhomogeneous materials, such as rules of mixture (isostrain and isostress models) and semiempirical formulae like the Halpin–Tsai equations (Halpin and Kardos, 1976), are not discussed here due to their typically rather weak physical background and their rather limited predictive capabilities. For brevity, a number of models with solid physical basis, such as expressions for self-similar composite sphere assemblages (CSA, (Hashin, 1962)) and composite cylinder assemblages (CCA, (Hashin and Rosen, 1964)), information theoretical approaches (Kreher, 1990), and the semiempirical methods proposed for describing the elastoplastic behavior of composites reinforced by aligned continuous fibers (Dvorak and Bahei-el Din, 1987), are not covered within the present discussions, either.

For studying materials that are inhomogeneous at a number of (sufficiently widely spread) length scales (e.g., materials in which well defined clusters of inhomogeneities are present), hierarchical procedures that use homogenization at more than one level are a natural extension of the above concepts. Such multi-scale models are the subject of a short discussion in chapter 8.

Chapter 2

Mean Field Methods

In this chapter relations are given for two-phase materials only, extensions to multi-phase materials being rather straightforward in most cases. Special emphasis is put on effective field methods of the Mori–Tanaka type, which may be viewed as the simplest mean field approaches for modeling inhomogeneous materials that encompass the full physical range of phase volume fractions[14]. Unless specifically stated otherwise, the material behavior of both reinforcements and matrix is taken to be linear (thermo)elastic. Perfect bonding between the constituents is assumed in all cases. There is an extensive body of literature covering mean field approaches, so that the following treatment is far from complete.

2.1 General Relations between Mean Fields in Thermoelastic Two-Phase Materials

Throughout this report additive decomposition of strains is used. For example, for the case of thermoelastoplastic material behavior the total strain tensor can be accordingly be written as

$$\boldsymbol{\varepsilon} = \boldsymbol{\varepsilon}_{\mathrm{el}} + \boldsymbol{\varepsilon}_{\mathrm{pl}} + \boldsymbol{\varepsilon}_{\mathrm{th}} \qquad , \tag{2.1}$$

where $\boldsymbol{\varepsilon}_{\mathrm{el}}$, $\boldsymbol{\varepsilon}_{\mathrm{pl}}$ and $\boldsymbol{\varepsilon}_{\mathrm{th}}$ denote the elastic, plastic and thermal strains, respectively. Strain and stress tensors can be split into volumetric and deviatoric contributions

$$\begin{aligned} \boldsymbol{\varepsilon} &= \boldsymbol{\varepsilon}_{\mathrm{vol}} + \boldsymbol{\varepsilon}_{\mathrm{dev}} = \mathbf{Q}_{\mathrm{vol}}\,\boldsymbol{\varepsilon} + \mathbf{Q}_{\mathrm{dev}}\,\boldsymbol{\varepsilon} \\ \boldsymbol{\sigma} &= \boldsymbol{\sigma}_{\mathrm{vol}} + \boldsymbol{\sigma}_{\mathrm{dev}} = \mathbf{Q}_{\mathrm{vol}}\,\boldsymbol{\sigma} + \mathbf{Q}_{\mathrm{dev}}\,\boldsymbol{\sigma} \qquad , \end{aligned} \tag{2.2}$$

$\mathbf{Q}_{\mathrm{vol}}$ and $\mathbf{Q}_{\mathrm{dev}}$ being the volumetric and deviatoric projection tensors.

For thermoelastic inhomogeneous materials, the macroscopic stress–strain relations can be written in the form

$$\begin{aligned} \langle\boldsymbol{\sigma}\rangle &= \mathbf{E}^*\langle\boldsymbol{\varepsilon}\rangle + \boldsymbol{\vartheta}^*\Delta T \\ \langle\boldsymbol{\varepsilon}\rangle &= \mathbf{C}^*\langle\boldsymbol{\sigma}\rangle + \boldsymbol{\alpha}^*\Delta T \qquad . \end{aligned} \tag{2.3}$$

[14] Because Eshelby and Mori–Tanaka methods are specifically suited for matrix–inclusion-type microtopologies, the expression "composite" is often used in the present chapter instead of the more general designation "inhomogeneous material".

Here the expression $\boldsymbol{\alpha}^*\Delta T$ corresponds to the macroscopic thermal strain tensor, $\boldsymbol{\vartheta}^* = -\mathbf{E}^*\boldsymbol{\alpha}^*$ is the macroscopic specific thermal stress tensor (i.e., the overall stress response of the fully constrained material to a purely thermal unit load), and ΔT stands for the (spatially homogeneous) temperature difference with respect to some stress-free reference temperature. The constituents, here a matrix $^{(\mathrm{m})}$ and inhomogeneities $^{(\mathrm{i})}$, are also assumed to behave thermoelastically, so that

$$\begin{aligned} \langle\boldsymbol{\sigma}\rangle^{(\mathrm{m})} &= \mathbf{E}^{(\mathrm{m})}\langle\boldsymbol{\varepsilon}\rangle^{(\mathrm{m})} + \boldsymbol{\vartheta}^{(\mathrm{m})}\Delta T & \qquad \langle\boldsymbol{\sigma}\rangle^{(\mathrm{i})} &= \mathbf{E}^{(\mathrm{i})}\langle\boldsymbol{\varepsilon}\rangle^{(\mathrm{i})} + \boldsymbol{\vartheta}^{(\mathrm{i})}\Delta T \\ \langle\boldsymbol{\varepsilon}\rangle^{(\mathrm{m})} &= \mathbf{C}^{(\mathrm{m})}\langle\boldsymbol{\sigma}\rangle^{(\mathrm{m})} + \boldsymbol{\alpha}^{(\mathrm{m})}\Delta T & \qquad \langle\boldsymbol{\varepsilon}\rangle^{(\mathrm{i})} &= \mathbf{C}^{(\mathrm{i})}\langle\boldsymbol{\sigma}\rangle^{(\mathrm{i})} + \boldsymbol{\alpha}^{(\mathrm{i})}\Delta T \end{aligned} \quad , \tag{2.4}$$

where the relations $\boldsymbol{\vartheta}^{(\mathrm{m})} = -\mathbf{E}^{(\mathrm{m})}\boldsymbol{\alpha}^{(\mathrm{m})}$ and $\boldsymbol{\vartheta}^{(\mathrm{i})} = -\mathbf{E}^{(\mathrm{i})}\boldsymbol{\alpha}^{(\mathrm{i})}$ hold.

From the definition of phase averaging, eqn. (1.13), the relations between the phase averaged fields,

$$\begin{aligned} \langle\boldsymbol{\varepsilon}\rangle &= \xi\langle\boldsymbol{\varepsilon}\rangle^{(\mathrm{i})} + (1-\xi)\langle\boldsymbol{\varepsilon}\rangle^{(\mathrm{m})} &= \boldsymbol{\varepsilon}^{\mathrm{a}} \\ \langle\boldsymbol{\sigma}\rangle &= \xi\langle\boldsymbol{\sigma}\rangle^{(\mathrm{i})} + (1-\xi)\langle\boldsymbol{\sigma}\rangle^{(\mathrm{m})} &= \boldsymbol{\sigma}^{\mathrm{a}} \end{aligned} \quad , \tag{2.5}$$

where $\xi = V^{(\mathrm{i})} = \Omega^{(\mathrm{i})}/\Omega_{\mathrm{s}}$ stands for the volume fraction of the reinforcements and $1-\xi = V^{(\mathrm{m})} = \Omega^{(\mathrm{m})}/\Omega_{\mathrm{s}}$ for the volume fraction of the matrix. $\boldsymbol{\varepsilon}^{\mathrm{a}}$ and $\boldsymbol{\sigma}^{\mathrm{a}}$ denote the far field (applied) homogeneous stress and strain tensors, respectively, with $\boldsymbol{\varepsilon}^{\mathrm{a}} = \mathbf{C}^*\boldsymbol{\sigma}^{\mathrm{a}}$. Perfect interfaces between the phases are assumed in expressing the macroscopic strain of the composite as the weighted sum of the phase averaged strains.

The phase averaged strains and stresses can be related to the overall strains and stresses by the phase strain and stress concentration tensors $\bar{\mathbf{A}}$, $\bar{\boldsymbol{\eta}}$, $\bar{\mathbf{B}}$, and $\bar{\boldsymbol{\beta}}$ (Hill, 1963), respectively, which are defined for thermoelastic inhomogeneous materials by the expressions

$$\begin{aligned} \langle\boldsymbol{\varepsilon}\rangle^{(\mathrm{m})} &= \bar{\mathbf{A}}^{(\mathrm{m})}\langle\boldsymbol{\varepsilon}\rangle + \bar{\boldsymbol{\eta}}^{(\mathrm{m})}\Delta T & \qquad \langle\boldsymbol{\varepsilon}\rangle^{(\mathrm{i})} &= \bar{\mathbf{A}}^{(\mathrm{i})}\langle\boldsymbol{\varepsilon}\rangle + \bar{\boldsymbol{\eta}}^{(\mathrm{i})}\Delta T \\ \langle\boldsymbol{\sigma}\rangle^{(\mathrm{m})} &= \bar{\mathbf{B}}^{(\mathrm{m})}\langle\boldsymbol{\sigma}\rangle + \bar{\boldsymbol{\beta}}^{(\mathrm{m})}\Delta T & \qquad \langle\boldsymbol{\sigma}\rangle^{(\mathrm{i})} &= \bar{\mathbf{B}}^{(\mathrm{i})}\langle\boldsymbol{\sigma}\rangle + \bar{\boldsymbol{\beta}}^{(\mathrm{i})}\Delta T \end{aligned} \quad , \tag{2.6}$$

compare eqn. (1.12) for the purely elastic case. $\bar{\mathbf{A}}$ and $\bar{\mathbf{B}}$ are referred to as the mechanical or (elastic) phase stress and strain concentration tensors, respectively, and $\bar{\boldsymbol{\eta}}$ as well as $\bar{\boldsymbol{\beta}}$ are the corresponding thermal concentration tensors.

By using eqns. (2.5) and (2.6), the strain and stress concentration tensors can be shown to fulfill the relations

$$\begin{aligned} \xi\bar{\mathbf{A}}^{(\mathrm{i})} + (1-\xi)\bar{\mathbf{A}}^{(\mathrm{m})} &= \mathbf{I} & \qquad \xi\bar{\boldsymbol{\eta}}^{(\mathrm{i})} + (1-\xi)\bar{\boldsymbol{\eta}}^{(\mathrm{m})} &= \mathbf{o} \\ \xi\bar{\mathbf{B}}^{(\mathrm{i})} + (1-\xi)\bar{\mathbf{B}}^{(\mathrm{m})} &= \mathbf{I} & \qquad \xi\bar{\boldsymbol{\beta}}^{(\mathrm{i})} + (1-\xi)\bar{\boldsymbol{\beta}}^{(\mathrm{m})} &= \mathbf{o} \end{aligned} \quad , \tag{2.7}$$

where $\mathbf{I}$ stands for the symmetric rank 4 unit tensor and $\mathbf{o}$ for the rank 2 null tensor.

The effective elasticity and compliance tensors of the composite can be obtained from the properties of the phases and from the mechanical concentration tensors as

$$\begin{aligned} \mathbf{E}^* &= \xi\mathbf{E}^{(\mathrm{i})}\bar{\mathbf{A}}^{(\mathrm{i})} + (1-\xi)\mathbf{E}^{(\mathrm{m})}\bar{\mathbf{A}}^{(\mathrm{m})} \\ &= \mathbf{E}^{(\mathrm{m})} + \xi[\mathbf{E}^{(\mathrm{i})} - \mathbf{E}^{(\mathrm{m})}]\bar{\mathbf{A}}^{(\mathrm{i})} = \mathbf{E}^{(\mathrm{i})} + (1-\xi)[\mathbf{E}^{(\mathrm{m})} - \mathbf{E}^{(\mathrm{i})}]\bar{\mathbf{A}}^{(\mathrm{m})} \end{aligned} \tag{2.8}$$

$$\begin{aligned}\mathbf{C}^* &= \xi\mathbf{C}^{(\mathfrak{i})}\bar{\mathbf{B}}^{(\mathfrak{i})} + (1-\xi)\mathbf{C}^{(\mathfrak{m})}\bar{\mathbf{B}}^{(\mathfrak{m})} \\ &= \mathbf{C}^{(\mathfrak{m})} + \xi[\mathbf{C}^{(\mathfrak{i})} - \mathbf{C}^{(\mathfrak{m})}]\bar{\mathbf{B}}^{(\mathfrak{i})} = \mathbf{C}^{(\mathfrak{i})} + (1-\xi)[\mathbf{C}^{(\mathfrak{m})} - \mathbf{C}^{(\mathfrak{i})}]\bar{\mathbf{B}}^{(\mathfrak{m})} \quad , \end{aligned} \tag{2.9}$$

compare eqn. (1.8). For multi-phase materials with N phases $(\mathfrak{p})$ the equivalents of eqn. (2.7) take the form

$$\begin{aligned} \sum_{(\mathfrak{p})} \bar{\mathbf{A}}^{(\mathfrak{p})} &= \mathbf{I} & \sum_{(\mathfrak{p})} \bar{\boldsymbol{\eta}}^{(\mathfrak{p})} &= \mathbf{o} \\ \sum_{(\mathfrak{p})} \bar{\mathbf{B}}^{(\mathfrak{p})} &= \mathbf{I} & \sum_{(\mathfrak{p})} \bar{\boldsymbol{\beta}}^{(\mathfrak{p})} &= \mathbf{o} \quad , \end{aligned} \tag{2.10}$$

and the effective elastic tensors can be evaluated as

$$\mathbf{E}^* = \sum_{(\mathfrak{p})} \xi^{(\mathfrak{p})}\mathbf{E}^{(\mathfrak{p})}\bar{\mathbf{A}}^{(\mathfrak{p})} \qquad \mathbf{C}^* = \sum_{(\mathfrak{p})} \xi^{(\mathfrak{p})}\mathbf{C}^{(\mathfrak{p})}\bar{\mathbf{B}}^{(\mathfrak{p})} \tag{2.11}$$

in analogy to eqns. (2.8) and (2.9).

The effective thermal expansion coefficient tensor, $\boldsymbol{\alpha}^*$, and the specific thermal stress tensor, $\boldsymbol{\vartheta}^*$, can be related to the thermoelastic phase behaviors and the thermal concentration tensors as

$$\begin{aligned}\boldsymbol{\alpha}^* &= \xi[\mathbf{C}^{(\mathfrak{i})}\bar{\boldsymbol{\beta}}^{(\mathfrak{i})} + \boldsymbol{\alpha}^{(\mathfrak{i})}] + (1-\xi)[\mathbf{C}^{(\mathfrak{m})}\bar{\boldsymbol{\beta}}^{(\mathfrak{m})} + \boldsymbol{\alpha}^{(\mathfrak{m})}] \\ &= \xi\boldsymbol{\alpha}^{(\mathfrak{i})} + (1-\xi)\boldsymbol{\alpha}^{(\mathfrak{m})} + (1-\xi)[\mathbf{C}^{(\mathfrak{m})} - \mathbf{C}^{(\mathfrak{i})}]\bar{\boldsymbol{\beta}}^{(\mathfrak{m})} \\ &= \xi\boldsymbol{\alpha}^{(\mathfrak{i})} + (1-\xi)\boldsymbol{\alpha}^{(\mathfrak{m})} + \xi[\mathbf{C}^{(\mathfrak{i})} - \mathbf{C}^{(\mathfrak{m})}]\bar{\boldsymbol{\beta}}^{(\mathfrak{i})} \quad . \end{aligned} \tag{2.12}$$

$$\begin{aligned}\boldsymbol{\vartheta}^* &= \xi[\mathbf{E}^{(\mathfrak{i})}\bar{\boldsymbol{\eta}}^{(\mathfrak{i})} + \boldsymbol{\vartheta}^{(\mathfrak{i})}] + (1-\xi)[\mathbf{E}^{(\mathfrak{m})}\bar{\boldsymbol{\eta}}^{(\mathfrak{m})} + \boldsymbol{\vartheta}^{(\mathfrak{m})}] \\ &= \xi\boldsymbol{\vartheta}^{(\mathfrak{i})} + (1-\xi)\boldsymbol{\vartheta}^{(\mathfrak{m})} + (1-\xi)[\mathbf{E}^{(\mathfrak{m})} - \mathbf{E}^{(\mathfrak{i})}]\bar{\boldsymbol{\eta}}^{(\mathfrak{m})} \\ &= \xi\boldsymbol{\vartheta}^{(\mathfrak{i})} + (1-\xi)\boldsymbol{\vartheta}^{(\mathfrak{m})} + \xi[\mathbf{E}^{(\mathfrak{i})} - \mathbf{E}^{(\mathfrak{m})}]\bar{\boldsymbol{\eta}}^{(\mathfrak{i})} \quad . \end{aligned} \tag{2.13}$$

The above expressions can be derived by inserting eqns. (2.4) and (2.6) into eqns. (2.5) and comparing with eqns. (2.3). Alternatively, the overall coefficients of thermal expansion of multi-phase materials can be obtained as

$$\boldsymbol{\alpha}^* = \sum_{(\mathfrak{p})} \xi^{(\mathfrak{p})}(\bar{\mathbf{B}}^{(\mathfrak{p})})^{\mathrm{T}}\boldsymbol{\alpha}^{(\mathfrak{p})} \quad , \tag{2.14}$$

compare (Mandel, 1965; Levin, 1967), an expression known as the Mandel–Levin formula. If the effective compliance tensor of a two-phase material is known eqn.(2.10) can be inserted into eqn.(2.14) to give the overall coefficients of thermal expansion as

$$\boldsymbol{\alpha}^* = (\mathbf{C}^* - \mathbf{C}^{(\mathfrak{m})})(\mathbf{C}^{(\mathfrak{i})} - \mathbf{C}^{(\mathfrak{m})})^{-1}\boldsymbol{\alpha}^{(\mathfrak{i})} - (\mathbf{C}^* - \mathbf{C}^{(\mathfrak{i})})(\mathbf{C}^{(\mathfrak{i})} - \mathbf{C}^{(\mathfrak{m})})^{-1}\boldsymbol{\alpha}^{(\mathfrak{m})} \quad . \tag{2.15}$$

The mechanical stress and strain concentration tensors for a given phase are linked to each other by expressions of the type

$$\begin{aligned}\bar{\mathbf{A}}^{(\mathfrak{m})} &= \mathbf{C}^{(\mathfrak{m})}\bar{\mathbf{B}}^{(\mathfrak{m})}\mathbf{E}^{(\mathfrak{i})}[\mathbf{I} + (1-\xi)(\mathbf{C}^{(\mathfrak{m})} - \mathbf{C}^{(\mathfrak{i})})\bar{\mathbf{B}}^{(\mathfrak{m})}\mathbf{E}^{(\mathfrak{i})}]^{-1} = \mathbf{C}^{(\mathfrak{m})}\bar{\mathbf{B}}^{(\mathfrak{m})}\mathbf{E}^* \\ \bar{\mathbf{B}}^{(\mathfrak{m})} &= \mathbf{E}^{(\mathfrak{m})}\bar{\mathbf{A}}^{(\mathfrak{m})}\mathbf{C}^{(\mathfrak{i})}[\mathbf{I} + (1-\xi)(\mathbf{E}^{(\mathfrak{m})} - \mathbf{E}^{(\mathfrak{i})})\bar{\mathbf{A}}^{(\mathfrak{m})}\mathbf{C}^{(\mathfrak{i})}]^{-1} = \mathbf{E}^{(\mathfrak{m})}\bar{\mathbf{A}}^{(\mathfrak{m})}\mathbf{C}^* \quad . \end{aligned} \tag{2.16}$$

In addition, by invoking the principle of virtual work relations were developed (Benveniste and Dvorak, 1990; Benveniste et al., 1991) which link the thermal strain concentration tensors, $\bar{\boldsymbol{\eta}}^{(\mathrm{p})}$, to the mechanical strain concentration tensors, $\bar{\mathbf{A}}^{(\mathrm{p})}$, and the thermal stress concentration tensors, $\bar{\boldsymbol{\beta}}^{(\mathrm{p})}$, to the mechanical stress concentration tensors, $\bar{\mathbf{B}}^{(\mathrm{p})}$, respectively, as

$$\begin{aligned}
\bar{\boldsymbol{\eta}}^{(\mathrm{m})} &= [\mathbf{I} - \bar{\mathbf{A}}^{(\mathrm{m})}][\mathbf{E}^{(\mathrm{i})} - \mathbf{E}^{(\mathrm{m})}]^{-1}[\boldsymbol{\vartheta}^{(\mathrm{m})} - \boldsymbol{\vartheta}^{(\mathrm{i})}] \\
\bar{\boldsymbol{\eta}}^{(\mathrm{i})} &= [\mathbf{I} - \bar{\mathbf{A}}^{(\mathrm{i})}][\mathbf{E}^{(\mathrm{m})} - \mathbf{E}^{(\mathrm{i})}]^{-1}[\boldsymbol{\vartheta}^{(\mathrm{i})} - \boldsymbol{\vartheta}^{(\mathrm{m})}] \\
\bar{\boldsymbol{\beta}}^{(\mathrm{m})} &= [\mathbf{I} - \bar{\mathbf{B}}^{(\mathrm{m})}][\mathbf{C}^{(\mathrm{i})} - \mathbf{C}^{(\mathrm{m})}]^{-1}[\boldsymbol{\alpha}^{(\mathrm{m})} - \boldsymbol{\alpha}^{(\mathrm{i})}] \\
\bar{\boldsymbol{\beta}}^{(\mathrm{i})} &= [\mathbf{I} - \bar{\mathbf{B}}^{(\mathrm{i})}][\mathbf{C}^{(\mathrm{m})} - \mathbf{C}^{(\mathrm{i})}]^{-1}[\boldsymbol{\alpha}^{(\mathrm{i})} - \boldsymbol{\alpha}^{(\mathrm{m})}] \qquad . \qquad (2.17)
\end{aligned}$$

From eqns. (2.9) to (2.17) it is evident that the knowledge of one elastic phase concentration tensor is sufficient for describing the full thermoelastic behavior of a two-phase inhomogeneous material within the mean field framework[15]. A fair number of additional relations between phase averaged tensors have been given in the literature which allow, e.g., the phase concentration tensors to be obtained from the overall and phase elastic tensors.

2.2 Eshelby Tensor and Dilute Matrix–Inclusion Composites

A large proportion of the mean field descriptions used in continuum micromechanics of materials are based on the work of Eshelby (1957), who studied the stress and strain distributions in homogeneous media that contain a subregion that spontaneously changes its shape and/or size (undergoes a "transformation") so that it no longer fits into its previous space in the "parent medium". Eshelby's results show that if an elastic homogeneous ellipsoidal inclusion (i.e., an inclusion consisting of the same material as the matrix) in an infinite matrix is subjected to a homogeneous strain $\boldsymbol{\varepsilon}_{\mathrm{t}}$ (called the "stress-free strain", "unconstrained strain", "eigenstrain", or "transformation strain"), the stress and strain states in the constrained inclusion are uniform[16], i.e., $\boldsymbol{\sigma}^{(\mathrm{i})} = \langle\boldsymbol{\sigma}\rangle^{(\mathrm{i})}$ and $\boldsymbol{\varepsilon}^{(\mathrm{i})} = \langle\boldsymbol{\varepsilon}\rangle^{(\mathrm{i})}$. The uniform strain in the constrained inclusion (the "constrained strain"), $\boldsymbol{\varepsilon}_{\mathrm{c}}$, is related to the stress-free strain $\boldsymbol{\varepsilon}_{\mathrm{t}}$ by the expression

$$\boldsymbol{\varepsilon}_{\mathrm{c}} = \mathbf{S}\boldsymbol{\varepsilon}_{\mathrm{t}} \qquad (2.18)$$

where $\mathbf{S}$ is referred to as the (interior point) Eshelby tensor. For eqn. (2.18) to hold, $\boldsymbol{\varepsilon}_{\mathrm{t}}$ may be any kind of eigenstrain that is uniform over the inclusion (e.g., a thermal strain or a strain due to some phase transformation which involves no changes in the elastic constants of the inclusion).

[15] Similarly, $n-1$ elastic phase concentration tensors must be known for describing the overall thermoelastic behavior of an n-phase material.

[16] This "Eshelby property" or "Eshelby uniformity" is limited to ellipsoidal shapes (Lubarda and Markenscoff, 1998). For certain nondilute periodic arrangements of inclusions, however, non-ellipsoidal shapes can give rise to homogeneous fields (Liu et al., 2007).

For mean field descriptions of dilute matrix–inclusion composites, of course, the interest is focused on the stress and strain fields in inhomogeneous inclusions ("inhomogeneities") that are embedded in a matrix. Such cases can be handled on the basis of Eshelby's theory for homogeneous inclusions, eqn. (2.18), by introducing the concept of equivalent homogeneous inclusions. This strategy involves replacing an actual perfectly bonded inhomogeneous inclusion, which has different material properties than the matrix and which is subjected to a given unconstrained eigenstrain $\boldsymbol{\varepsilon}_\mathrm{t}$, with a (fictitious) "equivalent" homogeneous inclusion on which a (fictitious) "equivalent" eigenstrain $\boldsymbol{\varepsilon}_\tau$ is made to act. This equivalent eigenstrain must be chosen in such a way that the inhomogeneous inclusion and the equivalent homogeneous inclusion attain the same stress state $\boldsymbol{\sigma}^{(\mathrm{i})}$ and the same constrained strain $\boldsymbol{\varepsilon}_\mathrm{c}$ (Eshelby, 1957; Withers et al., 1989). When $\boldsymbol{\sigma}^{(\mathrm{i})}$ is expressed in terms of the elastic strain in the inhomogeneity or inclusion, this condition translates into the equality

$$\boldsymbol{\sigma}^{(\mathrm{i})} = \mathbf{E}^{(\mathrm{i})}[\boldsymbol{\varepsilon}_\mathrm{c} - \boldsymbol{\varepsilon}_\mathrm{t}] = \mathbf{E}^{(\mathrm{m})}[\boldsymbol{\varepsilon}_\mathrm{c} - \boldsymbol{\varepsilon}_\tau] \qquad . \tag{2.19}$$

Here $\boldsymbol{\varepsilon}_\mathrm{c} - \boldsymbol{\varepsilon}_\mathrm{t}$ and $\boldsymbol{\varepsilon}_\mathrm{c} - \boldsymbol{\varepsilon}_\tau$ are the elastic strains in the inhomogeneity and the equivalent homogeneous inclusion, respectively. Obviously, in the general case the stress-free strains will be different for the equivalent inclusion and the real inhomogeneity, $\boldsymbol{\varepsilon}_\mathrm{t} \neq \boldsymbol{\varepsilon}_\tau$. Plugging the result of applying eqn. (2.18) to the equivalent eigenstrain, $\boldsymbol{\varepsilon}_\mathrm{c} = \mathbf{S}\boldsymbol{\varepsilon}_\tau$, into eqn. (2.19) leads to the relationship

$$\boldsymbol{\sigma}^{(\mathrm{i})} = \mathbf{E}^{(\mathrm{i})}[\mathbf{S}\boldsymbol{\varepsilon}_\tau - \boldsymbol{\varepsilon}_\mathrm{t}] = \mathbf{E}^{(\mathrm{m})}[\mathbf{S} - \mathbf{I}]\boldsymbol{\varepsilon}_\tau \qquad , \tag{2.20}$$

which can be rearranged to obtain the equivalent eigenstrain as a function of the known stress-free eigenstrain $\boldsymbol{\varepsilon}_\mathrm{t}$ of the real inclusion as

$$\boldsymbol{\varepsilon}_\tau = [(\mathbf{E}^{(\mathrm{i})} - \mathbf{E}^{(\mathrm{m})})\mathbf{S} + \mathbf{E}^{(\mathrm{m})}]^{-1}\mathbf{E}^{(\mathrm{i})}\boldsymbol{\varepsilon}_\mathrm{t} \qquad . \tag{2.21}$$

This, in turn, allows the stress in the inhomogeneity, $\boldsymbol{\sigma}^{(\mathrm{i})}$, to be expressed as

$$\boldsymbol{\sigma}^{(\mathrm{i})} = \mathbf{E}^{(\mathrm{m})}(\mathbf{S} - \mathbf{I})[(\mathbf{E}^{(\mathrm{i})} - \mathbf{E}^{(\mathrm{m})})\mathbf{S} + \mathbf{E}^{(\mathrm{m})}]^{-1}\mathbf{E}^{(\mathrm{i})}\boldsymbol{\varepsilon}_\mathrm{t} \qquad . \tag{2.22}$$

The concept of the equivalent homogeneous inclusion can be extended to cases where a uniform mechanical strain $\boldsymbol{\varepsilon}^\mathrm{a}$ or external stress $\boldsymbol{\sigma}^\mathrm{a}$ is applied to a perfectly bonded inhomogeneous elastic inclusion in an infinite matrix. Here, the strain in the inclusion, $\boldsymbol{\varepsilon}^{(\mathrm{i})}$, is a superposition of the applied strain and of a term $\boldsymbol{\varepsilon}_\mathrm{c}$ that accounts for the constraint effects of the surrounding matrix. A fair number of different expressions for concentration tensors obtained by such procedures have been reported in the literature, among the most handy being those proposed by Hill (1965b) and elaborated by Benveniste (1987). For deriving them, the conditions of equal stresses and strains in the actual inclusion (elasticity tensor $\mathbf{E}^{(\mathrm{i})}$) and the equivalent inclusion (elasticity tensor $\mathbf{E}^{(\mathrm{m})}$) under an applied far field strain $\boldsymbol{\varepsilon}^\mathrm{a}$ take the form

$$\boldsymbol{\sigma}^{(\mathrm{i})} = \mathbf{E}^{(\mathrm{i})}[\boldsymbol{\varepsilon}^\mathrm{a} + \boldsymbol{\varepsilon}_\mathrm{c}] = \mathbf{E}^{(\mathrm{m})}[\boldsymbol{\varepsilon}^\mathrm{a} + \boldsymbol{\varepsilon}_\mathrm{c} - \boldsymbol{\varepsilon}_\tau] \tag{2.23}$$

and

$$\boldsymbol{\varepsilon}^{(\mathrm{i})} = \boldsymbol{\varepsilon}^\mathrm{a} + \boldsymbol{\varepsilon}_\mathrm{c} = \boldsymbol{\varepsilon}^\mathrm{a} + \mathbf{S}\boldsymbol{\varepsilon}_\tau \qquad , \tag{2.24}$$

respectively, where eqn. (2.18) is used to describe the constrained strain of the equivalent homogeneous inclusion. On the basis of these relationships the strain in the inhomogeneity can be expressed as

$$\boldsymbol{\varepsilon}^{(\mathrm{i})} = [\mathbf{I} + \mathbf{S}\mathbf{C}^{(\mathrm{m})}(\mathbf{E}^{(\mathrm{i})} - \mathbf{E}^{(\mathrm{m})})]^{-1}\boldsymbol{\varepsilon}^\mathrm{a} \qquad . \tag{2.25}$$

Because the strain in the inhomogeneity is homogeneous, $\boldsymbol{\varepsilon}^{(\mathrm{i})} = \langle\boldsymbol{\varepsilon}\rangle^{(\mathrm{i})}$, the strain concentration tensor for dilute inhomogeneities follows directly as

$$\bar{\mathbf{A}}^{(\mathrm{i})}_{\mathrm{dil}} = [\mathbf{I} + \mathbf{S}\mathbf{C}^{(\mathrm{m})}(\mathbf{E}^{(\mathrm{i})} - \mathbf{E}^{(\mathrm{m})})]^{-1} \qquad . \tag{2.26}$$

By setting $\langle\boldsymbol{\varepsilon}\rangle^{(\mathrm{i})} = \mathbf{C}^{(\mathrm{i})}\langle\boldsymbol{\sigma}\rangle^{(\mathrm{i})}$ and using $\boldsymbol{\varepsilon}^{\mathrm{a}} = \mathbf{C}^{(\mathrm{m})}\boldsymbol{\sigma}^{\mathrm{a}}$, the dilute stress concentration tensor for the inhomogeneities is found from eqn. (2.26) as

$$\begin{aligned} \bar{\mathbf{B}}^{(\mathrm{i})}_{\mathrm{dil}} &= \mathbf{E}^{(\mathrm{i})}[\mathbf{I} + \mathbf{S}\mathbf{C}^{(\mathrm{m})}(\mathbf{E}^{(\mathrm{i})} - \mathbf{E}^{(\mathrm{m})})]^{-1}\mathbf{C}^{(\mathrm{m})} \\ &= [\mathbf{I} + \mathbf{E}^{(\mathrm{m})}(\mathbf{I} - \mathbf{S})(\mathbf{C}^{(\mathrm{i})} - \mathbf{C}^{(\mathrm{m})})]^{-1} \qquad . \end{aligned} \tag{2.27}$$

Alternative expressions for dilute mechanical and thermal inclusion concentration tensors were given, e.g., by Mura (1987), Wakashima et al. (1988) and Clyne and Withers (1993). All of the above relations were derived under the assumption that the inhomogeneities are dilutely dispersed in the matrix and thus do not "feel" any effects due to their neighbors (i.e., they are loaded by the unperturbed applied stress $\boldsymbol{\sigma}^{\mathrm{a}}$ or applied strain $\boldsymbol{\varepsilon}^{\mathrm{a}}$, the so called dilute case). Accordingly, the inclusion concentration tensors are independent of the reinforcement volume fraction ξ.

The stress and strain fields outside a transformed homogeneous or inhomogeneous inclusion in an infinite matrix are not uniform on the microscale[17] (Eshelby, 1959). Within the framework of mean field theories, which aim to link the average fields in matrix and inhomogeneities with the overall response of inhomogeneous materials, however, it is only the average matrix stresses and strains that are of interest. For dilute composites, such expressions follow directly by combining eqns. (2.26) and (2.27) with eqn. (2.7). Estimates for the overall elastic and thermal expansion tensors can, of course, be obtained in a straightforward way from the concentration tensors by using eqns. (2.8) to (2.17). It must be kept in mind, however, that the dilute expressions are strictly valid only for vanishingly small inhomogeneity volume fractions and give dependable results only for $\xi \ll 0.1$.

The Eshelby tensor $\mathbf{S}$ depends only on the material properties of the matrix and on the aspect ratio a of the inclusions, i.e., expressions for the Eshelby tensor of ellipsoidal inhomogeneities are independent of the material symmetry and properties of the inhomogeneities. Expressions for the Eshelby tensor of spheroidal inclusions in an isotropic matrix are given, e.g., by Pedersen (1983), Tandon and Weng (1984), Mura (1987) or Clyne and Withers (1993)[18], the formulae being very simple for continuous fibers of circular cross-section ($a \to \infty$), spherical inclusions ($a = 1$), and thin circular disks ($a \to 0$). Closed form expressions for the Eshelby tensor have also been reported for spheroidal inclusions in a matrix of transversely isotropic (Withers, 1989) or cubic material symmetry (Mura, 1987), provided the material axes of the matrix constituents are aligned with the orientations of non-spherical inclusions. In cases where no analytical solutions are available, the Eshelby tensor can be evaluated numerically, compare Gavazzi and Lagoudas (1990).

[17] The fields outside a single inclusion can be described via the (exterior point) Eshelby tensor, see, e.g., Ju and Sun (1999). From the (constant) interior point fields and the (position) dependent exterior point fields the stress and strain jumps at the interface between inclusion and matrix can be evaluated.

[18] Instead of evaluating the Eshelby tensor for a given configuration, the so called mean polarization factor tensor $\mathbf{Q} = \mathbf{E}^{(\mathrm{m})}(\mathbf{I} - \mathbf{S})$ may be evaluated instead, see, e.g., Ponte Castañeda (1996).

2.3 Mean Field Methods for Thermoelastic Composites with Aligned Reinforcements

Theoretical descriptions of the overall thermoelastic behavior of composites with reinforcement volume fractions of more than a few percent must explicitly account for interactions between inhomogeneities, i.e., for the effects of all surrounding reinforcements on the stress and strain fields experienced by a given fiber or particle. Within the mean field framework such interaction effects as well as the concomitant perturbations of the stress and strain fields in the matrix are accounted for in a collective way via suitable phase-wise constant approximations. Beyond these "background effects", there are interactions between individual reinforcements which, on the one hand, give rise to inhomogeneous stress and strain fields within each inhomogeneity ("intra-particle fluctuations") and in the matrix. On the other hand, they cause the levels of the average stresses and strains in individual inhomogeneities to differ ("inter-particle fluctuations"). These interactions and fluctuations are not resolved by mean field methods.

Mori–Tanaka-Type Estimates

One way of introducing collective interactions between inhomogeneities consists of approximating the stresses acting on an inhomogeneity, which may be viewed as perturbation stresses caused by the presence of other inhomogeneities ("image stresses", "background stresses") superimposed on the applied far field stress, by an appropriate average matrix stress. The idea of combining such a concept of an average matrix stress with Eshelby-type equivalent inclusion expressions goes back to Brown and Stobbs (1971) as well as Mori and Tanaka (1973). Effective field theories of this type are generically referred to as Mori–Tanaka methods. By construction they do not invoke explicit (e.g., pair-wise) interactions between "individual" inhomogeneities, but rather operate on a level of collective interactions.

Benveniste (1987) pointed out that in the isothermal case the central assumption involved in Mori–Tanaka approaches can be denoted as

$$\begin{aligned} \langle \boldsymbol{\varepsilon} \rangle^{(\mathrm{i})} &= \bar{\mathbf{A}}^{(\mathrm{i})}_{\mathrm{dil}} \langle \boldsymbol{\varepsilon} \rangle^{(\mathrm{m})} \\ \langle \boldsymbol{\sigma} \rangle^{(\mathrm{i})} &= \bar{\mathbf{B}}^{(\mathrm{i})}_{\mathrm{dil}} \langle \boldsymbol{\sigma} \rangle^{(\mathrm{m})} \quad . \end{aligned} \tag{2.28}$$

Thus, the methodology developed for dilute inhomogeneities is retained and the interactions with the surrounding inhomogeneities are accounted for by suitably modifying the stresses or strains acting on each inhomogeneity. Equation (2.28) may then be viewed as a modification of eqn. (1.12) in which the macroscopic strain or stress, $\langle \boldsymbol{\varepsilon} \rangle$ or $\langle \boldsymbol{\sigma} \rangle$, is replaced by the phase averaged matrix strain or stress, $\langle \boldsymbol{\varepsilon} \rangle^{(\mathrm{m})}$ and $\langle \boldsymbol{\sigma} \rangle^{(\mathrm{m})}$, respectively.

In a next step suitable expressions for $\langle \boldsymbol{\varepsilon} \rangle^{(\mathrm{m})}$ and/or $\langle \boldsymbol{\sigma} \rangle^{(\mathrm{m})}$ must be introduced into the scheme. This can be easily done by inserting eqn. (2.28) into eqn. (2.5), leading to the expressions

$$\begin{aligned} \langle \boldsymbol{\varepsilon} \rangle^{(\mathrm{m})} &= [(1-\xi)\mathbf{I} + \xi \bar{\mathbf{A}}^{(\mathrm{i})}_{\mathrm{dil}}]^{-1} \langle \boldsymbol{\varepsilon} \rangle \\ \langle \boldsymbol{\sigma} \rangle^{(\mathrm{m})} &= [(1-\xi)\mathbf{I} + \xi \bar{\mathbf{B}}^{(\mathrm{i})}_{\mathrm{dil}}]^{-1} \langle \boldsymbol{\sigma} \rangle \quad . \end{aligned} \tag{2.29}$$

These, in turn, allow the Mori–Tanaka strain and stress concentration tensors for matrix and inhomogeneities to be written in terms of the dilute concentration tensors as

$$\begin{aligned} \bar{\mathbf{A}}^{(\mathrm{m})}_{\mathrm{MT}} &= [(1-\xi)\mathbf{I} + \xi\bar{\mathbf{A}}^{(\mathrm{i})}_{\mathrm{dil}}]^{-1} & \bar{\mathbf{A}}^{(\mathrm{i})}_{\mathrm{MT}} &= \bar{\mathbf{A}}^{(\mathrm{i})}_{\mathrm{dil}}[(1-\xi)\mathbf{I} + \xi\bar{\mathbf{A}}^{(\mathrm{i})}_{\mathrm{dil}}]^{-1} \\ \bar{\mathbf{B}}^{(\mathrm{m})}_{\mathrm{MT}} &= [(1-\xi)\mathbf{I} + \xi\bar{\mathbf{B}}^{(\mathrm{i})}_{\mathrm{dil}}]^{-1} & \bar{\mathbf{B}}^{(\mathrm{i})}_{\mathrm{MT}} &= \bar{\mathbf{B}}^{(\mathrm{i})}_{\mathrm{dil}}[(1-\xi)\mathbf{I} + \xi\bar{\mathbf{B}}^{(\mathrm{i})}_{\mathrm{dil}}]^{-1} \end{aligned} \qquad (2.30)$$

(Benveniste, 1987). Equations (2.30) may be evaluated with any strain and stress concentration tensors $\bar{\mathbf{A}}^{(\mathrm{i})}_{\mathrm{dil}}$ and $\bar{\mathbf{B}}^{(\mathrm{i})}_{\mathrm{dil}}$ pertaining to dilute inhomogeneities embedded in a matrix. If, for example, the equivalent inclusion expressions, eqns. (2.26) and (2.27), are employed, the Mori–Tanaka matrix strain and stress concentration tensors for the non-dilute composite take the form

$$\begin{aligned} \bar{\mathbf{A}}^{(\mathrm{m})}_{\mathrm{MT}} &= \{(1-\xi)\mathbf{I} + \xi[\mathbf{I} + \mathbf{S}\mathbf{C}^{(\mathrm{m})}(\mathbf{E}^{(\mathrm{i})} - \mathbf{E}^{(\mathrm{m})})]^{-1}\}^{-1} \\ \bar{\mathbf{B}}^{(\mathrm{m})}_{\mathrm{MT}} &= \{(1-\xi)\mathbf{I} + \xi\mathbf{E}^{(\mathrm{i})}[\mathbf{I} + \mathbf{S}\mathbf{C}^{(\mathrm{m})}(\mathbf{E}^{(\mathrm{i})} - \mathbf{E}^{(\mathrm{m})})]^{-1}\mathbf{C}^{(\mathrm{m})} \end{aligned} \quad , \qquad (2.31)$$

compare Benveniste (1987), Benveniste and Dvorak (1990) or Benveniste et al. (1991). The Mori–Tanaka approximations to the effective elastic tensors are obtained by inserting eqns.(2.30) and/or (2.31) into eqns.(2.8) and (2.9).

A number of authors gave different but essentially equivalent Mori–Tanaka-type expressions for the phase concentration tensors and effective thermoelastic tensors of inhomogeneous materials, among them Pedersen (1983), Wakashima et al. (1988), Taya et al. (1991), Pedersen and Withers (1992) as well as Clyne and Withers (1993). Alternatively, the Mori–Tanaka method can be formulated to directly give the macroscopic elasticity tensor as

$$\mathbf{E}^{*}_{\mathrm{T}} = \mathbf{E}^{(\mathrm{m})}\big\{\mathbf{I} - \xi[(\mathbf{E}^{(\mathrm{i})} - \mathbf{E}^{(\mathrm{m})})\big(\mathbf{S} - \xi(\mathbf{S}-\mathbf{I})\big) + \mathbf{E}^{(\mathrm{m})}]^{-1}[\mathbf{E}^{(\mathrm{i})} - \mathbf{E}^{(\mathrm{m})}]\big\}^{-1} \qquad (2.32)$$

(Tandon and Weng, 1984). Because eqn. (2.32) does not explicitly use the compliance tensor of the inhomogeneities, $\mathbf{C}^{(\mathrm{i})}$, it can be modified in a straightforward way to describe the macroscopic stiffness of porous materials by setting $\mathbf{E}^{(\mathrm{i})} \to \mathbf{0}$, giving rise to the relationship

$$\mathbf{E}_{\mathrm{T,por}} = \mathbf{E}^{(\mathrm{m})}\big[\mathbf{I} + \frac{\xi}{1-\xi}(\mathbf{I}-\mathbf{S})^{-1}\big]^{-1} \quad . \qquad (2.33)$$

which, however, should not be used for void volume fractions that are in excess of, say, $\xi = 0.25$[19].

As is evident from their derivation, Mori–Tanaka-type theories at all volume fractions describe composites consisting of aligned ellipsoidal inhomogeneities embedded in a matrix, i.e., inhomogeneous materials with a distinct matrix–inclusion microtopology. More precisely, it was shown by Ponte Castañeda and Willis (1995) that Mori–Tanaka methods are a special case of Hashin–Shtrikman variational estimates (compare section 2.4) in which

[19]Mori–Tanaka theories are based on the assumption that the shape of the inhomogeneities can be described by ellipsoids of a given aspect ratio throughout the deformation history. In porous materials with high void volume fractions deformation at the microscale takes place mainly by bending and buckling cell walls or struts (Gibson and Ashby, 1988), which implies changes of the shapes of the voids. Such effects are not described by Mori–Tanaka models, which, consequently, tend to overestimate the effective stiffness of cellular materials by far.

the spatial arrangement of the inhomogeneities follows an aligned ellipsoidal distribution, which is characterized by the same aspect ratio as the shape of the inhomogeneities themselves, compare fig. 2.1.

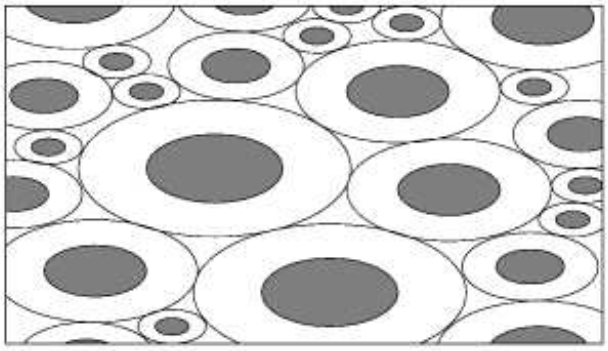

Figure 2.1: Sketch of ellipsoidal inhomogeneities in an aligned ellipsoidally distributed spatial arrangement as used implicitly in Mori–Tanaka-type approaches (a=2.0).

For two-phase composites Mori–Tanaka estimates coincide with Hashin–Shtrikman-type bounds (compare section 3.1) and, accordingly, their predictions for the overall Young's and shear moduli are always on the low side for composites reinforced by aligned or spherical reinforcements that are stiffer than the matrix (see the comparisons in section 3.4 as well as tables 5.1 to 5.3) and on the high side for materials containing compliant reinforcements in a stiffer matrix. In high contrast situations they tend to under- or overestimate the effective elastic properties by a considerable margin, compare table 5.3. For discussions of further issues with respect to the range of validity of Mori–Tanaka theories for elastic inhomogeneous two-phase materials see Christensen et al. (1992).

For multi-phase materials consisting of a matrix (m) into which $N-1$ inhomogeneity phases are embedded the Mori–Tanaka phase concentration tensors take the form

$$\begin{aligned}
\bar{\mathbf{A}}^{(\mathrm{m})}_{\mathrm{MT}} &= \Big[\xi^{(\mathrm{m})}\mathbf{I} + \sum_{(\mathrm{j})\neq(\mathrm{m})} \xi^{(\mathrm{j})}\bar{\mathbf{A}}^{(\mathrm{j})}_{\mathrm{dil}}\Big]^{-1} \qquad & \bar{\mathbf{A}}^{(\mathrm{i})}_{\mathrm{MT}} &= \bar{\mathbf{A}}^{(\mathrm{i})}_{\mathrm{dil}}\Big[\xi^{(\mathrm{m})}\mathbf{I} + \sum_{(\mathrm{j})\neq(\mathrm{m})} \xi^{(\mathrm{j})}\bar{\mathbf{A}}^{(\mathrm{j})}_{\mathrm{dil}}\Big]^{-1} \\
\bar{\mathbf{B}}^{(\mathrm{m})}_{\mathrm{MT}} &= \Big[\xi^{(\mathrm{m})}\mathbf{I} + \sum_{(\mathrm{j})\neq(\mathrm{m})} \xi^{(\mathrm{j})}\bar{\mathbf{B}}^{(\mathrm{j})}_{\mathrm{dil}}\Big]^{-1} \qquad & \bar{\mathbf{B}}^{(\mathrm{i})}_{\mathrm{MT}} &= \bar{\mathbf{A}}^{(\mathrm{i})}_{\mathrm{dil}}\Big[\xi^{(\mathrm{m})}\mathbf{I} + \sum_{(\mathrm{j})\neq(\mathrm{m})} \xi^{(\mathrm{j})}\bar{\mathbf{B}}^{(\mathrm{j})}_{\mathrm{dil}}\Big]^{-1}
\end{aligned} \tag{2.34}$$

and the macroscopic elastic tensors are obtained as

$$\begin{aligned}
\mathbf{E}^{*}_{\mathrm{MT}} &= \Big[\xi^{(\mathrm{m})}\mathbf{E}^{(\mathrm{m})} + \sum_{(\mathrm{i})\neq(\mathrm{m})} \xi^{(\mathrm{i})}\mathbf{E}^{(\mathrm{i})}\bar{\mathbf{A}}^{(\mathrm{i})}_{\mathrm{dil}}\Big]\Big[\xi^{(\mathrm{m})}\mathbf{I} + \sum_{(\mathrm{i})\neq(\mathrm{m})} \xi^{(\mathrm{i})}\bar{\mathbf{A}}^{(\mathrm{i})}_{\mathrm{dil}}\Big]^{-1} \\
\mathbf{C}^{*}_{\mathrm{MT}} &= \Big[\xi^{(\mathrm{m})}\mathbf{C}^{(\mathrm{m})} + \sum_{(\mathrm{i})\neq(\mathrm{m})} \xi^{(\mathrm{i})}\mathbf{C}^{(\mathrm{i})}\bar{\mathbf{B}}^{(\mathrm{i})}_{\mathrm{dil}}\Big]\Big[\xi^{(\mathrm{m})}\mathbf{I} + \sum_{(\mathrm{i})\neq(\mathrm{m})} \xi^{(\mathrm{i})}\bar{\mathbf{B}}^{(\mathrm{i})}_{\mathrm{dil}}\Big]^{-1} \quad .
\end{aligned} \tag{2.35}$$

These expressions are rigorous bounds only if the matrix is the most compliant or the stiffest constituent.

Mori–Tanaka-type theories can be implemented into computer programs in a straightforward way. Because they are explicit algorithms, all that is required are matrix additions, multiplications, and inversions plus expressions for the Eshelby tensor. Despite their limitations, Mori–Tanaka approaches provide useful accuracy for the elastic contrasts pertaining to most practically relevant composites. This combination of features makes them important tools for evaluating the stiffness and thermal expansion properties of inhomogeneous materials that show a matrix–inclusion topology with aligned inhomogeneities or voids. Mori–Tanaka-type approaches for thermoelastoplastic materials are discussed in section 2.4 and "extended" Mori–Tanaka approaches for nonaligned reinforcements in section 2.7.

Classical Self-Consistent Estimates

Another group of estimates for the overall thermomechanical behavior of inhomogeneous materials are effective medium theories, in which an inhomogeneity or some phase arrangement, the kernel, is embedded in the effective material (the properties of which are not known a priori). Figure 2.2 shows a schematic comparison of the material and loading configurations underlying Eshelby models, effective field (Mori–Tanaka) methods and two effective medium approaches, the classical self-consistent and generalized self-consistent (compare section 2.4) schemes[20].

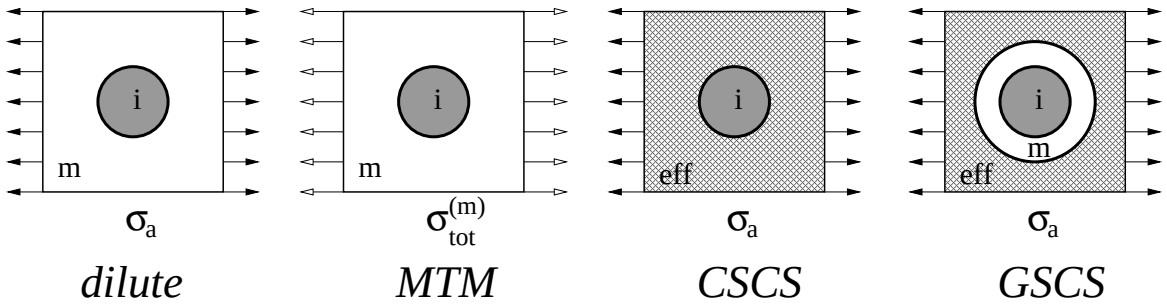

Figure 2.2: Schematic comparison of the Eshelby method for dilute composites, Mori–Tanaka approaches and classical as well as generalized self-consistent schemes.

If the kernel consists of a dilute inhomogeneity, classical (or two-phase) self-consistent schemes are obtained (CSCS), see, e.g., Hill (1965b). They are based on rewriting eqn. (2.26) and (2.27) for an inhomogeneity that is surrounded by the effective medium instead of the matrix, i.e., $\mathbf{E}^{(\mathrm{m})} \rightarrow \mathbf{E}^*$ and $\mathbf{C}^{(\mathrm{m})} \rightarrow \mathbf{C}^*$, so that $\bar{\mathbf{A}}^{(\mathrm{i})}_{\mathrm{dil}} \rightarrow \bar{\mathbf{A}}^{(\mathrm{i})}_{\mathrm{dil}}(\mathbf{E}^*, \mathbf{C}^*)$ and $\bar{\mathbf{B}}^{(\mathrm{i})}_{\mathrm{dil}} \rightarrow \bar{\mathbf{B}}^{(\mathrm{i})}_{\mathrm{dil}}(\mathbf{E}^*, \mathbf{C}^*)$. The results of the above formal procedure can be inserted into eqn. (2.8), giving rise to the relationships

$$\begin{aligned}
\mathbf{E}^*_{\mathrm{SCS}} &= \mathbf{E}^{(\mathrm{m})} + \xi[\mathbf{E}^{(\mathrm{i})} - \mathbf{E}^{(\mathrm{m})}]\, \bar{\mathbf{A}}^{(\mathrm{i})}_{\mathrm{dil}}(\mathbf{E}^*, \mathbf{C}^*) \\
&= \mathbf{E}^{(\mathrm{m})} + \xi[\mathbf{E}^{(\mathrm{i})} - \mathbf{E}^{(\mathrm{m})}]\, [\mathbf{I} + \mathbf{SC}(\mathbf{E}^{(\mathrm{i})} - \mathbf{E}^*_{\mathrm{SCS}})]^{-1} \\
\mathbf{C}^*_{\mathrm{SCS}} &= \mathbf{C}^{(\mathrm{m})} + \xi[\mathbf{C}^{(\mathrm{i})} - \mathbf{C}^{(\mathrm{m})}]\, \bar{\mathbf{B}}^{(\mathrm{i})}_{\mathrm{dil}}(\mathbf{E}^*, \mathbf{C}^*) \\
&= \mathbf{C}^{(\mathrm{m})} + \xi[\mathbf{C}^{(\mathrm{i})} - \mathbf{C}^{(\mathrm{m})}]\, [\mathbf{I} + \mathbf{E}^*(\mathbf{I} - \mathbf{S})(\mathbf{C}^{(\mathrm{i})} - \mathbf{C}^*_{\mathrm{SCS}})]^{-1} \quad , \qquad (2.36)
\end{aligned}$$

[20]Within the classification of micromechanical methods given in section 1.5, self-consistent mean field methods can also be viewed as as analytical embedding approaches.

where $\mathbf{S}$ has to be evaluated with respect to the effective material. Equations (2.36) can be interpreted as an implicit nonlinear system of equations for the unknown elastic tensors $\mathbf{E}^* = \mathbf{E}^*_{\mathrm{SCS}}$ and $\mathbf{C}^* = \mathbf{C}^*_{\mathrm{SCS}}$, which describe the behavior of the effective medium. This system can be solved by self-consistent iterative schemes of the type

$$\begin{aligned} \mathbf{E}_{n+1} &= \mathbf{E}^{(\mathrm{m})} + \xi[\mathbf{E}^{(\mathrm{i})} - \mathbf{E}^{(\mathrm{m})}][\mathbf{I} + \mathbf{S}_n\mathbf{C}_n(\mathbf{E}^{(\mathrm{i})} - \mathbf{E}_n)]^{-1} \\ \mathbf{C}_{n+1} &= \left[\mathbf{E}_{n+1}\right]^{-1} \quad . \end{aligned} \tag{2.37}$$

The Eshelby tensor $\mathbf{S}_n$ in eqn. (2.37) describes the response of an inhomogeneity embedded in the n-th iteration of the effective medium; it must be recomputed for each iteration[21].

For multi-phase composites the classical self-consistent estimate for the effective elasticity tensor takes the form

$$\begin{aligned} \mathbf{E}^*_{\mathrm{SC},n} &= \sum_{(\mathrm{p})} \mathbf{E}^{(\mathrm{p})}\left\{\mathbf{I} + \mathbf{S}^{(\mathrm{p})}_{n-1}\mathbf{C}_{\mathrm{SC},n-1}[\mathbf{E}^{(\mathrm{p})} - \mathbf{E}_{\mathrm{SC},n-1}]\right\}^{-1} \\ \mathbf{C}^*_{\mathrm{SC},n} &= (\mathbf{E}^*_{\mathrm{SC},n})^{-1} \quad , \end{aligned} \tag{2.38}$$

where $\mathbf{S}^{(\mathrm{p})}_{n-1}$ pertains to an ellipsoidal inhomogeneity with the shape of phase (p).

The predictions of the CSCS differ noticeably from those of Mori–Tanaka methods in being close to the Hashin–Shtrikman lower bounds (see section 4) for low reinforcement volume fractions, but close to the upper bounds for reinforcement volume fractions approaching unity (compare figs. 3.1 to 3.7). Generally, two-phase self-consistent schemes are best suited to describing the overall properties of two-phase materials that do not show a matrix–inclusion microtopology at some or all of the volume fractions of interest[22]. Essentially, the microstructures described by two-phase CSCS are characterized by interpenetrating phases around $\xi = 0.5$, with one of the materials acting as the matrix for $\xi \to 0$ and the other for $\xi \to 1$. Consequently, the CSCS is typically not the best choice for describing composites showing a matrix–inclusion topology, but is well suited to studying Functionally Graded Materials (FGMs) in which the volume fraction of a constituent can vary from 0 to 1 through the thickness of a sample. Multi-phase versions of the CSCS, such as eqn.(2.38) are important methods for modeling polycrystals. When microgeometries described by the CSCS show a geometrical anisotropy, this anisotropy determines the shapes or aspect ratios of the "inhomogeneity" used in the model.

For porous materials classical self-consistent schemes predict a breakdown of the stiffness due to the percolation of the pores at $\xi = \frac{1}{2}$ for spherical voids and at $\xi = \frac{1}{3}$ for aligned cylindrical voids (Torquato, 2002).

Because self-consistent schemes are by definition implicit methods, their computational requirements are in general higher than those of Mori–Tanaka-type approaches. Like ef-

[21] For aligned spheroidal but non-spherical inhomogeneities the effective medium shows transversely isotropic behavior, so that an appropriate evaluation procedure for evaluating the Eshelby tensor must be used.

[22] Classical self-consistent schemes can be shown to correspond to perfectly disordered materials (Kröner, 1978) or self-similar hierarchical materials (Torquato, 2002). Note that in contrast to eqn. (2.11), in the CSCS expression, eqn. (2.38), all phases are treated on an equal footing.

fective field models, they can form the basis for describing the behavior of nonlinear inhomogeneous materials.

Differential Schemes

A further important group of mean field approaches are differential schemes (McLaughlin, 1977; Norris, 1985), which may be envisaged as involving repeated cycles of adding small concentrations of inhomogeneities to a material and then homogenizing. Following Hashin (1988) the overall elastic tensors can accordingly be described by the differential equations

$$\begin{aligned} \frac{\mathrm{d}\mathbf{E}^*_{\mathrm{D}}}{\mathrm{d}\xi} &= \frac{1}{1-\xi}\,[\mathbf{E}^{(\mathrm{i})} - \mathbf{E}^*_{\mathrm{D}}]\bar{\mathbf{A}}_{\mathrm{dil}}(\mathbf{E}^*_{\mathrm{D}}) \\ \frac{\mathrm{d}\mathbf{C}^*_{\mathrm{D}}}{\mathrm{d}\xi} &= \frac{1}{1-\xi}\,[\mathbf{C}^{(\mathrm{i})} - \mathbf{C}^*_{\mathrm{D}}]\bar{\mathbf{B}}_{\mathrm{dil}}(\mathbf{E}^*_{\mathrm{D}}) \end{aligned} \tag{2.39}$$

with the initial conditions $\mathbf{E}^*_{\mathrm{D}}{=}\mathbf{E}^{(\mathrm{m})}$ and $\mathbf{C}^*_{\mathrm{D}}{=}\mathbf{C}^{(\mathrm{m})}$, respectively, at $\xi{=}0$. In analogy to eqn. (2.36) $\bar{\mathbf{A}}_{\mathrm{dil}}$ and $\bar{\mathbf{B}}_{\mathrm{dil}}$ depend on $\mathbf{E}^*_{\mathrm{D}}$ and $\mathbf{C}^*_{\mathrm{D}}$, respectively. Equations (2.39) can be integrated with standard numerical algorithms for initial value problems, e.g., Runge–Kutta schemes.

Differential schemes can be related to matrix–inclusion microgeometries with polydisperse distributions of the sizes of the inhomogeneities (corresponding to the repeated homogenization steps) [23]. Because of their association with specific microgeometries that are not typical of "classical composites" (in which reinforcement size distributions usually are not very wide[24]) and due to their higher mathematical complexity (as compared, e.g., to Mori–Tanaka models) Differential Schemes have seen limited use in studying the mechanical behavior of composite materials.

2.4 Hashin–Shtrikman Estimates

The stress field in an inhomogeneous material can be expressed in terms of a homogeneous comparison (or reference) medium having an elasticity tensor $\mathbf{E}^0$ as

$$\boldsymbol{\sigma}(\mathbf{x}) = \mathbf{E}(\mathbf{x})\,\boldsymbol{\varepsilon}(\mathbf{x}) = \mathbf{E}^0\,\boldsymbol{\varepsilon}(\mathbf{x}) + \boldsymbol{\tau}^0(\mathbf{x}) \qquad . \tag{2.40}$$

where $\boldsymbol{\tau}^0(\mathbf{x}) = (\mathbf{E}(\mathbf{x}) - \mathbf{E}^0)\,\boldsymbol{\varepsilon}(\mathbf{x})$ is known as the polarization tensor. Phase averaging of $\boldsymbol{\tau}^0(\mathbf{x})$ over phase (p) leads to the phase averaged polarization tensor

$$\langle\boldsymbol{\tau}^0\rangle^{(\mathrm{p})} = [\mathbf{E}^{(\mathrm{p})} - \mathbf{E}^0]\langle\boldsymbol{\varepsilon}\rangle^{(\mathrm{p})} = \langle\boldsymbol{\sigma}\rangle^{(\mathrm{p})} - \mathbf{E}^0\langle\boldsymbol{\varepsilon}\rangle^{(\mathrm{p})} \qquad , \tag{2.41}$$

[23] The interpretation of differential schemes of involving the repeated addition of infinitesimal volume fractions of inhomogeneities of increasingly larger size, followed each time by homogenization, is due to Roscoe (1973). It was pointed out, however, by Hashin (1988) that the requirements of infinitesimal volume fraction and growing size of the inhomogeneities may lead to contradictions.

[24] However, with the exception of the CSCS for two-dimensional conduction (Torquato and Hyun, 2001), none of the mean field methods discussed in section 2.3 corresponds to a realization in the form of a monodisperse matrix–inclusion microgeometry.

which can be directly used in a mean field framework.

Equation (2.41) can be used as the starting point for deriving general mean field strain concentration tensors in dependence on the elasticity tensor of a reference materials. Following Bornert (2001) these concentration tensors take the form

$$\begin{aligned} \bar{\mathbf{A}}_{\mathrm{HS}}^{(\mathrm{m})} &= [\mathbf{L}^0 + \mathbf{E}^{(\mathrm{m})}]^{-1}\big[\xi(\mathbf{L}^0 + \mathbf{E}^{(\mathrm{i})})^{-1} + (1-\xi)(\mathbf{L}^0 + \mathbf{E}^{(\mathrm{m})})^{-1}\big]^{-1} \\ \bar{\mathbf{A}}_{\mathrm{HS}}^{(\mathrm{i})} &= [\mathbf{L}^0 + \mathbf{E}^{(\mathrm{i})}]^{-1}\big[\xi(\mathbf{L}^0 + \mathbf{E}^{(\mathrm{i})})^{-1} + (1-\xi)(\mathbf{L}^0 + \mathbf{E}^{(\mathrm{m})})^{-1}\big]^{-1} \quad , \end{aligned} \tag{2.42}$$

where the tensor $\mathbf{L}^0$, which is known as the overall constraint tensor (Hill, 1965b) or Hill's influence tensor, is defined as

$$\mathbf{L}^0 = \mathbf{E}^0[(\mathbf{S}^0)^{-1} - \mathbf{I}] \quad . \tag{2.43}$$

The Eshelby tensor $\mathbf{S}^0$ has to be evaluated with respect to the comparison material. Equations (2.42) lead to estimates for the overall elastic stiffness of two-phase materials in the form

$$\mathbf{E}_{\mathrm{HS}}^{*} = \mathbf{E}^{(\mathrm{m})} + \xi(\mathbf{E}^{(\mathrm{i})} - \mathbf{E}^{(\mathrm{m})})\big[\mathbf{I} + (1-\xi)(\mathbf{L}^0 + \mathbf{E}^{(\mathrm{m})})^{-1}(\mathbf{E}^{(\mathrm{i})} - \mathbf{E}^{(\mathrm{m})})\big]^{-1} \quad , \tag{2.44}$$

which are referred to as Hashin–Shtrikman elastic tensors (Bornert, 2001).

Standard mean field models can be obtained as special cases of Hashin–Shtrikman methods by appropriate choices of the comparison material. For example, using the matrix as the comparison material results in Mori–Tanaka methods, whereas the selection of the effective material as comparison material leads to classical self-consistent schemes.

Generalized Self-Consistent Estimates

The above Hashin–Shtrikman formalism can be extended in a number of ways, one of which consists in not only studying inhomogeneities but also more complex geometrical entities, called patterns or motifs, embedded in a matrix, see Bornert (1996) and Bornert (2001). Typically the stress and strain fields in such patterns are inhomogeneous even in the dilute case and numerical methods must be used for evaluating the corresponding overall constraint tensors. The simplest example of such a pattern consists of a spherical particle or cylindrical fiber surrounded by a constant-thickness layer of matrix at an appropriate volume fraction, which, when embedded in the effective material, allows to recover the three-phase or generalized self-consistent scheme (GSCS) of Christensen and Lo (1979), compare fig. 2.2 and see also (Christensen and Lo, 1986). GSCS expressions for the overall elastic moduli can also be obtained by considering the differential equations describing the elastic response of such three-phase regions under appropriate boundary and loading conditions. The GSCS in its original version is limited to inhomogeneities of spherical or cylindrical shape, where it is closely related but not identical to microgeometries of the CSA and CCA types (Christensen, 1998), respectively. It gives rise to third-order equations for the shear modulus G and the transverse shear modulus G_{T}, and its results for the bulk and transverse bulk moduli coincide with those obtained from the CSA and CCA, respectively. Extensions of the GSCS to multi-layered spherical inhomogeneities (Hervé and Zaoui, 1993) and to aligned ellipsoidal inhomogeneities (Huang and Hu, 1995) were

also reported in the literature.

Generalized self-consistent schemes give excellent results for inhomogeneous materials with matrix–inclusion topologies and are accordingly highly suited for obtaining estimates for the thermoelastic moduli of composite materials reinforced by spherical or equiaxed particles or aligned continuous fibers. They are, however, not mean-field schemes in the sense of section 2.3.

2.5 Other Analytical Estimates for Elastic Composites with Aligned Reinforcements

Interpolative schemes can be constructed that generate estimates between mean-field models describing, on the one hand, some composite and, on the other hand, a material in which the roles of matrix and reinforcements are interchanged (referred to, e.g., as Mori–Tanaka and Inverse Mori–Tanaka schemes), see, e.g., Lielens et al. (1997). Such approaches, while being capable of providing useful estimates for given composites, have the drawback of typically not being associated with realizable microgeometries.

Ponte Castañeda and Willis (1995) proposed a refined mean field scheme for inhomogeneous materials that consist of ellipsoidal arrangements of ellipsoidal inhomogeneities embedded in a matrix. In such systems the spatial correlations of the inhomogeneity arrangement can be described by an Eshelby tensor $\mathbf{S}_\mathrm{d}$, whereas the shapes of the inhomogeneities are introduced via the Eshelby tensor $\mathbf{S}_\mathrm{i}$. The corresponding phase arrangements can be visualized by extending fig. 2.1 to non-overlapping "safety ellipsoids" that contain aligned or non-aligned ellipsoidal inhomogeneities, the aspect ratios of the safety ellipsoids and the inhomogeneities being different. The inclusion strain concentration tensors of such microgeometries can be expressed as

$$\begin{aligned} \bar{\mathbf{A}}^{(\mathfrak{i})}_{\mathrm{PW}} &= \big[\mathbf{I} + (\mathbf{S}_\mathrm{i} - \xi\mathbf{S}_\mathrm{d})\mathbf{C}^{(\mathfrak{m})}(\mathbf{E}^{(\mathfrak{i})} - \mathbf{E}^{(\mathfrak{m})})\big]^{-1} \\ &= \big[(\mathbf{E}^{(\mathfrak{i})} - \mathbf{E}^{(\mathfrak{m})})^{-1} - \xi\bar{\mathbf{A}}^{(\mathfrak{i})}_{\mathrm{dil}}\,\mathbf{S}_\mathrm{d}\mathbf{C}^{(\mathfrak{m})}\big]^{-1} \quad , \end{aligned} \tag{2.45}$$

from which the macroscopic elasticity tensor follows as

$$\begin{aligned} \mathbf{E}^{*}_{\mathrm{PW}} &= \mathbf{E}^{(\mathfrak{m})} + \xi[\mathbf{E}^{(\mathfrak{i})} - \mathbf{E}^{(\mathfrak{m})}]\big[\mathbf{I} + (\mathbf{S}_\mathrm{i} - \xi\mathbf{S}_\mathrm{d})\mathbf{C}^{(\mathfrak{m})}(\mathbf{E}^{(\mathfrak{i})} - \mathbf{E}^{(\mathfrak{m})})\big]^{-1} \\ &= \mathbf{E}^{(\mathfrak{m})} + \xi\big[(\mathbf{E}^{(\mathfrak{i})} - \mathbf{E}^{(\mathfrak{m})})^{-1} - \xi\bar{\mathbf{A}}^{(\mathfrak{i})}_{\mathrm{dil}}\,\mathbf{S}_\mathrm{d}\mathbf{C}^{(\mathfrak{m})}\big]^{-1}\bar{\mathbf{A}}^{(\mathfrak{i})}_{\mathrm{dil}} \end{aligned} \tag{2.46}$$

via eqn.(2.8). This model is known as the Hashin–Shtrikman estimates of Ponte Castañeda and Willis (1995) and it is strictly valid as long as the inhomogeneities do not penetrate their respective safety ellipsoids. When both the inhomogeneities and the safety ellipsoids are aligned and $\mathbf{S}_\mathrm{i} = \mathbf{S}_\mathrm{d}$, eqn. (2.46) becomes equivalent to the corresponding Mori–Tanaka expression, which shows that Mori–Tanaka methods are a special case of the Hashin–Shtrikman estimates. For a discussion of the latters' relationship to other micromechanical schemes see Hu and Weng (2000). For multi-phase composites the Ponte–Willis estimates for the elasticity tensor take the form

$$\mathbf{E}^{*}_{\mathrm{PW}} = \mathbf{E}^{(\mathfrak{m})} + \sum_{(\mathfrak{i})\neq(\mathfrak{m})} \xi^{(\mathfrak{i})}\Big[\mathbf{I} - \sum_{(\mathfrak{j})\neq(\mathfrak{m})} \xi^{(\mathfrak{j})}(\mathbf{E}^{(\mathfrak{j})} - \mathbf{E}^{(\mathfrak{m})})\bar{\mathbf{A}}^{(\mathfrak{j})}_{\mathrm{dil}}\,\mathbf{S}^{(\mathfrak{i})}_\mathrm{d}\mathbf{C}^{(\mathfrak{m})}\Big]^{-1}(\mathbf{E}^{(\mathfrak{j})} - \mathbf{E}^{(\mathfrak{m})})\bar{\mathbf{A}}^{(\mathfrak{i})}_{\mathrm{dil}} \tag{2.47}$$

and the strain concentration tensor for inhomogeneity (i) is

$$\bar{\mathbf{A}}^{(i)}_{\mathrm{PW}} = \bar{\mathbf{A}}^{(i)}_{\mathrm{dil}}\big[\mathbf{I} - \sum_{(j)\neq(m)} \xi^{(j)}\mathbf{S}^{(i)}_{\mathrm{d}}\mathbf{C}^{(m)}(\mathbf{E}^{(j)} - \mathbf{E}^{(m)})\bar{\mathbf{A}}^{(j)}_{\mathrm{dil}}\big] \quad . \tag{2.48}$$

Here $\mathbf{S}^{(i)}_{\mathrm{d}}$ describes the "safety ellipsoids" pertaining to phase (i). Analogous results can be obtained with the Interaction Direct Derivative (IDD) approach of Du and Zheng (2002).

An important group of analytical models for the macroscopic elastic response of inhomogeneous materials are estimates based on n-point statistics, which are not mean field approaches in the sense of most other methods discussed in chapter 2. Three-point estimates for the thermoelastic properties of two-phase materials were developed by Torquato (1998) and use the same pair of three-point microstructural parameters, η and ζ, employed by the three-point bounds discussed in section 3.2. These estimates lie between the corresponding bounds and give excellent analytical predictions for the overall thermoelastic response of inhomogeneous materials that show the appropriate microgeometries and are free of flaws. For discussion of further estimates for the overall elastic properties of inhomogeneous materials see, e.g., Torquato (2002).

2.6 Mean Field Methods for Inelastic Composites

Over the past two decades considerable efforts have been directed at modeling the mechanical behavior of inhomogeneous materials in which one or more constituents show viscoelastic, elastoplastic or viscoelastoplastic responses. The main motivation of such studies has been need to describe the time dependent behavior of polymer matrix composites and the responses of composites with metallic phases. Mean field methods have been developed for and successfully adapted to studying many aspects of such problems.

If the behavior of an inhomogeneous material is not only inelastic, but also nonlinear, suitable linearization schemes are required, which reduce the nonlinear problem to a sequence of linear ones. In continuum micromechanics, the most important approaches of this type this are secant (Tandon and Weng, 1988) and incremental (Hill, 1965a) methods. In addition, tangent concepts (Molinari et al., 1987) and, recently, affine formulations (Masson et al., 2000; Brenner et al., 2001) have been reported.

Viscoelastic Composites

Viscoelastic materials show hereditary behavior, i.e., their response at a given time depends on their previous load history. Important issues in the mechanical behavior of viscoelastic composites are, on the one hand, quasi-static responses such as relaxation and creep, which can be described via relaxation relaxation function and creep compliance tensors. The dynamic behavior under periodic excitations, on the other hand, can be studied via complex modulus tensors.

Correspondence principles are available (Hashin, 1965, 1970) that directly relate the analysis of linear viscoelastic composites to that of elastic composites of identical phase ge-

ometry of both of the above sets of problems, see also Schapery (1974) and Hashin (1983). For the quasi-static case the correspondence principle requires formulating the quasi-static viscoelastic problem in the Carson–Laplace transformed domain, where expressions for the transformed relaxation function and creep compliance tensors are equivalent to estimates for the elasticity and compliance tensors, respectively, in elastic micromechanics. On this basis replacement schemes can be defined (Hashin, 1972) that allow to obtain Laplace transformed macroscopic moduli, modulus tensors and phase averaged microfields of viscoelastic materials from mean field results such as the ones discussed in sections 2.3 to 2.5. The back transformation from the Carson–Laplace to the time domain, however, typically is not straightforward and does not provide closed form solutions in most cases, approximations having to be introduced or numerical methods to be used, compare Schapery (1962) and Lévesque et al. (2007). The correspondence principle for periodic excitations uses transforms to Fourier space and the resulting replacement scheme (Hashin, 1972) directly generates effective complex modulus tensors from the effective elastic tensors obtained for a given microgeometry[25].

For in-depth discussions of and alternative concepts for mean field models of linear and nonlinear viscoelastic composites see, e.g., Paquin et al. (1999), Brenner and Masson (2005), Lévesque et al. (2007), as well as Lahellec and Suquet (2007).

(Thermo)Elastoplastic Composites

The following discussion is restricted to mean field models based on continuum plasticity[26]. Nearly all work reported on such models for elastoplastic or viscoelastoplastic inhomogeneous materials has relied on secant, incremental, tangent or affine linearization strategies. A fairly recent overview of mean field methods for elastoplastic composites was given by Ponte Castañeda and Suquet (1998).

The main difficulties in applying mean field methods to composites with elastoplastic constituents lie in the path dependence of plastic behavior and in the typically strong intraphase fluctuations of the microstress and microstrain fields in elastoplastic inhomogeneous materials. Accordingly, each material point in an elastoplastic phase tends to follow a different trajectory in stress space, so that even a two-phase elastoplastic composite effectively behaves as a multi-phase material and phase averages over matrix and reinforcements are less useful descriptors than in the linear elastic case. As a consequence, in mean field models of elastoplastic composites choices have to be made with respect to the linearization procedure, the linear homogenization model, and the phase-wise equivalent stresses and equivalent strains to be used in evaluating the elastoplastic constituent material behavior (Zaoui, 2001).

[25]The correspondence principles can be applied, on the one hand, to analytical expressions, such as the CSA and CCA models (Hashin, 1972), and on the other hand, to numerical results obtained with the Discrete Microfield Approaches discussed in chapters 5 to 7, see, e.g., Brinson and Lin (1998) or Yi et al. (1998).

[26]In a separate line of development, phase averaged stress fields obtained by Eshelby-based methods have been used in dislocation-based descriptions of elastoplastic matrix behavior, see, e.g., Taya and Mori (1987).

Secant Methods for Elastoplastic Composites

Secant plasticity concepts in continuum micromechanics, see, e.g., Tandon and Weng (1988) or Dunn and Ledbetter (1997), are based on the deformation theory of plasticity, in which elastoplastic behavior is approximated by nonlinear elastic models.

In the simplest case of an isotropic elastoplastic phase that is described by J_2 plasticity, the secant "elastic" and "compliance" tensors, $\mathbf{E}^{(\mathfrak{p})}_{\mathrm{sec}}$ and $\mathbf{C}^{(\mathfrak{p})}_{\mathrm{sec}}$, take the form

$$\mathbf{E}^{(\mathfrak{p})}_{\mathrm{sec}} = 3K^{(\mathfrak{p})}\mathbf{Q}^{\mathrm{E}}_{\mathrm{vol}} + 2G^{(\mathfrak{p})}_{\mathrm{sec}}\mathbf{Q}^{\mathrm{E}}_{\mathrm{dev}} \qquad \text{and} \qquad \mathbf{C}^{(\mathfrak{p})}_{\mathrm{sec}} = \frac{1}{3K^{(\mathfrak{p})}}\mathbf{Q}^{\mathrm{C}}_{\mathrm{vol}} + \frac{1}{2G^{(\mathfrak{p})}_{\mathrm{sec}}}\mathbf{Q}^{\mathrm{C}}_{\mathrm{dev}} \qquad , \tag{2.49}$$

respectively. Here $\mathbf{Q}^{\mathrm{E}}$ and $\mathbf{Q}^{\mathrm{C}}$ are the volumetric and deviatoric "partitioning tensors" for elasticities and compliances[27], respectively. The secant shear modulus $G^{(\mathfrak{p})}_{\mathrm{sec}}$ is equal to the elastic shear modulus of the matrix, $G^{(\mathfrak{p})}$, in the elastic range. In the post-yield regime it can be obtained from the current phase averages of the equivalent stress $\langle\sigma_{\mathrm{eqv}}\rangle^{(\mathfrak{p})}$ and the equivalent plastic strain $\langle\varepsilon_{\mathrm{eqv,pl}}\rangle^{(\mathfrak{p})}$ as

$$G^{(\mathfrak{p})}_{\mathrm{sec}} = \frac{G^{(\mathfrak{p})}\,\langle\sigma_{\mathrm{eqv}}\rangle^{(\mathfrak{p})}}{\langle\sigma_{\mathrm{eqv}}\rangle^{(\mathfrak{p})} + 3G^{(\mathfrak{p})}\langle\varepsilon_{\mathrm{eqv,pl}}\rangle^{(\mathfrak{p})}} \tag{2.50}$$

on the basis of an additive strain decomposition, compare eqn. (2.1). $\varepsilon_{\mathrm{eqv,pl}}$ must be evaluated from σ_{eqv} via an appropriate hardening law.

Expressions for the macroscopic secant tensors $\mathbf{E}^{*}_{\mathrm{sec}}$ and $\mathbf{C}^{*}_{\mathrm{sec}}$ can be obtained from the phase secant tensors, eqn. (2.49), by mean field relationships equivalent to eqns. (2.8) and (2.9). For the case of elastic inhomogeneities embedded in an elastoplastic matrix these take the form

$$\begin{aligned} \mathbf{E}^{*}_{\mathrm{sec}} &= \mathbf{E}^{(\mathfrak{m})}_{\mathrm{sec}} + \xi(\mathbf{E}^{(\mathfrak{i})} - \mathbf{E}^{(\mathfrak{m})}_{\mathrm{sec}})\bar{\mathbf{A}}^{(\mathfrak{m})}_{\mathrm{sec}} \\ \mathbf{C}^{*}_{\mathrm{sec}} &= \mathbf{C}^{(\mathfrak{m})}_{\mathrm{sec}} + \xi(\mathbf{C}^{(\mathfrak{i})} - \mathbf{C}^{(\mathfrak{m})}_{\mathrm{sec}})\bar{\mathbf{B}}^{(\mathfrak{m})}_{\mathrm{sec}} \qquad . \end{aligned} \tag{2.51}$$

The non-dilute secant strain and stress concentration tensors, $\bar{\mathbf{A}}^{(\mathfrak{m})}_{\mathrm{sec}}$ and $\bar{\mathbf{B}}^{(\mathfrak{m})}_{\mathrm{sec}}$, can be generated from dilute secant concentration tensors, $\bar{\mathbf{A}}^{(\mathfrak{m})}_{\mathrm{dil,sec}}$ and $\bar{\mathbf{B}}^{(\mathfrak{m})}_{\mathrm{dil,sec}}$, via a suitable mean field theory, e.g., a Mori–Tanaka method or a self-consistent scheme, compare section 2.3. The dilute secant concentration tensors and the Eshelby tensors contained in them, in turn, must be evaluated using the current secant tensors of the constituents. Iterative procedures are required for obtaining solutions corresponding to prescribed macroscopic strain or stress states.

In first order methods, the phase average of the equivalent stress required in eqn. (2.50) is approximated from the phase averaged stress tensor,

$$\langle\sigma_{\mathrm{eqv}}\rangle^{(\mathfrak{p})} \approx \left[\frac{3}{2}\,\langle\boldsymbol{\sigma}\rangle^{T}_{\mathrm{dev}}\langle\boldsymbol{\sigma}\rangle_{\mathrm{dev}}\right]^{\frac{1}{2}} \qquad , \tag{2.52}$$

[27] In index notation the $\mathbf{Q}^{\mathrm{E}}$ and $\mathbf{Q}^{\mathrm{C}}$ are equal to each other and to the volumetric and deviatoric projection tensors $\mathbf{Q}$ defined in eqn. (2.2). The use of shear angles in the present engineering notation, however, leads to differences in the shear terms of $\mathbf{Q}^{\mathrm{E}}_{\mathrm{dev}}$, $\mathbf{Q}^{\mathrm{C}}_{\mathrm{dev}}$ and $\mathbf{Q}_{\mathrm{dev}}$.

which neglects contributions from the local stress fluctuations and, accordingly, tends to underestimate $\langle\sigma_{\mathrm{eqv}}\rangle^{(\mathrm{p})}$, leading to underestimates of the macroscopic effective stress[28]. Improved results can be obtained by second order approximations that obtain the phase averaged equivalent stress in terms of the second order moments of stress, $\left\langle \boldsymbol{\sigma}\otimes\boldsymbol{\sigma}\right\rangle^{(\mathrm{p})}$, (Suquet, 1995; Buryachenko, 1996; Hu, 1997; Ju and Sun, 2001) or on the basis of energy considerations (Qiu and Weng, 1992).

Alternatively, secant theories for composites with nonlinear constituents can be obtained from variational principles (Ponte Castañeda, 1991) or they can be formulated in terms of potentials (Bornert and Suquet, 2001), which allows for a concise mathematical presentation. Because secant models treat elastoplastic composites as nonlinearly elastic materials they are limited to strictly monotonic loading and to radial (or approximately radial) trajectories of the phase averaged stresses of the constituents in stress space[29], which precludes their use as micromechanically based constitutive models or as lower scale models in multi-scale analysis.

"Modified secant models" (Ponte Castañeda and Suquet, 1998) that use second order approximations for $\langle\sigma_{\mathrm{eqv}}\rangle^{(\mathrm{p})}$, however, have been found to be highly suitable for materials characterization of elastoplastic composites, where they have shown excellent agreement with predictions from multi-particle unit cell models (Segurado et al., 2002a) and experiments. Modified secant models have also proved quite flexible. For example, method of this type was adapted to incorporate a nonlocal plasticity model for the matrix (Hu et al., 2005) in order to study particle size effects on the macroscopic yield behavior of particle reinforced MMCs.

Incremental Methods for Elastoplastic Composites

Incremental mean field methods can be formulated on the basis of strain and stress rate tensors for elastoplastic phases $^{(\mathrm{p})}$, $\mathrm{d}\langle\boldsymbol{\varepsilon}\rangle^{(\mathrm{p})}$ and $\mathrm{d}\langle\boldsymbol{\sigma}\rangle^{(\mathrm{p})}$, which can be expressed in analogy to eqn. (2.6) as

$$\begin{aligned}\mathrm{d}\langle\boldsymbol{\varepsilon}\rangle^{(\mathrm{p})} &= \bar{\mathbf{A}}_{\mathrm{t}}^{(\mathrm{p})}\mathrm{d}\langle\boldsymbol{\varepsilon}\rangle + \bar{\boldsymbol{\eta}}_{\mathrm{t}}^{(\mathrm{p})}\mathrm{d}T \\ \mathrm{d}\langle\boldsymbol{\sigma}\rangle^{(\mathrm{p})} &= \bar{\mathbf{B}}_{\mathrm{t}}^{(\mathrm{p})}\mathrm{d}\langle\boldsymbol{\sigma}\rangle + \bar{\boldsymbol{\beta}}_{\mathrm{t}}^{(\mathrm{p})}\mathrm{d}T \qquad ,\end{aligned} \tag{2.53}$$

where $\mathrm{d}\langle\boldsymbol{\varepsilon}\rangle$ stands for the macroscopic strain rate tensor, $\mathrm{d}\langle\boldsymbol{\sigma}\rangle$ for the macroscopic stress rate tensor, and $\mathrm{d}T$ for a homogeneous temperature rate. $\bar{\mathbf{A}}_{\mathrm{t}}^{(\mathrm{p})}$, $\bar{\boldsymbol{\eta}}_{\mathrm{t}}^{(\mathrm{p})}$, $\bar{\mathbf{B}}_{\mathrm{t}}^{(\mathrm{p})}$, and $\bar{\boldsymbol{\beta}}_{\mathrm{t}}^{(\mathrm{p})}$ are instantaneous strain and stress concentration tensors, respectively. Assuming the inhomogeneities to show elastic and the matrix to show elastoplastic material behavior[30], the

[28] As an extreme case, using eqn. (2.52) for evaluating the equivalent stress leads to predictions that materials with spherical reinforcements will not yield under macroscopically hydrostatic loads or unconstrained thermal expansion. This is in contradiction to experimental and other theoretical results.

[29] The condition of radial loading paths in stress space at the constituent level is generally violated by a considerable margin in the phases of elastoplastic inhomogeneous materials, even for macroscopic loading paths that are perfectly radial (Pettermann, 1997). This behavior is due to changes in the accommodation of the phase stresses and strains in inhomogeneous materials upon yielding of a constituent and, to a much lesser extent, in the strain hardening regime.

[30] Analogous expressions can be derived for elastoplastic inhomogeneities in an elastic matrix or, in general, for composites containing any required number of elastoplastic phases.

overall instantaneous (tangent) stiffness tensor can be written in terms of the phase properties and the instantaneous concentration tensors as

$$\begin{aligned} \mathbf{E}_{\mathrm{t}}^{*} &= \mathbf{E}^{(\mathrm{i})} + (1-\xi)[\mathbf{E}_{\mathrm{t}}^{(\mathrm{m})} - \mathbf{E}^{(\mathrm{i})}]\bar{\mathbf{A}}_{\mathrm{t}}^{(\mathrm{m})} \\ &= [\mathbf{C}^{(\mathrm{i})} + (1-\xi)[\mathbf{C}_{\mathrm{t}}^{(\mathrm{m})} - \mathbf{C}^{(\mathrm{i})}]\bar{\mathbf{B}}_{\mathrm{t}}^{(\mathrm{m})}]^{-1} \quad , \end{aligned} \tag{2.54}$$

compare eqns. (2.8) and (2.9).

Using the Mori–Tanaka formalism of Benveniste (1987), the instantaneous matrix concentration tensors take the form

$$\begin{aligned} \bar{\mathbf{A}}_{\mathrm{t}}^{(\mathrm{m})} &= \{(1-\xi)\mathbf{I} + \xi[\mathbf{I} + \mathbf{S}_{\mathrm{t}}\mathbf{C}_{\mathrm{t}}^{(\mathrm{m})}(\mathbf{E}^{(\mathrm{i})} - \mathbf{E}_{\mathrm{t}}^{(\mathrm{m})})]^{-1}\}^{-1} \\ \bar{\mathbf{B}}_{\mathrm{t}}^{(\mathrm{m})} &= \{(1-\xi)\mathbf{I} + \xi\mathbf{E}^{(\mathrm{i})}[\mathbf{I} + \mathbf{S}_{\mathrm{t}}\mathbf{C}_{\mathrm{t}}^{(\mathrm{m})}(\mathbf{E}^{(\mathrm{i})} - \mathbf{E}_{\mathrm{t}}^{(\mathrm{m})})]^{-1}\mathbf{C}_{\mathrm{t}}^{(\mathrm{m})}\}^{-1} \quad , \end{aligned} \tag{2.55}$$

compare eqn. (2.31). Expressions for the instantaneous thermal concentration tensors and instantaneous coefficients of thermal expansion can be derived in analogy to the corresponding thermoelastic relations, e.g., eqns. (2.13) and (2.17). Equations (2.55) use the instantaneous Eshelby tensor $\mathbf{S}_{\mathrm{t}}$, which depends on the current state of the (elastoplastic) matrix material, $\mathbf{E}_{\mathrm{t}}^{(\mathrm{m})}$, and, in general, has to be evaluated numerically.

By replacing rates such as $\mathrm{d}\langle\boldsymbol{\sigma}\rangle^{(\mathrm{p})}$ with finite increments such as $\Delta\langle\boldsymbol{\sigma}\rangle^{(\mathrm{p})}$ formulations of eqns. (2.53) to (2.55) can be obtained that are suitable for implementation as micromechanically based constitutive models at the integration point level within Finite Element codes. The resulting incremental Mori–Tanaka (IMT) methods make no assumptions on the overall yield surface and the overall flow potential, the effective material behavior being entirely determined by the incremental mean field equations and the constitutive behavior of the phases. As a consequence, mapping of the stresses onto the yield surface cannot be handled at the level of the homogenized material and radial return mapping must be applied to the matrix at the microscale instead. This implies that the constitutive equations describing the overall behavior cannot be integrated directly (as is the case for homogeneous elastoplastic materials), and iterative algorithms are required. For example, Pettermann (1997) used an implicit Euler scheme in an implementation of an incremental Mori–Tanaka method as a user supplied material routine (UMAT) for the Finite Element code ABAQUS (Simulia, Pawtucket, RI). Extended versions of such algorithms can also handle thermal expansion effects[31] and temperature dependent material parameters.

Incremental mean field models of the type discussed above tend to overestimate the macroscopic strain hardening in the post-yield regime to such an extent that their practical applicability is rather limited, especially for matrix dominated deformation modes, compare, e.g., the discussions by Gilormini (1995) and Suquet (1997). Recent developments involve the use of tangent operators that reflect the macroscopic symmetry of the composite, e.g., "isotropized" operators[32] for statistically isotropic materials (Bornert, 2001),

[31] Elastoplastic inhomogeneous materials such as metal matrix composites typically show a hysteretic thermal expansion response, i.e., the "coefficients of thermal expansion" are not material properties in the strict sense. This dependence of the thermal expansion behavior on the instantaneous mechanical response requires special treatment within the IMT framework, compare Pettermann (1997).

[32] For a discussion of a number of issues pertaining to the use of "isotropic" versus "anisotropic" tangent operators see, e.g., Chaboche and Kanouté (2003).

and algorithmic modifications (Doghri and Ouaar, 2003; Doghri and Friebel, 2005). These improvements have succeeded in markedly reducing the above weaknesses of incremental mean field models such as incremental Mori–Tanaka methods for particle reinforced composites, rendering them highly useful for practical applications and making them attractive candidates for use at the lower length scale in multi-scale models of ductile matrix composites, compare chapter 8. IMTs were also successfully extended to the large strain regime (Huber et al., 2007).

Incremental mean field models have typically used eqn. (2.52) for evaluating the phase averaged equivalent stresses, which, accordingly, tend to be underestimated. The improved estimators for $\langle \sigma_{\mathrm{eqv}} \rangle^{(\mathrm{p})}$ used in modified secant models are not suitable for incremental methods, for which an empirical correction was proposed by Delannay et al. (2007). Furthermore, because they assume elastoplastic phases to yield as a whole once the phase averaged equivalent stress exceeds the yield stress of the elastoplastic constituent, mean field approaches predict sharp transitions from elastic to plastic states instead of a more realistic gradual progress of yielded regions at the microscale.

Other mean field schemes can also be combined with secant and incremental approaches to obtain descriptions for elastoplastic inhomogeneous materials, the most important application having been the use of classical self-consistent schemes for describing the elastoplastic behavior of polycrystalline materials, see, e.g., (Hill, 1965a; Hutchinson, 1970; Berveiller and Zaoui, 1981). In the case of incremental methods what has to be done is replacing elastic, Eshelby and concentration tensors with the corresponding instantaneous tensors for each elastoplastic phase in expressions such as eqns. (2.36), (2.38), (2.46) or (2.47). The weaknesses and strengths of such procedures are closely related to those discussed above for the Mori–Tanaka method. In addition, mean field approaches have been employed to obtain estimates for the nonlinear response of inhomogeneous materials due to microscopic damage or to combinations of damage and plasticity, see, e.g., (Tohgo and Chou, 1996; Guo et al., 1997).

As an alternative to directly extending mean field theories into secant or incremental plasticity, they can also be combined with Dvorak's Transformation Field Analysis (Dvorak, 1992) in order to obtain descriptions of the overall behavior of inhomogeneous materials in the plastic range, see, e.g., Plankensteiner (2000). Such approaches tend to markedly overestimate the markedly strain hardening of elastoplastic composites because they use elastic accommodation of microstresses and strains throughout the loading history. For modifications aimed at improving this behavior of the Transformation Field Analysis see Chaboche et al. (2001).

2.7 Mean Field Methods for Composites with Nonaligned Reinforcements

The macroscopic symmetry of composites reinforced by nonaligned short fibers in many cases is isotropic (random fiber orientations) or transversely isotropic (fiber arrangements with axisymmetric orientation distributions, e.g., fibers with planar random orientation).

However, processing conditions can give rise to a wide range of fiber orientation distributions and, consequently, to lower overall symmetries, compare, e.g., Allen and Lee (1990).

The statistics of the microgeometries of nonaligned matrix–inclusion composites can be typically described on the basis of orientation distribution functions (ODFs) and aspect ratio or length distribution functions (LDFs) of the reinforcements, both of which can be determined experimentally. In addition, information is required on the type of phase geometry to be described. At elevated fiber volume fractions local domains of (nearly) aligned fibers are typically observed in short fiber reinforced composites, which give rise to a "grain-type" mesostructure, referred to as an aggregate system by Eduljee and McCullough (1993). Composites of this type are appropriately modeled via two-step homogenization schemes that involve meso-level averages at the grain level, see, e.g., Camacho et al. (1990) and Pierard et al. (2004). At low to moderate fiber volume fractions, in contrast, the orientations of neighboring fibers are essentially independent within the geometrical constraints of non-penetration. Such dispersed systems (Eduljee and McCullough, 1993) can be studied via single-step mean field schemes involving configurational averaging procedures, which may encompass aspect ratio averaging in addition to orientational averaging.

Studying the responses of nonaligned composites obviously requires orientational averaging of tensor valued variables, which can be done by direct (numerical) integration, see, e.g., Pettermann et al. (1997), or on the basis of expansions of the ODF in terms of generalized spherical harmonics (Viglin (1961) expansions), compare, e.g., Advani and Tucker (1987). The latter approach can be formulated in a number of ways, e.g., via texture coefficients or texture matrices, compare Siegmund et al. (2004). For a discussion of a number of issues relevant to configurational averaging see Eduljee and McCullough (1993).

Mori–Tanaka methods have been extended to describing the elastic behavior of such materials, the typical starting point being dilute concentration tensors $\bar{\mathbf{B}}_{\mathrm{dil}}^{(\mathrm{i})\angle}(\varphi,\psi,\theta)$ for reinforcements having orientations with respect to the global coordinate system that are described by the Euler angles φ, ψ and θ. A phase averaged dilute fiber stress concentration tensor can be obtained as the orientational average

$$\overline{\mathbf{B}}_{\mathrm{dil}}^{(\mathfrak{i})} = \left\langle\left\langle \bar{\mathbf{B}}_{\mathrm{dil}}^{(\mathrm{i})\angle}\rho\right\rangle\right\rangle = \int_0^{2\pi}\int_0^{2\pi}\int_0^{\pi} \bar{\mathbf{B}}_{\mathrm{dil}}^{(\mathrm{i})\angle}(\varphi,\psi,\theta)\,\rho(\varphi,\psi,\theta)\,\mathrm{d}\varphi\,\mathrm{d}\psi\,\mathrm{d}\theta \quad , \tag{2.56}$$

where the orientation distribution function $\rho(\varphi,\psi,\theta)$ is normalized to give $\langle\langle\rho\rangle\rangle = 1$. Using such an "equivalent phase of aligned inclusions" the core statement of the Mori–Tanaka approach, eqn. (2.28), can be written in the form

$$\langle\boldsymbol{\sigma}\rangle^{(\mathfrak{i})} = \overline{\mathbf{B}}_{\mathrm{dil}}^{(\mathfrak{i})}\langle\boldsymbol{\sigma}\rangle^{(\mathfrak{m})} = \overline{\mathbf{B}}_{\mathrm{dil}}^{(\mathfrak{i})}\,\overline{\mathbf{B}}_{\mathrm{MT}}^{(\mathfrak{m})}\langle\boldsymbol{\sigma}\rangle = \overline{\mathbf{B}}_{\mathrm{MT}}^{(\mathfrak{i})}\langle\boldsymbol{\sigma}\rangle \qquad , \tag{2.57}$$

which allows the phase concentration tensors $\overline{\mathbf{B}}_{\mathrm{MT}}^{(\mathfrak{m})}$ and $\overline{\mathbf{B}}_{\mathrm{MT}}^{(\mathfrak{i})}$ to be evaluated as

$$\begin{aligned} \overline{\mathbf{B}}_{\mathrm{MT}}^{(\mathfrak{m})} &= [(1-\xi)\mathbf{I} + \xi\overline{\mathbf{B}}_{\mathrm{dil}}]^{-1} \\ \overline{\mathbf{B}}_{\mathrm{MT}}^{(\mathfrak{i})} &= \overline{\mathbf{B}}_{\mathrm{dil}}\,[(1-\xi)\mathbf{I} + \xi\overline{\mathbf{B}}_{\mathrm{dil}}]^{-1} \end{aligned} \tag{2.58}$$

in analogy to eqns. (2.30) and (2.31). On the basis of eqns. (2.35) the corresponding

effective macroscopic elasticity tensors take the form

$$\begin{aligned}\mathbf{E}^{*}_{\mathrm{MT}} &= \left[(1-\xi)\mathbf{E}^{(\mathrm{m})} + \xi\left\langle\!\left\langle \mathbf{E}^{(\mathrm{i})}\bar{\mathbf{A}}^{(\mathrm{i})}_{\mathrm{dil}}\,\rho\right\rangle\!\right\rangle\right]\left[(1-\xi)\mathbf{I} + \xi\left\langle\!\left\langle \bar{\mathbf{A}}^{(\mathrm{i})}_{\mathrm{dil}}\,\rho\right\rangle\!\right\rangle\right]^{-1} \\ \mathbf{C}^{*}_{\mathrm{MT}} &= \left[(1-\xi)\mathbf{C}^{(\mathrm{m})} + \xi\left\langle\!\left\langle \mathbf{C}^{(\mathrm{i})}\bar{\mathbf{B}}^{(\mathrm{i})}_{\mathrm{dil}}\,\rho\right\rangle\!\right\rangle\right]\left[(1-\xi)\mathbf{I} + \xi\left\langle\!\left\langle \bar{\mathbf{B}}^{(\mathrm{i})}_{\mathrm{dil}}\,\rho\right\rangle\!\right\rangle\right]^{-1} \quad . \end{aligned} \tag{2.59}$$

The stress $\langle\boldsymbol{\sigma}\rangle^{(\mathrm{i})}$ obtained from eqn. (2.57) is an average over all inhomogeneities, irrespective of their orientation, and, accordingly, provides only limited information. The average stresses in inhomogeneities of a given orientation (φ, ψ, θ), which is of higher practical interest, can be evaluated as

$$\langle\boldsymbol{\sigma}\rangle^{(\mathrm{i})\angle} = \bar{\mathbf{B}}^{(\mathrm{i})\angle}_{\mathrm{dil}}\,\overline{\mathbf{B}}^{(\mathrm{m})}_{\mathrm{MT}}\langle\boldsymbol{\sigma}\rangle \quad . \tag{2.60}$$

Results obtained with the above relation are in good agreement with numerical predictions for moderate reinforcement volume fractions and elastic contrasts, compare fig. 2.3.

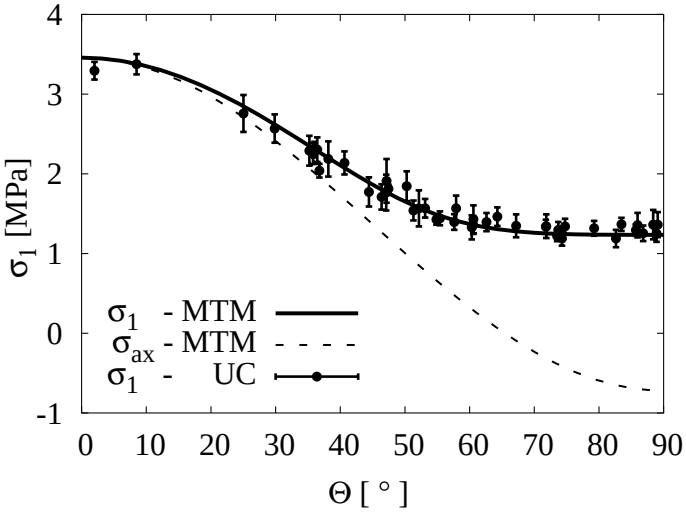

Figure 2.3: Dependence of the averaged stresses in individual fibers on the fiber orientation angle Θ predicted for a uniaxially loaded SiC/Al MMC reinforced by randomly oriented fibers of aspect ratio $a = 5$ (Duschlbauer et al., 2003). Results for the maximum principal stress σ_1 and the axial stress σ_{ax} obtained with an "extended" Mori–Tanaka scheme are shown as solid and dashed lines, respectively. Unit cell results are presented in terms of the mean values (solid circles) and standard deviations within individual fibers (error bars). Θ describes the angle between a given fiber and the loading direction.

"Extended" Mori–Tanaka methods for modeling the elastic behavior of microstructures that contain nonaligned inhomogeneities were developed by a number of authors (Benveniste, 1990; Dunn and Ledbetter, 1997; Pettermann et al., 1997; Mlekusch, 1999). These models differ mainly in the algorithms employed for orientational or configurational averaging[33]. Methods of this type tend to be very useful for many practical applications and have also been used for studying elastic fabric reinforced composites, the orientation of the fiber tows being described by appropriate "equivalent orientations" (Gommers et al., 1998). Extended Mori–Tanaka methods are, however, of a somewhat ad-hoc nature and

[33] Alternative modified Mori–Tanaka models for nonaligned composites can be obtained by using spatially averaged Eshelby tensors, see, e.g., Johannesson and Pedersen (1998).

can lead to non-symmetric effective stiffness tensors[34] in certain situations (Benveniste et al., 1991; Ferrari, 1991).

Mean field approaches based on orientational averaging and Mori–Tanaka approaches have also been employed in studies of the nonlinear behavior of nonaligned composites. Secant plasticity schemes of the above type were used for describing ductile matrix materials (Bhattacharyya and Weng, 1994; Dunn and Ledbetter, 1997) and incremental approaches for modeling composites consisting of an elastoplastic matrix reinforced by nonaligned or random short fibers were proposed by Doghri and Tinel (2005) as well as Lee and Simunovic (2000), with the latter work also accounting for debonding between reinforcements and matrix.

An improved approach to studying composites with nonaligned reinforcements is provided by the Hashin–Shtrikman estimates of Ponte Castañeda and Willis (1995). As discussed in section 2.5 this method is based on "ellipsoid-in-ellipsoid" phase arrangements, with different Eshelby tensors pertaining to the ellipsoids describing the two-point correlations of the phase arrangement and to those describing the shapes of the inhomogeneities. Equation (2.47) can be directly extended to nonaligned reinforcements by converting the inner sum to an orientation average to give

$$\mathbf{E}^{*}_{\mathrm{PW}} = \mathbf{E}^{(\mathfrak{m})} + \xi^{(\mathfrak{i})}\Big[\mathbf{I} - \xi^{(\mathfrak{i})}\,\big\langle\big\langle(\mathbf{E}^{(\mathfrak{j})} - \mathbf{E}^{(\mathfrak{m})})\,\bar{\mathbf{A}}^{(\mathfrak{j})}_{\mathrm{dil}}\,\rho\big\rangle\big\rangle\,\mathbf{S}_{\mathrm{d}}\mathbf{C}^{(\mathfrak{m})}\Big]^{-1}\big\langle\big\langle(\mathbf{E}^{(\mathfrak{j})} - \mathbf{E}^{(\mathfrak{m})})\,\bar{\mathbf{A}}^{(\mathfrak{j})}_{\mathrm{dil}}\,\rho\big\rangle\big\rangle \qquad (2.61)$$

These Hashin–Shtrikman estimates are rigorous provided none of the (aligned) "safety ellipsoids" described by $\mathbf{S}_{\mathrm{d}}$ overlap and none of the (non-aligned) inhomogeneities penetrate outside the associated safety ellipsoids. This results in a limited range of strict applicability in terms of inhomogeneity volume fractions, which can be rather small for markedly prolate or oblate reinforcements that show a considerable degree of misalignment.

For the special case of randomly oriented fibers or platelets of a given aspect ratio, "symmetrized" dilute strain concentration tensors may be constructed, which are known as Wu tensors (Wu, 1966). They can be combined with Mori–Tanaka methods[35] (Benveniste, 1987) or classical self-consistent schemes (Berryman, 1980) to describe composites with randomly oriented phases of matrix–inclusion and interpenetrating topologies. Another mean field approach for such materials, the Kuster and Toksöz (1974) model, essentially is a dilute description applicable to matrix–inclusion topologies and tends to give unphysical results at high reinforcement volume fractions. For recent discussions on the relationships between some of the above approaches see, e.g., Berryman and Berge (1996) as well as Hu and Weng (2000). Due to the overall isotropic behavior of composites reinforced by randomly oriented fibers or platelets, their elastic response must comply with the "standard" Hashin–Shtrikman bounds (Hashin and Shtrikman, 1963), see also table 5.2 in section 5.5.

In addition to mean field and unit cell models (section 5.5) a number of other methods have been proposed for studying composites with nonaligned reinforcements. Most of them

[34] The reason for these difficulties lies in the aligned ellipsoidal symmetry of the phase arrangement that is inherent to Mori–Tanaka methods, compare fig. 2.1.

[35] When used for describing randomly oriented reinforcements via a Wu tensor, Mori–Tanaka methods are not liable to giving nonsymmetric overall elastic tensors.

are based on the assumption that the contribution of a given fiber to the overall stiffness and strength depends solely on its orientation with respect to the applied load and on its length, interactions between neighboring fibers being neglected. The paper physics approach (Cox, 1952) and the Fukuda–Kawata theory (Fukuda and Kawata, 1974) are based on summing up stiffness contributions of fibers crossing an arbitrary normal section on the basis of fiber orientation and length distribution functions, compare also Jayaraman and Kortschot (1996). Such theories use shear lag models (Cox, 1952; Fukuda and Chou, 1982) or modifications thereof (Fukuda and Kawata, 1974) to describe the behavior of a single fiber embedded in matrix material, the results being typically given as modified rules of mixtures with fiber direction and fiber length corrections. Laminate analogy approaches, see, e.g., Fu and Lauke (1998), approximate nonaligned reinforcement arrangements by a stack of layers each of which pertains to one fiber orientation and, where appropriate, one fiber length. Like related models that are based on orientational averaging of the elastic tensors corresponding to different fiber orientations (Huang, 2001) and the so-called aggregate models (Toll, 1992), laminate analogy approaches use Voigt (strain coupling) approximations. Such schemes can be useful especially for describing composites with planar random fiber orientations (Huang, 2001).

2.8 Mean Field Methods for Non-Ellipsoidal Reinforcements

When non-ellipsoidal, inhomogeneous or coated inclusions are subjected to a homogeneous eigenstrain the resulting stress and strain fields are in general inhomogeneous. As a consequence, the interior field Eshelby tensors and dilute inclusion concentration tensors depend on the position within such inhomogeneities. Analytical solutions are available only for certain inclusion shapes, see, e.g., Mura (1987) and Onaka (2001).

A straightforward extension of the mean field concept for such cases consists in using Eshelby or dilute inclusion concentration tensors that are averaged over the inhomogeneity (Duschlbauer, 2004). The corresponding averaged (or "replacement") dilute inclusion concentration tensors, $\bar{\mathbf{A}}_{\mathrm{dil}}^{(\mathrm{i,r})}$ and $\bar{\mathbf{B}}_{\mathrm{dil}}^{(\mathrm{i,r})}$, can be obtained from models with a single dilute inhomogeneity. By generating solutions for six linearly independent load cases via the Finite Element method, and using eqn. (4.1), the average strains and stresses in the phases can be computed and the replacement concentration tensors evaluated.

In order to achieve a workable formulation it is necessary, in addition, to replace the elastic tensors of the inhomogeneities, $\mathbf{E}^{(\mathrm{i})}$ and $\mathbf{C}^{(\mathrm{i})}$, with "replacement elastic tensors" following the expressions

$$\begin{aligned} \mathbf{E}^{(\mathrm{i,r})} &= \mathbf{E}^{(\mathrm{m})} + \frac{1}{\xi_{\mathrm{dil}}}(\mathbf{E}^{*}_{\mathrm{dil}} - \mathbf{E}^{(\mathrm{m})})[\bar{\mathbf{A}}_{\mathrm{dil}}^{(\mathrm{i,r})}]^{-1} \\ \mathbf{C}^{(\mathrm{i,r})} &= \mathbf{C}^{(\mathrm{m})} + \frac{1}{\xi_{\mathrm{dil}}}(\mathbf{C}^{*}_{\mathrm{dil}} - \mathbf{C}^{(\mathrm{m})})[\bar{\mathbf{B}}_{\mathrm{dil}}^{(\mathrm{i,r})}]^{-1} \end{aligned} \quad , \tag{2.62}$$

where $\mathbf{E}^{*}_{\mathrm{dil}}$ and $\mathbf{C}^{*}_{\mathrm{dil}}$ are the effective elastic tensors of the dilute single-inhomogeneity configurations, and ξ_{dil} is the corresponding reinforcement volume fraction. These replacement

elastic tensors ensure consistency within the mean field framework by enforcing eqns. (2.9) to be fulfilled. The replacement tensors can then be inserted in lieu of the "standard" concentration and elastic tensors into the mean field theories described in sections 2.2 and 2.3 in order to obtain estimates for composites reinforced by nonellipsoidal inhomogeneities. This works especially well with explicit algorithms such as Mori–Tanaka methods.

A related method for handling non-ellipsoidal inhomogeneities in a mean field framework is available in the form of the compliance contribution tensor formalism proposed by Kachanov et al. (1994). It uses the difference between the compliance tensors of the matrix and of the dilutely reinforced material,

$$\mathbf{H}_{\mathrm{dil}}^{(\mathrm{i,m})} = \mathbf{C}_{\mathrm{dil}}^{*} - \mathbf{C}^{(\mathrm{m})} \qquad , \tag{2.63}$$

which is referred to as the compliance contribution tensor, to formulate mean field expressions for the overall responses of inhomogeneous materials containing reinforcements or holes of general shape. The $\mathbf{C}_{\mathrm{dil}}^{*}$, like above, must be evaluated from appropriate dilute single-inhomogeneity configurations.

Both the replacement inclusion approach and the compliance contribution formalism are approximations applicable to non-ellipsoidal inhomogeneities of general shapes, and both inhomogeneities and matrix may have general elastic symmetries.

For some configurations volume averaged Eshelby tensors are available, which provide an alternative route to obtaining mean field algorithms for composites reinforced by non-ellipsoidal inhomogeneities, see, e.g., Hashemi et al. (2009).

2.9 Mean Field Methods for Diffusion-Type Problems

The mathematical descriptions of steady-state thermoelasticity and thermal conduction of heterogeneous materials share many common features and can be attacked using similar techniques. Table 2.1 lists the principal variables of these two groups of problems such that the analogies between them are highlighted. Other steady-state diffusion phenomena are mathematically analogous to heat conduction (Hashin, 1983), among them electrical conduction and diffusion of moisture[36]. For further related problems see Torquato (2002).

An important difference between elasticity and conduction problems concerns the orders of the tensors involved, which is lower in the latter case. The displacements $\mathbf{u}$ are vectors whereas the temperatures T are scalars, stresses $\boldsymbol{\sigma}$ and strains $\boldsymbol{\varepsilon}$ are tensors of order 2, whereas the heat fluxes $\mathbf{q}$ and thermal gradients $\mathbf{d}$ are vectors, and the elasticity tensor $\mathbf{E}$ as well as its inverse, the compliance tensor $\mathbf{C} = \mathbf{E}^{-1}$, are of order 4, whereas the conductivity tensor $\mathcal{K}$ and its inverse, the resistivity tensor $\mathcal{R} = \mathcal{K}^{-1}$, are of order 2. The differences in the orders of the tensors directly affect the number of generalized moduli required for describing the generalized material property tensors as well as their symmetry properties (Nye, 1957). For example, cubic geometrical symmetry gives rise

[36]The differential equations describing antiplane shear in elastic solids, d'Arcy creep flow in porous media, and equilibrium properties such as overall dielectric constants and magnetic permeabilities are also of the Poisson type and thus mathematically equivalent to diffusive transport problems.

Table 2.1: Principal variables in steady state elasticity and heat conduction problems.

physical problem	elasticity	thermal conduction
field variable	displacement field $\mathbf{u}$ [m]	temperature field T [K]
generalized intensity	strain field $\boldsymbol{\varepsilon}$ [ ]	thermal gradient field $\mathbf{d}$ [Km^{-1}]
generalized flux	stress field $\boldsymbol{\sigma}$ [Pa]	heat flux field $\mathbf{q}$ [Wm^{-2}]
generalized property	elasticity $\mathbf{E}$ [Pa] compliance $\mathbf{C}$ [Pa^{-1}]	thermal conductivity $\mathcal{K}$ [$\mathrm{Wm}^{-1}\mathrm{K}^{-1}$] thermal resistivity $\mathcal{R}$ [$\mathrm{W}^{-1}\mathrm{mK}$]

to macroscopic cubic symmetry in elasticity (with three independent elastic moduli) but isotropic symmetry in thermal conduction.

In diffusion-type problems the effects of dilute inhomogeneous inclusions can be described via the depolarization tensor (or "diffusion Eshelby tensor"), $\mathcal{S}$, of order 2, which is directly analogous to the "mechanical" Eshelby tensor, $\mathbf{S}$, discussed in section 2.2. In the case of spheroidal inhomogeneities embedded in an isotropic matrix the depolarization tensor depends only on the formers' aspect ratio, see, e.g., Hatta and Taya (1986) and Torquato (2002), whereas for transversally isotropic matrix behavior the latter's material behavior also comes into play, see Giraud et al. (2007). For diffusion problems the Eshelby property takes the form of constant fluxes and constant gradients within dilute ellipsoidal inclusions subjected to uniform far-field loads, and dilute gradient and flux concentration tensors can be obtained in analogy to eqns. (2.26) and (2.27) as

$$\begin{aligned} \mathcal{A}^{(\mathrm{i})}_{\mathrm{dil}} &= [\mathcal{I} + \mathcal{S}\mathcal{R}^{(\mathrm{m})}(\mathcal{K}^{(\mathrm{i})} - \mathcal{K}^{(\mathrm{m})})]^{-1} \\ \mathcal{B}^{(\mathrm{i})}_{\mathrm{dil}} &= [\mathcal{I} + \mathcal{K}^{(\mathrm{m})}(\mathcal{I} - \mathcal{S})(\mathcal{R}^{(\mathrm{i})} - \mathcal{R}^{(\mathrm{m})})]^{-1} \quad . \end{aligned} \tag{2.64}$$

Equivalents to many of the general relations for mechanical problems discussed in section 2.1 hold, a typical example being the expressions for the effective conductivity and resistivity tensors,

$$\begin{aligned} \mathcal{K}^{*} &= \xi\mathcal{K}^{(\mathrm{i})}\bar{\mathcal{A}}^{(\mathrm{i})} + (1-\xi)\mathcal{K}^{(\mathrm{m})}\bar{\mathcal{A}}^{(\mathrm{m})} \\ \mathcal{R}^{*} &= \xi\mathcal{R}^{(\mathrm{i})}\bar{\mathcal{B}}^{(\mathrm{i})} + (1-\xi)\mathcal{R}^{(\mathrm{m})}\bar{\mathcal{B}}^{(\mathrm{m})} \quad , \end{aligned} \tag{2.65}$$

which are directly equivalent to eqns. (2.8) and (2.9).

For diffusive transport in nondilute inhomogeneous materials analoga of the Mori–Tanaka and self-consistent approaches introduced in sections 2.3, 2.4 and 2.7 can be derived, see, e.g., Hatta and Taya (1986), Miloh and Benveniste (1988), Dunn and Taya (1993), Chen (1997) as well as Torquato (2002). In the case of Mori–Tanaka methods the phase concentration tensors can be evaluated from their dilute equivalents as

$$\begin{aligned} \bar{\mathcal{A}}^{(\mathrm{m})}_{\mathrm{MT}} &= [(1-\xi)\mathcal{I} + \xi\mathcal{A}^{(\mathrm{i})}_{\mathrm{dil}}]^{-1} & \bar{\mathcal{A}}^{(\mathrm{i})}_{\mathrm{MT}} &= \mathcal{A}^{(\mathrm{i})}_{\mathrm{dil}}[(1-\xi)\mathcal{I} + \xi\mathcal{A}^{(\mathrm{i})}_{\mathrm{dil}}]^{-1} \\ \bar{\mathcal{B}}^{(\mathrm{m})}_{\mathrm{MT}} &= [(1-\xi)\mathcal{I} + \xi\mathcal{B}^{(\mathrm{i})}_{\mathrm{dil}}]^{-1} & \bar{\mathcal{B}}^{(\mathrm{i})}_{\mathrm{MT}} &= \mathcal{B}^{(\mathrm{i})}_{\mathrm{dil}}[(1-\xi)\mathcal{I} + \xi\mathcal{B}^{(\mathrm{i})}_{\mathrm{dil}}]^{-1} \end{aligned} \tag{2.66}$$

in direct analogy to eqns. (2.29) and (2.30). Estimates for the effective conductivity tensor according to the classical self-consistent scheme takes the form

$$\begin{aligned} \mathcal{K}_{n+1} &= \mathcal{K}^{(\mathrm{m})} + \xi[\mathcal{K}^{(\mathrm{i})} - \mathcal{K}^{(\mathrm{m})}][\mathcal{I} + \mathcal{S}_n\mathcal{R}_n(\mathcal{K}^{(\mathrm{i})} - \mathcal{K}_n)]^{-1} \\ \mathcal{R}_{n+1} &= \left[\mathcal{K}_{n+1}\right]^{-1} \qquad , \end{aligned} \tag{2.67}$$

which is equivalent to eqn. (2.37). The differential scheme for the effective conductivity tensor can be written as

$$\frac{\mathrm{d}\mathcal{K}^*_{\mathrm{D}}}{\mathrm{d}\xi} = \frac{1}{1-\xi}\left[\mathcal{K}^{(\mathrm{i})} - \mathcal{K}^*_{\mathrm{D}}\right]\mathcal{A}_{\mathrm{dil}}(\mathcal{K}^*_{\mathrm{D}}) \qquad , \tag{2.68}$$

compare eqn. (2.39).

Replacement inhomogeneity models in analogy to section 2.8 can be used to handle the conduction behavior of composites containing non-ellipsoidal inhomogeneities as well as reinforcements with finite interfacial conductances. In the latter case, which is of considerable practical importance, provision must be made for the "replacement inhomogeneity" to account for the interfacial temperature jumps, see the discussion by Duschlbauer (2004). Replacement conductivities or resistivities must be evaluated from consistency conditions equivalent to eqns. (2.62), i.e.,

$$\begin{aligned} \mathcal{K}^{(\mathrm{i,r})} &= \mathcal{K}^{(\mathrm{m})} + \frac{1}{\xi_{\mathrm{dil}}}(\mathcal{K}^*_{\mathrm{dil}} - \mathcal{K}^{(\mathrm{m})})[\bar{\mathcal{A}}^{(\mathrm{i,r})}_{\mathrm{dil}}]^{-1} \\ \mathcal{R}^{(\mathrm{i,r})} &= \mathcal{R}^{(\mathrm{m})} + \frac{1}{\xi_{\mathrm{dil}}}(\mathcal{R}^*_{\mathrm{dil}} - \mathcal{R}^{(\mathrm{m})})[\bar{\mathcal{B}}^{(\mathrm{i,r})}_{\mathrm{dil}}]^{-1} \qquad . \end{aligned} \tag{2.69}$$

In contrast to standard methods for evaluating the effects of non-ideal interfaces on the macroscopic conductivity of composites (Hasselman and Johnson, 1987), the replacement inhomogeneity formalism can handle inhomogeneously distributed interfacial conductances (Nogales and Böhm, 2008). Both types of methods predict that finite interfacial conductances give rise to a marked size effect in the macroscopic conductivities, i.e., below some critical size even highly conductive reinforcements fail to improve the overall conductivity of composites. Diffusive transport in composites containing non-ellipsoidal inhomogeneities can also be described by resistance contribution tensors in analogy to the compliance contribution tensor formalism, eqn. (2.63).

Due to the lower rank of the tensors involved in diffusion-type problems the latter tend to be more benign and easier to handle than mechanical ones. Extensive discussions of diffusion-type problems in inhomogeneous media can be found, e.g., in Markov (2000), Torquato (2002) and Milton (2002). Analogous mean field descriptions can also be devised for a number of coupled problems, such as the electromechanical behavior of inhomogeneous materials with at least one piezoelectric constituent, see, e.g., Huang and Yu (1994).

Chapter 3

Bounding Methods

Whereas mean field methods, unit cell approaches and embedding strategies can typically be used for both homogenization and localization tasks, bounding methods are limited to homogenization. Discussions in this chapter again are restricted to materials consisting of two perfectly bonded constituents.

Rigorous bounds on the overall elastic properties of inhomogeneous materials are typically obtained from appropriate variational (minimum energy) principles. In what follows only outlines of bounding methods are given; formal treatments can be found, e.g., in Nemat-Nasser and Hori (1993), Bornert (1996), Ponte Castañeda and Suquet (1998), Markov (2000), Torquato (2002) and Milton (2002).

3.1 Classical Bounds

Hill Bounds

Classical expressions for the minimum potential energy and the minimum complementary energy in combination with uniform stress and strain trial functions lead to the simplest variational bounding expressions, the upper bounds of Voigt (1889) and the lower bounds of Reuss (1929). In their tensorial form (Hill, 1952) they are known as the Hill bounds and can be written as

$$\left[\sum\nolimits_{(\mathrm{p})} V^{(\mathrm{p})}\mathbf{C}^{(\mathrm{p})}\right]^{-1} \leq \mathbf{E} \leq \sum\nolimits_{(\mathrm{p})} V^{(\mathrm{p})}\mathbf{E}^{(\mathrm{p})} \quad . \tag{3.1}$$

These bounds, while universal and very simple, do not contain any information on the microgeometry of an inhomogeneous material beyond the phase volume fractions, and are too slack for many practical purposes[39]. However, in contrast to the Hashin–Shtrikman and higher-order bounds, they also hold for volume elements that are too small to be proper RVEs.

[39]The bounds on the Young's and shear moduli obtained from eqn. (3.1) are equivalent to Voigt and Reuss expressions in terms of the corresponding phase moduli only if the constituents have Poisson's ratios that give rise to equal Poisson contractions. Due to the homogeneous stress and strain assumptions used for obtaining the Hill bounds, the corresponding phase strain and stress concentration tensors are $\bar{\mathbf{A}}_{\mathrm{V}}^{(\mathrm{p})} = \mathbf{I}$ and $\bar{\mathbf{B}}_{\mathrm{R}}^{(\mathrm{p})} = \mathbf{I}$, respectively.

Hashin–Shtrikman-Type Bounds

Considerably tighter bounds on the macroscopic behavior of inhomogeneous materials can be obtained from a variational formulation due Hashin and Shtrikman (1961). They are formulated in terms of a homogeneous reference material and of polarization fields $\boldsymbol{\tau}(\mathbf{x})$ that describe the difference between microscopic stress fields in the inhomogeneous material and a homogeneous reference medium, compare eqn. (2.40). In combination with the macrohomogeneity condition, eqn. (1.6) polarization fields allow the complementary energy of the composite to be formulated in such a way that the "fast" and "slow" contributions are separated, giving rise to the Hashin–Shtrikman variational principle. The latter can be written in the form

$$F_{\mathrm{HS}}(\boldsymbol{\tau}(\mathbf{x})) = \frac{1}{V}\int_V \{\boldsymbol{\tau}^T(\mathbf{x})[\mathbf{E}^0 - \mathbf{E}(\mathbf{x})]^{-1}\,\boldsymbol{\tau}(\mathbf{x}) + [\boldsymbol{\tau}(\mathbf{x}) - \langle\boldsymbol{\tau}\rangle^*]^T\,\boldsymbol{\varepsilon}'(\boldsymbol{\tau}(\mathbf{x})) + 2\boldsymbol{\tau}^T\boldsymbol{\varepsilon}^0\}\,\mathrm{d}\Omega \qquad , \tag{3.2}$$

compare, e.g., Gross and Seelig (2001). The definitions of the variables in eqn. (3.2) follow those in eqn. (2.40). The stationary values of F_{HS} take the form

$$F_{\mathrm{HS}} = \boldsymbol{\varepsilon}^{0T}\,(\mathbf{E}^* - \mathbf{E}^0)\,\boldsymbol{\varepsilon}^0$$

and are maxima when $(\mathbf{E}(\mathbf{x}) - \mathbf{E}^0)$ is positive definite and minima when $(\mathbf{E}(\mathbf{x}) - \mathbf{E}^0)$ is negative definite.

In order to allow an analytical solution for the above variational problem, the highly complex position dependent polarizations $\boldsymbol{\tau}(\mathbf{x})$ are approximated by phase-wise constant polarizations $\boldsymbol{\tau}^{(\mathfrak{p})}$, compare eqn. (2.41). This has the consequence that the strain fluctuations $\boldsymbol{\varepsilon}'(\boldsymbol{\tau}^{(\mathfrak{p})})$ can be evaluated by an Eshelby-type eigenstrain procedure. It can be shown that for the case of isotropic constituents and isotropic overall behavior the proper Eshelby tensor to be used is the one for spheres. By optimizing the Hashin–Shtrikman variational principle with respect to the $\boldsymbol{\tau}^{(\mathfrak{p})}$ the tightest possible bounds within the Hashin–Shtrikman scheme are found.

In the case of two-phase materials with isotropic constituents, in which the matrix is softer than the reinforcements, i.e., for $(K^{(\mathfrak{i})} - K^{(\mathfrak{m})}) > 0$ and $(G^{(\mathfrak{i})} - G^{(\mathfrak{m})}) > 0$, the above procedure leads to lower bounds for the elasticity tensors of the form

$$\begin{aligned}\mathbf{E}^*_{\mathrm{HS}-} &= \mathbf{E}^{(\mathfrak{m})} + \xi\Big[(\mathbf{E}^{(\mathfrak{i})} - \mathbf{E}^{(\mathfrak{m})})^{-1} + (1-\xi)\mathbf{S}^{(\mathfrak{m})}\mathbf{C}^{(\mathfrak{m})}\Big]^{-1} \\ &= \mathbf{E}^{(\mathfrak{m})} + \xi(\mathbf{E}^{(\mathfrak{i})} - \mathbf{E}^{(\mathfrak{m})})\,\bar{\mathbf{A}}^{(\mathfrak{i})}_{\mathrm{HS}-} \qquad ,\end{aligned} \tag{3.3}$$

the strain concentration tensor $\bar{\mathbf{A}}^{(\mathfrak{i})}_{\mathrm{HS}-}$ being equal to a Mori–Tanaka strain concentration tensor, eqn. (2.30), evaluated with a dilute concentration tensor of the type given in eqn. (2.26). The upper bound Hashin–Shtrikman elasticity tensors are obtained by exchanging the roles of matrix and inhomogeneities as

$$\mathbf{E}^*_{\mathrm{HS}+} = \mathbf{E}^{(\mathfrak{i})} + (1-\xi)\Big[(\mathbf{E}^{(\mathfrak{m})} - \mathbf{E}^{(\mathfrak{i})})^{-1} + \xi\mathbf{S}^{(\mathfrak{i})}\mathbf{C}^{(\mathfrak{i})}\Big]^{-1} \qquad . \tag{3.4}$$

The Hashin–Shtrikman bounds proper, eqn. (3.3) and (3.4), were stated by Hashin and Shtrikman (1963) in terms of bounds on the effective bulk modulus K^* and the effective shear modulus[40] G^*. They apply to essentially all practically relevant inhomogeneous materials with isotropic phases that show (statistically) isotropic overall symmetry[41] and fulfill the condition $(K^{(\mathrm{i})} - K^{(\mathrm{m})})(G^{(\mathrm{i})} - G^{(\mathrm{m})}) > 0$. The Hashin–Shtrikman formalism also allows to recover the Voigt and Reuss bounds when the reference material is chosen to be much stiffer or much softer than either of the constituents.

A different set of Hashin–Shtrikman bounds is applicable to (statistically) transverse isotropic composites reinforced by aligned continuous fibers[42] (Hashin and Shtrikman, 1962). For a discussion of evaluating these bounds for composites reinforced by transversely isotropic fibers see Hashin (1983).

Further developments led to the Walpole (1966) and Willis (1977) bounds, which pertain to thermoelastically anisotropic overall behavior due to anisotropic constituents, statistically anisotropic phase arrangements, and/or non-spherical reinforcements, a typical example being the aligned ellipsoidal microgeometry sketched in fig. 2.1. These bounds include the Hashin–Shtrikman bounds discussed above as special cases and they can also handle situations where a "softest" and "stiffest" constituent cannot be identified unequivocally so that a fictive reference material must be used.

Hashin–Shtrikman-type bounds are not restricted to materials with matrix–inclusion topologies, but hold for any phase arrangement of the appropriate symmetry and phase volume fraction. In addition, it is worth noting that Hashin–Shtrikman-type bounds are sharp, i.e., they are the tightest bounds that can be given for the type of geometrical information used (volume fraction and overall symmetry, corresponding to two-point correlations). From the practical point of view it is of interest that for two-phase materials Mori–Tanaka estimates are equal to one of the Willis bounds (Weng, 1990), while the other bound can be obtained after a "color inversion" (i.e., after exchanging the roles of inhomogeneities and matrix)[43]. Accordingly, the bounds can be evaluated for fairly general

[40] Whereas engineers tend to describe elastic material behavior in terms of Young's moduli and Poisson's ratios (which can be measured experimentally in a relatively straightforward way), many homogenization expressions are best formulated in terms of bulk and shear moduli, which directly describe the physically relevant hydrostatic and deviatoric responses of materials. For obtaining bounds on the effective Young's modulus E^* from the results on K^* and G^* see Hashin (1983), and for bounding expressions on the Poisson numbers ν^* see Zimmerman (1992).

[41] Avellaneda and Milton (1989) constructed hierarchical laminates that are statistically isotropic but show overall conductivities that do not fall within the pertinent Hashin–Shtrikman bounds. Accordingly, statistical isotropy by itself is not a sufficient condition for guaranteeing the validity of expressions such as eqns. (3.3) and (3.4). For a discussion of Hashin–Shtrikman-type bounds of macroscopically isotropic composites consisting of anisotropic constituents see, e.g., Nadeau and Ferrari (2001).

[42] These bounds apply to general (transversely isotropic) two-phase materials, the ("in-plane") phase geometries of which are translation invariant in the "out-of-plane" or "axial" direction.

[43] Put more precisely, the lower bounds for two-phase materials are obtained from Mori–Tanaka methods when the more compliant material is used as matrix phase, and the upper bounds when it is used as inclusion phase. For matrix–inclusion materials with more than two constituents, Mori–Tanaka expressions are bounds if the matrix is the stiffest or the softest phase, and fall between the appropriate bounds otherwise (Weng, 1990). Note, however, that extended Mori–Tanaka methods for nonaligned composites as discussed in sections 2.7 and 2.8 in general do not coincide with bounds.

aligned phase geometries by simple matrix algebra such as eqn. (2.32). For elevated phase contrasts the lower and upper Hashin–Shtrikman-type bounds tend to be rather far apart, however.

Composites reinforced by randomly oriented fibers or platelets follow the Hashin–Shtrikman bounds for statistically isotropic materials, eqns. (3.3) and (3.4). A discussion of Hashin–Shtrikman-type bounds on the elastic responses of composites with more general fiber orientation distributions can be found in Eduljee and McCullough (1993). In the case of porous materials (where the pores may be viewed as an ideally compliant phase) only upper Hashin–Shtrikman bounds can be obtained, the lower bounds for the elastic moduli being zero. The opposite situation holds in case one of the constituents is rigid.

Hashin–Shtrikman-type variational formulations can also be employed for generating bounds for more general phase arrangements. Evaluating the polarizations for "composite regions" consisting of inhomogeneities embedded in matrix gives rise to Hervé–Stolz–Zaoui bounds (Hervé et al., 1991). When complex phase patterns are to be considered (Bornert, 1996; Bornert et al., 1996) numerical methods must be used for evaluating the polarization fields.

Bounds for Discrete Microgeometries

Hashin–Shtrikman-type bounds can also be derived for (simple) periodic phase arrangements, see, e.g., Nemat-Nasser and Hori (1993). Among other bounding approaches for such phase arrangements are those of Bisegna and Luciano (1996), which uses approximate variational principles evaluated from periodic unit cells via Finite Element models, and of Teply and Dvorak (1988), which evaluates bounds for the elastoplastic behavior of fiber reinforced composites with periodic hexagonal phase arrangements.

3.2 Improved Bounds

When more complex trial functions are used in variational bounding, their optimization requires statistical information on the phase arrangement in the form of n-point correlations. This way improved bounds can be generated that are significantly tighter than Hashin–Shtrikman-type expressions.

Three-point bounds for statistically isotropic two-phase materials can be formulated in such a way that the information on the phase arrangement statistics is contained in two three-point microstructural parameters, $\eta(\xi)$ and $\zeta(\xi)$, compare Torquato (2002). Evaluating these parameters for given arrangement statistics is a considerable task. However, analytical expressions or tabulated data in terms of the reinforcement volume fraction ξ are available for a number of generic microgeometries of practical importance, among them statistically homogeneous isotropic materials containing identical, bidisperse and polydisperse impenetrable ("hard") spheres (that describe matrix–inclusion composites) as well as monodisperse interpenetrating spheres ("boolean models" that can describe many interwoven phase arrangements), and statistically homogeneous transversely isotropic materials

reinforced by impenetrable or interpenetrating aligned cylinders. References to some three-point bounds and to a number of expressions for η and ζ applicable to some two-phase composites can be found in section 3.4, where results from mean field and bounding approaches are compared. For reviews of higher-order bounds for elastic (as well as other) properties of inhomogeneous materials see, e.g., Quintanilla (1999), Torquato (1991) and Torquato (2002).

Improved bounds can provide highly useful information for low and moderate phase contrasts (as typically found in technical composites), but even they tend to be rather slack for elevated phase contrasts.

3.3 Bounds on Nonlinear Mechanical Behavior

Analoga to the Hill bounds for nonlinear inhomogeneous materials were introduced by Bishop and Hill (1951). For polycrystals the nonlinear equivalents to Voigt and Reuss expressions are usually referred to as Taylor and Sachs bounds, respectively.

In analogy to mean field estimates for elastoplastic material behavior, nonlinear bounds are typically obtained by evaluating a sequence of linear bounds. Talbot and Willis (1985) extended the Hashin–Shtrikman variational principles to obtain one-sided bounds (i.e., upper or lower bounds, depending on the material combination) on the nonlinear mechanical behavior of inhomogeneous materials.

An important development took place with the derivation of a variational principle by Ponte Castañeda (1992) which provides upper bounds on the effective nonlinear behavior of inhomogeneous materials on the basis of upper bounds for the elastic response[44]. It uses a sequence of inhomogeneous reference materials, the properties of which have to be obtained by optimization procedures for each strain level. Essentially, the variational principle guarantees the best choice for the comparison material at a given load. The Ponte Castañeda bounds are closely related to mean field approaches using improved secant plasticity methods, compare section 2.6. For higher-order bounds on the nonlinear response of inhomogeneous materials see, e.g., Talbot and Willis (1998).

The study of bounds — like the development of improved estimates — for the overall nonlinear mechanical behavior of inhomogeneous materials has been an active field of research during the past decade, see the recent reviews by Suquet (1997), Ponte Castañeda and Suquet (1998) and Willis (2000).

[44]The Ponte Castañeda bounds are rigorous for nonlinear elastic inhomogeneous materials and, on the basis of deformation theory, are very good approximations for materials with at least one elastoplastic constituent. Applying the Ponte Castañeda variational procedure to elastic lower bounds does not necessarily lead to a lower bound for the inelastic behavior.

3.4 Comparisons of Mean Field and Bounding Predictions for Macroscopic Elastic Responses

In order to give some idea of the type of predictions that can be obtained by different mean field (and related) approaches and by bounding methods for the thermomechanical responses of inhomogeneous thermoelastic materials, results for the overall elastic moduli and coefficients of thermal expansion are presented as functions of the reinforcement volume fraction ξ in this section. All comparisons are based on E-glass particles or fibers embedded in an epoxy matrix. The elastic contrast of these constituents is $c \approx 21$ and the thermal expansion contrast takes a value of approximately 0.14, see table 3.1.

Table 3.1: Constituent material parameters of epoxy matrix and E-glass reinforcements used in generating figs. 3.1 to 3.7.

	E[GPa]	ν[ ]	α[1/K]
matrix	3.5	0.35	36.0
reinforcements	74.0	0.2	4.9

Figures 3.1 and 3.2 show predictions for the overall Young's and shear moduli of a particle reinforced composite using the above constituent parameters. The Hill bounds can be seen to be very slack. The Mori–Tanaka estimates (MTM) — as mentioned before — coincide with the lower Hashin–Shtrikman bounds (H/S LB), whereas the classical self-consistent scheme (CSCS) shows a typical behavior in that it is close to one Hashin–Shtrikman bound at low volume fractions, approaches the other at high volume fractions, and displays a transitional behavior in the form of a sigmoid curve in-between. The three-

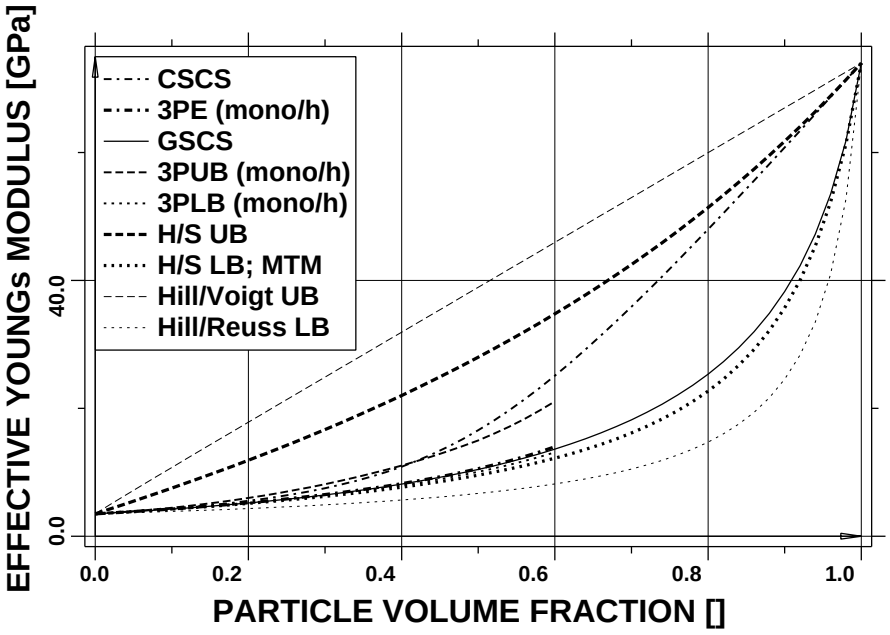

Figure 3.1: Bounds and estimates for the effective Young's moduli of glass/epoxy particle reinforced composites as functions of the particle volume fraction.

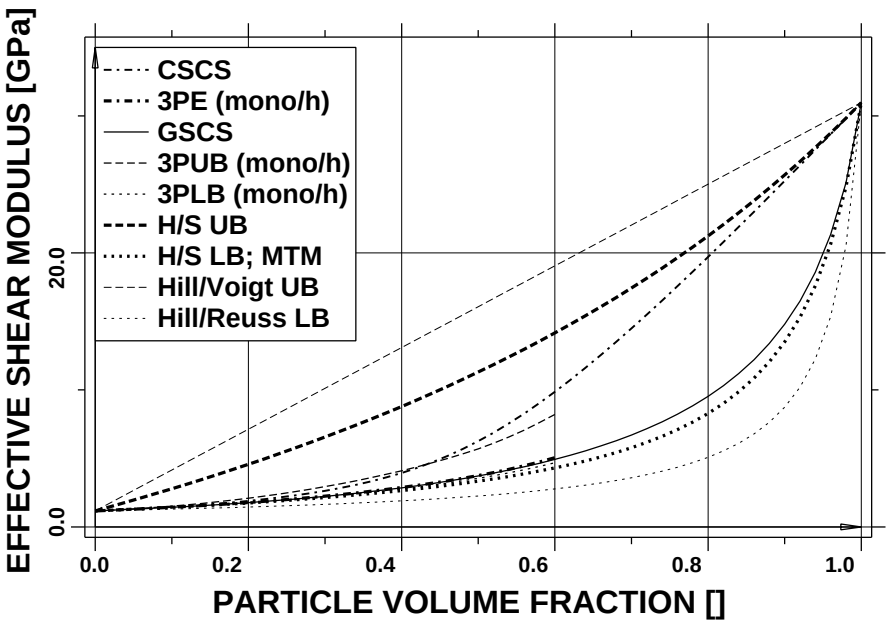

Figure 3.2: Bounds and estimates for the effective shear moduli of glass/epoxy particle reinforced composites as functions of the particle volume fraction.

point bounds (3PLB and 3PUB) shown in figs. 3.1 and 3.2 are based on formalisms developed by Beran and Molyneux (1966), Milton (1981) as well as Phan-Thien and Milton (1983). They apply to impenetrable spherical particles of equal size and use expressions for the statistical parameters η and ζ that were reported by Miller and Torquato (1990) and Torquato et al. (1987), respectively. These expressions are available for reinforcement volume fractions up to $\xi = 0.6$[45]. The three-point estimates (3PE) of Torquato (1998) were evaluated with the same choice of η and ζ and can be seen to lie between the three-point bounds. For the case considered here the results from the generalized self-consistent scheme, which predicts a slightly stiffer behavior than the Mori–Tanaka method, are very close to the lower three-point bounds even though microgeometries corresponding to the GSCS are not monodisperse in the sizes of the inhomogeneities.

Predictions for the coefficients of thermal expansion of statistically isotropic inhomogeneous materials are presented in fig. 3.3. Levin's formula, eqn.(2.14), was combined the Hashin–Shtrikman bounds, the three-point bounds and the three-point estimates for the effective bulk modulus to obtain the corresponding bounds and estimates for the CTE. Because they are based on the same estimates for the effective bulk modulus, the results given for the GSCS and the Mori–Tanaka-scheme coincide with the upper Levin/Hashin–Shtrikman bounds.

In figs. 3.3 to 3.7 results are presented for the overall transverse Young's moduli, overall axial and transverse shear moduli, as well as overall axial and transverse coefficients of

[45]This value approaches the maximum volume fraction achievable in random packings of spheres, which is $\xi = 0.64$ (Weisstein, 2000).

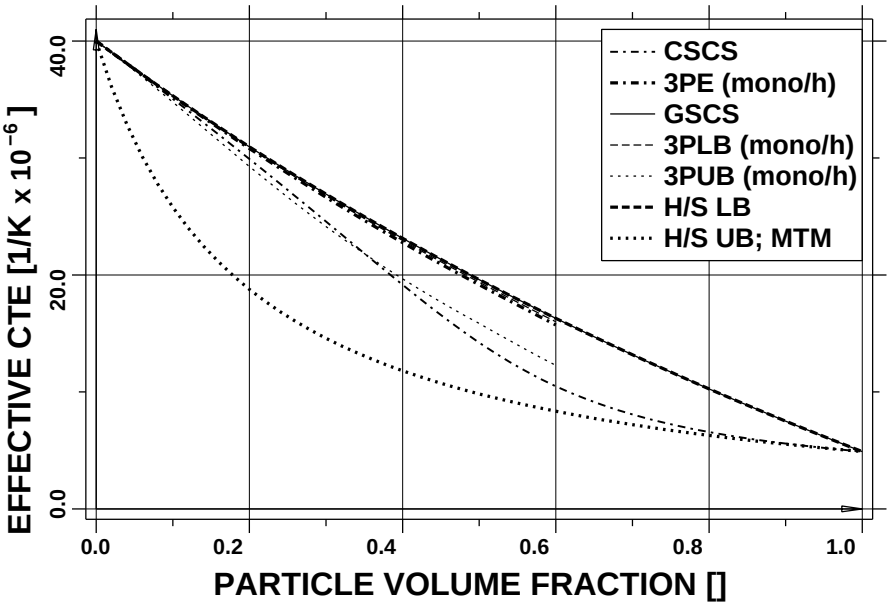

Figure 3.3: Bounds and estimates for the effective CTEs of glass/epoxy particle reinforced composites as functions of the particle volume fraction.

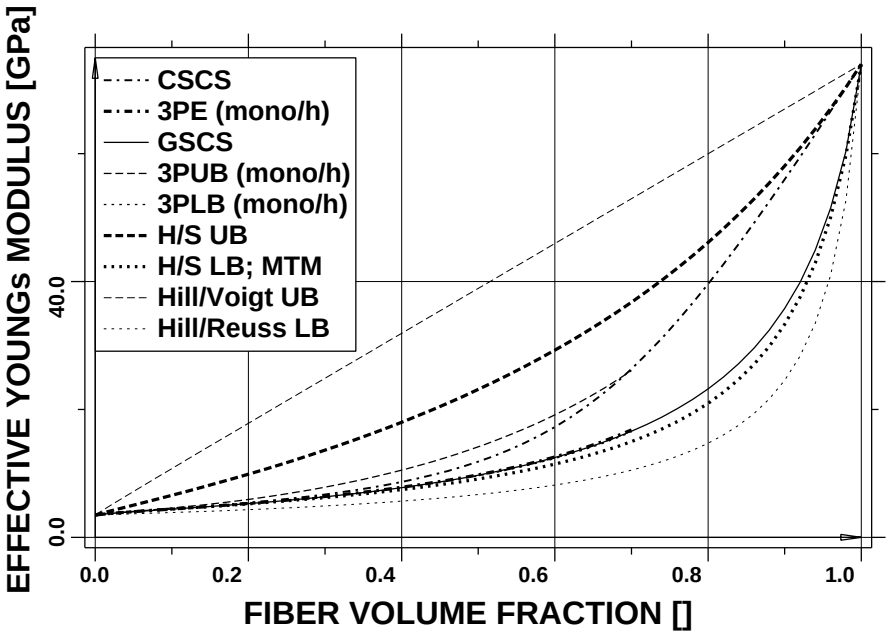

Figure 3.4: Bounds and estimates for the effective transverse Young's moduli of glass/epoxy fiber reinforced composites as functions of the fiber volume fraction.

thermal expansion of composites reinforced by aligned continuous fibers[46]. The results for the three-point bounds shown follow the formalism of Silnutzer (1972) and Milton (1981),

[46]In the case of the axial Young's moduli the estimates and bounds are nearly indistinguishable from each other (and from the rule of mixture result, $E^*_{\mathrm{A}} = \xi E^{(\mathrm{i})}_{\mathrm{A}} + (1-\xi)E^{(\mathrm{m})}$, for the material parameters and scaling used in fig. 3.4 and are, accordingly, not given here. It is, however, worth noting that the effective axial Young's modulus of a composite reinforced by aligned continuous fibers is always equal to or larger than the rules of mixture result.

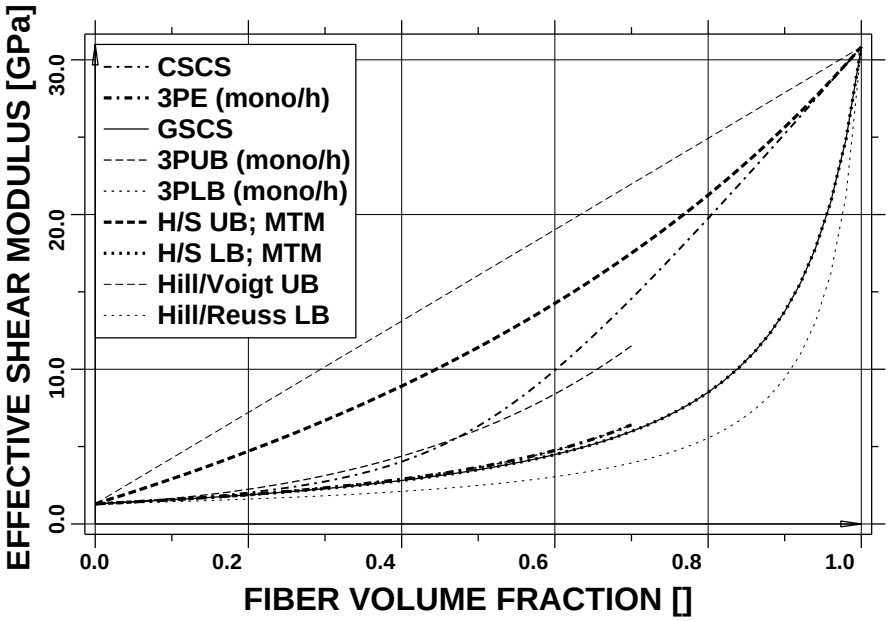

Figure 3.5: Bounds and estimates for the effective axial shear moduli of glass/epoxy fiber reinforced composites as functions of the fiber volume fraction.

correspond to the case of aligned impenetrable circular cylindrical fibers of equal diameter and use statistical parameters evaluated by Torquato and Lado (1992) for fiber volume fractions $\xi \lessapprox 0.7$. Generally, a qualitatively similar behavior to the particle reinforced case can be observed. It is noteworthy, however, that the overall transverse CTEs in fig. 3.7 at low fiber volume fractions exceeds the CTEs of both constituents. Such behavior is

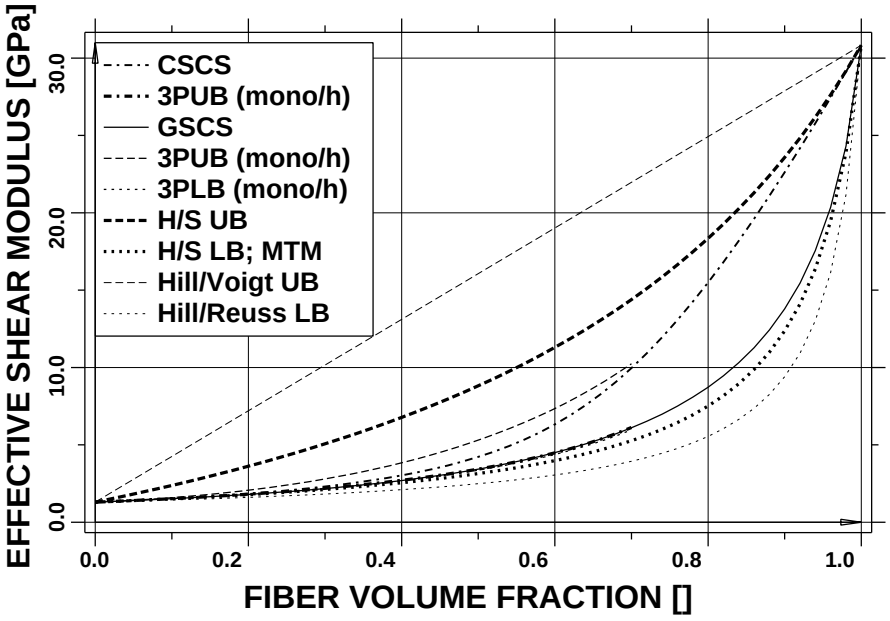

Figure 3.6: Bounds and estimates for the effective transverse shear moduli of glass/epoxy fiber reinforced composites as functions of the fiber volume fraction.

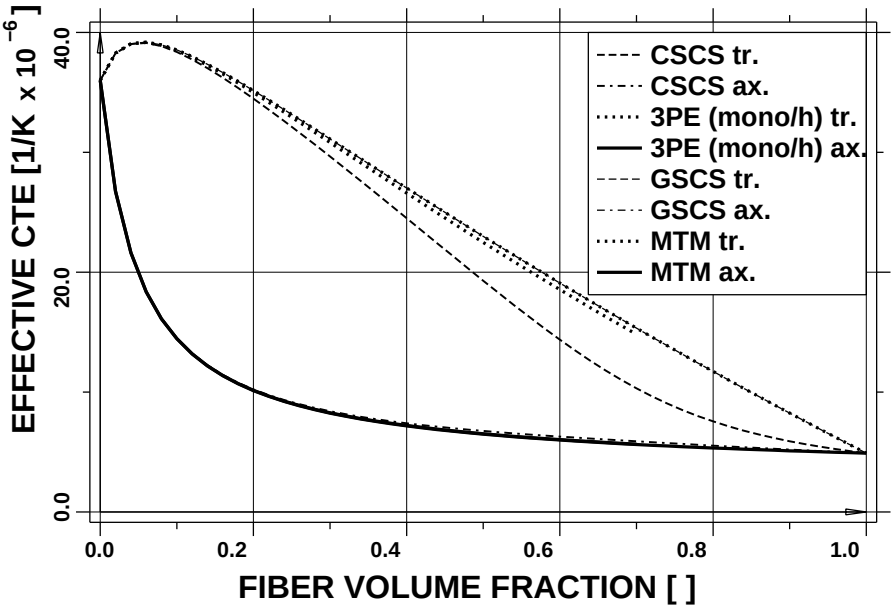

Figure 3.7: Estimates for the effective axial and transverse CTEs of glass/epoxy fiber reinforced composites as functions of the fiber volume fraction.

typical for continuously reinforced composites and is caused by the marked axial constraint enforced by the fibers.

In figs. 3.1 to 3.7 the classical self-consistent scheme — as expected — is not in good agreement with the three-point bounds shown, which explicitly correspond to matrix–inclusion topologies. Considerably better agreement with the CSCS is found by using three-point parameters of the interpenetrating sphere or cylinder type (which can also describe cases where both phases percolate, but are not as symmetrical with respect to the constituents as the CSCS). From a practical point of view it is worth noting that despite their sophistication improved bounds (and higher order estimates) may give overly optimistic predictions for the overall moduli because they describe ideal composites, whereas in actual materials it is practically impossible to avoid flaws such as porosity.

Before closing this chapter it should be mentioned that more complex responses may be obtained when one or both of the constituents are transversely isotropic with a high stiffness contrast between the axial and transverse directions (note that e.g. carbon fibers typically exhibit transverse Young's moduli that are much smaller than the Young's moduli of, say, metallic matrices, whereas the opposite holds true for the axial Young's moduli). Such effects may be especially marked in the nonlinear range. Also, the angular dependences of stiffnesses and CTEs in fiber reinforced materials can be quite rich, compare, e.g., Pettermann et al. (1997).

Chapter 4

General Remarks on Modeling Approaches Based on Discrete Microgeometries

In the following micromechanical approaches based on discrete microgeometries are understood to encompass the periodic homogenization, embedding and windowing methods discussed in chapters 5 to 7. Broadly speaking, these models trade off restrictions to the generality of the phase arrangements against the capability of using fine grained geometrical descriptions and of resolving details of the stress and strain fields at the length scale of the inhomogeneities. The main fields of application of these methods are studying the nonlinear behavior of inhomogeneous materials and evaluating the microscopic stress and strain fields of relevant microgeometries at high resolution. This information, on the one hand, may be required when the local stress and strain fields fluctuate strongly and are, accordingly, difficult to describe by averaged fields. On the other hand, it is important for understanding the damage and failure behavior of inhomogeneous materials, which can depend on details of their microgeometry.

4.1 Microgeometries

The heterogeneous volume elements ("microgeometries") used in discrete microstructure models range from highly idealized periodic geometries, such as simple cubic arrays of spheres in a matrix, to phase arrangements that aim at closely approximating the geometrical complexity of actual inhomogeneous materials. There are two philosophies for obtaining heterogeneous volume elements for modeling, viz., generating them by computer algorithms or basing them directly on geometries obtained by experiment.

Computer Generated Phase Arrangements

Computer generated volume elements may be classified into two groups, one of which is based on generic arrangements of a number of reinforcements that are randomly positioned and, where appropriate, randomly oriented. The other group aims at generating more specific phase arrangements that have identical phase distribution statistics as some target

material. A further possible approach to generating realistic volume elements by computer algorithms, which consists of modeling the actual production process, has seen little use to date for composites due to the complexity of the task.

The generation of generic microgeometrical models with random phase arrangements typically involves random sequential addition methods[46] and, in many cases, random perturbation or relaxation techniques. The reinforcement volume fractions that can be reached by RSA methods tend to be moderate due to jamming (geometrical frustration) and their representativeness for actual phase arrangements generated by mixing processes is open to question (Stroeven et al., 2004). Major improvements on both counts can be obtained by using RSA geometries as starting configurations for random perturbation or hard core shaking models (HCSM, also referred to as dynamic simulations), see, e.g., Buryachenko et al. (2003), that apply small random displacements to each inhomogeneity to obtain more tightly packed arrangements of reinforcements as the size of the volume element is reduced to increase the inhomogeneity volume fraction. Methods of the above types have been used to generate statistically homogeneous distributions of particular or fibrous reinforcements, see, e.g., Gusev (1997), Böhm and Han (2001), Lusti et al. (2002) or Duschlbauer et al. (2006), as well as idealized clustered microgeometries (Segurado et al., 2003).

The alternative strategy for generating volume elements by simulation aims at obtaining "statistically reconstructed" phase arrangements, which are not identical to any given sample, but rather are statistically equivalent to a target material. Statistical reconstruction typically results in optimization problems in which some starting configuration (e.g., a periodic phase arrangement of appropriate volume fraction) is modified such that suitable statistical descriptors of the phase distributions closely approach or become equal to the chosen target descriptor. Procedures for reconstructing matrix–inclusion and more general microgeometries have been reported that employ simulated annealing procedures (Rintoul and Torquato, 1997; Torquato, 1998; Bochenek and Pyrz, 2002), genetic algorithms (Zeman and Šejnoha, 2001), and other minimization methods (Roberts and Garboczi, 1999). For in-depth discussions of the underlying issues, such as statistical descriptors for the phase arrangements of inhomogeneous materials, see, e.g., Torquato (2002) and Zeman (2003). Statistical reconstruction studies have been based on a number of statistical descriptors of phase arrangement, among them n-point distribution functions, radial distribution functions and correlation functions. Obviously, the statistical reconstruction of microgeometries is closely connected to the concept of geometrical RVEs, compare section 1.3.

For volume elements that contain considerable numbers of inhomogeneities or other microstructural features, statistically reconstructed phase arrangements are definitely more specific to a given target material than are generic random microgeometries. However, because at present computational requirements put rather strong limits on the sizes of

[46] In random sequential addition (RSA) algorithms (also known as random sequential insertion or, in two-dimensional cases, random sequential adhesion models, and sometimes referred to as static simulations), positions and, where applicable, orientations for new reinforcements are created by random processes, a candidate inhomogeneity being accepted if it does not "collide" with any of the existing ones and rejected otherwise. In contrast to random packing, in generating microgeometrical models a "collision" typically involves the violation of some minimum distance rather than an actual overlap between neighboring inhomogeneities.

volume elements that can be handled by numerical engineering methods, this advantage tends to be limited in practice.

Computer generated microgeometries have tended to employ idealized reinforcement shapes, equiaxed particles embedded in a matrix, for example, being often represented by spheres, and fibers by cylinders or prolate spheroids[47] of appropriate aspect ratio. Recently work employing polyhedral inhomogeneities has also been reported, see, e.g., (Nogales and Böhm, 2008).

Real Structure Phase Arrangements

Instead of generating phase arrangements by computer algorithms, volume elements may be chosen to follow as closely as possible the microgeometry in part of a given sample of the material to be modeled, obtained from metallographic sections (Fischmeister and Karlsson, 1977), serial sections (Terada and Kikuchi, 1996; Li et al., 1999), tomographic data (Hollister et al., 1994; Kenesei et al., 2004; Chawla and Chawla, 2006; Buffière et al., 2008), etc. The resulting descriptions are often referred to as "real structure" models.

Recently the generation of real structure models from pixel (digital images) or voxel (tomographic) data describing the geometries of inhomogeneous materials has been the focus of considerable research efforts. Such work typically has been based on digital images. It involves the steps of selecting from experimental data sets appropriate volume elements for analysis ("registration") and of identifying the regions occupied by the different constituents by thresholding of the grey values of the pixels or voxels ("segmentation"). At this stage pixel or voxel models (compare section 4.2) can be generated directly from the segmented data set or contouring procedures may be used for obtaining "smooth" phase domains, the latter operation typically being more manpower intensive and difficult to automatize. In the past decade tomography has proven especially useful for determining the microgeometries of inhomogeneous materials with constituents that show markedly different X-ray absorption, e.g., porous and cellular materials.

Real microstructure models can provide accurate descriptions of actual phase arrangements, but they may depend to a considerable extent on details of the underlying experiments, e.g., the resolution of the digital images, and of the registration, segmentation and, where applicable, smoothing procedures. In general, they are non-periodic and, accordingly, cannot be used directly with the periodic homogenization techniques discussed in section 5.

[47] For uniform boundary conditions it can be shown that the overall elastic behavior of matrix–inclusion type composites can be bounded by approximating the actual shape of particles by inner and outer envelopes of "smooth" shape, e.g., inscribed and circumscribed ellipsoids. This is known as the Hill modification theorem (or Hill's comparison theorem, Hill's auxiliary theorem), compare Hill (1963) and Huet et al. (1990). Approximations of actual inhomogeneity shapes by ellipsoids typically work considerably better for convex than for non-convex particle shapes (Kachanov and Sevostianov, 2005).

Sizes of Volume Elements

When complex discrete phase arrangements are employed in discrete microfield simulations the predicted macroscopic responses predicted from small volume elements has been found to show a marked dependence on colume element size, see, e.g., Iorga et al. (2008). This immediately raises the question of the size of volume element required for adequately capturing the macroscopic physical behavior of the material to be studied. On the one hand, the requirement of limiting numerical costs obviously puts a premium on using the smallest viable volume element but, on the other hand, accuracy requirements are best fulfilled by using close approximations to representative volume elements (RVEs, compare section 1.3). These conflicting demands led to the concepts of "minimum RVEs" by Ren and Zheng (2004) and of statistical RVEs (SRVEs) by Trias et al. (2006).

When the philosophy of geometrical RVEs is followed, the assessment of a suitable size of volume element for analysis can be made on the basis of the microgeometry of the inhomogeneous material, the physical property to be modeled playing no role. In this context adequate sizes of model geometries may be estimated, e.g., on the basis of experimentally obtained correlation lengths (Bulsara et al., 1999) or covariances (Jeulin, 2001) of the phase arrangement or by posing the requirement of having at least two statistically independent inhomogeneities in the volume element (Zeman and Šejnoha, 2001). Such approaches have proven successful for micromechanical models of the elastic behavior of inhomogeneous materials. The concept of physical RVEs, in contrast, implies that the suitability of a given size of volume element for micromechanical modeling depends on the physical property to be studied. This suitability can be assessed via windowing analysis, compare chapter 7, identical predictions of the macroscopic behavior with macroscopically homogeneous stress and strain boundary conditions, respectively, being a necessary condition for physical RVEs. Weaker criteria involve comparisons of macroscopic properties (e.g., moduli) or responses (e.g., homogenized stress vs. strain curves) between different volume elements of equal size, or deviations from some macroscopic material symmetry. A comparison of different geometry and microfield based criteria for choosing the size of model geometries was given by Trias et al. (2006).

Assessments based on geometry alone or on the overall elastic behavior predict that relatively small volume elements can give quite accurate results. Zeman (2003) reported that the transverse elastic behavior of composites reinforced by continuous fibers can be satisfactorily described by unit cells containing reconstructed arrangements of 10 to 20 fibers. Using a nonlocal Hashin–Shtrikman model Drugan and Willis (1996) found that for statistically isotropic composites consisting of a matrix reinforced by spherical particles volume elements with sizes of some two and five particle diameters are sufficient for obtaining errors of less than 5% and less than 1%, respectively, in terms of the macroscopic elastic behavior irrespective of the particle volume fraction. Considerably larger volume elements are required for aligned ellipsoidal inhomogeneity, the independence of the model size from the volume fraction being lost (Monetto and Drugan, 2009).

When inelastic constituent behavior is present, however, a number of numerical studies (Zohdi, 1999; Jiang et al., 2001; Böhm and Han, 2001) have indicated that larger volume elements may be required for satisfactorily approximating the overall symmetries and

obtaining good agreement, especially at elevated strains, between the responses of phase arrangements designed to be statistically equivalent. The reason for this behavior lies in the marked inhomogeneity of the microscopic strain fields that is typically present in nonlinear composites. For example, there tend to be contiguous zones of high plastic strains, which can evolve to become considerably larger than individual geometrical inhomogeneities, thus effectively introducing a new length scale into the problem[48].

When a number of volume elements of comparable size and pertaining to a given composite are available, they may be viewed as being realizations of some statistical process. In the typical case, where individual model geometries obtained by a computer model or from real structures are smaller than proper RVEs, ensemble averaging over a number of results obtained from such equivalent volume elements can be used to obtain improved estimates for the effective material properties, compare, e.g., Kanit et al. (2003) and Stroeven et al. (2004). The number of different volume elements required for a given accuracy of the ensemble averages decreases as the sizes of the models increase (Khisaeva and Ostoja-Starzewski, 2006). Finally, it is worth mentioning that the size of volume elements affects not only the macroscopic responses of composites but also the microfields, which tend to be less sensitive to boundary condition effects when large phase arrangements are studied (Shen and Brinson, 2006).

4.2 Numerical Engineering Methods

The majority of published continuum micromechanical analyses of discrete microstructures have employed standard numerical engineering methods for resolving the microfields. Work reported in the literature has used Finite Difference (FD) and Finite Volume algorithms, compare Adams and Doner (1967) and Bansal and Pindera (2006), spring lattice models, compare Ostoja-Starzewski (1996), the Boundary Element Method (BEM), compare Achenbach and Zhu (1989) or Liu et al. (2005b), as well as the Finite Element Method (FEM) and its developments such as Extended Finite Element Methods, mesh-free and particle methods, compare Sukumar et al. (2001) and Missoum-Benziane et al. (2007), or FE-based discrete dislocation models (Cleveringa et al., 1997). Generally speaking, spring lattice models tend to have advantages in handling pure traction boundary conditions and in modeling the progress of microcracks due to local (brittle) failure. Boundary elements tend to be at their best in studying geometrically complex linear elastic problems.

In addition, techniques using Fast Fourier Transforms (FFT), compare Moulinec and Suquet (1994), and Discrete Fourier Transforms (DFT), compare Müller (1996), have been used. They were mainly applied to analyzing periodic phase arrangements, for which they tend to be highly efficient, compare, e.g., Michel et al. (1999), and their fixed regular

[48]For elastoplastic matrices, weaker strain hardening tends to give rise to more inhomogeneous microstrains, which leads to a requirement for bigger volume elements that contain a higher number of inhomogeneities. Very large volumes tend to be necessary when one of the phases shows softening, e.g., due to damage (Zohdi and Wriggers, 2001; Swaminathan and Ghosh, 2006; Gitman, 2006). Eliminating the dependence of the homogenized response on the size of the SRVE may, in fact, be impossible (Gitman et al., 2007) in the latter case. For elastic polycrystals, the anisotropy and shape of the grains were also reported to influence the required size of volume elements (Ren and Zheng, 2004).

grids make them also well suited for for studying the evolution of microstructures (Dreyer et al., 1999). The Transformation Field Analysis of Dvorak (1992) allows the prediction of the nonlinear response of inhomogeneous materials based on either mean field descriptions (compare the remarks in section 2.6) or on discrete microfield approximations. High computational efficiency is claimed for "classical" TFA models involving piecewise uniform transformation fields (Dvorak et al., 1994), but very fine discretizations of the phases are required to achieve good accuracy. A developed version of the TFA, the Nonuniform Transformation Field Analysis (Michel and Suquet, 2004) expands anelastic strains into a number of nonuniform, incompressible and orthogonal "plastic flow modes" to achieve efficient descriptions of the nonlinear mechanical behavior of inhomogeneous materials.

A number of further approaches that are specialized to continuum micromechanics are discussed in connection with periodic microfield analyses, see section 5. For all numerical engineering methods the characteristic length of the discretization ("mesh size") must be considerably smaller than the microscale of a given problem in order to obtain spatially well resolved results.

At present, the FEM is the most popular numerical scheme for evaluating discrete microgeometries, especially in the nonlinear range, where its flexibility and capability of supporting a wide range of constitutive models for the constituents and for the interfaces between them are especially appreciated[49]. An additional asset of the FEM in the context of continuum micromechanics is its ability to handle discontinuities in the stress and strain components (which typically occur at interfaces between different constituents) in a natural way via appropriately placed element boundaries.

Applications of the FEM to micromechanical studies tend to fall into four main groups, compare fig. 4.1. In most published works the phase arrangements are discretized by an often high number of "standard" continuum elements, the mesh being designed in such a way that element boundaries (and, where appropriate, special interface elements) are positioned at all interfaces between constituents. Such approaches use unstructured meshes and have the advantage that in principle any microgeometry can be discretized at a prescribed level of accuracy. The resulting meshes are suitable for analysis with readily available commercial FE packages. However, the actual modeling of complex phase configurations in many cases requires sophisticated and/or specialized preprocessors for generating the mesh, a task that may be work intensive and has been found to be difficult to automatatize[50]. In addition, the resulting stiffness matrices may show unfavorable conditioning due to suboptimal element shapes and the requirement of satisfactory resolution of the microfields at local "hot spots" (e.g., between closely neighboring reinforcements) can lead to very large models indeed. Nevertheless, the possibility of providing for mesh refinements where they

[49] Constitutive models for constituents used in FEM-based micromechanics have included a wide range of elastoplastic, viscoelastoplastic and continuum damage mechanics descriptions as well as crystal plasticity models, see, e.g., McHugh et al. (1993), and nonlocal models, compare Bassani et al. (2001) and Drabek and Böhm (2006). In addition, the FEM has supported a range of modeling options for interfaces between phases.

[50] Most preprocessors for Finite Element analysis are not geared towards discretizing matrix–inclusion topologies with thin matrix bridges between closely approaching inclusions. Other major sources of difficulties are intersections between phase and cell boundaries at very acute or obtuse angles and the generation of periodic meshes for PMAs.

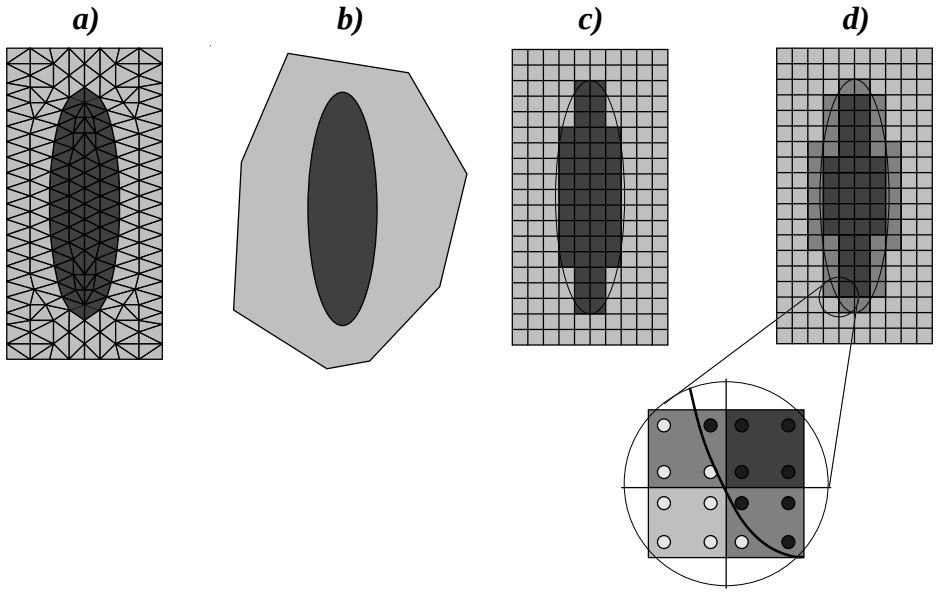

Figure 4.1: Sketch of FEM approaches used in micromechanics: a) discretization by standard elements, b) special hybrid elements, c) pixel/voxel discretization, d) "multi-phase elements"

are required and of using standard mesh refinement approaches are major strengths of this discretization strategy.

Alternatively, a smaller number of special hybrid elements may be used, which are specifically formulated to model the deformation, stress, and strain fields in an inhomogeneous region consisting of a single inhomogeneity or void together with the surrounding matrix on the basis of some appropriate analytical theory (Accorsi, 1988). The most highly developed approach of this type at present is the Voronoi Finite Element Method (Ghosh et al., 1996), in which the mesh for the hybrid elements is obtained from Voronoi tessellations based on the positions of the reinforcements. Large planar multi-inclusion arrangements can be analyzed this way using a limited number of (albeit rather complex) elements, and good accuracy as well as significant gains in efficiency have been claimed. Numerous damage models have been implemented into the method and an extension to three dimensions was reported recently (Ghosh and Moorthy, 2004). Modeling approaches of this type are specifically tailored to inhomogeneous materials with matrix–inclusion topologies.

A computational strategy that occupies an intermediate position between the above two approaches uses static condensation to remove the degrees of freedom of the interior nodes of the inhomogeneities (or, in the case of coated reinforcements, of inhomogeneities and interface) from the stiffness matrix of a heterogeneous volume element (Liu et al., 2005a).

Especially when the phase arrangements to be studied are based on digital images of actual microgeometries, a third approach for discretizing microgeometries of interest. It consists of using a structured mesh that consists of regular, rectangular or hexahedral elements of fixed size and has the same resolution as the digital data, each element being

assigned to one of the constituents by operations such as thresholding of the grey values of the corresponding pixel or voxel, respectively. Such meshes have the advantage of allowing a straightforward automatic model generation from appropriate experimental data (metallographic sections, tomographic scans) and of avoiding ambiguities in smoothing the digital data (which are generally present if a "standard" FE mesh is employed to discretize experimental data of this type). Obviously "pixel element" and "voxel element" strategies lead to ragged phase boundaries, which may give rise to some oscillatory behavior of the solutions (Niebur et al., 1999), can cause high local stress maxima (Terada et al., 1997), may degrade accuracy, and restrict detailed modeling of interfacial effects. Such "digital image based" (DIB) models are, however, claimed not to cause unacceptably large errors even for relatively coarse discretizations, at least in the linear elastic range (Guldberg et al., 1998). Good spatial resolution, i.e., a high number of pixels or voxels, of course, is especially beneficial in such models.

A fourth approach also uses structured FE meshes, but assigns phase properties at the integration point level of standard elements ("multi-phase elements"), see, e.g., Schmauder et al. (1996) or Quilici and Cailletaud (1999). Essentially, this amounts to trading off ragged boundaries at element edges for smeared-out (and typically degraded) microfields within those elements that contain a phase boundary, because stress or strain discontinuities within elements cannot be adequately handled by standard FE shape functions. With respect to the element stiffnesses the latter concern can be much reduced by over-integrating elements containing phase boundaries, which leads to good approximations of integrals involving non-smooth displacements by numerical quadrature, see Zohdi and Wriggers (2001). The resulting stress and strain distributions, however, remain smeared-out approximations in elements that contain phase boundaries, the rate of convergence of the microfields being accordingly slow. Multiphase element models also are limited in their capabilities for detailed modeling of interfaces. Some of the above drawbacks are avoided by algorithmic developments such as Extended Finite Element methods, which use a background mesh that does not have to conform to phase boundaries, which are accounted for, e.g., by appropriately enriching the shape functions (Moës et al., 2003).

A fairly recent development for studying microgeometries involving a considerable number of inhomogeneities (tens to thousands) by Finite Element methods involves programs specially geared towards solving micromechanical problems. Such codes may be based on matrix-free iterative solvers such as Conjugate Gradient (CG) methods, analytical solutions for the microfields (e.g., constant strain approximations corresponding to the upper Hill bounds, eqn. (3.1), being used as starting solutions to speed convergence[51]. For studies involving such programs see, e.g., Gusev (1997), Zohdi and Wriggers (2001) or Arbenz et al. (2008). Fast solvers of this type open the possibility of solving inverse problems, e.g., for finding optimal particle shapes for given load cases and damage modes, compare Zohdi (2003).

Special Finite Element formulations (and, as a consequence, dedicated Finite Element programs) are typically required for asymptotic homogenization models (compare section 5.3) and for other schemes that concurrently solve the macroscopic and microscopic prob-

[51]Essentially, in such a scheme the initial guess gives a good estimate of "long wavelength" contributions to the solution, and the CG iterations take care of "short wavelength" variations.

lems, see, e.g., Urbański (1999).

Discrete microgeometry approaches employing numerical engineering methods are best suited for phase arrangements in which the characteristic lengths of important geometrical features do not differ markedly. If this is not the case, very large volume elements may be required, meshing tends to become very difficult, and the numerical effort for studying the models may become excessive, especially for three-dimensional configurations. Typical cases in point are composites reinforced by short fibers with aspect ratios in excess of, say, 25 or by polydispersely sized particles for which the minimum and maximum diameters differ by more than a factor of, say, 5.

4.3 Evaluation of Results

When elastic or thermoelastic inhomogeneous materials are studied, the major aim of homogenization in discrete microstructure approaches consists in evaluating the effective tensors, $\mathbf{E}^*$ and $\boldsymbol{\alpha}^*$. In homogenization studies of elastoplastic, thermoelastoplastic or viscoelastoplastic materials, in contrast, usually the evolution of appropriate scalar macroscopic variables is followed, e.g., in the form of stress–strain diagrams[52].

In general six linearly independent mechanical load cases must be applied to the volume element for evaluating macroscopic elastic tensors, and a homogeneous temperature change is required for obtaining the macroscopic thermal expansion tensor. The effective elastic tensors of inhomogeneous materials with orthotropic or higher symmetry show the same structure as those of isotropic or transversely isotropic symmetry, see eqns. 1.9 and 1.10, i.e., in Nye notation all terms are zero with the exception of the upper left submatrix and the diagonal of the lower right submatrix. However, volume elements corresponding to real structures or obtained with stochastics-based computer models in general show lower symmetries. This is mainly due to their limited size, which introduces "sub-orthotropic" contributions into the elastic matrix that are smaller than the "orthotropic contributions" discussed above, but do not vanish. In addition, small perturbations of the tensor elements due to roundoff errors in the numerical engineering methods must be expected.

Accordingly, volume elements aimed at describing statistically isotropic, transversely isotropic or orthotropic material behavior actually return lower material symmetries. These errors, which tend to decrease with growing size of the volume elements, can in principle be corrected by looking for that elastic tensor of the required symmetry which is closest to the "raw" elastic tensor evaluated from homogenization, resulting in optimization problems. Little pertinent work, however, has been published. Pahr and Böhm (2008) proposed a simplified approach in which the sub-orthotropic contributions to the elastic tensor of a unit cell like the one shown in fig. 5.4, which aims at describing a statistically isotropic composite, is coarsely "orthotropized" by setting all sub-orthotropic terms to zero and,

[52]Homogenized tangent tensors for given load states can also be evaluated, compare, e.g., (Ghosh et al., 1996). This is of interest mainly in multi-scale analysis employing discrete microstructure models as implicit material models for Finite Element models on the macroscale.

if necessary, symmetrizing the "raw tensor"[53]. The closest isotropic tensor to such an "orthotropized" elastic tensor can then be obtained as the isotropic term of a generalized spherical harmonics expansion of the orthotropic elongation and bulk modulus orientation distribution functions, using expressions developed by He and Curnier (1997); for an alternative approach to finding the isotropic tensor that is closest to an elasticity tensor of general anisotropy see Norris (2006). Moduli evaluated from the resulting "isotropized" elasticity tensor provide better approximations to effective moduli than do averages over, say, tensile responses in the coordinate directions.

Microscopic fields can usually be directly obtained from the numerical engineering methods. Some care is necessary, however, because, on the one hand, the extreme values of microscopic stresses and strains tend to depend markedly on details of the microgeometry and, on the other hand, idiosyncrasies of the numerical methods may come into play. For example, due to limitations in the extrapolation and averaging algorithms used by Finite Element methods stresses and strains tend to be evaluated with lower accuracy at phase boundaries than within bulk phases.

For evaluating phase averaged quantities from unit cell analyses, it is good practice to use direct volume integration according to eqn. (1.13)[54]. In many FE codes this can be done by approximate numerical quadrature according to

$$\langle f \rangle = \frac{1}{\Omega} \int_{\Omega} f(\mathbf{z}) d\Omega \approx \frac{1}{\Omega} \sum_{l=1}^{N} f_l \, \Omega_l \tag{4.1}$$

Here f_l and Ω_l are the function value and the integration weight (in terms of the volume of the integration point), respectively, associated with the l-th integration point within a given integration volume Ω that contains N integration points[55] When macroscopic values or phase averages are to be generated of variables that are nonlinear functions of the stress or strain components (e.g., equivalent stresses, equivalent strains, stress triaxialities), only direct volume averaging should be used, because evaluation of nonlinear variables on the basis of averaged components may lead to unacceptable inaccuracies, compare also section 2.6. Besides generating overall and phase averages, microscopic variables can also be evaluated in terms of averages in individual inhomogeneities. In addition, distribution functions ("stress spectra", see, e.g., Bornert et al. (1994), Böhm and Rammerstorfer (1995) or Böhm and Han (2001)) and higher statistical moments of microfields can be evaluated from discrete microstructure models for the whole composite, for a given phase or for individual inhomogeneities, compare the fiber level standard deviations of the maximum principal stress displayed in fig. 2.3.

[53] Actually, in finding the orthotropic elasticity tensor that is closest to a "raw" elastic tensor the orientations of the former's principal axes must also be considered. In "raw" elastic tensors obtained by periodic homogenization, compare section 5, typically only very small deviations from symmetry due to roundoff errors are found, whereas applying windowing methods, compare section 7, to sub-orthotropic volume elements can give rise to considerably higher anisotropies.

[54] It is of some practical interest that volume averaged and phase averaged microfields obtained from discrete microfield analysis must fulfill all relations given in section 2.1 and can thus be conveniently used to check the consistency of a given model by inserting them into eqns. (2.5). Note, however, that for finite deformations appropriate stress and strain measures must be used for this purpose (Nemat-Nasser, 1999).

[55] Such procedures may also be used for evaluating other volume integrals, e.g., in computing Weibull-type fracture probabilities for reinforcements (Antretter, 1998; Böhm et al., 2002).

Chapter 5

Periodic Microfield Models

Periodic Microfield Approaches (PMAs) aim at approximating the macroscopic and microscopic behavior of inhomogeneous materials by studying model materials that have periodic microstructures.

5.1 Basic Concepts of Unit Cell Models

Periodic microfield approaches analyze the behavior of infinite (one, two- or three-dimensional) periodic phase arrangements under the action of far field mechanical loads or uniform temperature fields[56]. The most common approach for studying the stress and strain fields in such periodic configurations is based on describing the microgeometry by a periodically repeating unit cell[57] (RUC) to which the investigations may be limited without loss of information or generality, at least for static analysis[58].

The literature on periodic microfield models of inhomogeneous materials is fairly extensive, and well developed mathematical theories are available on scale transitions in periodic structures, compare Michel et al. (2001). A wide variety of unit cells have been

[56]Standard PMAs cannot handle macroscopic gradients in mechanical loads, temperature or composition in any direction in which periodicity of the fields is prescribed. Gradients and free boundaries can be studied, however, in directions where periodicity is not prescribed, a typical case being layer-type models that are non-periodic in one direction and periodic in the other(s), see, e.g., Wittig and Allen (1994), Reiter et al. (1997) and Weissenbek et al. (1997).

[57]In the present work the designation "unit cell" is used for any volume element that can generate a periodic microgeometry. Accordingly, a unit cell may comprise a simple periodic base unit (or part of it), a collective of simple periodic base units, or a phase arrangement of arbitrary geometrical complexity (multi-fiber or multi-particle unit cell) that shows translational periodicity. With increasing size unit cells approximate geometrical and/or physical RVEs increasingly more closely.

[58]Periodic phase arrangements are typically not well suited to dynamic analysis, because they act as filters that exclude all waves with frequencies outside certain bands, see, e.g., Suzuki and Yu (1998). In addition, due to the boundary conditions required for obtaining periodicity, unit cell methods can only handle wavelengths that are smaller than or equal to the relevant cell dimension, and only standing waves can be dealt with.
In analogy, in stability analysis unit cells can directly resolve only buckling modes of specific wavelengths, so that considerable care is required in using them for such purposes, compare Vonach (2001) as well as Pahr and Rammerstorfer (2006). However, bifurcation modes with wavelengths exceeding the size of the unit cell can be resolved in periodic linear models by using the Bloch theorem from solid state physics (Gong et al., 2005).

employed in such studies, ranging from geometries that describe simple periodic arrays of inhomogeneities to highly complex phase arrangements, such as multi-inhomogeneity unit cells ("supercells"). For some simple periodic phase arrangements and for linear material behavior it has proved possible to find analytical solutions based on series expansions that make explicit use of the periodicity (Sangani and Lu, 1987; Cohen, 2004) or on appropriate potential methods (Wang et al., 2000).

Even though most PMA studies in the literature have used standard numerical engineering methods as described in chapter 4, other numerical schemes have been proposed that are specialized to periodic phase arrangements. One of them, known as the Method of Cells (Aboudi, 1989, 1991), in its basic form discretizes unit cells that correspond to square arrangements of square fibers into four subcells, within each of which displacements are approximated by low-order polynomials. Traction and displacement continuity conditions at the faces of the subcells are imposed in an average sense and analytical and/or semi-analytical approximations to the deformation fields are obtained in the elastic and inelastic ranges. While using highly idealized microgeometries, providing only limited information on the microscopic stress and strain fields, and having limited capabilities for handling axial shear, the resulting models pose relatively low computational requirements and can be used as a constitutive model for analyzing structures made of continuously reinforced composites, see, e.g., Arenburg and Reddy (1991). Developments of the algorithm led to the Generalized Method of Cells (Aboudi, 1996), which is more flexible geometrically and allows finer discretizations of unit cells for fiber and particle reinforced composites, reinforcement and matrix being essentially split into a number of "subregions" of rectangular or hexahedral shape. For some comparisons with microfields obtained by Finite Element based unit cells see, e.g., Iyer et al. (2000) or Pahr and Arnold (2002). Recently, higher order displacement interpolants were introduced to obtain the High-Fidelity Generalized Method of Cells (Aboudi, 2004), which provides an alternative to Finite Element algorithms for "pixel element" micromechanical models (compare section 4.2).

A further group of solution strategies for PMAs reported in the literature (Axelsen and Pyrz, 1995; Fond et al., 2001; Schjødt-Thomsen and Pyrz, 2004) use numerically evaluated equivalent inclusion approaches that account for interacting inhomogeneities as provided, e.g., by the work of Moschovidis and Mura (1975). Alternatively, the elastic fields in periodic inhomogeneous materials can be evaluated numerically via variational approaches for determining stress-free strain fields (Wang et al., 2002).

In periodic homogenization the strain and stress fields are decomposed into constant macroscopic strain and stress contributions ("slow variables"), $\langle\boldsymbol{\varepsilon}\rangle$ and $\langle\boldsymbol{\sigma}\rangle$, and periodically varying microscopic fluctuations ("fast variables"), $\boldsymbol{\varepsilon}'(\mathbf{z})$ and $\boldsymbol{\sigma}'(\mathbf{z})$, in analogy to eqn. (1.1). Here $\mathbf{z}$ is a "microscopic coordinate" that has sufficient resolution for describing the variations on the microscale. The corresponding expression for the displacements takes the form (Michel et al., 1999)

$$\mathbf{u}(\mathbf{z}) = \langle\boldsymbol{\varepsilon}\rangle\mathbf{z} + \mathbf{u}'(\mathbf{z}) \qquad . \tag{5.1}$$

Volume integrals for obtaining averages, eqns.(1.3) and (1.5), must, of course, be solved over the volume of the unit cell, Ω_{UC}. Formal derivations of the above relationships for

periodically varying microstrains and microstresses show that the work done by the fluctuating stress and strain contributions vanishes, compare Michel et al. (2001).

Evidently, in periodic microfield approaches each unit of periodicity (unit cell) contributes the same increment of the displacement vector $\Delta\mathbf{u}$ so that the homogenized displacements vary (multi)linearly. An idealized depiction of such a situation is presented in fig. 5.1, which shows the variations of the strains $\varepsilon_{\mathrm{s}}(s) = \langle\varepsilon_{\mathrm{s}}\rangle + \varepsilon'_{\mathrm{s}}(s)$ and of the corresponding displacements $u_{\mathrm{s}}(s) = \langle\varepsilon_{\mathrm{s}}\rangle\, s + u'_{\mathrm{s}}(s)$ along some line s in a hypothetical periodic two-phase material consisting of constituents A and B. Obviously, the relation $\langle\varepsilon_{\mathrm{s}}\rangle = \Delta u_{\mathrm{s}}/c_{\mathrm{u}}$ holds for linear displacement–strain relations, where c_{u} stands for the length of a unit cell in direction s and Δu_{s} for the corresponding displacement increment. The periodicity of the strains and of the displacements is immediately apparent.

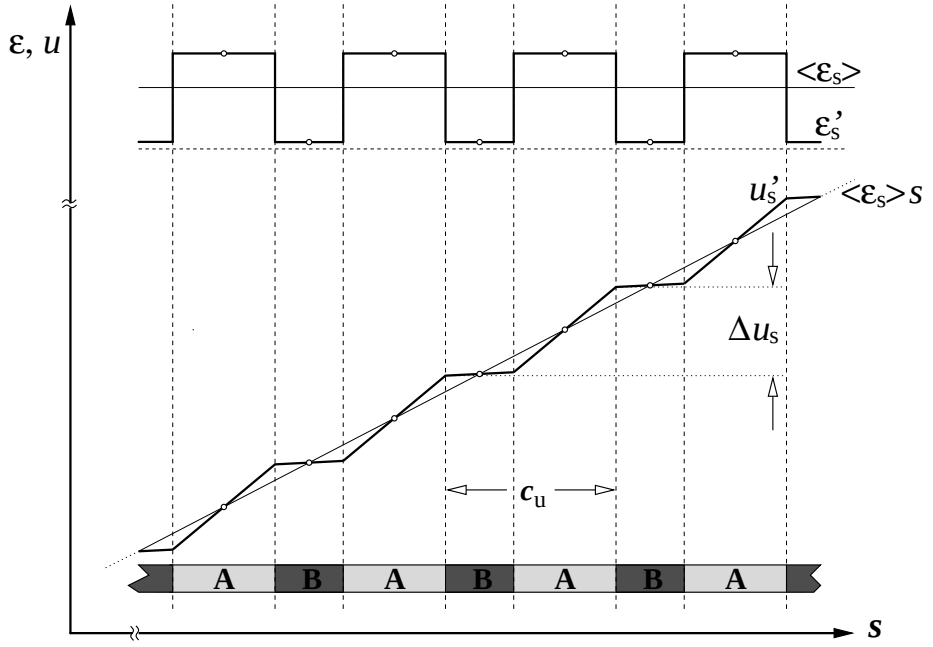

Figure 5.1: Schematic depiction of the variation of the strains $\varepsilon_{\mathrm{s}}(s)$ and the displacements $u_{\mathrm{s}}(s)$ along a generic "one-dimensional composite" (coordinate s) consisting of constituents A and B. Symmetry points of $\varepsilon_{\mathrm{s}}(s)$ and $u_{\mathrm{s}}(s)$ are indicated by small circles.

5.2 Boundary Conditions

Unit cells together with the boundary conditions (B.C.s) prescribed on them must generate valid tilings both for the undeformed geometry and for all deformed states pertinent to the investigation. Accordingly, gaps and overlaps between neighboring unit cells as well as unphysical constraints on their deformations must not be allowed, i.e., the cells must be geometrically compatible. In order to achieve this, the boundary conditions for the unit cells must be specified in such a way that all deformation modes appropriate for the load cases to be studied can be attained. The three major types of boundary conditions used in periodic microfield analysis are periodicity, symmetry, and antisymmetry (or point

symmetry) B.C.s[59]. In PMA models one of these three types of boundary conditions (or a combination of them) must be used, irrespective of the numerical method employed for solving the equilibrium equations.

Generally, for a given periodic phase arrangement unit cells are non-unique, the range of possible shapes being especially wide when point or mirror symmetries are present in the microgeometry. As an example, fig. 5.2 depicts a (two-dimensional) periodic hexagonal array of circular inhomogeneities (e.g., fibers oriented normally to the plane) and some of the unit cells that can be used to study aspects of the behavior of this phase arrangement. There are considerable differences in the sizes and capabilities of the unit cells shown.

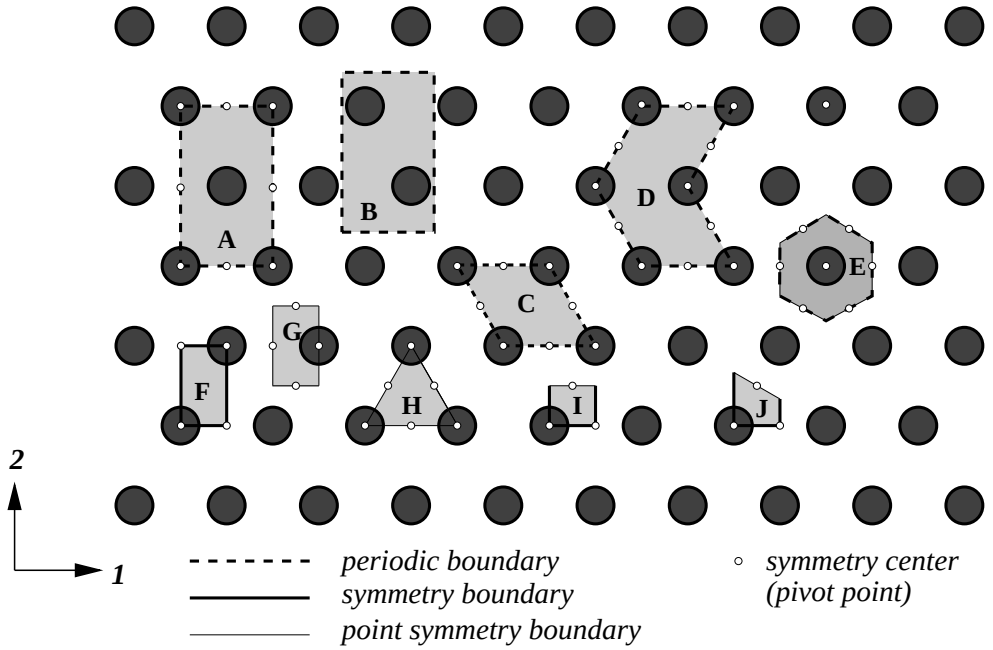

Figure 5.2: Periodic hexagonal array of circular inhomogeneities in a matrix and 10 unit cells that can be used to describe the mechanical responses of this arrangement under loads acting parallel to the coordinate axes.

In the following a nomenclature is used in which the faces of two-dimensional quadrilateral unit cells are denoted as N, S, E and W (for North, South, East, and West which are used as in topographical maps), vertices being named according to the adjoining cell faces, compare figs. 5.5, 5.6 and 5.7. The faces of three-dimensional cells of hexahedral shape are, in analogy, referred to as N, S, E, W, B and T (the latter standing for bottom and top), and edges as well as vertices are referred to by the adjoining faces (e.g., SE or SWB), see fig. 5.4.

[59]For more formal treatments of boundary conditions for unit cells than given here see, e.g., Anthoine (1995) or Michel et al. (1999). In the case of layer-type models, which can be generated by specifying free surfaces at appropriate boundaries, macroscopic rotational degrees of freedom, i.e., macroscopic bending and twisting, can be studied by appropriately modifying the above standard B.C.s. When such macroscopic rotational degrees of freedom are present, out-of-plane shear loads must be accompanied by appropriate bending moments to achieve stress equilibrium, compare, e.g., Urbański (1999).

Periodicity Boundary Conditions

The most general boundary conditions for unit cells in continuum micromechanics are periodicity ("toroidal", "cyclic") B.C.s, which can handle any physically valid deformation state of the cell and, consequently, of the inhomogeneous material to be modeled. Periodicity boundary conditions make use of translatoric symmetries of a given geometry; in fig. 5.2 cells A to E belong to this group.

In order to describe an N-dimensional phase arrangement with translatoric periodicity, a suitable unit cell and a set of N linearly independent periodicity vectors $\mathbf{p}_n$ are required. These periodicity vectors are neither unique nor do they have to be orthogonal. For any given periodic microgeometry the minimum volume of pertinent unit cells is well defined, but such "minimum unit cells" can take a wide range of shapes as is shown for a simple two-dimensional case in fig. 5.3. The surface of each proper unit cell must consist of at least N pairs of faces (or parts of faces) Γ_k, and the surface elements making up a pair, k^- and k^+, must be identical but shifted relative to each other by "shift vectors" $\mathbf{c}_k$. Each shift vector, in turn, must be a linear combination of the periodicity vectors, i.e., $\mathbf{c}_k = \sum_l c_l^k \mathbf{p}_l$, where the c_l^k are integer numbers. In fig. 5.3 pairs of faces (or, in the case of some cell, parts of faces) Γ_k are marked by being drawn with the same line style.

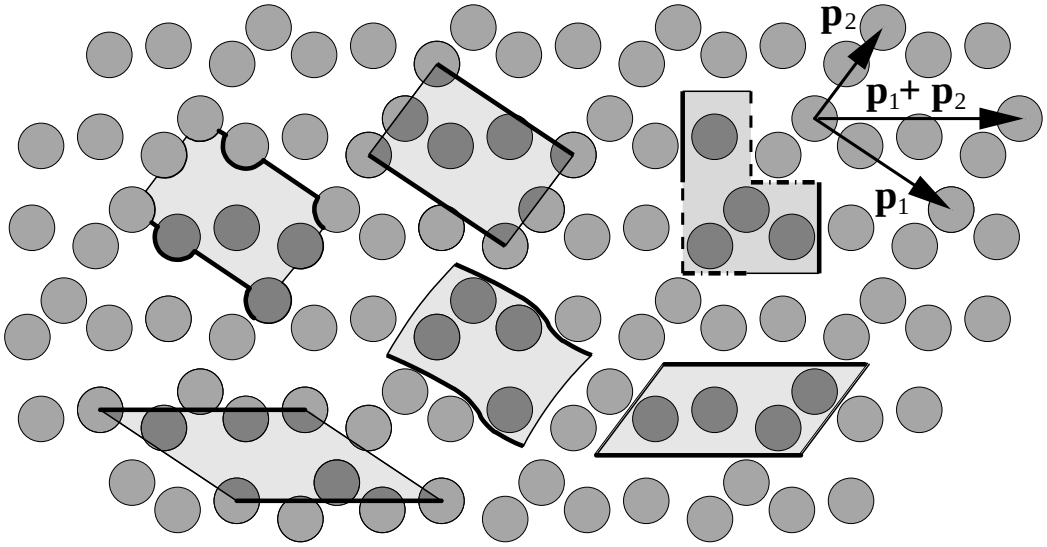

Figure 5.3: Six different but equivalent periodic minimum-size unit cells for a two-dimensional periodic matrix–inclusion medium with two (slightly) non-orthogonal translation vectors $\mathbf{p}_1$ and $\mathbf{p}_2$. Paired faces (or parts of faces) Γ_k are marked by identical line styles and regions belonging to one of the cells are highlighted by shading.

Computer generated periodic volume elements are often set up such that the translation vectors are orthogonal, which allows to generate unit cells that are rectangles or right hexahedra, compare fig. 5.4. Unit cells of simple shape to some extent facilitate the application of periodicity boundary conditions. However, low-angle intersections between phase boundaries and cell faces as well as phase boundaries that closely approach cell faces often make such cells difficult to mesh for FE analysis. This issues can be alleviated or avoided by choosing suitably shaped and positioned unit cells.

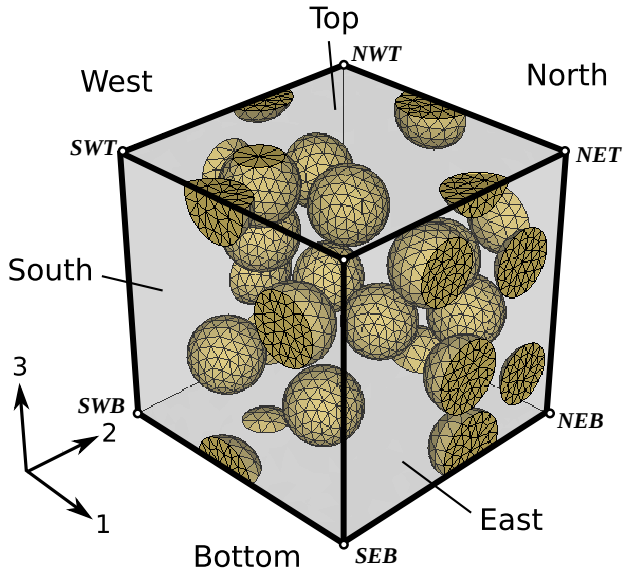

Figure 5.4: Cube-shaped periodic unit cell containing 15 randomly positioned spherical particles of equal size at a volume fraction of $\xi^{(i)}$=0.15. Designators of the six faces (East, West, North, South, Top, Bottom) and of the vertices are given (Pahr and Böhm, 2008).

Because the unit cells tile the computational space by translation, neighboring cells (and, consequently, the "opposite" faces of a given cell) must fit into each other like the pieces of a jigsaw puzzle in both undeformed and deformed states. For each pair of surface elements, Γ_k, eqn.(5.1) allows to express the boundary conditions for the mechanical problem in the small strain regime as

$$\Delta\mathbf{u}_k = \mathbf{u}_{k^+} - \mathbf{u}_{k^-} = \mathbf{u}(\tilde{\mathbf{s}}_k + \mathbf{c}_k) - \mathbf{u}(\tilde{\mathbf{s}}_k) = \langle\boldsymbol{\varepsilon}\rangle * \mathbf{c}_k \qquad , \tag{5.2}$$

where $\mathbf{u}_{k^+}$ and $\mathbf{u}_{k^-}$ are the displacements at corresponding points $\tilde{\mathbf{s}}_k + \mathbf{c}_k$ and $\tilde{\mathbf{s}}_k$ of the surface elements k^+ and k^- (which could, e.g., correspond to that faces N and S in fig. 5.4), respectively. $\tilde{\mathbf{s}}_k$ is a local coordinate on surface element k^- and $\langle\boldsymbol{\varepsilon}\rangle$ is the macroscopic strain, which is prescribed in displacement controlled analysis and must be determined in load controlled analysis. These conditions enforce a "seamless fit" between neighboring unit cells for all possible deformed states.

For the special case of initially rectangular two-dimensional unit cells, such as the one shown in fig. 5.5, this leads to the expressions

$$\mathbf{u}_{\mathrm{N}}(\tilde{s}_1) = \mathbf{u}_{\mathrm{S}}(\tilde{s}_1) + \mathbf{u}_{\mathrm{NW}} \qquad \mathbf{u}_{\mathrm{E}}(\tilde{s}_2) = \mathbf{u}_{\mathrm{W}}(\tilde{s}_2) + \mathbf{u}_{\mathrm{SE}} \qquad , \tag{5.3}$$

where vertex SW is assumed to be fixed. Equations (5.3) directly imply that

$$\mathbf{u}_{\mathrm{NE}} = \mathbf{u}_{\mathrm{NW}} + \mathbf{u}_{\mathrm{SE}} \qquad .$$

For numerical analysis the two faces making up a pair Γ_k must be discretized in a compatible way, i.e., the nodal points on then must be positioned at equal values of the "face coordinates" $\tilde{\mathbf{s}}_k$. Equations (5.2) then become sets of linear constraints each of which links

three nodal displacement DOFs[60]. Comparing eqns.(5.2) and (5.3) shows that the displacements of the "master nodes" SE and NW contain the information on the macroscopic strain tensor $\langle \boldsymbol{\varepsilon} \rangle$. In addition, the displacements of the master nodes and of faces S and W fully control the displacements of the "slave faces" N and E.

Conditions analogous to eqn. (5.3) can be specified for any periodic, space-filling and regular two-dimensional cell that has an even number of sides (squares, rectangles, and hexagons) or three-dimensional cell that has an even number of faces (cubes, hexahedra, rhombic dodecahedra, and regular tetrakaidecahedra). The scheme can also be extended to unit cells of less regular shape that have even numbers of faces, compare Cruz and Patera (1995) or Xia et al. (2003) as well as figs. 5.2 and 5.3. Periodicity B.C.s generally are the least restrictive option for multi-inhomogeneity unit cell models using phase arrangements generated by statistics-based algorithms.

In practice FE-based unit cell studies using periodicity boundary conditions can be rather expensive in terms of computing time and memory requirements, because the multi-point constraints required for implementing eqn. (5.3) or its equivalents tend to degrade the band structure of the system matrix, especially in three-dimensional problems. In addition it is worth noting that — especially for simple phase arrangements — care may be required to prevent over- and underconstraining due to inappropriate selection of regions with periodicity boundary conditions, compare Pettermann and Suresh (2000).

Symmetry Boundary Conditions

For rectangular and hexahedral unit cells in which the faces of the cell coincide with symmetry planes of the phase arrangement and for which this property is retained for all deformed states that are to be studied, periodicity B.C.s simplify to symmetry boundary

[60] In principle, all variables (i.e., for mechanical analysis the displacements, strains and stresses) must be linked by appropriate periodicity conditions. When a displacement based FE code is used, however, such conditions can be specified explicitly only for the displacement components (including, where appropriate, rotational DOFs). The periodicity of the stresses is then typically fulfilled only approximately, mainly because in most implementations nodal stresses are not averaged across cell boundaries, even though they ought to be.
As a consequence of the periodicity of stresses the traction vectors at unit cell boundaries are antiperiodic.

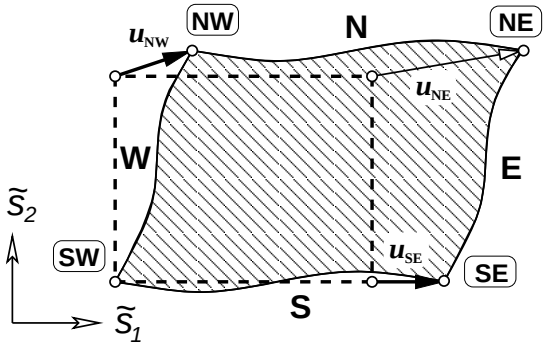

Figure 5.5: Sketch of periodicity boundary conditions as used with an initially rectangular two-dimensional unit cell.

conditions. Following the nomenclature of fig. 5.6 these B.C.s take the form

$$u_{\mathrm{E}}(\tilde{s}_2) = u_{\mathrm{SE}} \qquad v_{\mathrm{N}}(\tilde{s}_1) = v_{\mathrm{NW}} \qquad u_{\mathrm{W}}(\tilde{s}_2) = 0 \qquad v_{\mathrm{S}}(\tilde{s}_1) = 0 \qquad , \tag{5.4}$$

where u and v stand for the displacement components in 1- and 2-direction, respectively. Equation (5.4) puts constraints on the normal components of the at the unit cells' surfaces, but leaves the tangential displacements free, thus enforcing the condition that pairs of master and slave faces must stay parallel throughout the deformation history. For symmetry B.C.s there are no requirements with respect to compatibility of phase arrangements or meshes at different faces.

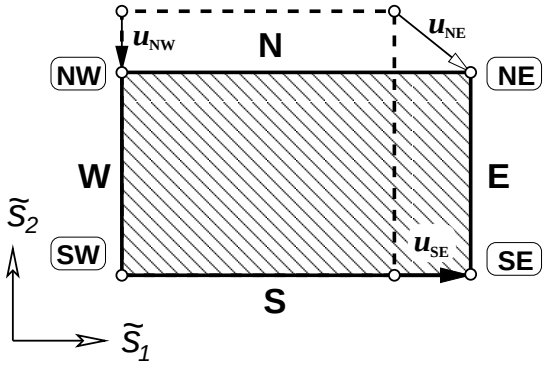

Figure 5.6: Sketch of symmetry boundary conditions as used with a rectangular two-dimensional unit cell.

Symmetry boundary conditions are fairly easy to use and tend to give rise to small unit cells for simply periodic phase arrangements. However, the load cases that can be handled are limited to uniform thermal loads, mechanical loads that act in directions normal to one or more pairs of faces, and combinations of the above[61]. In fig. 5.2 unit cell F uses boundary conditions of this type. Symmetry boundary conditions are typically very useful for describing relatively simple microgeometries, but tend to be restrictive for modeling phase arrangements generated by statistics-based algorithms or obtained from micrographs.

Antisymmetry Boundary Conditions

Antisymmetry (or point symmetry) boundary conditions require the presence of centers of point symmetry ("pivot points") and are, accordingly, even more limited in terms of the microgeometries that they can handle. In contrast to symmetry boundary conditions, however, unit cells employing them on all faces are subject to few restrictions with respect to the load cases that can be handled. Among the unit cells shown in fig. 5.2, cells G and H use point symmetry B.C.s on all faces and can handle any in-plane deformation[62].

[61] Because these load cases include different normal loads acting on each pair of faces, loading by macroscopic extensional shear (obtained, e.g., in the two-dimensional case by applying normal stresses σ_{a} to the vertical and $-\sigma_{\mathrm{a}}$ to the horizontal faces), hydrostatic loading, and (hygro)thermal loading, symmetry B.C.s are typically sufficient for materials characterization. However, for macroscopically anisotropic materials the normal and shear stresses evaluated as above do not pertain to the same coordinate system because extensional shear corresponds to simple shear in a coordinate system rotated by 45°.

[62] Triangular unit cells similar to cell H in fig. 5.2 were used, e.g., by Teply and Dvorak (1988) to study the transverse mechanical behavior of hexagonal arrays of fibers. Rectangular cells with point symmetries

Alternatively, antisymmetry B.C.s can be combined with symmetry B.C.s to obtain very small unit cells that are restricted to loads acting normal to the symmetry faces, compare unit cells I and J in fig. 5.2. Figure 5.7 shows such a "reduced" unit cell, the antisymmetry boundary conditions being applied on face E where a pivot point P is present. For this configuration the boundary conditions

$$\begin{aligned} \mathbf{u}_{\mathrm{U}}(\tilde{s}_{\mathrm{P}}) + \mathbf{u}_{\mathrm{L}}(-\tilde{s}_{\mathrm{P}}) &= 2\mathbf{u}_{\mathrm{P}} \\ v_{\mathrm{N}}(\tilde{s}_1) &= v_{\mathrm{NW}} = 2v_{\mathrm{P}} \qquad v_{\mathrm{S}}(\tilde{s}_1) = 0 \qquad u_{\mathrm{W}}(\tilde{s}_2) = 0 \qquad , \end{aligned} \tag{5.5}$$

must be fulfilled, where $\mathbf{u}_{\mathrm{U}}(\tilde{s}_{\mathrm{P}})$ and $\mathbf{u}_{\mathrm{L}}(-\tilde{s}_{\mathrm{P}})$ are the displacement vectors of pairs of points U and L that are positioned symmetrically with respect to the pivot point P. As indicated in fig. 5.7 the local coordinate system $\tilde{s}$ is defined on face E and centered on P. The undeformed geometry of such a face also must be antisymmetric with respect to the pivot point P, and the phase arrangements as well as the discretizations on both halves of face E must be compatible. Three-dimensional unit cells employing combinations of symmetry and point symmetry B.C.s can, e.g., be used to advantage for studying cubic arrays of particles, see Weissenbek et al. (1994).

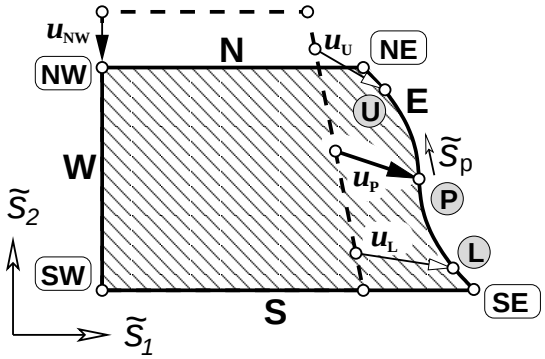

Figure 5.7: Sketch of a quadrilateral two-dimensional unit cell that combines antisymmetry boundary conditions on face E with symmetry boundary conditions on faces N, S and W.

Within the nomenclature of fig. 5.7, the displacements at the master nodes SE and NW, $\mathbf{u}_{\mathrm{SE}}$ and $\mathbf{u}_{\mathrm{NW}}$, control the overall deformation of the unit cell in the 1- and 2-directions and can be used to evaluate the macroscopic strain of the corresponding periodic model material, compare eqn. (5.15). With respect to unit cell models that use the FEM for evaluating the microfields, it is worth noting that all of the above types of boundary conditions can be handled by any code that provides linear multipoint constraints between degrees of freedom and thus allows the linking of three or more D.O.F.s by linear equations.

Obviously, the description of real materials, which in general are not periodic, by periodic model materials entails some geometrical approximations. In the case of real structure geometries this may entail applying periodicity constraints to non-periodic geometries or modifying the geometries such that they become periodic[63]. The effects of such approximations are perturbations in the vicinity of the cell surfaces which diminish in importance

on each boundary were introduced by Marketz and Fischer (1994) for perturbed square arrangements of inhomogeneities. The periodic cells D and E also show point symmetry on their faces.

[63]The simplest way of "periodifying" a non-periodic rectangular or cuboidal volume element consists

with growing size of the model. At least in the linear range the use of windowing with appropriate mixed boundary conditions, compare chapter 7, provides a superior alternative to such ad-hoc "periodification" procedures.

Periodicity boundary conditions that are conceptually similar to eqn. (5.3) can be devised for cases where standard conditions for homogenization are not met, gradient (nonlocal) theories are employed on the macroscale, and higher-order stresses as well as strain gradients figure in coupling the length scales (Geers et al., 2001b).

5.3 Application of Loads and Evaluation of Fields

Once suitable unit cells have been defined and appropriate boundary conditions applied, the volume elements must be subjected to appropriate loads in the form of macroscopic stresses, strains and/or temperature excursions, i.e., the microscopic and macroscopic fields must be linked. Whereas loading by uniform temperature differences does not pose major difficulties, applying far field stresses or strains is not necessarily straightforward. For example, the variations of the stresses along the faces of a unit cell in general are not known a priori, so that it is not possible to prescribe the boundary tractions via distributed loads. There are two major approaches to implementing the micro–macro linkage.

Asymptotic Homogenization

The most versatile and elegant strategy for linking the macroscopic and microscopic fields in periodic microfield models is based on a mathematical framework referred to as asymptotic homogenization, asymptotic expansion homogenization, or homogenization theory, see, e.g., Suquet (1987). It is based on explicitly introducing macroscopic and microscopic coordinates, $\mathbf{Z}$ and $\mathbf{z}$, respectively, into the formulation of the problem. The microscopic and macroscopic coordinates are linked by the expression

$$z_i = x_i/\epsilon \tag{5.6}$$

where $\epsilon = \ell/L \ll 1$ is a scaling parameter. L and ℓ stand for the characteristic lengths of the macro- and microscales[64]. The displacement field in the unit cell can then be represented by an asymptotic expansion of the type

$$u_i(\mathbf{Z},\mathbf{z},\epsilon) = u_i^{(0)}(\mathbf{Z}) + \epsilon\, u_i^{(1)}(\mathbf{Z},\mathbf{z}) + \epsilon^2\, u_i^{(2)}(\mathbf{Z},\mathbf{z}) + \text{H.O.T.} \qquad , \tag{5.7}$$

where the $u_i^{(0)}$ are the effective or macroscopic displacements and $u_i^{(1)}$ stands for the periodically varying displacement perturbations due to the microstructure[65].

in mirroring it with respect to 2 or 3 of its surfaces, respectively, and doing periodic homogenization on the resulting larger unit cell. Such operations, however, tend to lead to undesired shapes of reinforcement and to changes in the arrangement statistics. The alternative expedient of specifying symmetry B.C.s for rectangular or cuboidal real structure cells amounts to an even larger modification of the microgeometry and introduces marked local constraints. Nevertheless, for sufficiently large multi-inhomogeneity cells useful results can be obtained with the latter strategy, see, e.g., (Terada et al., 2000).

[64]Equation (5.6) may be viewed as "stretching" the microscale so it becomes comparable to the macroscale, $f(\mathbf{x}) \to f(\mathbf{Z},\mathbf{Z}/\epsilon) = f(\mathbf{Z},\mathbf{z})$.

[65]The nomenclature used in eqns. (5.6) to (5.13) follows typical usage in asymptotic homogenization. It is more general than but can be directly compared with the one used in eqns. (1.1) to (5.5), where no macroscopic coordinates $\mathbf{Z}$ are employed.

Using the chain rule, i.e.,

$$\frac{\partial}{\partial \mathbf{x}} f(\mathbf{Z}(\mathbf{x}), \mathbf{z}(\mathbf{x}), \epsilon) \quad \rightarrow \quad \frac{\partial}{\partial \mathbf{Z}} f + \frac{1}{\epsilon} \frac{\partial}{\partial \mathbf{z}} f \qquad , \tag{5.8}$$

the strains can be related to the displacements in the small strain elastic regime as

$$\begin{aligned} \varepsilon_{ij}(\mathbf{Z}, \mathbf{z}, \epsilon) &= \frac{1}{2}\Big\{ \left(\frac{\partial}{\partial Z_j} u_i^{(0)} + \frac{\partial}{\partial Z_i} u_j^{(0)} \right) + \left(\frac{\partial}{\partial z_j} u_i^{(1)} + \frac{\partial}{\partial z_i} u_j^{(1)} \right) \Big\} \\ &+ \frac{\epsilon}{2}\Big\{ \left(\frac{\partial}{\partial Z_j} u_i^{(1)} + \frac{\partial}{\partial Z_i} u_j^{(1)} \right) + \left(\frac{\partial}{\partial z_j} u_i^{(2)} + \frac{\partial}{\partial z_i} u_j^{(2)} \right) \Big\} + \text{H.O.T.} \\ &= \varepsilon_{ij}^{(1)}(\mathbf{Z}, \mathbf{z}) + \epsilon\, \varepsilon_{ij}^{(2)}(\mathbf{Z}, \mathbf{z}) + \text{H.O.T.} \qquad , \end{aligned} \tag{5.9}$$

where terms of the type $\varepsilon_{ij}^{(0)} = \frac{1}{\epsilon} \frac{\partial}{\partial z_j} u_i^{(0)}$ are deleted due to the underlying assumption that the variations of slow variables are negligible at the microscale. In analogy the stresses can be expanded into the expression

$$\sigma_{ij}(\mathbf{Z}, \mathbf{z}, \epsilon) = \sigma_{ij}^{(1)}(\mathbf{Z}, \mathbf{z}) + \epsilon\, \sigma_{ij}^{(2)}(\mathbf{Z}, \mathbf{z}) + \text{H.O.T.} \qquad . \tag{5.10}$$

Using the two-scale assumption and, as a consequence, eqn. (5.8), the equilibrium equations take the form

$$\left(\frac{\partial}{\partial Z_j} + \frac{1}{\epsilon} \frac{\partial}{\partial z_j} \right) \sigma_{ij}(\mathbf{Z}, \mathbf{z}, \epsilon) + f_i(\mathbf{Z}) = 0 \qquad , \tag{5.11}$$

the f_i being macroscopic body forces. By inserting eqn. (5.10) into this expression and sorting the resulting terms by order of ϵ a hierarchical system of partial differential equations is obtained

$$\begin{aligned} \frac{\partial}{\partial z_j} \sigma_{ij}^{(1)} = 0 \qquad & \text{(order} \quad \epsilon^{-1}) \\ \frac{\partial}{\partial Z_j} \sigma_{ij}^{(1)} + \frac{\partial}{\partial z_j} \sigma_{ij}^{(2)} + f_i = 0 \qquad & \text{(order} \quad \epsilon^{0}) \qquad , \end{aligned} \tag{5.12}$$

the first of which gives rise to a boundary value problem at the unit cell level that is referred to as the "micro equation". By making a specific ansatz for the strains at unit cell level and by volume averaging over the second equation in the system (5.12), which is known as the "macro equation", the microscopic and macroscopic fields can be linked such that the homogenized elasticity tensor is obtained as

$$E_{ijkl} = \frac{1}{\Omega_{\text{UC}}} \int_{\Omega_{\text{UC}}} E_{ijkl}(\mathbf{z}) \left[I_{klmn} + \frac{\partial}{\partial z_l} \chi_{kmn}(\mathbf{z}) \right] \mathrm{d}\Omega \qquad . \tag{5.13}$$

Here Ω_{UC} is the volume of the unit cell, $E_{ijkl}(\mathbf{z})$ is the phase-level (microscopic) elasticity tensor, and the "characteristic function" $\chi_{kmn}(\mathbf{z})$ describes the deformation modes of the unit cell[66] and, accordingly, relates the micro- and macrofields. Analogous expressions can be derived for the tangent modulus tensors used in elastoplastic analysis, compare Ghosh

[66] Even though eqns. (5.12) and (5.13) are derived from an explicit two-scale formulation neither of them contains the scale parameter ϵ, see the discussion by Chung et al. (2001).

et al. (1996).

The above relations can be used as the basis of Finite Element algorithms that solve for the characteristic function $\chi_{ijk}(\mathbf{z})$, a task that typically has required special analysis codes. For detailed discussions of asymptotic homogenization methods within the framework of FEM-based micromechanics see, e.g., Hollister et al. (1991), Ghosh et al. (1996), Hassani and Hinton (1999) or Chung et al. (2001). An asymptotic homogenization procedure for elastic composites that uses standard elements within a commercial FE package was proposed by Banks-Sills and Leiderman (1997).

Asymptotic homogenization allows to directly couple FE models on the macro- and microscales, compare, e.g., Ghosh et al. (1996) or Terada et al. (2003), an approach that has been used in a number of multi-scale studies (compare chapter 8) and is sometimes referred to as the FE^2 method (Feyel, 2003). A treatment of homogenization in the vicinity of macroscopic boundaries can be found in Schrefler et al. (1997). Asymptotic homogenization schemes have also been employed for problems involving higher-order stresses and strain gradients (Kouznetsova et al., 2002)[67], an approach referred to as higher order homogenization.

Recently, an alternative unit-cell based asymptotic homogenization scheme for linear problems, the Variational Asymptotical Method for Unit Cell Homogenization (VAMUC), was reported (Yu and Tang, 2007), which can also be implemented within a Finite Element framework.

Method of Macroscopic Degrees of Freedom

When asymptotic homogenization is not used, it is good practice to apply far field stresses and strains to a given unit cell via concentrated nodal forces or prescribed displacements, respectively, at the master nodes and/or pivot points, an approach termed the "method of macroscopic degrees of freedom" by Michel et al. (1999). Employing the divergence theorem and using the nomenclature and configuration of fig. 5.5, for load controlled analysis the forces to be applied to the master nodes SE and NW, $\mathbf{P}_{\mathrm{SE}}$ and $\mathbf{P}_{\mathrm{NW}}$, of a two-dimensional unit cell with periodicity boundary conditions can be shown to be given by the surface integrals

$$\mathbf{P}_{\mathrm{SE}} = \int_{\Gamma_{\mathrm{E}}} \mathbf{t}^{\mathrm{a}}(\mathbf{z})\, \mathrm{d}\Gamma \qquad \mathbf{P}_{\mathrm{NW}} = \int_{\Gamma_{\mathrm{N}}} \mathbf{t}^{\mathrm{a}}(\mathbf{z})\, \mathrm{d}\Gamma \qquad . \tag{5.14}$$

[67] Such methods are especially useful for problems in which the length scales are not well separated; in them the "unit cells" do not necessarily remain periodic during the deformation process.

Here $\mathbf{t}^{\mathrm{a}}(\mathbf{z}) = \boldsymbol{\sigma}^{\mathrm{a}} * \mathbf{n}_\Gamma(\mathbf{z})$ stands for the homogeneous surface traction vector corresponding to the applied (far field) stress field[68] at some given point $\mathbf{z}$ on the cell's surface Γ_{UC}, and $\mathbf{n}_\Gamma(\mathbf{z})$ is the local normal vector of the appropriate face. Equation (5.14) can be generalized to require that each master node is loaded by a force corresponding to the surface integral of the surface traction vectors over the face slaved to it via an equivalent of eqns. (5.14), compare Smit et al. (1998). Analogous procedures hold for three-dimensional cases, and symmetry as well as antisymmetry boundary conditions as described by eqns. (5.4) and (5.5) can be handled by eqn. (5.14).

For applying far field strains to periodic volume elements, the displacements to be prescribed to the master nodes must be obtained from the macroscopic strains via appropriate strain–displacement relations. For example, using the notation of eqns. (5.3), the displacements to be prescribed to the master nodes NE and SW of the unit cell shown in fig. 5.5 can be evaluated from eqn. (5.2) as

$$\begin{aligned} u_{\mathrm{SE}} &= \varepsilon^{\mathrm{a}}_{11}\, c_1 \quad v_{\mathrm{SE}} = \gamma^{\mathrm{a}}_{12}\, c_1 \\ u_{\mathrm{NW}} &= \gamma^{\mathrm{a}}_{21}\, c_2 \quad v_{\mathrm{NW}} = \varepsilon^{\mathrm{a}}_{22}\, c_2 \end{aligned} \tag{5.15}$$

for an applied strain $\boldsymbol{\varepsilon}^{\mathrm{a}}$ and linear strain–displacement relations[69]. For the case considered here, the projections of the shift vectors, c_1 and c_2, are equal to the side lengths of the cell in the undeformed state. In order to obtain the elastic tensors of periodic phase arrangements, six linearly independent load cases must be evaluated. Typically strain controlled unit cell analysis is easier to handle than stress controlled models[70].

In general, the overall stress and strain tensors within a unit cell can be evaluated by volume averaging[71] or by using the equivalent surface integrals given in eqn. (1.3), i.e.,

$$\begin{aligned} \langle \boldsymbol{\sigma} \rangle &= \frac{1}{\Omega_{\mathrm{UC}}} \int_{\Omega_{\mathrm{UC}}} \boldsymbol{\sigma}(\mathbf{z})\, \mathrm{d}\Omega = \frac{1}{\Omega_{\mathrm{UC}}} \int_{\Gamma_{\mathrm{UC}}} \mathbf{t} \otimes \mathbf{z}\, \mathrm{d}\Gamma \\ \langle \boldsymbol{\varepsilon} \rangle &= \frac{1}{\Omega_{\mathrm{UC}}} \int_{\Omega_{\mathrm{UC}}} \boldsymbol{\varepsilon}(\mathbf{z})\, \mathrm{d}\Omega = \frac{1}{2\Omega_{\mathrm{UC}}} \int_{\Gamma_{\mathrm{UC}}} (\mathbf{u} \otimes \mathbf{n}_\Gamma + \mathbf{n}_\Gamma \otimes \mathbf{u})\, \mathrm{d}\Gamma \quad . \end{aligned} \tag{5.16}$$

In practice, it is typically fairly straightforward to evaluate volume integrals by numerical integration schemes such as eqn. (4.1), whereas no comparable approximations are available for surface integrals.

[68] Note that the $\mathbf{t}^{\mathrm{a}}(\mathbf{z})$ are not identical with the actual local values of the tractions, $\mathbf{t}(\mathbf{z})$, at the cell boundaries, but are equal to them in an integral sense over the cell face. For geometrically nonlinear analysis eqn. (5.14) must be applied to the current configuration. Because the far field stress $\boldsymbol{\sigma}^{\mathrm{a}}$ is constant it can be factored out of the surface integrals, so that the force applied to a master node $\mathbf{P}_{\mathrm{M}}$ takes the form $\mathbf{P}_{\mathrm{M}} = \boldsymbol{\sigma}^{\mathrm{a}} * \int_{\Gamma_{\mathrm{S}}} \mathbf{n}_\Gamma(\mathbf{z})\, \mathrm{d}\Gamma$, which is the projection of the applied stress to the current average surface normal of the slave face Γ_{S} times the current area of the face.

[69] Equations (5.15) can be directly extended to three-dimensional problems and to handling nonlinear strain–displacement relations as well as deformation gradients (Huber et al., 2007).

[70] Even though the loads acting on the master nodes obtained from eqn. (5.14) are equilibrated, in stress controlled analysis solid body rotations may be induced through small numerical errors. When these solid body rotations are suppressed by deactivating degrees of freedom beyond those required for enforcing periodicity, the quality of the solutions may be degraded or transformations of the averaged stresses and strains may be required.

[71] For large strain analysis the consistent procedure is to first average the deformation gradients and then evaluate the strains from these averages.

In the case of rectangular or hexahedral unit cells that are aligned with the coordinate axes, averaged engineering stress and strain components can, of course, be evaluated by dividing the applied or reaction forces at the master nodes by the appropriate surface areas and by dividing the displacements of the master nodes by the appropriate cell lengths, respectively.

5.4 Unit Cell Models for Composites Reinforced by Continuous Fibers

Unit cell modes have been reported for three groups of continuously reinforced composites, unidirectionally reinforced, angle-ply and cross-ply materials as well as fabric reinforced composites.

Composites Reinforced by Unidirectional Continuous Fibers

Composites reinforced by continuous aligned fibers typically show a statistically transversely isotropic overall behavior and can be studied well with periodic homogenization. Materials characterization with the exception of the overall axial shear behavior can be carried out with two-dimensional unit cell models employing generalized plane strain elements that use a global degree of freedom to describe the axial deformation of the whole model[72]. For handling the overall axial shear response special generalized plane strain elements (Adams and Crane, 1984; Sørensen, 1992) or three-dimensional analyses with appropriate boundary conditions (Pettermann and Suresh, 2000) are required[73]. Three-dimensional modeling is also relevant for the materials characterization of composites reinforced by continuous aligned fibers when the effects of fiber misalignment, of fiber waviness (Garnich and Karami, 2004), or of broken fibers[74] (Mahishi, 1986) are to be studied. Unit cell models used for nonlinear constitutive modeling, of course, must be fully three-dimensional and employ periodicity boundary conditions.

Basic generalized plane strain models of continuously reinforced composites make use of simple periodic fiber arrangements as shown in fig. 5.8, all of which can be described by rather small unit cells using symmetry and/or antisymmetry B.Cs. The simplest among these arrangements are the periodic hexagonal (PH0) and periodic square (PS0) arrays. Models with hexagonal symmetry (PH0,CH1,RH2,CH3) give rise to transversely isotropic thermoelastic overall behavior, whereas the other fiber arrangements shown in fig. 5.8

[72] Generalized plane strain elements suitable for such analysis are implemented in a number of commercial FE codes. Because the axial stiffness of composites reinforced by continuous aligned fibers can usually be satisfactorily described by Voigt-type ("rule of mixture") models unit cell studies of such materials have tended to concentrate on the transverse behavior. Note that plain strain models can describe neither the axial constraints nor the axial components of microstresses and microstrains.

[73] For linear elastic material behavior there is the additional option of making use of the formal analogy between out-of-plane (antiplane) shear and diffusion problems.

[74] For investigating the axial failure behavior of continuously reinforced MMCs, statistical methods concentrating on fiber fragmentation or more elaborate spring lattice models, see, e.g., Zhou and Curtin (1995), have been used successfully.

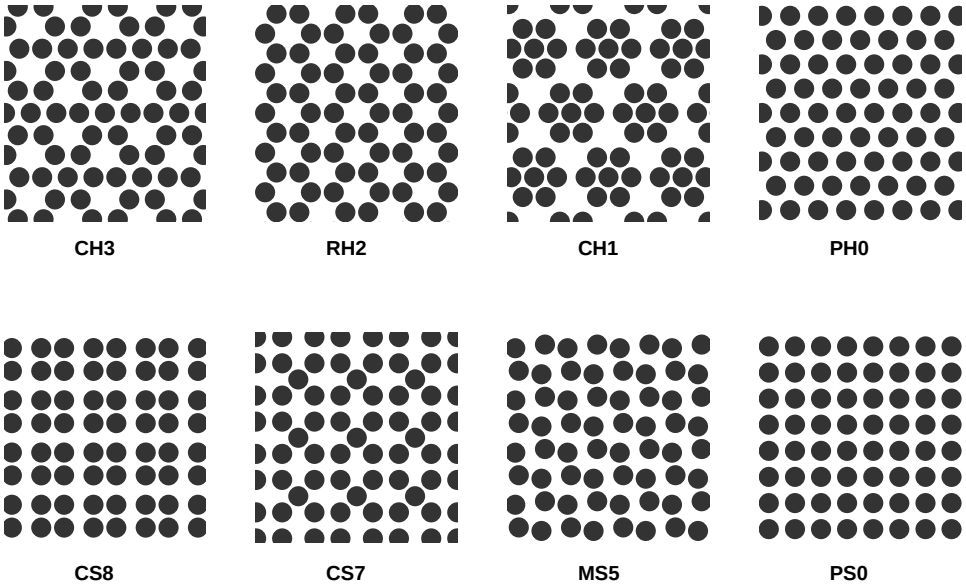

Figure 5.8: Eight simple periodic fiber arrangements of fiber volume fraction ξ=0.475 for modeling continuously fiber reinforced composites (Böhm and Rammerstorfer, 1995).

have tetragonal (PS0,CS7,CS8) or monoclinic (MS5) overall symmetry. In the elastoplastic range the macroscopic symmetries of the fiber arrangements degrade under most load cases, see fig. 5.9. This behavior is due to the low symmetry of the local material properties of the matrix (especially the plastic strain and, as a consequence, the strain hardening), which depend on the load history a given point has undergone. In many cases simple periodic microgeometries do not provide satisfactory descriptions of fiber reinforced materials, most of which show at least some randomness in the fiber positions. Much improved models can be obtained by periodic multi-fiber unit cells that employ quasi-random fiber positions. Such models can either use symmetry B.C.s, compare the unit cell shown in fig. 5.10, which is based on the work of Nakamura and Suresh (1993), or periodicity B.C.s (Moulinec and Suquet, 1997; Gusev et al., 2000; Zeman and Šejnoha, 2007).

In table 5.1 thermoelastic moduli of an aligned continuously reinforced ALTEX/Al MMC as predicted by bounding methods, MFAs and unit cells methods using arrangements PH0, CH1 and PS0 (compare fig. 5.8) as well as DN (see fig. 5.10) are listed. For this material combination all unit cell results (even PS0, which is not transversally isotropic) fall within the Hashin–Shtrikman bounds[75], but the predictions for the square arrangement show clear in-plane anisotropy and do not follow the three-point bounds. The results for the multi-fiber arrangement indicate some minor deviation from transversely isotropic macroscopic behavior.

The fiber arrangements shown in figs. 5.8 and 5.10 give nearly identical results for the overall thermoelastoplastic behavior of continuously reinforced composites under axial mechanical loading, and the predicted overall axial and transverse responses under thermal

[75]The constituents' material properties underlying table 3 show a low elastic contrast of $C \approx 3$, making them relatively insensitive to perturbations of macroscopic symmetry. In general the elastic stiffnesses obtained from square-type arrangements may violate the Hashin–Shtrikman bounds and usually lie outside the three-point bounds.

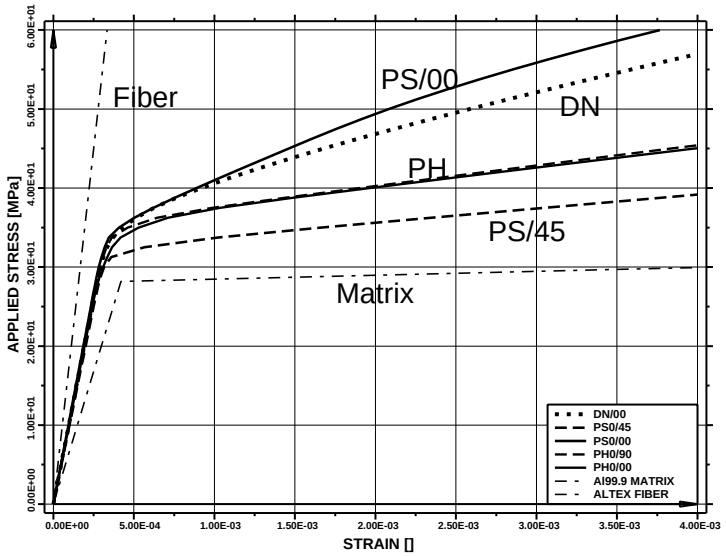

Figure 5.9: Transverse elastoplastic response of a unidirectional continuously reinforced ALTEX/Al MMC (ξ=0.453, elastoplastic matrix with linear hardening) to transverse uniaxial loading as predicted by unit cell models PH0, PS0 and DN.

loading are also very similar. The overall behavior under transverse mechanical loading, however, depends markedly on the phase arrangement, see fig. 5.9. For fiber arrangements of tetragonal or lower symmetry (e.g., PS0, MS5, CS7 and CS8) the predicted transverse stiffness depends strongly on the loading direction. The behavior of the hexagonal arrangements is sandwiched between the stiff (0°) and the compliant (45°) responses of periodic square arrangements in both the elastic and elastoplastic ranges. Multi-fiber unit cells that approach statistical transverse isotropy (such as the one shown in fig. 5.10) tend to show noticeably stronger strain hardening compared to periodic hexagonal arrangements,

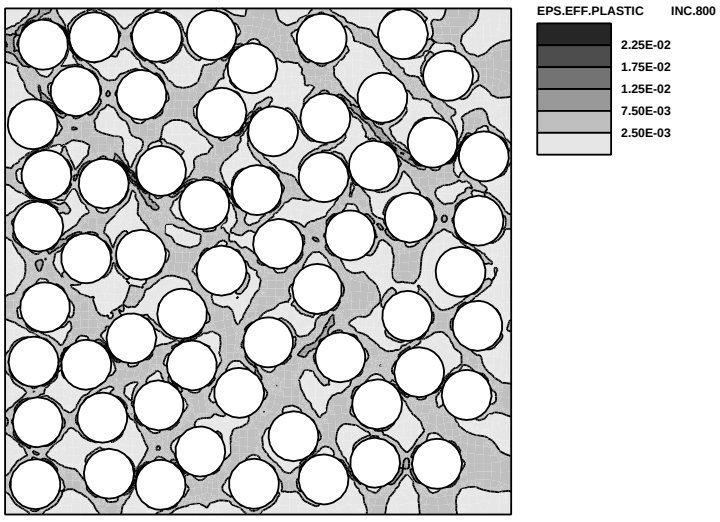

Figure 5.10: Microscopic distributions of the accumulated equivalent plastic strain in the matrix of a transversely loaded unidirectional continuously reinforced ALTEX/Al MMC (ξ=0.453) as predicted by a multi-fiber unit cell (arrangement DN).

Table 5.1: Overall thermoelastic moduli of a unidirectional continuously reinforced ALTEX/Al MMC (ξ=0.453 nominal) as predicted by the Hashin–Shtrikman (HS) and three-point (3PB) bounds, by the Mori–Tanaka method (MTM) and the generalized self-consistent scheme (GSCS), by Torquato's three-point estimates (3PE), as well as by unit cell analysis using periodic arrangements shown in fig. 5.8 (PH0, CH1, PS0) and the multi-fiber cell displayed in fig. 5.10 (DN). For arrangement PS0 responses in the 0° and 45°, and for arrangement DN responses in the 0° and 90° directions are listed.

	E^*_A [GPa]	E^*_T [GPa]	ν^*_A []	ν^*_T []	α^*_A $[K^{-1}\times10^{-6}]$	α^*_T $[K^{-1}\times10^{-6}]$
fibers	180.0	180.0	0.20	0.20	6.0	6.0
matrix	67.2	67.2	0.35	0.35	23.0	23.0
HS/lo	118.8	103.1	0.276	0.277	—	—
HS/hi	119.3	107.1	0.279	0.394	—	—
3PB/lo	118.8	103.8	0.278	0.326	—	—
3PB/hi	118.9	104.5	0.279	0.347	—	—
MTM	118.8	103.1	0.279	0.342	11.84	16.46
GSCS	118.8	103.9	0.279	0.337	11.84	16.46
3PE	118.8	103.9	0.279	0.338	11.89	16.40
PH0	118.8	103.7	0.279	0.340	11.84	16.46
CH1	118.7	103.9	0.279	0.338	11.90	16.42
PS0/00	118.8	107.6	0.279	0.314	11.85	16.45
PS0/45	118.8	99.9	0.279	0.363	11.85	16.45
DN/00	118.8	104.8	0.278	0.334	11.90	16.31
DN/90	118.8	104.6	0.278	0.333	11.90	16.46

of the same fiber volume fraction, compare Moulinec and Suquet (1997). Generally the macroscopic yield surfaces of uniaxially reinforced MMCs are not of the Hill (1948) type, but can be described by a bimodal description (Dvorak and Bahei-el Din, 1987).

The distributions of microstresses and microstrains in fibers and matrix tend to depend strongly on the fiber arrangement, especially under thermal and transverse mechanical loading. In the plastic regime, the microscopic distributions of equivalent and hydrostatic stresses, equivalent plastic strains and stress triaxialities tend to be markedly inhomogeneous[76], see, e.g., fig. 5.10. As a consequence of the inhomogeneity of the microfields, there tend to be strong constrained plasticity effects in continuously reinforced MMCs and the onset of damage in the matrix, of fracture of the fibers, and of interfacial decohesion at the fiber–matrix interfaces show a strong dependence on the fiber arrangement.

Cross-Ply and Angle-Ply Composites

Another group of composite materials reinforced by continuous fibers that can be studied to advantage by unit cell methods are laminates consisting of plies the thickness of which is not much greater than the fiber diameter. The left side of fig. 5.11 depicts a unit cell

[76]The corresponding distribution functions, phase averages, and higher statistical moments are also significantly influenced by the fiber arrangement, compare Böhm and Rammerstorfer (1995).

for a cross-ply laminate with double layers of fibers which is suitable for use with periodicity and symmetry boundary conditions. In the the center a minimum unit cell for cross

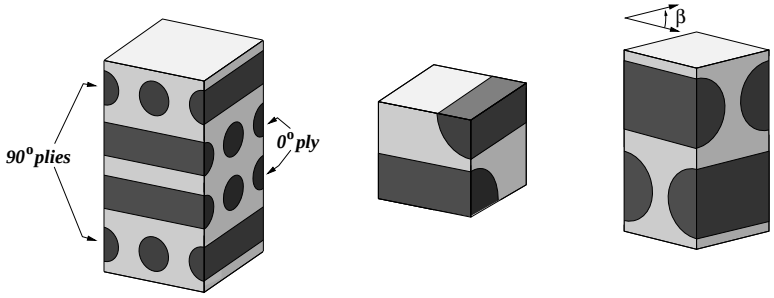

Figure 5.11: Unit cell for a double layer cross-ply laminate (left), minimum unit cell for a cross ply-laminate (center) and unit cell for an angle-ply laminate with ply angle β (right).

ply laminates with one fiber layer per ply is shown, which requires the use of symmetry boundary conditions. A unit cell for studying angle-ply laminates with a general ply angle β via periodicity boundary conditions is displayed on the right side of fig. 5.11.

Unit cells with symmetry boundary conditions were used for studying the thermomechanical behavior of cross ply laminates by Lerch et al. (1991) as well as Ismar and Schröter (2000). For unit cell studies of angle ply laminates see Xia et al. (2003) and Abolfathi et al. (2008).

Fabric Reinforced Composites

Periodic microfield methods have played an important role in modeling the behavior of fabric reinforced composites, i.e., materials containing woven, braided, or knitted reinforcements. In such "textile composites" the reinforcing phase usually takes the form of textile-like structures consisting of bundles of continuous fibers (tows). Unit cell models for such materials are typically based on modeling fiber bundles as a "mesophase" with smeared out material properties, which, in turn, are obtained from analyzing unidirectionally continuously reinforced composites[77]. Free surface boundary conditions are typically specified for the out-of-plane faces of the cell, and a number of cells may be stacked on top of each other in order to account for in-plane offsets and constraint effects between the layers (Byström et al., 2000). Symmetry boundary conditions can be specified for the in-plane faces, which gives reasonably small unit cells as shown in fig. 5.12, but restricts the load cases that can be handled in in-plane normal and thermal loads. By applying extended periodicity boundary conditions to larger unit cells macroscopic rotational degrees of freedom can be introduced to allow studying all deformation models, including the macroscopic warping and twisting of the laminae.

There is a wide range of weaves as well as knitting and braiding architectures that can be modeled with PMAs. Unit cells for woven, knitted and braided composites tend to be fairly complex geometrically, may be difficult to mesh for Finite Element analysis and may

[77]This modeling strategy obviously is a type of multiscale modeling as discussed in chapter 8.

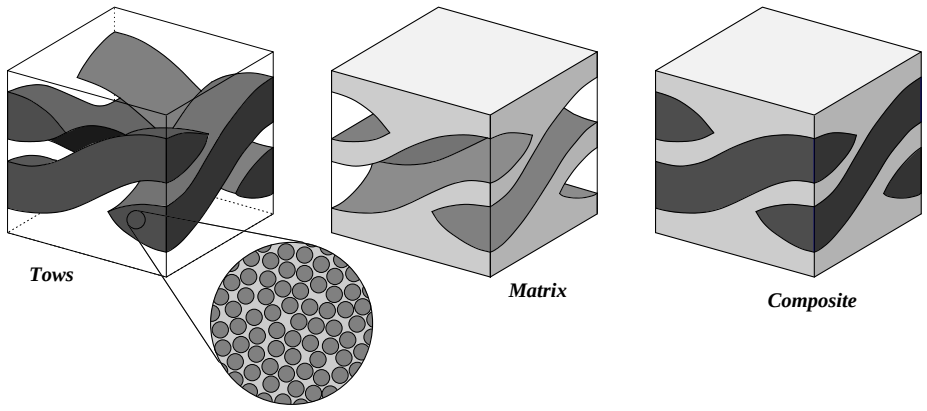

Figure 5.12: A unit cell for modeling a plain weave lamina using symmetry boundary conditions. The tow region (left), the matrix region (center) and the "assembled" unit cell (right) are shown.

pose considerable computational requirements, especially when nonlinear behavior is to be studied. Over the past 20 years a considerable number of studies have been published on unit cell modeling of fabric reinforced composites, see, e.g., Cox and Flanagan (1997), Huang and Ramakrishna (2000), Tang and Whitcomb (2003) or Lomov et al. (2006), and on software for generating appropriate unit cells (Robitaille et al., 2003; Sherburn, 2007).

5.5 Unit Cell Models for Short Fiber Reinforced Composites

The overall symmetry of short fiber reinforced composites in many cases is isotropic (for random fiber orientations) or transversely isotropic (for aligned fibers, planar random fibers and other fiber arrangements with axisymmetric orientation distributions). However, processing conditions can give rise to a wide range of fiber orientation distributions and, consequently, lower overall symmetries (Allen and Lee, 1990). The thermoelastic and thermoelastoplastic behavior of aligned short fiber reinforced composites has been successfully estimated by Mori–Tanaka methods, which can also be extended to nonaligned fibers and reinforcements showing an aspect ratio distribution, compare section 2.7. Such mean-field approaches are, however, limited in resolving details of fiber arrangements, especially for inelastic material behavior. At present the most powerful tools for studying the influence of fiber shapes and orientations, of clustering effects, of the interaction of fibers of different sizes, and of local stress and strain fields between neighboring fibers are periodic microfield methods. Platelet reinforced composites can be described in analogy to short fiber reinforced materials.

Composites Reinforced by Aligned Short Fibers

In contrast to continuously reinforced composites, the phase arrangements of discontinuously reinforced materials are inherently three-dimensional. The simplest three-dimensional unit cell models of aligned short fiber reinforced composites have used periodic square ar-

rangements of non-staggered or staggered aligned cylindrical fibers[78], see, e.g., Levy and Papazian (1991) and compare fig. 5.13. Such geometries are relatively simple to set up and do not pose major computational requirements, but are rather restrictive in terms of fiber arrangements and load conditions that can be handled. By setting up larger unit cells supporting periodicity boundary conditions are used the full thermomechanical behavior of the fiber arrangements can be studied. Analogous microgeometries based on periodic hexagonal arrangements of non-staggered (Järvstråt, 1992) or staggered (Tucker and Liang, 1999) fibers as well as ellipsoidal unit cells aimed at describing composite "ellipsoid assembly" microgeometries (Järvstråt, 1993) were also proposed[79].

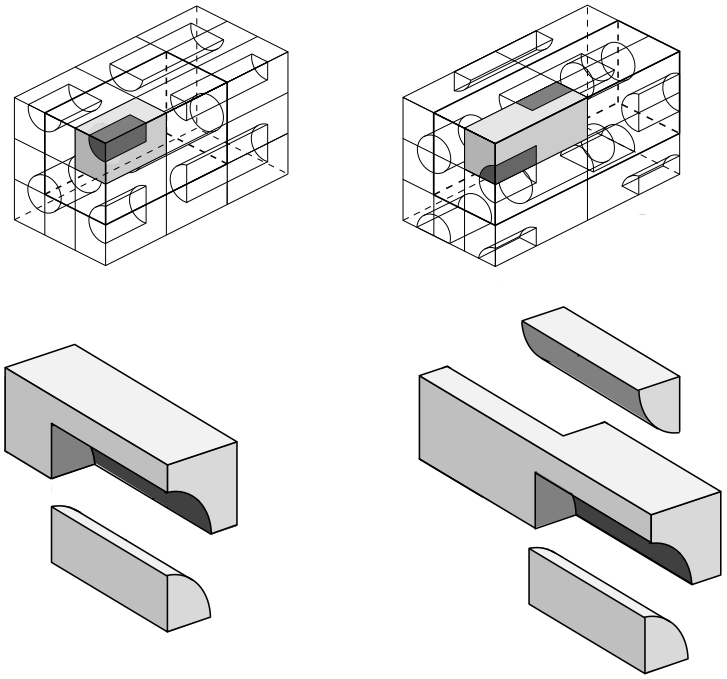

Figure 5.13: Three-dimensional unit cells for modeling non-staggered (left) and staggered (right) square arrangements of aligned short fibers. The shaded cells require symmetry B.C., cells outlined in bold can use periodicity B.C.

For many materials characterization studies, a more economical alternative to the above three-dimensional unit cells takes the form axisymmetric models describing the axial behavior of non-staggered or staggered arrays of aligned cylindrical short fibers in an approximate way. The basic idea behind these models is to replace unit cells for square or hexagonal arrangements by circular composite cylinders of equivalent cross sectional area (and volume fraction) as sketched in 5.14. The resulting axisymmetric cells are not unit cells in the strict sense, because they overlap and are not space filling. In addition, they do not have the same transverse fiber spacing as the corresponding three-dimensional arrangements and cannot be used to study the response to most transverse mechanical loading conditions.

[78]Such square arrangements give rise to tetragonal overall symmetry, and, consequently, the transverse overall properties are direction dependent. Figure 5.13 shows unit cells set up for symmetry B.C., which minimize computational cost but are suitable for materials characterization only.

[79]For a comparison between unit cell and analytical predictions for the overall elastic properties for short fiber reinforced composites see, e.g., Tucker and Liang (1999).

However, they have the advantage of significantly reduced computational requirements, which makes them especially suitable for qualitative studies of highly nonlinear behavior such as damage.

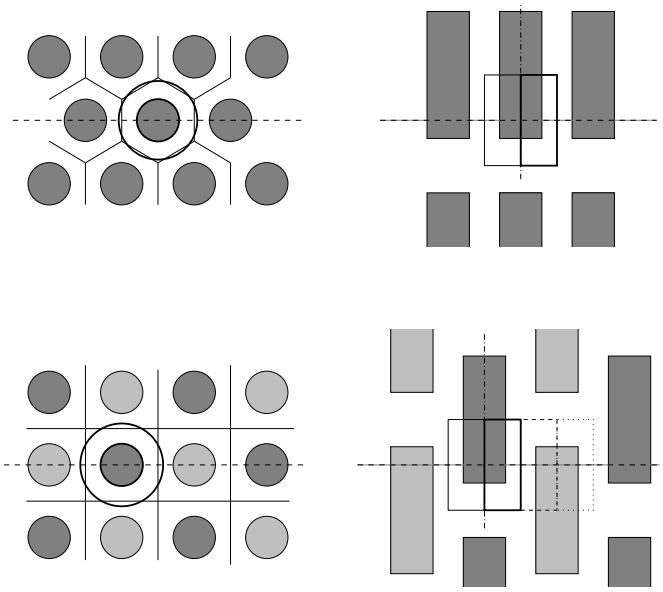

Figure 5.14: Periodic arrays of aligned non-staggered (top) and staggered (bottom) short fibers and corresponding axisymmetric cells (left: sections in transverse plane; right: sections parallel to fibers).

Symmetry boundary conditions are used for the top and bottom faces of these cells, and the B.C.s at the "outer" (circumferential) surface are chosen to enforce the same cross sectional area along the axial direction for an aggregate of cells. In the case of non-staggered fibers this can be easily done by specifying symmetry-type boundary conditions for the outer surfaces, whereas for staggered arrangements a pair of cells with different fiber positions is considered, for which the total cross sectional area is required to be independent of the axial coordinate[80]. Using the nomenclature of fig. 5.15 and the notation of eqns. (5.3) to (5.5), this leads to nonlinear relations for the radial displacements u and linear constraints for the axial displacements v at the outer surface,

$$(r_{\mathrm{U}} + u_{\mathrm{U}})^2 + (r_{\mathrm{L}} + u_{\mathrm{L}})^2 = 2(r_{\mathrm{P}} + u_{\mathrm{P}})^2 \qquad \text{and} \qquad v_{\mathrm{U}} + v_{\mathrm{L}} = 2v_{\mathrm{P}} \qquad , \tag{5.17}$$

respectively, where r is the radius of the undeformed cell. The two cells making up the pair are antisymmetric with respect to the pivot point P and can, in consequence, be described by a single cell with an antisymmetric outer (E-) face, U and L being nodes on this face that are positioned symmetrically with respect to the pivot. Nonlinear constraints such as eqn. (5.17) may, however, not be available or be cumbersome to use in a given FE code[81]. For most applications the boundary conditions for the radial displacements at the outer

[80] As originally proposed by Tvergaard (1990) the nonlinear displacement boundary conditions in eqn. (5.17) were combined with antisymmetry traction B.C.s for use with a hybrid FE formulation.

[81] For an example of the use of the nonlinear B.C.s described in eqn. (5.17) with a commercial FE code see Ishikawa et al. (2000), where cells of truncated cone shape are employed to describe bcc arrangements of particles.

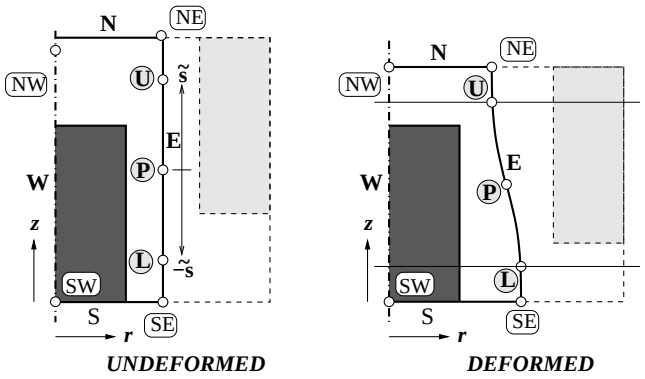

Figure 5.15: Axisymmetric cell for staggered arrangement of short fibers: undeformed and deformed shapes.

surfaces of the cylinders, eqn. (5.17), can be linearized without major loss in accuracy to give the set of boundary conditions

$$u_{\mathrm{U}} + u_{\mathrm{L}} = 2u_{\mathrm{P}} \qquad \text{and} \qquad v_{\mathrm{U}} + v_{\mathrm{L}} = 2v_{\mathrm{P}} \qquad . \tag{5.18}$$

which are identical to antisymmetry B.C.s, eqn. (5.5).

For the past 15 years axisymmetric cell models of the types shown in fig. 5.14 have been the workhorses of PMA studies of short fiber reinforced composites, see, e.g., Povirk et al. (1992) or Tvergaard (1994). Typically, descriptions using staggered arrangements allow a wider range of microgeometries to be covered, compare Böhm et al. (1993) or Tvergaard (2003), and give more realistic descriptions of actual composites. Both staggered and non-staggered axisymmetric models can be extended to studying a considerable range of arrangements incorporating aligned fibers of different size and/or aspect ratio by coupling two or more different cells via the condition of keeping the cross sectional area of the aggregate independent of the axial coordinate (Böhm et al., 1993).

Three-dimensional unit cells and axisymmetric cells have been used successfully for studying the nonlinear thermomechanical behavior of aligned short fiber reinforced MMCs, e.g., with respect to the their stress–strain responses, to the pseudo-Bauschinger effect, and to thermal residual stresses. They have provided valuable insight into causes and effects of matrix, interface and fiber damage.

Composites Reinforced by Nonaligned Short Fibers

Whereas a considerable number of unit cell studies of materials reinforced by aligned discontinuous fibers have been reported, the literature contains rather few such models dealing with nonaligned fibers, among them three-dimensional studies of composites reinforced by alternatingly tilted misaligned fibers (Sørensen et al., 1995) and plane-stress models describing planar random short fibers (Courage and Schreurs, 1992). The situation with respect to mean field models for such materials is not fully satisfactory for the elastic range, either, compare section 2.7, and little work has been done on the inelastic thermomechanical behavior.

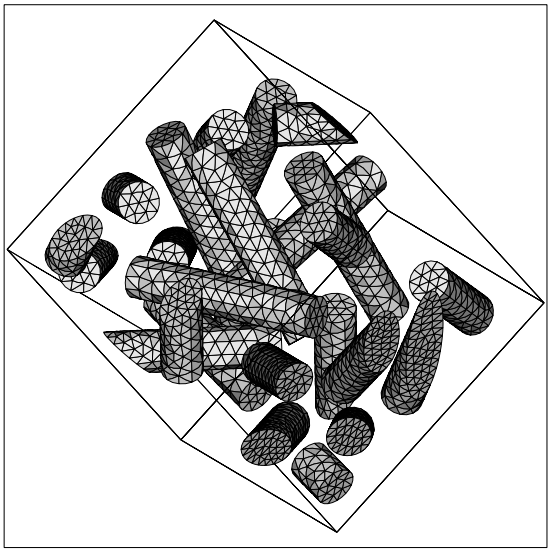

Figure 5.16: Unit cell a composite reinforced by randomly oriented short fibers (Böhm et al., 2002). The nominal fiber volume fraction is $\xi = 0.15$ and the 15 cylindrical fibers in the cell have an aspect ratio of $a = 5$.

At present the most promising modeling strategy for nonaligned short fiber reinforced composites consists of using three-dimensional multi-fiber unit cells in which the fibers are randomly positioned and oriented such that the required ODF is fulfilled approximately. Such multi-fiber unit cells were reported, e.g., for spatially random fiber orientation by Böhm et al. (2002) as well as Lusti et al. (2002) and for planar random fiber orientations by Duschlbauer et al. (2006) as well as Iorga et al. (2008). Such unit cell models can also account for the distributions of fiber sizes and/or aspect ratios. This modeling approach, however, tends to pose considerable challenges in generating appropriate fiber arrangements at nondilute volume fractions due to geometrical frustration and because relatively large volume elements are required for handling periodic microgeometries with fiber aspect ratio in excess of, say, 5. The meshing of the resulting phase arrangements for use with the FEM also may be difficult, compare Shephard et al. (1995), and analyzing the mechanical response of the resulting cells may require considerable computing power, especially for nonlinear constituent behavior. The first studies of this type were, accordingly, restricted to the linear elastic range, where the BEM has been found to answer well, see, e.g., Banerjee and Henry (1992).

As an example of a multi-fiber unit cell for a composite reinforced by nonaligned short fibers, fig. 5.16 shows a cube-shaped cell that contains 15 randomly oriented cylindrical fibers of aspect ratio $a = 5$, supports periodicity boundary conditions, was generated by random sequential addition, and is discretized by tetrahedral elements. The phase arrangement is set up in such a way that spheroidal fibers of the same aspect ratio, volume fractions, center points, and orientations can also be used in order to allow studying fiber shape effects (Böhm et al., 2002). Unit cells corresponding to higher fiber volume fractions can be generated by hard core shaking models, as implemented, e.g., in the commercial micromechanics code PALMYRA (MatSim Ges.m.b.H., Zurich, Switzerland).

In table 5.2 predictions are given for the overall elastic response of a composite rein-

forced by randomly positioned and oriented fibers obtained by analytical estimates and bounds as well as results of the above type of unit cell, for which data are shown pertaining to cylindrical and spheroidal fibers. Interestingly, considerable differences were found between the predictions for reinforcement by cylindrical and spheroidal fibers that have the same fiber volume fraction and aspect ratio, occupy the same positions and show the same orientations, with the spheroidal reinforcements leading to a softer response, especially in the inelastic regime. Satisfactory results were obtained despite the low number of fibers in the unit cell (chosen in view of the available computational resources) and excellent agreement with analytical descriptions was achieved in terms of the orientation dependence of the stresses in individual fibers, compare fig. 2.3. It should be noted, however, that from the point of view of the representativeness of the phase arrangement and for use in the elastoplastic range unit cells containing a considerably higher number of fibers are certainly desirable.

5.6 Unit Cell Models for Particle Reinforced Composites

Actual particle reinforced composite materials often show rather irregular particle shapes, and anisotropy in the microgeometry as well as in the overall response may be introduced by processing effects such as extrusion textures. Nevertheless, for materials reinforced by statistically uniformly distributed equiaxed particles isotropic macroscopic behavior is a good approximation that has been used in many modeling studies. The thermoelastic behavior of macroscopically isotropic composites has been successfully described by mean field methods that approximate the particles as spheres, see section 2.3. Extensions of the mean field solutions into the nonlinear range are available, compare section 2.6, but they are subject to some limitations in predicting the overall thermomechanical response in the

Table 5.2: Overall elastic properties of a SiC/Al2618 MMC reinforced by randomly oriented fibers ($a = 5, \xi$=0.15) as predicted by the Hashin–Shtrikman bounds (HS), by the Mori–Tanaka method (MTM), by the classical self-consistent scheme (CSCS) of Berryman (1980), by the Kuster and Toksöz (1974) model (KTM) and by multi-fiber unit cells of the type shown in fig. 5.16 (MFUC), which contain 15 spheroidal or cylindrical fibers (Böhm et al., 2002).

	E^* [GPa]	ν^* []
fibers	450.0	0.17
matrix	70.0	0.30
HS/lo	87.6	0.246
HS/hi	106.1	0.305
MTM	89.8	0.285
CSCS	91.2	0.284
KTM	90.3	0.285
MFUC/sph	89.4	0.285
MFUC/cyl	90.0	0.284

post-yield regime. In addition, mean field models cannot account for many particle shape, clustering, and size distribution effects and cannot resolve local fluctuations of the local stress and strain fields. As a consequence, there has been considerable interest in unit cell models for particle reinforced composites.

One issue in applying unit cell approaches to the modeling of particle reinforced materials with overall isotropic behavior is that there exists no simple periodic three-dimensional phase arrangement that shows matrix–inclusion toplogy and is inherently elastically isotropic[82]. Together with the wide variation in microgeometries and particle shapes in actual materials, this causes studies using generic phase arrangements to be subject to nontrivial tradeoffs between keeping computational requirements at manageable levels (favoring simple particle shapes combined with two-dimensional models or simple three-dimensional microgeometries) and obtaining sufficiently realistic models for a given purpose (often leading to requirements for unit cells containing a high number of particles of complex shape). In many respects, however, periodic microfield models of particle reinforced composites are subject to similar constraints and use analogous approaches as work on short fiber reinforced composites.

Many three-dimensional unit cell studies of generic microgeometries for particle reinforced composites have been based on simple cubic (sc), face centered cubic (fcc) and body centered cubic (bcc) arrangements of spherical, cylindrical and cube-shaped particles, compare Hom and McMeeking (1991). By invoking the symmetries of these arrangements and using symmetry as well as antisymmetry boundary conditions, small unit cells for materials characterization can be obtained[83], compare Weissenbek et al. (1994) and see figs. 5.17 and 5.18. In addition, work employing hexagonal or tetrakaidecahedral particle arrangements (Rodin, 1993) and Voronoi cells for cubic arrangements of particles (Li and Wongsto, 2004) was reported.

The effective elastic moduli obtained from cubic arrangements of particles show cubic symmetry[84], do not necessarily fulfill the Hashin–Shtrikman bounds and typically lie outside the three-point bounds, compare table 5.3. Of the unit cells shown in fig. 5.17, simple cubic models are the easiest to handle, but they show a more marked anisotropy than bcc and fcc ones.

During the past decade three-dimensional studies based on more complex phase arrangements have begun to appear in the literature. Gusev (1997) used Finite Element methods in combination with unit cells containing up to 64 statistically positioned parti-

[82]Even though pentagonal dodecahedra and icosahedra have the appropriate symmetry properties (Christensen, 1987), they are not space filling.

[83]Among the unit cells shown in fig. 5.18 the one on the left uses symmetry boundary conditions and is restricted in the load cases that can be handled. The other two cells employ antisymmetry B.C.s and can be used more freely. Unit cells with periodicity boundary conditions are considerably larger, but allow unrestricted modeling of the full thermomechanical response of cubic phase arrangements.

[84]Cubic symmetry is a special case of orthotropy with equal responses in all principal directions and requires three independent moduli for describing the elastic behavior. For a discussion of the elastic anisotropy of cubic materials see, e.g., Cazzani and Rovati (2003). The diffusion behavior of materials with cubic symmetry is isotropic.

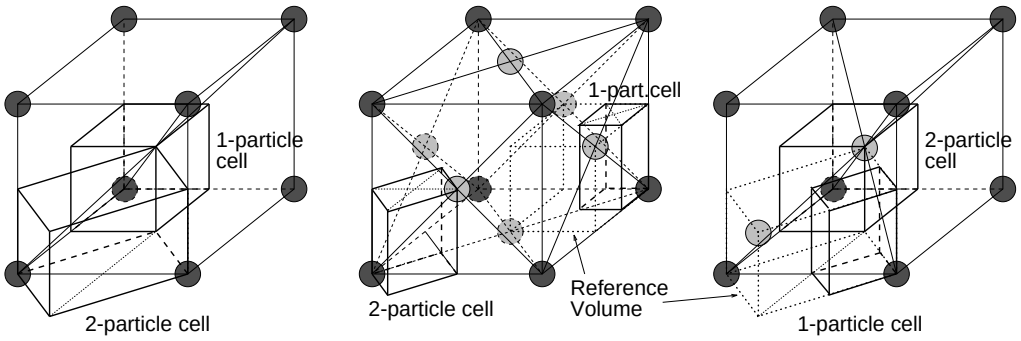

Figure 5.17: Simple cubic, face centered cubic, and body centered cubic arrangements of particles plus some pertinent small unit cells Weissenbek et al. (1994).

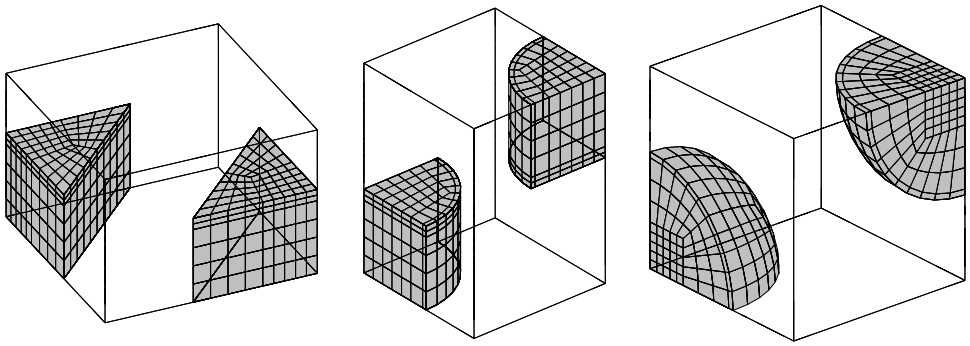

Figure 5.18: Some unit cells for particle reinforced composites using cubic arrangements of inhomogeneities: s.c. arrangement of cubes, b.c.c. arrangement of cylinders and f.c.c. arrangement of spheres Weissenbek et al. (1994).

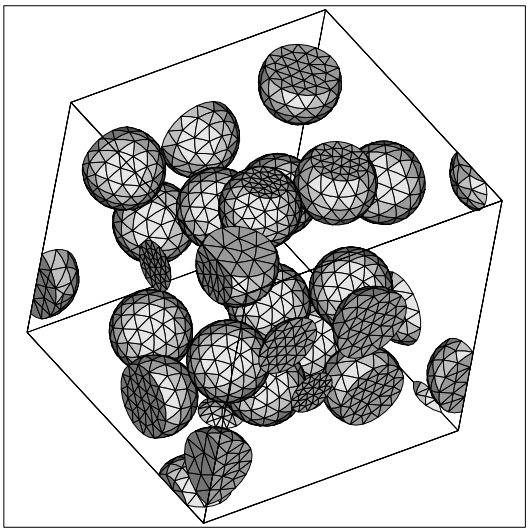

Figure 5.19: Unit cell for a particle reinforced MMC (ξ=0.2) containing 20 spherical particles in a quasi-random arrangement that is suitable for using periodicity B.C. (Böhm and Han, 2001).

cles to describe the overall behavior of elastic particle reinforced composites. Hexahedral unit cells containing up to 10 particles in a perturbed cubic configuration (Watt et al.,

1996) as well as cube shaped cells incorporating at least 15 spherical particles in quasi-random arrangements (Böhm et al., 1999; Böhm and Han, 2001), compare fig. 5.19, or clusters of particles (Segurado et al., 2003) were proposed for studying elastoplastic particle reinforced MMCs and related materials. Three-dimensional simulations involving high numbers of particles have been reported for investigating elastic composites (Michel et al., 1999), for studying brittle matrix composites that develop damage (Zohdi and Wriggers, 2001), and for rubber reinforced polymers (Fond et al., 2001).

In analogy to short fiber reinforced materials, compare fig. 5.14, axisymmetric cell models with staggered or non-staggered particles can be used for materials characterization of particle reinforced composites. By appropriate choice of the dimensions of the axisymmetric cells, sc, fcc and bcc arrangements of particles can even be approximated this way. Axisymmetric cell models have been a mainstay of PMA modeling of materials containing particulate inhomogeneities, see, e.g., Bao et al. (1991) or LLorca (1996).

Due to their relatively low computational requirements, planar unit cell models of particle reinforced materials have also been used to a considerable extent. Typically, plane stress models (which actually describe "reinforced sheets" or the stress states at the surface of inhomogeneous bodies) show a more compliant and plane strain models (which correspond to reinforcement by aligned continuous fibers rather than particles) show a stiffer overall response than three-dimensional descriptions, compare table 5.3. With respect to the overall behavior, plane stress analyses may be preferable to plane strain analyses, compare (Weissenbek, 1994), but no two-dimensional model gives satisfactory results in terms of the predicted microstress and microstrain distributions[85] (Böhm and Han, 2001). Axisymmetric cell models typically provide considerably better results than planar ones.

In table 5.3 bounds, MFA results and a number of PMA predictions for the overall thermoelastic moduli of a particle reinforced SiC/Al MMC (elastic contrast $C \approx 5.5$) are compared, the loading directions for the cubic arrangements being identified by Miller indices. It is noteworthy that — for the loading directions considered here, which do not span the full range of possible responses of the cells — none of the cubic arrangements gives results that fall within the third order bounds for identical spherical particles[86]. The overall anisotropy of the simple cubic arrangement is marked, whereas the body centered and face centered arrays deviate much less from overall isotropy. The predictions of the axisymmetric analyses can be seen to be of comparable quality in terms of the elastic moduli to those of the corresponding cubic arrays, but typically give an anisotropic thermal expansion behavior. The results listed for the three-dimensional multi-particle models are ensemble averages over a number of unit cells and loading directions (compare the discus-

[85] Plane stress configurations tend to predict much higher levels of equivalent plastic strains in the matrix and weaker overall hardening than do plane strain and generalized plane strain models using the same phase geometry. For a given particle volume fraction, results from three-dimensional arrangements typically lie between those of the above planar models. Evidently, the configurations of regions of concentrated strains that underlie this behavior depend strongly on the geometrical constraints (Iung and Grange, 1995; Gänser et al., 1998; Böhm et al., 1999; Shen and Lissenden, 2002). For continuously reinforced composites under transverse loading the equivalent plastic strains tend to concentrate in bands oriented at 45° to the loading directions, whereas the patterns are qualitatively different in particle reinforced materials.

[86] For cubic symmetries the extremal values of the Young's modulus are found for loading in the [100] and [111] directions (Nye, 1957).

Table 5.3: Overall thermoelastic properties of a particle reinforced SiC/Al MMC (spherical particles, ξ=0.2) as predicted by the Hashin–Shtrikman (HS) and third order (3PB) bounds, by the Mori–Tanaka method (MTM), by the generalized self-consistent scheme (GSCS), by Torquato's three-point estimates (3PE), as well as by unit cell analysis using three-dimensional cubic arrangements, axisymmetric cells approximating sc, fcc and bcc arrangements, two-dimensional multi-particle models based on plane stress (2/D PST) and plane strain (2/D PSE) kinematics, as well as the three-dimensional multi-particle model shown in fig. 5.19.

	E^* [GPa]	$E^*[100]$ [GPa]	$E^*[110]$ [GPa]	ν^* []	α_A^* $[K^{-1}\times 10^{-6}]$
particles	429.0	—	—	0.17	4.3
matrix	67.2	—	—	0.35	23.0
HS/lo	90.8	—	—	0.286	16.8
HS/hi	114.6	—	—	0.340	18.6
3PB/lo	91.4	—	—	0.323	18.5
3PB/hi	93.9	—	—	0.328	18.6
MTM	90.8	—	—	0.329	18.6
GSCS	91.5	—	—	0.327	18.6
3PE	91.8	—	—	0.327	18.6
sc	—	96.4	90.5		18.7
fcc	—	89.0	91.7		18.6
bcc	—	90.0	90.6		18.6
axi/sc	95.4	—	—		18.6/18.6
axi/fcc	88.1	—	—		18.1/19.0
axi/bcc	87.9	—	—		18.4/18.8
2/D PST	85.5	—	—	0.334	
2/D PSE	98.7	—	—	0.500	
3/D	92.4	—	—	0.326	

sion in section 4.1), and they show very good agreement with the three-point bounds and estimates, whereas there are marked differences to the plane stress and plane strain models. For the composite studied here, predicted overall moduli evaluated from the individual multi-particle cells differ by about 2%, and due to the use of a periodic pseudo-random rather than a statistically homogeneous particle distribution, the estimates of Drugan and Willis (1996) for the errors in the overall moduli are exceeded slightly.

Similarly to fiber reinforced MMCs, particle reinforced composites typically display highly inhomogeneous microscopic stress and strain distributions, especially for the matrix in the nonlinear range. As an example, fig. 5.20, shows the predicted equivalent plastic strains of the elastoplastic matrix inside the multi-particle unit cell model of an MMC shown in fig. 5.19. This behavior tends to give rise to microscopic "structures" that can be considerably larger than individual particles, leading to longer ranged interactions between inhomogeneities[87]. The latter, in turn, underlie the need for larger control volumes for

[87]Due to the filtering effect of periodic phase arrangements mentioned in section 5.1, the length of such features can exceed the size of the unit cell only in certain directions (parallel to the faces and diagonals

studying composites with nonlinear matrix behavior mentioned in chapter 4.

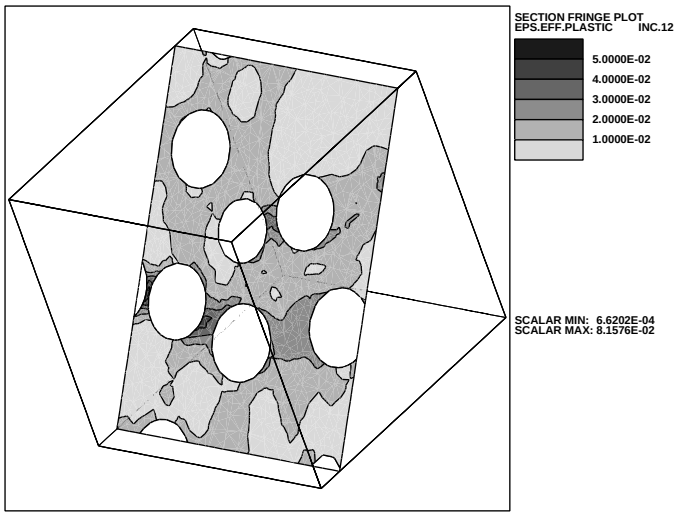

Figure 5.20: Predicted equivalent plastic strain in a particle reinforced MMC (ξ=0.2) subjected to uniaxial tensile loading obtained by a unit cell with 20 spherical particles in a quasi-random arrangement (Böhm and Han, 2001).

If the particles are highly irregular in shape or if their volume fraction markedly exceeds 0.5 (as is typically the case for cermets such as WC/Co), generic unit cell models employing relatively regular particle shapes may not result in satisfactory microgeometries. For such materials a useful approach consists of basing PMA models on modified real structures obtained from metallographic sections, compare, e.g., Fischmeister and Karlsson (1977). Due to the nature of the underlying experimental data, models of this type have often taken the form of planar analysis, the limitations of which are discussed above. This difficulty can be overcome, e.g., by voxel-based discretization schemes using digitized serial sections, see Terada and Kikuchi (1996), or microtomography data, see, e.g., Borbély et al. (2006). Alternatively, more or less irregular particles identified by such procedures may be approximated by equivalent ellipsoids, compare Li et al. (1999).

5.7 Unit Cell Models for Porous and Cellular Materials

Elastoplastic porous materials have been the subject of a considerable number of PMA studies due to their relevance to the ductile damage and failure of metallic materials[88]. Generally, modeling concepts for porous materials are closely related to the ones employed for particle reinforced composites, the main difference being that the shapes of the voids

of the cells), which may induce a spurious direction dependence into the predicted large-strain behavior of sub-RVE unit cells.

[88]Many models and constitutive descriptions of the ductile damage and failure of metals, among them contributions by Rice and Tracey (1969), Gurson (1977), Tvergaard and Needleman (1984), Gologanu et al. (1997) as well as Benzerga and Besson (2001), are based on micromechanical studies of the growth of pre-existing voids in a ductile matrix.

may evolve significantly through the loading history[89]. Three-dimensional unit cells based on cubic arrangements of voids (McMeeking and Hom, 1990; Segurado et al., 2002b) and axisymmetric cells of the types discussed in section 5.6 (Koplik and Needleman, 1988; Gărăjeu et al., 2000) have been used in the majority of the pertinent PMA studies. Recently, studies of void growth in ductile materials based on multi-void cells and using geometry data from serial sectioning were reported (Shan and Gokhale, 2001).

In cellular materials, such as foams, wood and cancellous bone, the volume fraction of the solid phase is low (often amounting to no more than a few percent) and the void phase may be topologically connected (open cell foams), unconnected (closed cell foams, syntactic foams) or both of the above (e.g., hollow sphere foams). The linear elastic responses of cellular materials are typically limited to a very small range of macroscopic strains, and marked differences tend to be present between tensile and compressive responses. As strains increase gross shape changes of the cells typically take place with bending, elastic buckling, plastic buckling and brittle failure of struts and cells walls playing major roles on the microscale, especially under compressive loading. For compression-dominated load cases this regime tends to give rise to a stress plateau on the macroscale, which underlies the favorable energy absorption properties of many cellular materials. No comparable behavior is present under tensile and shear loading. At some elevated strain the effective stiffness typically rises sharply under compression, the cellular structure having collapsed to such an extent that many cell walls or struts are in contact.

Periodic microfield methods are well suited to studying the thermomechanical behavior of cellular materials. The widely used analytical results of Gibson and Ashby (1988) were derived by analytically studying arrangements of beams (for open cell foams) or plates (for closed cell foams). They express macroscopic moduli and other physical properties of cellular materials as power laws

$$\frac{E^*}{E^{(\mathrm{m})}} \propto \left(\frac{\rho^*}{\rho^{(\mathrm{m})}}\right)^n \tag{5.19}$$

in terms of the relative density[90], $\rho^*/\rho^{(\mathrm{m})}$.

In Finite Element based models of cellular materials the solid phase may be described either by continuum elements or by structural elements (shells for the cell walls of closed cell foams and beams for the struts in open cell foams)[91]. In order to describe buckling and compaction phenomena, unit cells for cellular materials require explicit provision for

[89]The evolution of the shapes of initially spheroidal voids under non-hydrostatic loads has been the subject of intensive studies by mean field type methods, compare Kailasam et al. (2000). Such models are based on the assumption that initially spherical pores will stay ellipsoids throughout the deformation history, which axisymmetric cell analyses (Gărăjeu et al., 2000) have shown to be an excellent approximation for axisymmetric tensile load cases. For compressive loading, however, initially spherical pores may evolve into markedly different shapes (Segurado et al., 2002b). Void size effects (Tvergaard, 1996) and void coalescence (Faleskog and Shih, 1997) introduce additional complexity into studies of the ductile damage and failure of metals.

[90]The exponent in eqn. (5.19) allows to infer the dominant local deformation mode of a cellular microgeometry, with n=2 implying deformation by the bending and n=3 by axial elongation/compression of struts in open cell foams. The Gibson-Ashby cell for open cell foams gives n=2 and, as a consequence, tends to underestimate stiffness of actual open-cell foams.

[91]At high porosities it is typically necessary to account for the overlap of shell elements at edges and of beam elements at vertices when evaluating the phase volume fractions of the discretized unit cells. When

handling large deformations of and contact between cell walls or struts. Boundary conditions must be applied to the unit cells such that they do not interfere with buckling modes. Specifically, models must be sufficiently large so that nontrivial deformation and buckling patterns can develop, or Bloch wave theory (Gong et al., 2005) must be used to account for long wavelength buckling modes[92].

The geometrically simplest cellular materials are regular honeycombs, which can be modeled by planar hexagonal cell models. Somewhat less ordered two-dimensional arrangements have been used for studying the crushing behavior of soft woods (Holmberg et al., 1999), and highly irregular planar arrangements, compare fig. 5.21, can be used to investigate aspects of the geometry dependence of the mechanical response of cellular materials, such as metallic foams.

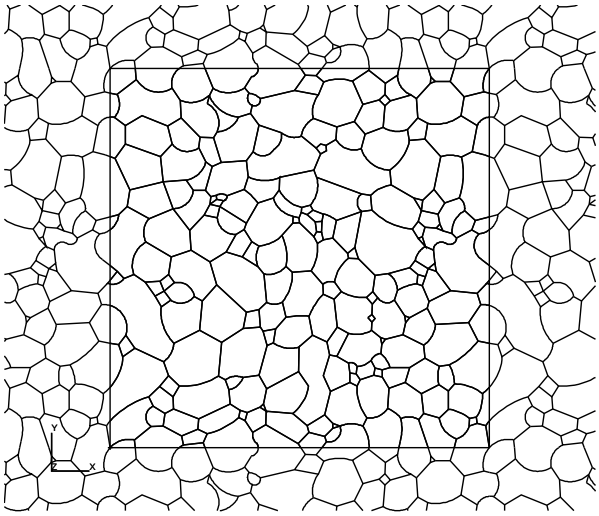

Figure 5.21: Planar periodic unit cell for studying irregular cellular materials (Daxner, 2003).

For three-dimensional studies of closed cell foams various generic microgeometries based on cubic cells, see, e.g., Hollister et al. (1991), truncated cubes plus small cubes (Santosa and Wierzbicki, 1998), rhombic dodecahedra, regular tetrakaidecahedra (Grenestedt, 1998; Simone and Gibson, 1998), compare fig. 5.22, as well as Kelvin, Williams and Weaire–Phelan[93] (Kraynik and Reinelt, 1996; Daxner et al., 2007) geometries, compare fig. 5.23, have been used. Analogous regular microgeometries have formed the basis for analytical and numerical models of open cell foams, see, e.g., Zhu et al. (1997), Shulmeister et al. (1998) and Vajjhala et al. (2000), the struts connecting the nodes of the cellular structures

structural elements are used in unit cell studies periodicity conditions must be enforced in terms of both translational and rotational degrees of freedom.

[92]For perfectly regular structures such as hexagonal honeycombs the minimum size of a unit cell for capturing bifurcation effects can be obtained from extended homogenization theory (Saiki et al., 2002). When symmetry boundary conditions are employed care must be taken that cell walls that may buckle do not coincide with symmetry planes, and periodic contact may have to be provided for if periodicity boundary conditions are used.

[93]In Kelvin, Williams and Weaire–Phelan foams some of the cell walls are spatially distorted in order to minimize the total surface, whereas in polyhedral foams all cell walls are planar. These small distortions lead to noticeable differences in the overall elastic response at low solid volume fractions.

being typically modeled as beams. Tetrahedral arrangements (Sihn and Roy, 2005) and cubic arrangements of struts with additional "reinforcements" as well as perturbed strut configurations (Luxner et al., 2005) have been used for studying open cell microgeometries. Random Laguerre tessellations have recently been proposed for generating periodic multi-cell models of open cell and closed cell foams (Redenbach, 2009).

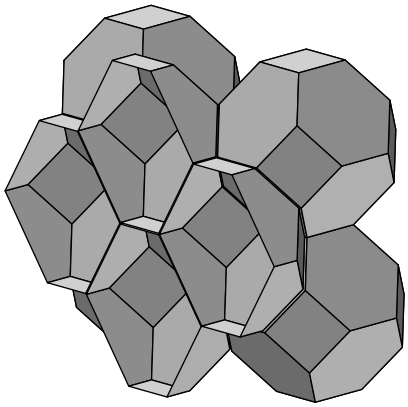

Figure 5.22: Foam microstructure modeled by regular tetrakaidecahedra (truncated octahedra).

The effects of details of the microgeometries of cellular materials (e.g., thickness distributions and geometrical imperfections or flaws of cell walls or struts or the Plateau borders formed at the intersections of cell walls), which can considerably influence the overall behavior have been an active field of research employing PMAs, see, e.g., Grenestedt (1998) and Daxner (2003). Even though unit cell analysis of cellular materials with realistic microgeometries tends to be rather complex and numerically demanding due to these materials' tendency to deform by local mechanisms and instabilities, analytical solutions have been reported for the linear elastic behavior of some simple periodic phase arrangements, see, e.g., Warren and Kraynik (1991).

The high flexibility of FE-based periodic homogenization allows its adaptation to non-standard microgeometries, such as hollow strut foams produced by coating a precursor cellular material. Figure 5.23 shows such a microgeometry that is based on a Weaire–Phelan model and was meshed by combinations of solid and shell elements (Daxner et al., 2007).

Due to the inherent absorption contrast between matrix and voids, cellular materials are well suited to high-resolution computed tomography, giving access to microgeometries that can be directly converted into voxel models[94] of open-cell and closed-cell foams, see, e.g., Maire et al. (2000) or Roberts and Garboczi (2001). Alternatively, image processing methods my be used to generate a surface model of the solid phase in the volume element to allow meshing with "standard" FE techniques (Youssef et al., 2005). Because the microgeometries extracted from the experiments are, in general, not periodic, windowing

[94]Roberts and Garboczi (2001) estimated the "systematic discretization error" to be of the order of 10% in terms of the overall moduli for voxel-based models of elastic open-cell and closed-cell foams.

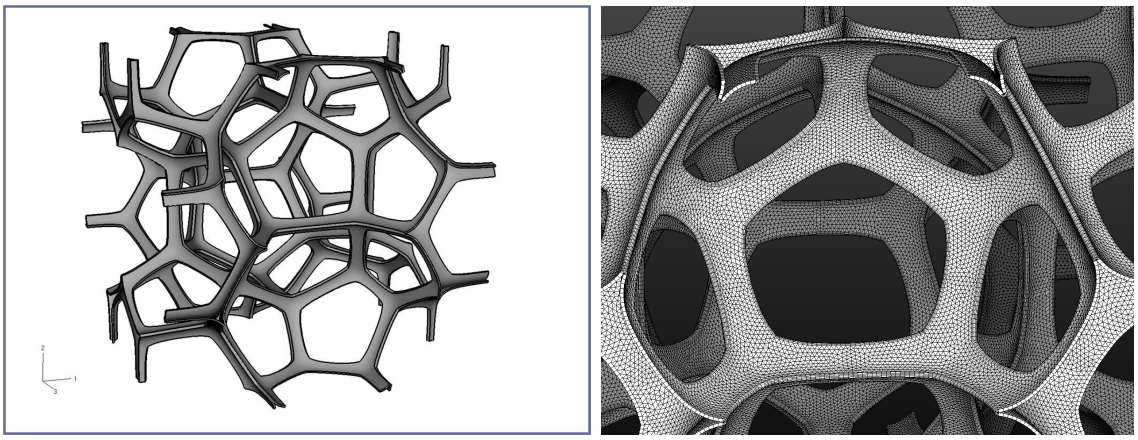

Figure 5.23: Weaire–Phelan model of an open cell foam with hollow struts (left) and detail of the FE-model (right), from Daxner et al. (2007).

approaches using homogeneous strain boundary conditions are preferable to unit cells in such models.

A specific group of cellular materials amenable to PMA modeling are syntactic foams (i.e., hollow spheres embedded in a solid matrix) and hollow sphere foams (in which the spaces between the spheres are "empty"), for which axisymmetric or three-dimensional cell models describing cubic arrangements of spheres can be used (Rammerstorfer and Böhm, 2000; Sanders and Gibson, 2003).

A further type of cellular material, cancellous (or spongy) bone, has attracted considerable research interest for the past twenty years[95]. Cancellous bone shows a wide range of microgeometries, which can be idealized as beam or beam–plate configurations (Gibson, 1985), and the solid phase again is an inhomogeneous material at lower length scales. In studying the mechanical behavior of cancellous bone, large three-dimensional unit cell models based on tomographic scans of actual samples and using voxel-based discretization schemes have become fairly widely used, see, e.g., Hollister et al. (1991), Hollister et al. (1994) or van Rietbergen et al. (1999).

5.8 Unit Cell Models for Some Other Inhomogeneous Materials

At the continuum level, the thermomechanical behavior of essentially any inhomogeneous material can be studied by periodic microfield techniques. For example, the elastic, elastoplastic, creep and damage behaviors of polycrystals, of high speed steels and dual phase steels, of intermetallics, of superalloys, and of graded materials have been the targets of unit cell models. In addition, "smart materials", such as piezoelectric composites and

[95]Like many materials of biological origin, bone is an inhomogeneous material at a number of length scales. The solid phase of spongy bone is inhomogeneous and can also be studied with micromechanical methods.

shape memory alloys, and solid state phase transitions in general have been studied. A comprehensive discussion of the models involved would by far exceed the present scope, so that the present section is limited to a small number of examples.

Generic PMA Models for Clustered, Graded, and Interpenetrating Microgeometries

Many commercially important steels may be viewed as matrix–inclusion-type composites. For example, high speed steels (HSS) contain carbidic inclusions in a steel matrix, with arrangements ranging from statistically homogeneous to highly clustered or layered (meso)geometries. Such materials can be modeled like particle reinforced MMCs. However, models encompassing elevated numbers of particles have been limited to two-dimensional analysis by computing power requirements. A straightforward and flexible strategy for setting up generic planar model geometries for such studies consists of tiling the computational plane with regular hexagonal cells which are assigned to one of the constituents by statistical or deterministic rules. If required, the shapes of the cells can be modified or randomly distorted and their sizes can be changed to adjust phase volume fractions. Such a Hexagonal Cell Tiling (HCT) concept can be used, e.g., to generate unit cells for analyzing layer structured HSSs, compare (Plankensteiner et al., 1997) and fig. 5.24, and clustered or random arrangements of inhomogeneities in a matrix. HCT and related models of matrix–inclusion topologies are, however, restricted to low reinforcement volume fractions.

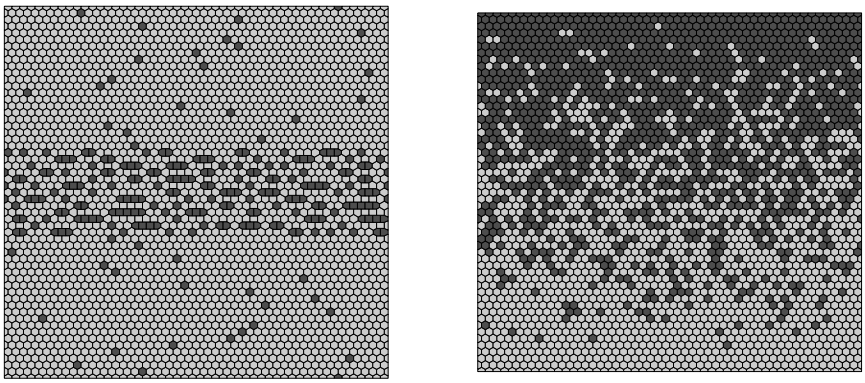

Figure 5.24: HCT unit cell models for a layer structured high-speed steel (left) and a functionally graded material (right).

Related concepts can be used to obtain generic geometries for planar models for studying functionally graded materials[96] (FGMs), in which the phase volume fractions run through the full physically possible range (Weissenbek et al., 1997; Reiter et al., 1997), so that there are regions that show matrix–inclusion microtopologies and others that do not, compare fig. 5.24 (right). A further application of such models have been investigations of the microstructure–property relationships in duplex steels, for which matrix–

[96]In contrast to most other materials discussed in the present reports, FGMs are statistically inhomogeneous materials and phase arrangements must be non-periodic in at least one direction, for which free-surface boundary conditions are used on the unit cells.

inclusion and interwoven phase arrangements were compared[97], see Siegmund et al. (1995) and Silberschmidt and Werner (2001). An FFT-based modeling scheme employing HCT-like geometries was developed by Michel et al. (1999) explicitly for studying interwoven microgeometries. There is no direct three-dimensional equivalent to HCT models, but unit cells partitioned into cube-shaped or tetrakaidecahedral subcells can be used in an analogous manner to obtain generic microgeometries. A related, but geometrically more flexible approach based on tetrahedral regions was reported by Galli et al. (2008).

PMA Models for Polycrystals

A large number of materials that are of technological interest are polycrystals and, accordingly, are inhomogeneous at some sufficiently small length scale. In the special case of metals and metallic alloys phenomena associated with plastic flow and ductile failure can be investigated at a number of length scales (McDowell, 2000), some of which are amenable to study by continuum micromechanical methods.

Micromechanical methods, especially analytical self-consistent approaches, have been applied to studying the mechanical behavior of polycrystals since the 1950s. The more recent concept of studying polycrystals by periodic microfield methods (and other discrete microgeometry approaches) is quite straightforward in principle — a planar or three-dimensional unit cell is partitioned into suitable subregions that correspond to individual grains[98]. For these grains appropriate material models must be prescribed, and suitable material as well as orientation parameters must be assigned to them. The generation of appropriate grain geometries may be based, e.g., on Voronoi tessellations using Poisson or hardcore distributed seed points. Such microgeometries may be linked to uniform and isotropic grain growth that stops at any point where neighboring grains contact each other, may be efficiently generated as well as meshed by appropriate software (Fritzen et al., 2009), and can provide periodic unit cells or non-periodic volume elements. Alternatively, the grain geometries can be based on experimental data obtained, e.g., by microscopy and serial sectioning.

Anisotropic elasticity and crystal plasticity models are best suited to describing the material behavior of the individual grains, the orientation of which can be described by stochastic models. The number of grains required to achieve a given accuracy in approximating the macroscopic elastic tensor has been shown to depend on the anisotropy of the individual grains (Nygårds, 2003). Analysis involving crystal plasticity tends to pose considerable demands on computational resources for three-dimensional analyses, compare Quilici and Cailletaud (1999). For a general discussion of the issues involved in micromechanical models in crystal plasticity and related fields see, e.g., Dawson (2000).

[97] In HSSs and FGMs particulate inhomogeneities are present at least in part of the volume fraction range, so that planar analyses must be viewed as compromises between modeling accuracy and computational requirements. Duplex steels, in contrast, typically show elongated aligned grains, which can be described well by generalized plane strain analysis in the transverse plane.

[98] Usually symmetry boundaries passing through grains must be avoided in models of this type because they give rise to "twin-like" pairs of grains that are unphysical in most situations.

PMA Models for Two-Phase Single Crystal Superalloys

Nickel-base single crystal superalloys, which consist of a γ matrix phase containing aligned cuboidal γ' precipitates, are of major technical importance due to their creep resistance at high temperatures. The most important field of application of superalloys is in the hot sections of gas turbines. Because these materials show relatively regular microgeometries that change under load, a process known as rafting, there has been considerable interest in micromechanical modeling for elucidating their thermomechanical behavior and for better understanding their microstructural evolution. The elastic behavior of two-phase superalloys can be handled relatively easily by hexahedral unit cells with appropriately oriented anisotropic phases. In the inelastic range, however, the highly constrained plastic flow in the γ channels is difficult to describe even by crystal plasticity models, see, e.g., Nouailhas and Cailletaud (1996).

5.9 Unit Cell Models Models for Diffusion-Type Problems

Periodic microfield methods analogous to those discussed in sections 5.1 to 5.8 can be used to study linear diffusion-type problems of the types mentioned in section 2.9. However, because symmetry boundary conditions, eqn. (5.4), imply insulating surfaces in conduction-type problems and, accordingly, are not compatible with macroscopic gradients normal to them, they cannot be used freely in such analysis. The Laplace solvers required for numerically-based homogenization in diffusion problems are widely available in FE packages, typically for modeling heat conduction. Specialized solvers are, however, required in some cases, e.g., when studying the frequency dependent dielectric properties of composites via complex potentials, see, e.g., Krakovsky and Myroshnychenko (2002).

For the most common application, thermal conduction, general periodicity boundary conditions equivalent to eqn. 5.2 take the form

$$\Delta T_k = T_{k^+} - T_{k^-} = T(\tilde{\mathbf{s}}_k + \mathbf{c}_k) - T(\tilde{\mathbf{s}}_k) = \langle \mathbf{d} \rangle \mathbf{c}_k \qquad , \tag{5.20}$$

where the nomenclature of table 2.1 is followed and $\langle \mathbf{d} \rangle$ is the volume averaged temperature gradient. Asymptotic homogenization for thermal conduction was discussed, e.g., by Auriault (1983), Tang and Yu (2007) or Matt and Cruz (2002), and the method of macroscopic degrees of freedom, compare section 5.3, can be formulated in terms of temperatures rather than displacements (Nogales, 2008). Volume and phase averages of fluxes are best evaluated according to eqn. (4.1). Finite interfacial conductances can be handled by using appropriate interface elements, compare, e.g., Matt and Cruz (2008) as well as Nogales and Böhm (2008).

There are, however, intrinsic conceptual difficulties in applying periodic homogenization to transport problems where nonlinear diffusivity of conductivity behavior of the constituents is present. Whereas in solid mechanics, material nonlinearities are typically formulated in terms of the microscopic stresses and strains, which may be viewed as "generalized intensity" and "generalized flux" fields (compare table 2.1, respectively, nonlinear

diffusivities in transport problems typically depend on the field variable, e.g., the temperature in heat conduction. As is evident from fig. 5.1, in PMAs the generalized intensities and fluxes are periodic (and have constant averages), whereas the field variables are sums of fluctuating and linear contributions, so that they accumulate from cell to cell. As a consequence, in solid mechanics problems the material properties of any given cell in a periodic arrangements are the same, whereas in transport problems they are not. This implies that — even though workable solutions in terms of both microscopic fields and homogenized macroscopic properties can be obtained from "unit cells" in which material nonlinearities of the above type are specified — the computational domain cannot be properly tiled with such cells and a periodic model material is not obtained[99]. Accordingly, embedding or windowing methods, see sections 6 and 7, rather than periodic homogenization should be used for studying nonlinear transport problems in inhomogeneous media.

[99]The fact that periodicity implies that the field variable can take values from $-\infty$ to $+\infty$ leads to another inconsistency in PMAs for thermal conduction, where the field variable T has a thermodynamical lower bound at absolute zero. However, no practical repercussions of this issue are known.

Chapter 6

Embedding Approaches and Related Models

Like periodic microfield methods, Embedded Cell Approaches (ECAs) aim at predicting the microfields in geometrically highly resolved models of inhomogeneous materials. ECA models consist of two major parts. On the one hand, there is a core (or "local heterogeneous region") consisting of a discrete microstructure, which can range from rather simple to highly detailed phase arrangements. On the other hand, there is an outer region ("embedding region", "effective region") into which the core is embedded and which serves mainly for transmitting the applied loads, compare fig. 6.1. This modeling strategy avoids some of the drawbacks of PMAs, especially the requirement that the microgeometry and all microfields must be strictly periodic[100].

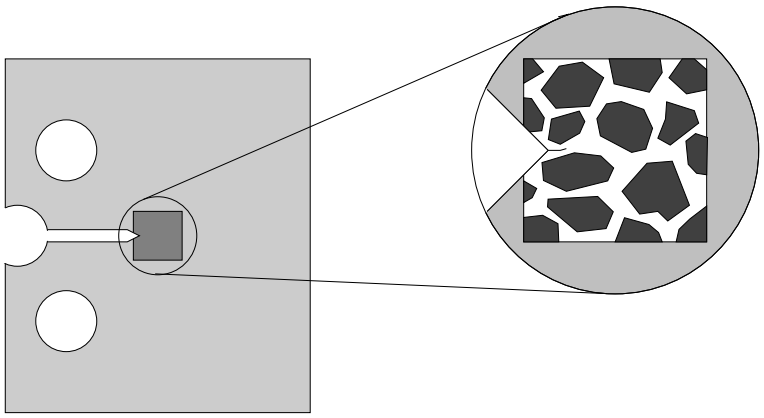

Figure 6.1: Schematic depiction of the arrangement of core and embedding region in an embedded cell model of a tensile test specimen.

An intrinsic feature of embedding models are spurious boundary layers that occur at the "interfaces" between the core and the embedding region and perturb the local stress

[100]Embedding analyses can be used without intrinsic restrictions at or in the vicinity of free surfaces and interfaces, they can handle gradients in composition and loads, and they can be used to study the interaction of macrocracks with microstructures. Also, the requirement of sufficiently separated length scales, compare section 1.1, does not necessarily apply to embedded models.

and strain fields[101]. Provision must be made to keep regions of specific interest, such as crack tips or process zones, away from the core's boundaries[102].

Three basic types of embedding approaches can be found in the literature. One of them uses discrete phase arrangements in both the core region and in the surrounding material, the latter, however, being discretized by a much coarser FE mesh, see, e.g., Sautter et al. (1993). Such models, which may approach descriptions of a full sample or structure that contain a refined mesh in some region(s) of interest, can avoid boundary layers to a large extent by using appropriately graded meshes. They tend, however, to be relatively expensive computationally. Mesh superposition techniques, which use a coarse mesh over the macroscopic model of some structure or sample together with a geometrically independent, much finer mesh in regions of interest (Takano et al., 2001) are conceptually similar to the above modeling strategy.

In the second group of embedding methods the behavior of the outer regions is described via appropriate "smeared-out" constitutive models. These typically take the form of semiempirical or micromechanically based constitutive laws that are prescribed a priori for the embedding zone and which must be chosen to correspond closely to the overall behavior of the core[103]. This way, conceptually simple models are obtained that are very well suited to studying local phenomena such as the stress and strain distributions in the vicinity of crack tips (Aoki et al., 1996), around local defects (Xia et al., 2001) or at macroscopic interfaces in composites (Chimani et al., 1997), the growth of cracks in inhomogeneous materials (van der Giessen and Tvergaard, 1994; Wulf et al., 1996; Motz et al., 2001; Mishnaevsky, 2004; González and LLorca, 2007) or damage due to the processing of composites (Monaghan and Brazil, 1997). For such applications, loads may be introduced via macrohomogeneous stress and/or strain fields, compare eqns. (7.2) and (7.3), or via displacement boundary conditions that impose a far field behavior obtained from a suitable analytical or numerical solution (e.g., the displacement field for the far field of a crack tip in elasticity or small-scale plasticity) pertinent to the appropriate effective material behavior. The modeling approach also allows complete specimens or components to be considered in "simulated experiments" as sketched in fig. 6.1, where loads can be applied via suitable concentrated forces that closely approximate the loading conditions of the actual samples.

[101]The interfaces between core and embedding region obviously are a consequence of the modeling approach and do not have any physical significance. In elasticity such boundary layers typically have a thickness of, say, the distance between the centers of neighboring inhomogeneities, but they may be longer ranged for nonlinear material behavior.

[102]Boundary layers and embedding regions may interfere with extended regions of concentrated strains, with shear bands, or with the growth of damaged regions. Such difficulties can only be avoided or mitigated by choosing a sufficiently large core region. In transient analysis the boundary layers tend to lead to reflection and/or refraction of waves. Special transition layers can, however, be introduced to mitigate boundary layer effects in the latter case.

[103]The material parameters used with these constitutive laws may be obtained from modeling or from experiments (Ayyar et al., 2008).
Care is required in modeling the behavior of elastoplastic inhomogeneous materials with continuous reinforcements via ECA models, because the homogenized response of the material is anisotropic, so that anisotropic plasticity models such as Hill (1948) plasticity must be used.
It is worth noting that by restricting damage effects to the core of a model and prescribing the behavior of the damage-free composite to the embedding material the size of the core effectively controls the volume fractions of damaged regions in ECA models, compare, e.g., Bao (1992).

A closely related modeling strategy makes use of submodeling techniques in which an inhomogeneous micromodel is coupled to a homogeneous macro model via appropriate coupling conditions (which may be implemented via the boundary conditions of the micromodel), compare, e.g., Heness et al. (1999) or Váradi et al. (1999).

The third type of embedding scheme employs the homogenized thermomechanical response of the core for determining the effective behavior of the surrounding medium in a self-consistent way. Models of this type have been mainly employed for materials characterization. The use of such approaches is, of course, predicated on the availability of suitable parameterizable constitutive laws for the embedding material that can follow the core's instantaneous homogenized behavior with high accuracy for all load cases and for any loading history. This requirement typically can be fulfilled easily in the linear range, see e.g., Yang et al. (1994) and Chen (1997), but may lead to considerable complexity when at least one of the constituents shows elastoplastic or viscoplastic material behavior[104]. Accordingly, approximations have to be used (the consequences of which may be difficult to assess in view of the nonlinearity and path dependence of, e.g., elastoplastic material behavior) and models of this type are best termed "quasi-self-consistent schemes". Such approaches were discussed, e.g., by Bornert et al. (1994) and by Dong and Schmauder (1996). They are the only embedding methods that do micromechanics in the strict sense in that they carry out scale transitions. When a periodic multi-inhomogeneity volume element is used as the core in a self-consistent or quasi-self-consistent embedding scheme, the relaxation of the periodicity constraints tends to make the overall responses of the embedded configuration softer compared to periodic homogenization of the same periodic arrangement (Bruzzi et al., 2001)[105]. For materials characterization embedded cell models are typically loaded by homogeneous far field stresses or strains applied to the outer boundaries.

Some analytical methods such as classical and generalized self-consistent schemes, see section 2.3, can obviously be viewed as embedding schemes that combine relatively simple cores with self-consistently defined material behavior of the embedding region. When geometrically more complex cores are considered in ECA-like frameworks, however, numerical engineering methods are best suited for resolving the discrete phase arrangements in the core region, compare Bornert (1996).

The core and embedding regions may be planar, axisymmetric or fully three-dimensional, and symmetries present in the geometries can, as usual, be employed to reduce the size of the model, compare Xia et al. (2001). Effective and phase averaged stresses and strains from embedded cell analyses are best evaluated with eqn. (5.16) or its equivalents, and in the case of geometrically complex phase arrangements it is good practice to use only

[104]Typically, the effective yielding behavior of elastoplastic composites shows some dependence on the first stress invariant, and, for low plastic strains, the homogenized response of the core tends to be strongly influenced by the fractions of the elastoplastic constituent(s) that have actually yielded. In addition, in many cases anisotropies of the yielding and hardening behavior are introduced by the phase geometry (e.g., aligned fibers) and by the phase arrangement of the core. At present, there appears to be no constitutive law that, on the one hand, can fully account for these phenomena and, on the other hand, has the capability of being adapted to the instantaneous response of the core by adjusting free parameters.

[105]In the study mentioned above, the difference between PMA and ECA results is relatively small. Identical responses can be expected from the two types of model if the phase arrangement is a proper RVE and the embedding material can fully describe the homogenized behavior of the core.

the central regions of the core for this purpose in order to avoid perturbations from the boundary layers.

Chapter 7

Windowing Approaches

The aim of windowing methods is to obtain estimates or bounds for the macroscopic properties of inhomogeneous materials on the basis of non-periodic volume elements that are referred to as "mesoscopic test windows" or, shorter, as "windows". These volume elements typically have simple shapes, are extracted at random positions and, in the case of macroscopically homogeneous materials, with random orientations from an inhomogeneous medium, compare fig. 7.1, and are smaller than RVEs. Because the results of windowing analysis pertain to individual samples rather than to a material, they are referred to as apparent (rather than effective) properties.

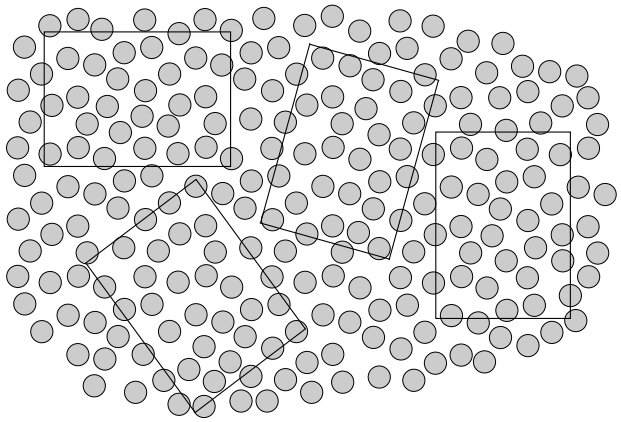

Figure 7.1: Schematic depiction of a composite and four rectangular windows of equal size.

Windowing methods are based on a surface integral version of the Hill condition, eqn. (1.6), that takes the form

$$\int_{\Gamma} \big[\mathbf{t}(\mathbf{x}) - \langle\boldsymbol{\sigma}\rangle * \mathbf{n}_{\Gamma}(\mathbf{x})\big]^{\mathrm{T}} \big[\mathbf{u}(\mathbf{x}) - \langle\boldsymbol{\varepsilon}\rangle * \mathbf{x}\big] \, \mathrm{d}\Gamma = 0 \quad , \tag{7.1}$$

see, e.g., Hazanov (1998). In general there are four ways of fulfilling this equation, three of them being based on uniform boundary conditions (Hazanov and Amieur, 1995; Ostoja-Starzewski, 2006).

First, the traction term in eqn. (7.1) can be set to zero by specifying appropriate Neumann boundary conditions for the tractions $\mathbf{t}(\mathbf{x})$. This can be achieved by prescribing

a given macroscopically homogeneous stress tensor $\boldsymbol{\sigma}^{\mathrm{a}}$ on all faces of the volume element,

$$\mathbf{t}(\mathbf{x}) = \boldsymbol{\sigma}^{\mathrm{a}} * \mathbf{n}_{\Gamma}(\mathbf{x}) \qquad \forall \mathbf{x} \in \Gamma \quad , \tag{7.2}$$

leading to statically uniform boundary conditions (SUBC).

Second, the right hand term in eqn. (7.1) can be set to zero by imposing a given macroscopically homogeneous strain tensor $\boldsymbol{\varepsilon}^{\mathrm{a}}$ on all boundaries,

$$\mathbf{u}(\mathbf{x}) = \boldsymbol{\varepsilon}^{\mathrm{a}} * \mathbf{x} \qquad \forall \mathbf{x} \in \Gamma \quad , \tag{7.3}$$

resulting in kinematically uniform boundary conditions (KUBC).

Third, mixed uniform boundary conditions (MUBC) may be specified, which enforce the scalar product under the integral to vanish separately for each face Γ_k making up the surface of the volume element,

$$\left[\mathbf{t}(\mathbf{x}) - \langle\boldsymbol{\sigma}\rangle * \mathbf{n}_{\Gamma}(\mathbf{x})\right]^{\mathrm{T}} \left[\mathbf{u}(\mathbf{x}) - \langle\boldsymbol{\varepsilon}\rangle * \mathbf{x}\right] \mathrm{d}\Gamma = 0 \qquad \forall \mathbf{x} \in \Gamma_k \quad . \tag{7.4}$$

This involves appropriate combinations of traction and strain components that are uniform over a given face of the volume element, but not macroscopically homogeneous. Mixed uniform boundary conditions that fulfill eqn. (7.1) must be orthogonal in the fluctuating contributions (Hazanov and Amieur, 1995).

Finally, the fluctuations of non-uniform boundary fields can be made to cancel out by pairing parallel faces of the volume element such that they show identical fluctuations but surface normals of opposite orientations. This strategy, which does not involve homogeneous fields, is used by the periodicity boundary conditions discussed in chapter 5.

Macrohomogeneous boundary conditions following eqns. (7.2) and (7.3) can be shown to give rise to lower and upper estimates, respectively, for the overall elastic tensor of a given mesoscopic volume element (Nemat-Nasser and Hori, 1993). Ensemble averages of such estimates obtained from windows of comparable size provide lower and upper bounds on the overall apparent tensors of these volume elements. These bounds are sometimes referred to as mesoscale bounds. By definition, for RVEs the lower and upper estimates and bounds on the overall elastic properties must coincide (Hill, 1963). Accordingly, hierarchies of bounds that are generated from sets of windows of sub-RVE volume elements and indicate the size of proper representative volume elements[106].

Equations (7.4) can be fulfilled by a range of different MUBC, resulting in different estimates for the apparent macroscopic tensors. A specific set of mixed uniform boundary conditions that avoids prescribing nonzero boundary tractions was proposed by Pahr and Zysset (2008) for obtaining the apparent elastic tensors of cellular materials. Table 7.1 lists these six load cases for volume elements that have the shape of right hexahedra aligned with

[106]Hierarchies of bounds for a given microgeometry can be generated by using series of windows of increasing size, which allows to assess the dependence of the predicted overall moduli on the size of the windows. However, the actual equality of the lower and upper mesoscale bounds is difficult to achieve in practice, the convergence of the two bounds being especially slow for softer inclusions in a stiffer matrix.

the coordinate system. Their edge lengths in the 1-, 2- and 3-directions are c_1, c_2 and c_3, respectively. The components of the prescribed strain tensor are denoted as $\varepsilon^{\mathrm{a}}_{ij}$ and those of the prescribed traction vector as τ^{a}_i. When applied to periodic volume elements with orthotropic phase arrangements, these MUBC were found to give the same predictions for the macroscopic elasticity tensor as periodic homogenization. Accordingly, they are referred to as periodicity compatible mixed uniform boundary conditions (PMUBC).

Table 7.1: The six linearly independent uniform strain load cases making up the periodicity compatible mixed boundary conditions (PMUBC) proposed by Pahr and Zysset (2008) and the pertinent boundary conditions for thermal loading; East, West, North, South, Top, and Bottom denote the faces of the hexahedral volume element, compare fig. 5.4, and the c_i are the lengths of its edges.

	East	West	North	South	Top	Bottom
Tensile 1	$u_1 = \varepsilon^{\mathrm{a}}_{11} c_1$ $\tau^{\mathrm{a}}_2 = \tau^{\mathrm{a}}_3 = 0$	$u_1 = -\varepsilon^{\mathrm{a}}_{11} c_1$ $\tau^{\mathrm{a}}_2 = \tau^{\mathrm{a}}_3 = 0$	$u_2 = 0$ $\tau^{\mathrm{a}}_1 = \tau^{\mathrm{a}}_3 = 0$	$u_2 = 0$ $\tau^{\mathrm{a}}_1 = \tau^{\mathrm{a}}_3 = 0$	$u_3 = 0$ $\tau^{\mathrm{a}}_1 = \tau^{\mathrm{a}}_2 = 0$	$u_3 = 0$ $\tau^{\mathrm{a}}_1 = \tau^{\mathrm{a}}_2 = 0$
Tensile 2	$u_1 = 0$ $\tau^{\mathrm{a}}_2 = \tau^{\mathrm{a}}_3 = 0$	$u_1 = 0$ $\tau^{\mathrm{a}}_2 = \tau^{\mathrm{a}}_3 = 0$	$u_2 = \varepsilon^{\mathrm{a}}_{22} c_2$ $\tau^{\mathrm{a}}_1 = \tau^{\mathrm{a}}_3 = 0$	$u_2 = -\varepsilon^{\mathrm{a}}_{22} c_2$ $\tau^{\mathrm{a}}_1 = \tau^{\mathrm{a}}_3 = 0$	$u_3 = 0$ $\tau^{\mathrm{a}}_1 = \tau^{\mathrm{a}}_2 = 0$	$u_3 = 0$ $\tau^{\mathrm{a}}_1 = \tau^{\mathrm{a}}_2 = 0$
Tensile 3	$u_1 = 0$ $\tau^{\mathrm{a}}_2 = \tau^{\mathrm{a}}_3 = 0$	$u_1 = 0$ $\tau^{\mathrm{a}}_2 = \tau^{\mathrm{a}}_3 = 0$	$u_2 = 0$ $\tau^{\mathrm{a}}_1 = \tau^{\mathrm{a}}_3 = 0$	$u_2 = 0$ $\tau^{\mathrm{a}}_1 = \tau^{\mathrm{a}}_3 = 0$	$u_3 = \varepsilon^{\mathrm{a}}_{33} c_3$ $\tau^{\mathrm{a}}_1 = \tau^{\mathrm{a}}_2 = 0$	$u_3 = -\varepsilon^{\mathrm{a}}_{33} c_3$ $\tau^{\mathrm{a}}_1 = \tau^{\mathrm{a}}_2 = 0$
Shear 12	$u_2 = \varepsilon^{\mathrm{a}}_{21} c_1$ $u_3 = 0$, $\tau^{\mathrm{a}}_1 = 0$	$u_2 = -\varepsilon^{\mathrm{a}}_{21} c_1$ $u_3 = 0$, $\tau^{\mathrm{a}}_1 = 0$	$u_1 = \varepsilon^{\mathrm{a}}_{12} c_2$ $u_3 = 0$, $\tau^{\mathrm{a}}_2 = 0$	$u_1 = -\varepsilon^{\mathrm{a}}_{12} c_2$ $u_3 = 0$, $\tau^{\mathrm{a}}_2 = 0$	$u_3 = 0$ $\tau^{\mathrm{a}}_1 = \tau^{\mathrm{a}}_2 = 0$	$u_3 = 0$ $\tau^{\mathrm{a}}_1 = \tau^{\mathrm{a}}_2 = 0$
Shear 13	$u_3 = \varepsilon^{\mathrm{a}}_{31} c_1$ $u_2 = 0$, $qta_1 = 0$	$u_3 = -\varepsilon^{\mathrm{a}}_{31} c_1$ $u_2 = 0$, $\tau^{\mathrm{a}}_1 = 0$	$u_2 = 0$ $\tau^{\mathrm{a}}_1 = \tau^{\mathrm{a}}_3 = 0$	$u_2 = 0$ $\tau^{\mathrm{a}}_1 = \tau^{\mathrm{a}}_3 = 0$	$u_1 = \varepsilon^{\mathrm{a}}_{13} c_3$ $u_2 = 0$, $\tau^{\mathrm{a}}_3 = 0$	$u_1 = -\varepsilon^{\mathrm{a}}_{13} c_3$ $u_2 = 0$, $\tau^{\mathrm{a}}_3 = 0$
Shear 23	$u_1 = 0$ $\tau^{\mathrm{a}}_2 = qta_3 = 0$	$u_1 = 0$ $\tau^{\mathrm{a}}_2 = \tau^{\mathrm{a}}_3 = 0$	$u_3 = \varepsilon^{\mathrm{a}}_{32} c_2$ $u_1 = 0$, $\tau^{\mathrm{a}}_2 = 0$	$u_3 = -\varepsilon^{\mathrm{a}}_{32} c_2$ $u_1 = 0$, $\tau^{\mathrm{a}}_2 = 0$	$u_2 = \varepsilon^{\mathrm{a}}_{23} c_3$ $u_1 = 0$, $\tau^{\mathrm{a}}_3 = 0$	$u_2 = -\varepsilon^{\mathrm{a}}_{23} c_3$ $u_1 = 0$, $\tau^{\mathrm{a}}_3 = 0$
Thermal Loading	$u_1 = 0$ $\tau^{\mathrm{a}}_2 = \tau^{\mathrm{a}}_3 = 0$	$u_1 = 0$ $\tau^{\mathrm{a}}_2 = \tau^{\mathrm{a}}_3 = 0$	$u_2 = 0$ $\tau^{\mathrm{a}}_1 = \tau^{\mathrm{a}}_3 = 0$	$u_2 = 0$ $\tau^{\mathrm{a}}_1 = \tau^{\mathrm{a}}_3 = 0$	$u_3 = 0$ $\tau^{\mathrm{a}}_1 = \tau^{\mathrm{a}}_2 = 0$	$u_3 = 0$ $\tau^{\mathrm{a}}_1 = \tau^{\mathrm{a}}_2 = 0$

The concept of periodicity compatible mixed uniform boundary conditions can be extended to thermoelasticity by adding a load case that constrains all displacements normal to the faces of the volume element, sets all in-plane tractions to zero, and applies a uniform temperature increment ΔT, see table 7.1. This allows to evaluate the volume averaged specific thermal stress tensor $\langle \boldsymbol{\vartheta} \rangle$, from which the apparent thermal expansion tensor can be obtained as $\boldsymbol{\alpha} = -\mathbf{C} \langle \boldsymbol{\vartheta} \rangle$.

It has been shown that the PMUBC listed in table 7.1 give valid results for periodic unit cells with sub-orthotropic symmetry (Pahr and Böhm, 2008), which indicates that they are also applicable to non-periodic volume elements provided the sub-orthotropic contributions to their overall symmetry is relatively small. The PMUBC accordingly offer an attractive option for evaluating estimates of the macroscopic elasticity and thermal expansion tensors of periodic and non-periodic volume elements. Boundary conditions that show an analogous behavior to the above PMUBC were reported by Jiang et al. (2002a) for thermal conduction in two-dimensional orthotropic periodic media.

In general, homogeneous strain and mixed uniform boundary conditions are more straightforward to apply than periodic B.C.s because there are no dependences between

phase geometries or discretizations on "opposite" faces, and the simpler constraint equations can make for reduced computational requirements. Homogeneous tangential tractions, however, must be prescribed in an FE framework via appropriate consistent tangential nodal forces, the application of which is not supported by many preprocessors.

The generation of lower and upper estimates by windowing using SUBC and KUBC can be shown to be valid in the context of nonlinear elasticity and deformation plasticity (Jiang et al., 2001). A discussion of windowing bounds in a finite strain elasticity setting was given by Khisaeva and Ostoja-Starzewski (2006). PMUBC, however, rely on the superposition principle for obtaining effective tensors and, accordingly, cannot be used for general load paths in the inelastic regime. They can, however, be employed for materials characterization of elastoplastic inhomogeneous materials (Pahr and Böhm, 2008).

For relatively small windows, within which the phase arrangement deviates significantly from statistical homogeneity, different boundary conditions, especially uniform kinematic and uniform static B.C.s, can give rise to marked differences in the distributions of the microfields, especially the plastic strains. When larger windows are used, however, increasingly similar statistical distributions of the microfields are obtained (Shen and Brinson, 2006). Again, improved predictions of the responses can be obtained by ensemble averaging over a number predictions obtained from small volume elements with the same B.C.s.

Like embedding methods windowing gives rise to perturbed boundary layer near the surfaces of the volume element, which may influence phase averages of microfields. The principal strength of windowing methods lies in providing an approach to studying the linear behavior of non-periodic volume

Chapter 8

Multi-Scale Models

The micromechanical methods discussed in chapters 2, 5, and 7 are designed to handle a single scale transition between a lower and a higher length scale ("microscale" and "macroscale"), overall responses being obtained by homogenization and/or local fields by localization. Many inhomogeneous materials, however, show more than two clearly distinct characteristic length scales, typical examples being laminated and woven composites (compare section 5.4), materials in which there are well defined clusters of particles, as well as most biomaterials. In such cases an obvious modeling strategy is a hierarchical (or multi-scale) approach that uses a sequence of scale transitions, i.e., the material response at any given length scale is described on the basis of the homogenized behavior of the next lower one[107]. Figure 8.1 schematically shows such a hierarchical model for a particle reinforced composite with a clustered mesostructure.

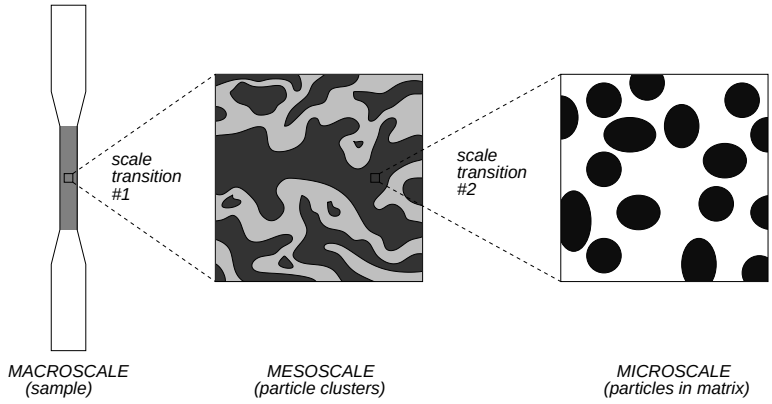

Figure 8.1: Schematic representation of a multi-scale approach for studying a material consisting of clustered inhomogeneities in a matrix. Two scale transitions, macro⟷meso and meso⟷micro, are used.

A multi-scale model can be viewed as involving a sequence of scale transitions and suitable micromechanical models, i.e., mean field, unit cell, windowing and, to some extent, embedding approaches, may be used as "building blocks" at any level within hierarchical

[107]Describing the material behavior at lower length scales by a homogenized model implies that characteristic lengths differ by more than, say, an order of magnitude, so that valid homogenization volumes can be defined. It is not technically correct to employ hierarchical approaches within "bands" of more or less less continuous distributions of length scales, as can be found, e.g., in some metallic foams with highly disperse cell sizes.

schemes[108]. Such multi-scale modeling strategies have the additional advantage of allowing the behavior of the constituents at all lower length scales to be assessed via the corresponding localization relations.

Because local stresses and strains at the lower length scales can differ markedly from the applied macroscopic conditions in both magnitude and orientation, it is advisable that the homogenized descriptions of the thermomechanical responses at all length scales (with the possible exception of the top one) take the form of proper constitutive models that are capable of handling any loading conditions and any loading history. In most cases, this requirement can be readily fulfilled by micromechanically based constitutive models that employ mean field methods or periodic microfield approaches.

Among the continuum mechanical multi-scale descriptions of the thermomechanical behavior of inhomogeneous materials reported in the literature, some combine mean field methods at the higher length scale with mean field (Hu et al., 1998; Tszeng, 1998) or periodic microfield approaches (González and LLorca, 2000) at the lower length scale. The most common strategy for multi-scale modeling, however, uses Finite Element based unit cell or embedding methods at the topmost length scale, which implies that the homogenized material models describing the lower level(s) of the hierarchy take the form of micromechanically based constitutive laws that can be evaluated at each integration point of the discretized model. This requirement typically does not give rise to extreme computational workloads in the elastic range, where the superposition principle can be used to obtain the full homogenized elasticity and thermal expansion tensors with a limited number of analyses[109] For simulating the thermomechanical response of nonlinear inhomogeneous materials, however, essentially a full micromechanical submodel has to be maintained and solved at each integration point in order to account for the history dependence of the local responses[110]. Although within such a framework the use of sophisticated unit cell based models at the lower length scales tends to be an expensive proposition in terms of computational requirements, considerable work of this type has been reported (Belsky et al., 1995; Ghosh et al., 1996; Smit et al., 1998; Feyel, 2003). Lower (but by no means negligible) computational costs can be achieved by using mean field models in lieu of constitutive models at the integration point level. Applications to elastoplastic composites have included incremental Mori–Tanaka methods, see, e.g., Pettermann (1997), mean field based versions of the Transformation Field Analysis, see, e.g., Fish and Shek (1998) or Plankensteiner (2000), and the nonuniform TFA (Michel and Suquet, 2004). It is also possible to handle the "lowest" scale transition by a combination of a mean field or TFA-type homogenization

[108]Micromechanical methods that by construction describe inhomogeneous materials with a wide range of length scales, e.g. differential schemes, are, however, of limited suitability for multi-scale analysis.

[109]In the elastic range decomposition techniques can be used to formulate the problems at the lower length scales in such a way that they are well suited for parallel processing, allowing the development of computationally highly efficient multi-scale procedures, see Oden and Zohdi (1997).

[110]Some approaches have been reported that aim at partially "decoupling" models at the higher and lower length scales by parameterizing results from unit cell analyses and using the stored data together with some interpolation scheme as an "approximate constitutive model", see, e.g., Terada and Kikuchi (1996), Gänser (1998), Schrefler et al. (1999) or Ghosh et al. (2001). The main difficulty in such modeling strategies lies in handling load history and load path dependences to account for elastoplastic constituents or microscopic damage to constituents. Appropriate representation of general multiaxial stress and/or strain states also tends to be a challenge.

procedure and unit-cell based localization algorithms, the latter being used only in regions of special interest (Fish et al., 1997).

Figure 8.2 shows a result obtained by applying multiscale approach that uses an incremental Mori–Tanaka method, compare section 2.6, at the integration point level of a meso-scale unit cell model for describing the elastoplastic behavior of a cluster-structured high speed steel. The particle-rich and particle-poor regions used for the description at the mesoscale are treated as particle reinforced MMCs with appropriate reinforcement volume fractions. Such an approach not only predicts macroscopic stress–strain curves, but also allows the mesoscopic distributions of phase averaged microscopic variables to be evaluated, compare (Plankensteiner, 2000). Alternatively, multiscale approaches may be rather "loosely coupled", essentially linking together quite different models to obtain an overall result, see, e.g., (Onck and van der Giessen, 1997).

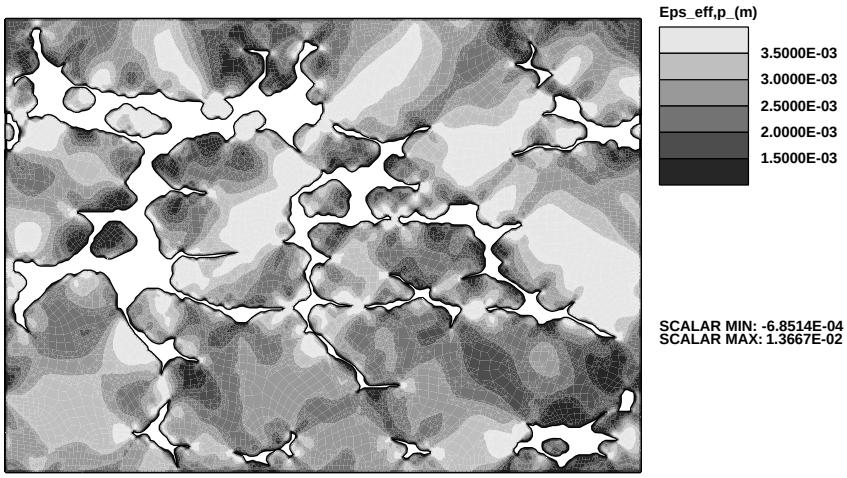

Figure 8.2: Phase averaged microscopic equivalent plastic strains in the matrix within the inhomogeneity-poor regions of a cluster-structured high speed steel under mechanical loading as predicted by a mesoscopic unit cell model combined with an incremental Mori–Tanaka model at the microscale (Plankensteiner, 2000).

For a number of years there has been a surge of research interest in developing and applying algorithms for the multi-scale and hierarchical continuum modeling of inhomogeneous materials (Lee and Ghosh, 1996; Zohdi et al., 1996; Fish and Shek, 2000; Feyel and Chaboche, 2000; Ibrahimbegović and Markovič, 2003; Moës et al., 2003). A recent development are multi-scale methods in which the computational domain is adaptively split into regions resolved at appropriate length scale. In an FE-based framework developed by Ghosh et al. (2001) "non-critical" regions are described by continuum elements with homogenized material properties, and at zones of high macroscopic stress and strain gradients PMA models are automatically activated at the integration points to monitor the phase behavior at the microscale. If violations of the homogenization conditions (e.g., onset of damage, mesoscopic interfaces, free edges) are detected, embedded models of the fully resolved microgeometry are activated at the appropriate positions, compare Raghavan and Ghosh (2004). Such strategies allow detailed studies of critical regions in inhomogeneous

materials, e.g., near free edges. In an alternative approach, homogenization models employing generalized continua have been proposed for handling regions close to free surfaces and zones with high local field gradients (Feyel, 2003).

Finally, it is worth noting that multi-scale approaches are not limited to using the "standard" methods of continuum micromechanics as discussed above. Especially the capability of the Finite Element method of handling highly complex constitutive descriptions has been used to build multi-scale descriptions that employ, among others, material models based on crystal plasticity (McHugh et al., 1993), discrete dislocation plasticity (Cleveringa et al., 1997) and atomistics (Tadmor et al., 2000).

Chapter 9

Closing Remarks

The research field of continuum micromechanics of materials has enjoyed considerable success in the past four decades in furthering the understanding of the thermomechanical behavior of inhomogeneous materials and in providing predictive tools for engineers and materials scientists. However, its methods are subject to some practical limitations that should be kept in mind when employing them.

All the methods discussed in chapter 2 to 7 implicitly use the assumption that the constituents of the inhomogeneous material to be studied can be treated as homogeneous at the lower length scale, which, of course, does not necessarily hold. When the length scale of the inhomogeneities in a constituent is much smaller than the length scale of the phase arrangement to be studied, the above assumption is valid and multi-scale models ("successive homogenization") as discussed in chapter 8 can be used (Carrere, 2001). However, no rigorous theory appears to be available at present for handling scale transitions in materials that do not fulfill the above requirement (e.g., particle reinforced composites in which the grain size of the matrix is comparable to or even larger than the size of the particles[111]). Typically the best that can be done in such cases is either to use sufficiently large models with resolved microgeometry (a computationally very expensive proposition) or to employ homogenized phase properties and be aware of the approximation that is introduced.

A major practical difficulty in the use of continuum micromechanics approaches (which in many cases is closely related to the questions mentioned above) has been identifying appropriate constitutive models and obtaining material parameters for the constituents. Typically, available data pertain to the behavior of the bulk materials (as measured from homogeneous macroscopic samples), whereas the actual requirement is for parameters and, in some cases, constitutive theories that describe the in-situ response of the constituents at the microscale. For example, with respect to MMCs, on the one hand, there is considerable evidence that classical continuum plasticity theories (in which there is no absolute length scale) cannot adequately describe the behavior of metallic materials in the presence of strong strain gradients, where geometrically necessary dislocations can markedly influence the material behavior (Hutchinson, 2000). On the other hand, it is well known that the

[111] For this special case unit cell or embedding models employing anisotropic or crystal plasticity models for the phases may be used which, however, can become very large when the statistics of grain orientation are accounted for.

presence of reinforcements can lead to accelerated aging and refinement of the grain size in the matrix ("secondary strengthening"). Furthermore, in many cases reasonably accurate material parameters are essentially not available (e.g., strength parameters for most interfaces in inhomogeneous materials). In fact, the dearth of dependable material parameters is one of the reasons why predictions of the strength of inhomogeneous materials by micromechanical methods tend to be a considerable challenge.

Another point that should be kept in mind is that continuum micromechanical descriptions in most cases do not have absolute length scales unless a length scale is introduced, typically via the constitutive model(s) of one (or more) of the constituents[112]. In this vein, absolute length scales, on the one hand, may be provided explicitly via discrete dislocation models (Cleveringa et al., 1997), via gradient or nonlocal constitutive laws, see, e.g., Tomita et al. (2000) or Niordson and Tvergaard (2001), or via (nonlocal) damage models. On the other hand, they may be introduced in an ad-hoc fashion, e.g., by adjusting the phase material parameters to account for grain sizes via the Hall–Petch effect. Analysts should also be aware that absolute length scales may be introduced inadvertently into a model by mesh dependence effects of discretizing numerical methods, a "classical" example being strain localization due to softening material behavior of a constituent, compare also the discussions in the Appendix. When multi-scale models are used special care may be necessary to avoid introducing inconsistent length scales at different modeling levels.

In addition it is worth noting that usually the macroscopic response of inhomogeneous materials is much less sensitive to the phase arrangement (and to modeling approximations) than are the distributions of the microfields. Accordingly, whereas good agreement in the overall behavior of a given model with "benchmark" theoretical results or experimental data typically indicates that the phase averages of stresses and strains are described satisfactorily, this does not necessarily imply that the higher statistical moments of the stress and strain distributions (and thus the heterogeneity of these fields) are captured correctly.

It is important to be aware that work in the field of micromechanics of materials invariably involves finding viable compromises in terms of the complexity of the models, which, on the one hand, have to be able to account (at least approximately) for the physical phenomena relevant to the given problem, and, on the other hand, must be sufficiently simple to allow solutions to be obtained within the relevant constraints of time, cost, and computational resources. Obviously, actual problems cannot be solved without recourse to various approximations and tradeoffs — the important point is to be aware of them and to account for them in interpreting and assessing results. It is worth keeping in mind that there is no such thing as a "best micromechanical approach" for all applications.

[112] One important exception are models for studying macroscopic cracks (e.g., via embedded cells), where the crack length does introduce an absolute length scale.
Note that the behavior of nanocomposites is typically "interface dominated". Appropriately accounting for this behavior may require the introduction of an absolute length scale. Within the framework of mean field methods this may be achieved by introducing surface terms into the Eshelby tensor, see, e.g., Duan et al. (2005).

APPENDIX A:
Some Aspects of Modeling Damage at the Microlevel

Modeling efforts aimed at studying the damage and failure behavior of inhomogeneous materials may take the form of microscopic or macroscopic approaches. Methods belonging to the latter group often are based to some extent on micromechanical concepts and encompass, among others, the "classical" failure surfaces for continuously reinforced laminae such as the Tsai–Wu criterion (Tsai and Wu, 1971) and macroscopic continuum damage models of various degrees of complexity, compare, e.g., Chaboche et al. (1998) or Voyiadjis and Kattan (1999). Also on the macroscopic level the Considére criterion may be used in combination with micromechanical models to check for (macroscopic) plastic instability when studying the ductility of inhomogeneous elastoplastic materials, see, e.g., González and LLorca (1996). In what follows, however, only the modeling of damage on the microscale in the context of (mainly Finite Element based) micromechanical methods of the types discussed in chapters 4 to 8 are considered.

General Remarks

When damage and failure of inhomogeneous materials are to be studied at the microscale, it is physically intuitive to represent them as acting at the level of the constituents and of the interfaces between them, where appropriate damage and fracture models have to be provided. All of the resulting microscopic failure mechanisms contribute to the energetics of crack growth. Taking MMCs as an example, this concept translates into viewing damage and failure as involving a mutual interaction and competition between ductile damage of the matrix, brittle cleavage of the reinforcements, and decohesion of the interfaces, whereas in polycrystals intergranular and intragranular failure are typical damage mechanisms. The dominant microscopic damage process is determined by the individual constituents' strength and stiffness parameters, by the microgeometry, and by the loading conditions, compare Needleman et al. (1993). In fact, it may be markedly influenced by details of the phase arrangement, such as particle shape and size, see, e.g., Miserez et al. (2004), a behavior which strongly supports the concept of using micromechanics for damage modeling.

Generally, macrocracks as well as microcracks that have lengths comparable to the microscale of a given phase arrangement must be resolved explicitly in micromechanical studies[113]. Smaller cracks and voids, however, can be treated in a homogenized manner as damage. For describing cracks in micromechanical models "standard" FE models of cracks may be used; for an overview covering some of the relevant methods see, e.g., Liebowitz et al. (1995). "Standard" criteria for the initiation and/or growth of cracks, such as J-integral, CTOD or CTOA criteria, etc., can also be used.

If only information on the initiation of damage is required it may be sufficient to evaluate appropriate "damage relevant fields", such as the maximum principal stress in brittle materials, a ductile damage indicator, or the traction vectors at interfaces, without ac-

[113]Crack-like features that develop due to the failure of contiguous sets of elements in a damage-type model fulfill this requirement.

counting for the loss of stiffness that accompanies the evolution of damage. For the use of a ductile damage indicator in this context see, e.g., Gunawardena et al. (1993) or Böhm and Rammerstorfer (1996). Alternatively, it may be of interest to study microgeometries containing flaws (e.g., fiber breaks, matrix flaws) in order to assess the resulting microfields, see, e.g., Tsotsis and Weitsman (1990), where J-integrals were evaluated for specific matrix crack configurations.

If, however, the progress of damage and the interaction of damage modes at the constituent level as well as final failure are to be studied, two major modeling strategies are available at present. They are, on the one hand, the "volume oriented" damage-based approaches used in continuum damage mechanics and related models and, on the other hand, "surface oriented" methods that aim at following the progress of individual cracks. The remainder of the present section is devoted to a short discussion of some aspects of these two groups of methods.

When constituent damage at the microscale is modeled by continuum damage mechanics (CDM) and related approaches (lumped together as CDM-type models in what follows), the implicit assumption is made that the characteristic length scale of inhomogeneities underlying the damage (pores, microcracks, etc.) is much smaller than the characteristic length scale of phase arrangement to be studied. Essentially such models amount to multiscale methods as discussed in chapter 8. This group of approaches includes ductile rupture models for describing ductile damage, see, e.g., Gurson (1977) and Rousselier (1987), and damage indicator triggered (DDIT) techniques, in which the stiffness of an integration point is drastically reduced or the corresponding element is removed when some critical value of an appropriate damage indicator is reached[114]. CDM-type methods can account for the stiffness degradation due to the evolution of damage, which tends to give rise to localization and may lead to the formation of proper shear bands within the microscopic phase arrangement.

A numerical difficulty typically encountered with CDM-type models lies in their tendency to provide solutions that show a marked mesh dependence[115]. The characteristic size of the localized or failed region is typically found to be comparable to the dimensions of one element, regardless of the actual degree of mesh refinement, and the predicted energies for crack formation accordingly tend to decrease with decreasing mesh size, compare fig. 8.2. This behavior can be avoided or at least mitigated by using theories that are suitably regularized by enrichment with higher-order gradients, see e.g., Geers et al. (2001a), by nonlocal averaging of the rate of an appropriate damage variable, compare Tvergaard and Needleman (1995) or Jirásek and Rolshoven (2003), or by the use of time dependent formulations involving rate effects (e.g., viscoelasticity, viscoplasticity), compare Needleman (1987). The above procedures explicitly introduce an absolute length scale into the

[114] In FE models reductions of the stiffness at the element level can be enforced either by degrading the relevant material behavior or by applying (spurious) concentrated forces such that the net internal forces of the neighboring elements are suitably reduced (Beissel et al., 1998).

[115] Within classical continuum theory strain softening material behavior leads to ill-posed boundary value problems, i.e., the governing equations lose their ellipticity or hyperbolicity, giving rise to the mesh sensitivity of the solutions, compare, e.g., Baaser and Gross (2002). In order to provide an objective description of localization, the problem has to be regularized.

problem[116] A rather ad-hoc alternative to the above regularization methods consists in selecting a mesh size that leads to physically reasonable sizes of localization features[117].

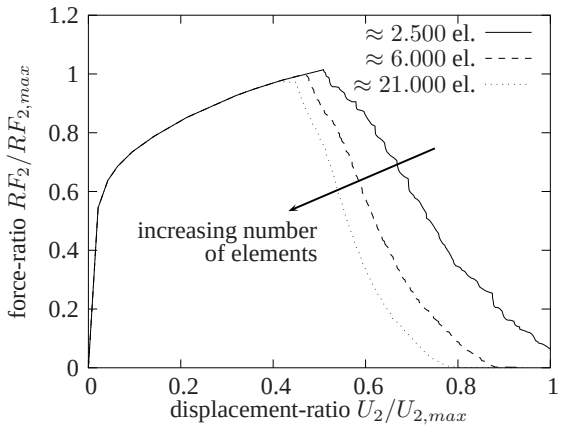

Figure A.1: Normalized overall force–displacement responses obtained for a column with a hole under transverse loading with a local Gurson–Tvergaard-Needleman ductile rupture model (Drabek and Böhm, 2006). A marked mesh dependence of the results is evident.

Surface-oriented numerical strategies for simulating the progress of cracks emphasize the concept that the nucleation and growth of cracks correspond to the creation of new free surface. In most such models crack growth involves breaking the connectivity between neighboring elements, e.g., by node release techniques (Bakuckas et al., 1993; Narasimhan, 1994) or by cohesive surface elements, compare, e.g., Elices et al. (2002). In "classical" models of this type crack paths are restricted to element boundaries, which tends to give rise to a mesh dependence in terms of the predicted crack paths unless the latter are known a priori. This difficulty can be counteracted by using very fine and irregular discretizations or by introducing remeshing schemes that locally adapt the element geometry for each crack growth increment, see, e.g., Fish et al. (1999) or Bouchard et al. (2003), and thus provide realistic crack paths. Both of these remedies tend to lead to complex and/or large models, so that in micromechanics of materials crack opening approaches have been reported mainly for interfacial cracks and for phase arrangements where the crack paths stay can be assumed to follow some plane of symmetry.

The mesh dependence of the crack paths predicted by surface oriented approaches can be removed by using specially formulated solid elements, known as embedded discontinuity elements, which employ appropriately enriched shape functions. Such elements, on the one hand, must allow discontinuities to develop at any position and in any direction within each element and, on the other hand, must provide for continuous crack paths across element boundaries, see e.g., Jirásek (2000) or Alfaiate et al. (2002). The actual opening of cracks is typically handled by formulations of the cohesive surface type. Embedded discontinuity elements at present are not fully not available in standard FE packages and up till now have been little used in the context of continuum micromechanics.

[116] A precondition for the proper regularization by higher-order gradients or by nonlocal averaging is that the discretization must be finer than than this absolute length scale.

[117] Local damage procedures may be interpreted as introducing characteristic lengths via the local element sizes. Material parameters identified on the basis of such procedures pertain to a given element size only.

Modeling of Reinforcement Damage and Failure

Studies of the damage to and failure of individual fibers or particles are limited to Discrete Microstructure Approaches. Mean field methods can, however, be used to assess what percentage of reinforcements has failed at a given load state.

Particulate and fibrous reinforcements in composites typically fail by brittle cleavage. Within the framework of micromechanical models using the FEM, the failure of such constituents can be modeled by following the extension of a crack through the the reinforcement, which implies that complex crack paths may have to be resolved, or by employing descriptions in which the crack opens instantaneously along some predefined "crack plane".

There are two groups of approaches to controlling the activation of cracks that are modeled as opening instantaneously. When deterministic (Rankine) criteria are used, a particle or fiber is induced to fail once a critical level of some stress or strain measure is reached or some fracture probability is exceeded. Studies using normal and maximum principal stress criteria, respectively, within such a framework were published, e.g., by Berns et al. (1998) and Ghosh and Moorthy (1998). In "fully probabilistic" models a random process (Monte-Carlo-type procedure) is provided which "decides" if a given reinforcement will fail at a given load level on the basis of appropriate fracture probabilities, compare, e.g., Pandorf (2000) and Eckschlager (2002). Within micromechanical descriptions such fracture probabilities can be evaluated from the predicted distributions of the microstresses by Weibull-type weakest-link models[118] that were originally developed for describing the failure statistics of bulk brittle materials. A simple Weibull expression for evaluating the failure probability P_n of a given particle n may take the form (Eckschlager, 2002)

$$P_\mathrm{n} = 1 - \exp\left\{ -\frac{1}{V_0} \int_{\Omega_\mathrm{n}:\sigma_1>0} \left(\frac{\sigma_1(\mathbf{x})}{\sigma_0} \right)^m \mathrm{d}\Omega \right\} \quad , \tag{A.1}$$

where $\sigma_1(\mathbf{x})$ is the field of microscopic maximum principal stresses in the inhomogeneity and $\Omega_\mathrm{n} : \sigma_1 > 0$ is that part of the particle volume in which the maximum principal stress is tensile. Equation (A.1) involves three material parameters, viz., σ_0, which stands for the particle's average strength, m, which is known as the Weibull modulus, and V_0, a control volume. Expressions such as eqn.(A.1) assign a failure probability to a particle or short fiber as a whole[119], which fits well with the concept of "instantaneous cleavage" of particles. Typically procedures of this type predict the onset of damage at rather low applied loads, with some of the reinforcements failing at low fracture probabilities. Because each simulation run provides a different realization of the underlying statistics, the results from fully

[118] Whereas there is agreement that the weakest-link behavior of long fibers is largely due to surface defects, the physical interpretation is not as clear for Weibull models of particles embedded in a ductile matrix. Weibull models based on eqn. (A.1) or similar expressions, however, have a number of advantages for the latter class of applications (Wallin et al., 1987), not the least of which is their capability for describing particle size effects. It should be noted, however, that simple Weibull-type models were reported to give predictions for the dependence of the number of fracture events per volume on particle size and volume fraction that do not agree with acoustic emission data from ductile matrix composites (Mummery et al., 1993).

[119] In modeling the fracture of continuous fibers data on the positions of transverse cracks are obviously required. Such information can be obtained by evaluating Weibull fracture probabilities for cylindrical subvolumes of the fibers.

probabilistic models for a given microgeometry are best evaluated in terms of ensemble averages over a number of analyses.

In models of discontinuously reinforced composites that use axisymmetric cells, a natural choice for the position of a predefined crack is a symmetry plane that is oriented normal to the axis of symmetry (which in such models coincides with the loading direction) and runs through the center of the inhomogeneity, compare, e.g., Bao (1992), Davis et al. (1998) or González and LLorca (1996). For more general arrangements of particles or short fibers an analogous approach takes the form of considering the stress state of each particle in selecting the crack plane[120], so that perturbations due to (possibly failed) neighboring particles can be accounted for. Due to their high computational requirements up till now such algorithms have only been reported for planar arrangements of ellipsoidal reinforcements, the crack being taken to pass through the position of maximum principal stress in the particle and to be oriented normally to the local maximum principal stress at this point (Ghosh et al., 2001).

For three-dimensional particle arrangements a simplified concept for approximating the orientations and positions of cracks within spherical particles can be based on the assumption that they pass through the particle center and are oriented normal to the average maximum principal stress in the inhomogeneity or to the macroscopic maximum principal stress (Eckschlager et al., 2001). Tomography data obtained on a model system consisting of aluminum reinforced by spheres of zirconia/silica at ξ=0.04 (Babout et al., 2004), however, show cracks that are oriented normally to the macroscopic maximum principcal stress but do not tend to run through the centers of particles.

The alternatives to the above approach of instantaneous particle cracking consist in using either cohesive surface models for opening predefined cracks in reinforcements, see, e.g., Finot et al. (1994) and Tvergaard (1994), or in applying continuum damage models to describing failure of the reinforcements, see, e.g., Zohdi and Wriggers (2001) or Mishnaevsky (2004). Such models are capable of resolving the growth sequence of a crack rather than "popping it open" instantaneously. Whereas predefined crack paths in the reinforcements have typically been used with cohesive surfaces, no such provision is required in the CDM-type models, which can describe geometrically complex cracks[121]. Both approaches, however, do not introduce effects of the absolute size of the reinforcements into micromechanical models.

Modeling of Matrix Failure

Discrete Microstructure Approaches in principle allow a detailed modeling of progressive matrix damage and failure of composites. The type of matrix failure to be covered obvi-

[120]For small monocrystalline particulates the crystallographic orientations can also be expected to play a role in determining the crack plane, thus introducing a statistical element into the problem. In particles of irregular shape local stress concentrations must be expected to influence the positions of cracks and for elongated particles or fibers the appearance of multiple cracks must be provided for. For experimental results on the orientation of cracks in particles see, e.g., Mawsouf (2000).

[121]From the physical point of view, continuum damage models are most appropriate in situations where a process zone, e.g. due to microcracks, is present. Because particle cleavage tends to produce "clean" cracks, it should preferably be handed by surface based models.

ously depends on the matrix material and thus on the composite system considered. In the case of metallic matrices ductile damage and failure must be considered, which either takes place by void nucleation, growth, and coalescence (void impingement) or by the formation of void sheets, compare, e.g., Horstemeyer et al. (2000). The former mechanism dominates at high stress triaxialities $\sigma_{\mathrm{m}}/\sigma_{\mathrm{eqv}}$, whereas the latter one leads to shear failure in the low triaxiality regime.

Over the past two decades the dominant approach to modeling the failure of ductile matrices in metal matrix composites have been descriptions based on the ductile rupture model of (Gurson, 1977) and its improved versions (Tvergaard and Needleman, 1984; Gărăjeu, 1995). Models of this type are implemented in a number of commercial Finite Element codes[122]. For micromechanical studies that employ Gurson-type models for describing ductile failure of the matrix of MMCs see, e.g., Needleman et al. (1993), Geni and Kikuchi (1999) and Hu et al. (2007). A version of the ductile damage model of Rousselier (1987) was used in micromechanical models by Drabek and Böhm (2004).

In the context of micromechanics element elimination models triggered by a ductile damage indicator ("DDIT models") have been used as an alternative to "ductile rupture" models of the above type[123]. The damage indicator most commonly used for such purposes was proposed by Gunawardena et al. (1991) on the basis of earlier studies on void growth (Rice and Tracey, 1969; Hancock and Mackenzie, 1976) and takes the form

$$D_{\mathrm{id}} = \int_0^{\varepsilon_{\mathrm{eqv,pl}}} \frac{\exp\left(\frac{3}{2}\sigma_{\mathrm{m}}/\sigma_{\mathrm{eqv}}\right)}{1.65\,\varepsilon_{\mathrm{f}}}\,\mathrm{d}\varepsilon_{\mathrm{eqv,pl}} \qquad , \tag{A.2}$$

where $\varepsilon_{\mathrm{eqv,pl}}$ stands for the accumulated equivalent plastic strain, σ_{m} for the mean (hydrostatic) stress, σ_{eqv} for the equivalent (von Mises) stress, and ε_{f} for the uniaxial failure strain of the material[124]. Like most ductile rupture models the damage indicator, eqn. (A.2), was derived for the high stress triaxiality regime[125], which is the more relevant one for micromechanical analysis of composites on account of the pronounced tendency towards highly constrained plasticity. Recently ductile damage indicators have been developed that can also account for local shear failure, see, e.g., Wilkins (1999).

DDIT-based element elimination schemes in the context of continuum micromechanics of inhomogeneous materials were reported, e.g., by Schmauder et al. (1996) and Berns

[122]Gurson models are are based on the behavior of spherical voids and are best suited for handling ductile damage in situations of high stress triaxaiality. A Gurson-type model that allows for evolution of the void shapes was developed by Gologanu et al. (1997). Nahshon and Hutchinson (2008) extended a Gurson-type model to the low-triaxiality situation of shear failure.

[123]In contrast to the physically interpretable damage variables used in ductile rupture and standard CDM models, which allow the effect of damage on all material properties to be handled consistently, only two values of the damage parameter D_{id} defined in eqn (A.2) have a direct physical interpretation: 0 indicates no damage and 1 ductile failure. Accordingly, ductile damage indicators per se cannot follow the degradation of stiffness as damage develops.

[124]The main advantage of this ductile damage indicator lies in requiring only one material parameter, ε_{f}, which can be evaluated experimentally in a relatively straightforward way (Fischer et al., 1995). Alternative ductile damage indicators were developed, e.g., by McClintock (1968) and Oyane (1972).

[125]For a discussion of the validity of eqn. (A.2) in the low to negative triaxiality regime, where the damage mechanism is shear failure rather than void growth and coalescence, see Gänser et al. (2001).

et al. (1998). Other criteria used for controlling element elimination in ductile matrices have included strain energy criteria (Mahishi and Adams, 1982), the so called s-criterion (Spiegler et al., 1990), plastic strain criteria (Adams, 1974), and stress triaxiality criteria (Steinkopff et al., 1995). Wulf et al. (1996) reported comparisons between predictions obtained by planar embedded cell models using element elimination models controlled by stress triaxiality, plastic strain, and Rice–Tracey criteria, the latter giving the best agreement with experimental results for that special case. The Finite Element code ABAQUS provides a set of hybrid schemes for modeling ductile and shear damage in metals, which combine a damage indicator-type concept for detecting "damage initiation"[126] with phenomenological CDM-like algorithms for describing the evolution of damage, leading finally to element elimination.

The use of nonlocal versions of ductile rupture models and DDIT schemes, which allow the mesh dependence of the solutions to be reduced or eliminated, was first proposed for micromechanical applications by Tvergaard and Needleman (1995). These methods have seen further development recently[127] see, e.g., Hu et al. (2004) or Drabek and Böhm (2004).

Alternatively, cohesive surface models may be used for modeling ductile failure, especially in cases where the crack path is known a priori, a typical example being ductile cracks propagating along a plane of symmetry, see, e.g., Finot et al. (1994). A possible drawback of cohesive surface models for studying ductile failure in a continuum micromechanics framework, however, has been revealed by recent studies, which indicate that the decohesion parameters tend to depend on the stress triaxialities, compare Chen et al. (2001).

Approaches to modeling matrix failure that do not fall into the above groups were reported, among others, by (Biner, 1996), who studied creep damage to the matrix of an MMC using the grain boundary cavitation model of Tvergaard (1994), and by Mahishi (1986), who combined a node release technique with an energy release criterion to study cracks in polymer matrices[128]. Composites with brittle elastic matrix behavior can be investigated via fracture mechanics based methods, see, e.g., Ismar and Reinert (1997), or Weibull-type criteria may be employed (Brockmüller et al., 1995).

Finally, for materials subjected to cyclic loading shakedown theorems may be used on the microscale to assess if elastic shakedown may take place in an inhomogeneous material or if low cycle fatigue will act on the microscale (Böhm, 1993; Schwabe, 2000).

[126] In this context the expression "damage initiation" is not used in the sense of metals physics, but rather signifies a state where damage effects on the behavior of some material volume become noticeable.

[127] As mentioned before, all elements subject to damage must be smaller than the characteristic length in nonlocal averaging. The average mesh size in nonlocal models, however, should not be much smaller than the characteristic length, either, because otherwise the high number of neighbors contributing to the nonlocal averages will make the algorithms too slow. These restrictions can considerably constrain the applicability of nonlocal averaging methods.
At present there is no agreement whether the characteristic length in ductile damage is a physical material property or a numerical modeling parameter. If, however, the characteristic length is assumed to be a physical parameter determined by void nucleation from small defects it can be expected to be inversely proportional to the third root of the defects' volume density (Rousselier, 1987).

[128] Because crack paths in inhomogeneous materials may be rather complicated, appropriate criteria for determining the crack direction have to be employed and remeshing typically is necessary when node release techniques are used (Vejen and Pyrz, 2002).

Modeling of Interface Failure

Most micromechanical studies of interfacial failure have been based on Dicrete Microstructure Approaches. Probably the most commonly used description for the debonding of a reinforcement from a matrix in numerical micromechanics has been a cohesive surface model developed by Needleman (1987). It is based on an interface potential that specifies the dependence of the normal and tangential interfacial tractions on the normal and tangential displacement differences across the interface and was extended by Tvergaard (1990) to handle the modeling of tangential separation. Interfacial behavior of this type is typically described in FE codes via special interface elements, which in many cases are also capable of handling contact and friction between reinforcement and matrix once interfacial decohesion has occurred. Micromechanical studies employing algorithms of the Needleman–Tvergaard type were carried out, e.g., by Nutt and Needleman (1987), Needleman et al. (1993) and Haddadi and Téodosiu (1999). A modified version of the above interfacial decohesion model was developed by Michel and Suquet (1994), and another related technique was reported by Zhong and Knauss (2000).

An alternative approach suitable for describing very weakly bonded reinforcements consists in using standard contact elements at the interface, the composite being assumed to be held together in a "shrink fit" by the thermal stresses caused by cooling down from the processing temperature, see, e.g., Gunawardena et al. (1993) or Sherwood and Quimby (1995). As an extension of this type of description, Coulomb-type models, i.e., a linkage between normal and shear stresses analogous to that employed for dry friction, may be used for the interface (Benabou, 2002).

Other interfacial decohesion models reported in the literature include strain softening interfacial springs (Vosbeek et al., 1993; Li and Wisnom, 1994) and node release techniques based on fracture mechanics solutions for bimaterial interfaces (Moshev and Kozhevnikova, 2002). Interphases, i.e., interfacial layers of finite thickness, were studied by various fictitious crack techniques, see, e.g., Ismar and Schmitt (1991), McHugh and Connolly (1994), or Walter et al. (1997) and thermomechanically based continuum damage models (Benabou, 2002).

A rather different approach has been developed specifically for accounting for the stiffness loss due to debonding within mean field models. It is based on describing debonded reinforcements by perfectly bonded (transversally isotropic) "fictitious inhomogeneities" of appropriately reduced stiffness. Within such a framework, the fraction of debonded reinforcements may be controlled via Weibull-type models, see, e.g., Zhao and Weng (1995) or Sun et al. (2003).

Models Involving Multiple Failure Modes

Modeling the interaction of different microscopic damage and failure modes of inhomogeneous materials poses considerable challenges. Such descriptions typically rely on combining suitable submodels for the damage or failure of the constituents and the interface. It is, however, also possible to use a single modeling approach, e.g., cohesive elements, with appropriate calibrations for all local damage modes (Haj-Ali, 2009). Whereas a number of

the works have been reported that involve two interacting micromechanical failure modes, only few attempts to concurrently model matrix, reinforcement and interfacial failure have been published. For two-dimensional studies of this type describing ductile matrix composites see, e.g., Berns et al. (1998) and Pandorf (2000), where generic particle arrangements in tool steels are compared with respect to their fracture properties, and Hu et al. (2007), where particle reinforced metal matrix composites are investigated.

Bibliography

N. Abolfathi, A. Naik, G. Karami, and C. Ulven. A micromechanical characterization of angular bidirectional fibrous composites. *Comput.Mater.Sci.*, 43:1193–1206, 2008.

J. Aboudi. The generalized method of cells and high-fidelity generalized method of cells micromechanical models — A review. *Mech.Adv.Mater.Struct.*, 11:329–366, 2004.

J. Aboudi. Micromechanical analysis of composites by the method of cells. *Appl.Mech.Rev.*, 42:193–221, 1989.

J. Aboudi. *Mechanics of Composite Materials*. Elsevier, Amsterdam, 1991.

J. Aboudi. Micromechanical analysis of composites by the method of cells — Update. *Appl. Mech. Rev.*, 49:83–S91, 1996.

M.L. Accorsi. A method for modeling microstructural material discontinuities in a finite element analysis. *Int.J.Num.Meth..Engng.*, 26:2187–2197, 1988.

J.D. Achenbach and H. Zhu. Effect of interfacial zone on mechanical behavior and failure of fiber-reinforced composites. *J.Mech.Phys.Sol.*, 37:381–393, 1989.

D.F. Adams. Practical problems associated with the application of the finite element method to composite material micromechanical analyses. *Fibre Sci.Technol.*, 7:111–122, 1974.

D.F. Adams and D.A. Crane. Finite element micromechanical analysis of a unidirectional composite including longitudinal shear loading. *Comput.Struct.*, 18:1153–1165, 1984.

D.F. Adams and D.R. Doner. Transverse normal loading of a uni-directional composite. *J.Compos.Mater.*, 1:152–164, 1967.

S.G. Advani and C.L. Tucker. The use of tensors to describe and predict fiber orientation in short fiber composites. *J.Rheol.*, 31:751–784, 1987.

J. Alfaiate, G.N. Wells, and L.J. Sluys. On the use of embedded discontinuity elements with crack path continuity for mode-I and mixed mode fracture. *Engng.Fract.Mech.*, 69: 661–686, 2002.

D.H. Allen and J.W. Lee. The effective thermoelastic properties of whisker-reinforced composites as functions of material forming parameters. In G.J. Weng, M. Taya, and H. Abé, editors, *Micromechanics and Inhomogeneity*, pages 17–40, New York, NY, 1990. Springer–Verlag.

A. Anthoine. Derivation of the in-plane elastic characteristics of masonry through homogenization theory. *Int.J.Sol.Struct.*, 32:137–163, 1995.

T. Antretter. *Micromechanical Modeling of High Speed Steel*. Reihe 18, Nr. 232. VDI–Verlag, Düsseldorf, 1998.

S. Aoki, Y. Moriya, K. Kishimoto, and S. Schmauder. Finite element fracture analysis of WC–Co alloys. *Engng.Fract.Mech.*, 55:275–287, 1996.

P. Arbenz, G.H. van Lenthe, U. Mennel, R. Müller, and M. Sala. Multi-level μ-finite element analysis for human bone structures. In B. Kagström, E. Elmroth, J. Dongarra, and J. Wasniewski, editors, *Applied Parallel Computing. State of the Art in Scientific Computing*, pages 240–250, Berlin, 2008. Springer–Verlag.

R.T. Arenburg and J.N. Reddy. Analysis of metal-matrix composite structures — I. Micromechanics constitutive theory. *Comput.Struct.*, 40:1357–1368, 1991.

J.L. Auriault. Effective macroscopic description for heat conduction in periodic composites. *Int.J.Heat Mass Trans.*, 26:861–869, 1983.

M. Avellaneda and G.W. Milton. Optimal bounds on the effective bulk modulus of polycrystals. *J.Appl.Math.*, 49:824–837, 1989.

M.S. Axelsen and R. Pyrz. Correlation between fracture toughness and the microstructure morphology in transversely loaded unidirectional composites. In R. Pyrz, editor, *Microstructure–Property Interactions in Composite Materials*, pages 15–26, Dordrecht, 1995. Kluwer Academic Publishers.

A. Ayyar, G.A. Crawford, J.J. Williams, and N. Chawla. Numerical simulation of the effect of partice spatial distribution and strength on tensile behavior of particle reinforced composites. *Comput.Mater.Sci.*, 44:496–506, 2008.

H. Baaser and D. Gross. On the limitations of CDM approaches to ductile fracture problems. In : H.A. Mang, F.G. Rammerstorfer, and J. Eberhardsteiner, editors, *Proc. Fifth World Congress on Computational Mechanics (WCCM V)*, page 81462, Vienna, 2002. Vienna University of Technology.

L. Babout, Y. Bréchet, E. Maire, and R. Fougères. On the competition between particle fracture and particle decohesion in metal matrix composites. *Acta mater.*, 52:4517–4525, 2004.

J.G. Bakuckas, T.M. Tan, A.C.W. Lau, and J. Awerbuch. A numerical model for predicting crack path and modes of damage in unidirectional metal matrix composites. *J.Reinf.Plast.Compos.*, 12:341–358, 1993.

P.K. Banerjee and D.P. Henry. Elastic analysis of three-dimensional solids with fiber inclusions by BEM. *Int.J.Sol.Struct.*, 29:2423–2440, 1992.

L. Banks-Sills and V. Leiderman. Macro-mechanical material model for fiber-reinforced metal matrix composites. In A.S. Khan, editor, *Physics and Mechanics of Finite Plastic and Viscoplastic Deformation*, pages 183–184, Fulton, MD, 1997. NEAT Press.

Y. Bansal and M.J. Pindera. Finite-volume direct averaging micromechanics of heterogeneous materials with elastic-plastic phases. *Int.J.Plast.*, 22:775–825, 2006.

G. Bao. Damage due to fracture of brittle reinforcements in a ductile matrix. *Acta.metall. mater.*, 40:2547–2555, 1992.

G. Bao, J.W. Hutchinson, and R.M. McMeeking. Particle reinforcement of ductile matrices against plastic flow and creep. *Acta metall.mater.*, 39:1871–1882, 1991.

R.B. Barello and M. Lévesque. Comparison between the relaxation spectra obtained from homogenization models and finite elements simulation for the same composite. *Int.J.Sol.Struct.*, 45:850–867, 2008.

J.L. Bassani, A. Needleman, and E. van der Giessen. Plastic flow in a composite: Comparison of nonlocal continuum and discrete dislocation predictions. *Int.J.Sol.Struct.*, 38: 833–853, 2001.

S.R. Beissel, G.R. Johnson, and C.H. Popelar. An element-failure algorithm for dynamic crack propagation in general directions. *Engng.Fract.Mech.*, 61:407–425, 1998.

V. Belsky, M.W. Beall, J. Fish, M.S. Shephard, and S. Gomaa. Computer-aided multiscale modeling tools for composite materials and structures. *Int.J.Comput.Syst.Engng.*, 6: 213–223, 1995.

L. Benabou. Comparative analysis of damage at interfaces of composites. *Composites B*, 33:215–224, 2002.

Y. Benveniste. A new approach to the application of Mori–Tanaka's theory in composite materials. *Mech.Mater.*, 6:147–157, 1987.

Y. Benveniste. Some remarks on three micromechanical models in composite media. *J.Appl.Mech.*, 57:474–476, 1990.

Y. Benveniste and G.J. Dvorak. On a correspondence between mechanical and thermal effects in two-phase composites. In G.J. Weng, M. Taya, and H. Abé, editors, *Micromechanics and Inhomogeneity*, pages 65–82, New York, NY, 1990. Springer–Verlag.

Y. Benveniste, G.J. Dvorak, and T. Chen. On diagonal and elastic symmetry of the approximate effective stiffness tensor of heterogeneous media. *J.Mech.Phys.Sol.*, 39: 927–946, 1991.

A.A. Benzerga and J. Besson. Plastic potentials for anisotropic porous solids. *Eur.J.Mech. A/Solids*, 20:397–434, 2001.

M.J. Beran and J. Molyneux. Use of classical variational principles to determine bounds for the effective bulk modulus in heterogeneous media. *Quart.Appl.Math.*, 24:107–118, 1966.

H. Berns, A. Melander, D. Weichert, N. Asnafi, C. Broeckmann, and A. Gross-Weege. A new material for cold forging tools. *Comput.Mater.Sci.*, 11:166–188, 1998.

J.G. Berryman. Long-wavelength propagation in composite elastic media, II. Ellipsoidal inclusions. *J.Acoust.Soc.Amer.*, 68:1820–1831, 1980.

J.G. Berryman and P.A. Berge. Critique of two explicit schemes for estimating elastic properties of multiphase composites. *Mech.Mater.*, 22:149–164, 1996.

M. Berveiller and A. Zaoui. A simplified self-consistent scheme for the plasticity of two-phase metals. *Res.Mech.Lett.*, 1:119–124, 1981.

A. Bhattacharyya and G.J. Weng. Plasticity of isotropic composites with randomly oriented packeted inclusions. *Int.J.Plast.*, 10:553–578, 1994.

S.B. Biner. A finite element method analysis of the role of interface behavior in the creep rupture characteristics of a discontinuously reinforced composite with sliding grain boundaries. *Mater.Sci.Engng.A*, 208:239–248, 1996.

P. Bisegna and R. Luciano. Variational bounds for the overall properties of piezoelectric composites. *J.Mech.Phys.Sol.*, 44:583–602, 1996.

J.F.W. Bishop and R. Hill. A theory of the plastic distortion of a polycrystalline aggregate under combined stress. *Phil.Mag.*, 42:414–427, 1951.

B. Bochenek and R. Pyrz. Reconstruction methodology for planar and spatial random microstructures. In R. Pyrz, J. Schjødt-Thomsen, J.C. Rauhe, T. Thomsen, and L.R. Jensen, editors, *New Challenges in Mesomechanics*, pages 565–572, Aalborg, 2002. Aalborg University.

H.J. Böhm. A short introduction to continuum micromechanics. In H.J. Böhm, editor, *Mechanics of Microstructured Materials*, pages 1–40, Springer–Verlag, Vienna, 2004a. CISM Courses and Lectures Vol. 464.

H.J. Böhm. Numerical investigation of microplasticity effects in unidirectional longfiber reinforced metal matrix composites. *Modell.Simul.Mater.Sci.Engng.*, 1:649–671, 1993.

H.J. Böhm and W. Han. Comparisons between three-dimensional and two-dimensional multi-particle unit cell models for particle reinforced metal matrix composites. *Modell.Simul.Mater.Sci.Engng.*, 9:47–65, 2001.

H.J. Böhm and F.G. Rammerstorfer. Fiber arrangement effects on the microscale stresses of continuously reinforced MMCs. In R. Pyrz, editor, *Microstructure–Property Interactions in Composite Materials*, pages 51–62, Dordrecht, 1995. Kluwer Academic Publishers.

H.J. Böhm and F.G. Rammerstorfer. Influence of the micro-arrangement on matrix and fiber damage in continuously reinforced MMCs. In A. Pineau and A. Zaoui, editors, *Micromechanics of Plasticity and Damage of Multiphase Materials*, pages 19–26, Dordrecht, 1996. Kluwer.

H.J. Böhm, F.G. Rammerstorfer, and E. Weissenbek. Some simple models for micromechanical investigations of fiber arrangement effects in MMCs. *Comput.Mater.Sci.*, 1: 177–194, 1993.

H.J. Böhm, A. Eckschlager, and W. Han. Modeling of phase arrangement effects in high speed tool steels;. In F. Jeglitsch, R. Ebner, and H. Leitner, editors, *Tool Steels in the Next Century*, pages 147–156, Leoben, 1999. Montanuniversität Leoben.

H.J. Böhm, A. Eckschlager, and W. Han. Multi-inclusion unit cell models for metal matrix composites with randomly oriented discontinuous reinforcements. *Comput.Mater.Sci.*, 25:42–53, 2002.

A. Borbély, P. Kenesei, and H. Biermann. Estimation of the effective properties of particle-reinforced metal-matrix composites from microtomographic reconstructions. *Acta mater.*, 54:2735–2744, 2006.

M. Bornert. Homogénéisation des milieux aléatoires: Bornes et estimations. In M. Bornert, T. Bretheau, and P. Gilormini, editors, *Homogénéisation en mécanique des matériaux 1. Matériaux aléatoires élastiques et milieux périodiques*, pages 133–221, Paris, 2001. Editions Hermès.

M. Bornert. *Morphologie microstructurale et comportement mécanique; charactérisations expérimentales, approches par bornes et estimations autocohérentes généralisées*. PhD thesis, Ecole Nationale des Ponts et Chaussées, Paris, France, 1996.

M. Bornert and P. Suquet. Propriétés non linéaires des composites: Approches par les potentiels. In M. Bornert, T. Bretheau, and P. Gilormini, editors, *Homogénéisation en mécanique des matériaux 2. Comportements non linéaires et problèmes ouverts*, pages 45–90, Paris, 2001. Editions Hermès.

M. Bornert, E. Hervé, C. Stolz, and A. Zaoui. Self consistent approaches and strain heterogeneities in two-phase elastoplastic materials. *Appl.Mech.Rev.*, 47:66–S76, 1994.

M. Bornert, C. Stolz, and A. Zaoui. Morphologically representative pattern-based bounding in elasticity. *J.Mech.Phys.Sol.*, 44:307–331, 1996.

M. Bornert, T. Bretheau, and P. Gilormini, editors. *Homogénéisation en mécanique des matériaux*. Editions Hermès, Paris, 2001.

P.O. Bouchard, F. Bay, and Y. Chastel. Numerical modelling of crack propagation: Automatic remeshing and comparison of different criteria. *Comput.Meth.Appl.Mech.Engng.*, 192:3887–3908, 2003.

R. Brenner and R. Masson. Improved affine estimates for nonlinear viscoelastic composites. *Eur.J.Mech. A/Solids*, 24:1002–1015, 2005.

R. Brenner, O. Castelnau, and P. Gilormini. A modified affine theory for the overall properties of nonlinear composites. *C.R.Acad.Sci.Paris, série IIb*, 329:649–654, 2001.

L.C. Brinson and W.S. Lin. Comparison of micromechanics methods for effective properties of multiphase viscoelastic composites. *Compos.Struct.*, 41:353–367, 1998.

K.M. Brockmüller, O. Bernhardi, and M. Maier. Determination of fracture stress and strain of highly oriented short fibre-reinforced composites using a fracture mechanics-based iterative finite-element method. *J.Mater.Sci.*, 30:481–487, 1995.

L.M. Brown and W.M. Stobbs. The work-hardening of copper–silica. I. A model based on internal stresses, with no plastic relaxation. *Phil.Mag.*, 23:1185–1199, 1971.

M.S. Bruzzi, P.E. McHugh, F. O'Rourke, and T. Linder. Micromechanical modelling of the static and cyclic loading of an Al 2141-SiC MMC. *Int.J.Plast.*, 17:565–599, 2001.

J.Y. Buffière, P. Cloetens, W. Ludwig, E. Maire, and L. Salvo. In situ X-ray tomography studies of microstructural evolution combined with 3D modeling. *MRS Bull.*, 33:611–619, 2008.

V.N. Bulsara, R. Talreja, and J. Qu. Damage initiation under transverse loading of unidirectional composites with arbitrarily distributed fibers. *Compos.Sci.Technol.*, 59:673–682, 1999.

V. Buryachenko. *Micromechanics of Heterogeneous Materials*. Springer–Verlag. Berlin, 2007.

V.A. Buryachenko. The overall elastoplastic behavior of multiphase materials with isotropic components. *Acta Mech.*, 119:93–117, 1996.

V.A. Buryachenko, N.J. Pagano, R.Y. Kim, and J.E. Spowart. Quantitative description and numerical simulation of random microstructures of composites and their elastic moduli. *Int.J.Sol.Struct.*, 40:47–72, 2003.

J. Byström, N. Jēkabsons, and J. Varna. An evaluation of different models for prediction of elastic properties of woven composites. *Composites B*, 31:7–20, 2000.

C.W. Camacho, C.L. Tucker, S. Yalvaç, and R.L. McGee. Stiffness and thermal expansion predictions for hybrid short fiber composites. *Polym.Compos.*, 11:229–239, 1990.

N. Carrere. *Sur l'analyse multiéchelle des matériaux composites à matrice métallique: application au calcul de structure*. PhD thesis, Ecole Polytechnique, Palaiseau, France, 2001.

A. Cazzani and M. Rovati. Extrema of Young's modulus for cubic and transversely isotropic solids. *Int.J.Sol.Struct.*, 40:1713–1744, 2003.

J.L. Chaboche and P. Kanouté. Sur les approximations "isotrope" et "anisotrope" de l'opérateur tangent pour les méthodes tangentes incrémentale et affine. *C.R.Mecanique*, 331:857–864, 2003.

J.L. Chaboche, S. Kruch, and T. Pottier. Micromechanics versus macromechanics: A combined approach for metal matrix composite constitutive modeling. *Eur.J.Mech. A/Solids*, 17:885–908, 1998.

J.L. Chaboche, S. Kruch, J.F. Maire, and T. Pottier. Towards a micromechanics based inelastic and damage modelling of composites. *Int.J.Plast.*, 17:411–439, 2001.

N. Chawla and K.K. Chawla. Microstructure based modeling of the deformation behavior of particle reinforced metal matrix composites. *J.Mater.Sci.*, 41:913–925, 2006.

C.R. Chen, I. Scheider, T. Siegmund, A. Tatschl, O. Kolednik, and F.D. Fischer. Fracture initiation and crack growth — Cohesive zone modeling and stereoscopic measurements. In K. Ravi-Chandar, B.L. Karihaloo, T. Kishi, R.O. Ritchie, and A.T. Yokobori, editors, *Advances in Fracture Research*, page 100409, Oxford, 2001. Elsevier.

T. Chen. Exact moduli and bounds of two-phase composites with coupled multifield linear responses. *J.Mech.Phys.Sol.*, 45:385–398, 1997.

C.M. Chimani, H.J. Böhm, and F.G. Rammerstorfer. On stress singularities at free edges of bimaterial junctions — A micromechanical study. *Scr.mater.*, 36:943–947, 1997.

R.M. Christensen. Sufficient symmetry conditions for isotropy of the elastic moduli tensor. *J.Appl.Mech.*, 54:772–777, 1987.

R.M. Christensen. Two theoretical elasticity micromodels. *J.Elasticity*, 50:15–25, 1998.

R.M. Christensen and K.H. Lo. Solutions for effective shear properties in three phase sphere and cylinder models. *J.Mech.Phys.Sol.*, 27:315–330, 1979.

R.M. Christensen and K.H. Lo. Erratum to Christensen and Lo, 1979. *J.Mech.Phys.Sol.*, 34:639, 1986.

R.M. Christensen, H. Schantz, and J. Shapiro. On the range of validity of the Mori–Tanaka method. *J.Mech.Phys.Sol.*, 40:69–73, 1992.

P.W. Chung, K.K. Tamma, and R.R. Namburu. Asymptotic expansion homogenization for heterogeneous media: Computational issues and applications. *Composites A*, 32: 1291–1301, 2001.

H.H.M. Cleveringa, E. van der Giessen, and A. Needleman. Comparison of discrete dislocation and continuum plasticity predictions for a composite material. *Acta mater.*, 45: 3163–3179, 1997.

T.W. Clyne and P.J. Withers. *An Introduction to Metal Matrix Composites*. Cambridge University Press, Cambridge, 1993.

I. Cohen. Simple algebraic approximations for the effective elastic moduli of cubic arrays of spheres. *J.Mech.Phys.Sol.*, 52:2167–2183, 2004.

W.M.G. Courage and P.J.G Schreurs. Effective material parameters for composites with randomly oriented short fibers. *Comput.Struct.*, 44:1179–1185, 1992.

B.N. Cox and G. Flanagan. Handbook of analytical methods for textile composites. Technical Report NASA–CR–4570, NASA, Washington, DC, 1997.

H.L. Cox. The elasticity and strength of paper and other fibrous materials. *Brit.J.Appl. Phys.*, 3:72–79, 1952.

M.E. Cruz and A.T. Patera. A parallel Monte-Carlo finite element procedure for the analysis of multicomponent random media. *Int.J.Num.Meth.Engng.*, 38:1087–1121, 1995.

L.C. Davis. Flow rule for the plastic deformation of particulate metal matrix composites. *Comput.Mater.Sci.*, 6:310–318, 1996.

L.C. Davis, C. Andres, and J.E. Allison. Microstructure and strengthening of metal matrix composites. *Mater.Sci.Engng.A*, 249:40–45, 1998.

P.R. Dawson. Computational crystal plasticity. *Int.J.Sol.Struct.*, 37:115–130, 2000.

T. Daxner. *Multi-Scale Modeling and Simulation of Metallic Foams*. Reihe 18, Nr. 285. VDI–Verlag, Düsseldorf, 2003.

T. Daxner, R.D. Bitsche, and H.J. Böhm. Micromechanical models of metallic sponges with hollow struts. In T. Chandra, K. Tsuzaki, M. Militzer, and C. Ravindran, editors, *Thermec 2006*, pages 1857–1862, Trans Tech Publications, Zurich, 2007. Materials Science Forum 539–543.

L. Delannay, I. Doghri, and O. Pierard. Prediction of tension–compression cycles in multiphase steel using a modified mean-field model. *Int.J.Sol.Struct.*, 44:7291–7306, 2007.

I. Doghri and C. Friebel. Effective elasto-plastic properties of inclusion-reinforced composites. Study of shape, orientation and cyclic response. *Mech.Mater.*, 37:45–68, 2005.

I. Doghri and A. Ouaar. Homogenization of two-phase elasto-plastic composite materials and structures. *Int.J.Sol.Struct.*, 40:1681–1712, 2003.

I. Doghri and L. Tinel. Micromechanical modeling and computation of elasto-plastic materials reinforced with distributed-orientation fibers. *Int.J.Plast.*, 21:1919–1940, 2005.

M. Dong and S. Schmauder. Modeling of metal matrix composites by a self-consistent embedded cell model. *Acta mater.*, 44:2465–2478, 1996.

T. Drabek and H.J. Böhm. Simulation of ductile damage in metal matrix composites. In S. Ghosh, J.M. Castro, and J.K. Lee, editors, *Proceedings of NUMIFORM 2004*, pages 1887–1892, Melville, NY, 2004. American Institute of Physics.

T. Drabek and H.J. Böhm. Micromechanical finite element analysis of metal matrix composites using nonlocal ductile failure models. *Comput.Mater.Sci.*, 37:29–36, 2006.

W. Dreyer, W.H. Müller, and J. Olschewski. An approximate analytical 2D-solution for the stresses and strains in eigenstrained cubic materials. *Acta Mech.*, 136:171–192, 1999.

W.J. Drugan and J.R. Willis. A micromechanics-based nonlocal constitutive equation and estimates of representative volume element size for elastic composites. *J.Mech.Phys.Sol.*, 44:497–524, 1996.

D.X. Du and Q.S. Zheng. A further exploration of the interaction direct derivative (IDD) estimate for the effective properties of multiphase composites taking into account inclusion distribution. *Acta Mech.*, 157:61–80, 2002.

H.L. Duan, J. Wang, Z.P. Huang, and Z.Y. Luo. Stress concentration tensors of inhomogeneities with interface effects. *Mech.Mater.*, 37:723–736, 2005.

M.L. Dunn and H. Ledbetter. Elastic–plastic behavior of textured short-fiber composites. *Acta mater.*, 45:3327–3340, 1997.

M.L. Dunn and M. Taya. Micromechanics predictions of the effective electroelastic moduli of piezoelectric composites. *Int.J.Sol.Struct.*, 30:161–175, 1993.

D. Duschlbauer. *Computational Simulation of the Thermal Conductivity of MMCs under Consideration of the Inclusion–Matrix Interface*. Reihe 5, Nr. 561. VDI–Verlag, Düsseldorf, 2004.

D. Duschlbauer, H.E. Pettermann, and H.J. Böhm. Mori–Tanaka based evaluation of inclusion stresses in composites with nonaligned reinforcements. *Scr.mater.*, 48:223–228, 2003.

D. Duschlbauer, H.J. Böhm, and H.E. Pettermann. Computational simulation of composites reinforced by planar random fibers: Homogenization and localization by unit cell and mean field approaches. *J.Compos.Mater.*, 40:2217–2234, 2006.

G.J. Dvorak. Transformation field analysis of inelastic composite materials. *Proc.Roy.Soc. London*, A437:311–327, 1992.

G.J. Dvorak and Y.A. Bahei-el Din. A bimodal plasticity theory of fibrous composite materials. *Acta Mech.*, 69:219–241, 1987.

G.J. Dvorak, Y.A. Bahei-el Din, and A.M. Wafa. The modeling of inelastic composite materials with the transformation field analysis. *Modell.Simul.Mater.Sci.Engng.*, 2:571–586, 1994.

A. Eckschlager. *Simulation of Particle Failure in Particle Reinforced Ductile Matrix Composites*. PhD thesis, TU Wien, Vienna, Austria, 2002.

A. Eckschlager, H.J. Böhm, and W. Han. Modeling of brittle particle failure in particle reinforced ductile matrix composites by 3D unit cells. In Y. Zhang, editor, *Proceedings of the 13th International Conference on Composite Materials (ICCM–13)*, page 1342, Beijing, 2001. Scientific and Technical Documents Publishing House.

R.F. Eduljee and R.L. McCullough. Elastic properties of composites. In R.W. Cahn, P. Haasen, and E.J. Kramer, editors, *Materials Science and Technology Vol.13: Structure and Properties of Composites*, pages 381–474, Weinheim, 1993. VCH.

M. Elices, G.V. Guinea, J. Gómez, and J. Planas. The cohesive zone model: Advantages, limitations and challenges. *Engng.Fract.Mech.*, 69:137–163, 2002.

J.D. Eshelby. The determination of the elastic field of an ellipsoidal inclusion and related problems. *Proc.Roy.Soc.London*, A241:376–396, 1957.

J.D. Eshelby. The elastic field outside an ellipsoidal inclusion. *Proc.Roy.Soc.London*, A252: 561–569, 1959.

J. Faleskog and C.F. Shih. Micromechanics of coalescence — I.: Synergistic effects of elasticity, plastic yielding and multi-size-scale voids. *J.Mech.Phys.Sol.*, 45:21–50, 1997.

M. Ferrari. Asymmetry and the high concentration limit of the Mori–Tanaka effective medium theory. *Mech.Mater.*, 11:251–256, 1991.

F. Feyel. A multilevel finite element method (FE^2) to describe the response of highly non-linear structures using generalized continua. *Comput.Meth.Appl.Mech.Engng.*, 192: 3233–3244, 2003.

F. Feyel and J.L. Chaboche. FE^2 multiscale approach for modelling the elastoviscoplastic behaviour of long fiber SiC/Ti composite materials. *Comput.Meth.Appl.Mech.Engng.*, 183:309–330, 2000.

M.A. Finot, Y.L. Shen, A. Needleman, and S. Suresh. Micromechanical modeling of reinforcement fracture in particle-reinforced metal-matrix composites. *Metall.Trans.*, 25A: 2403–2420, 1994.

F.D. Fischer, O. Kolednik, G.X. Shan, and F.G. Rammerstorfer. A note on calibration of ductile failure damage indicators. *Int.J.Fract.*, 73:345–357, 1995.

H.F. Fischmeister and B. Karlsson. Plastizitätseigenschaften grob-zweiphasiger Werkstoffe. *Z.Metallkd.*, 68:311–327, 1977.

J. Fish and K. Shek. Multiscale analysis of composite materials and structures. *Compos.Sci.Technol.*, 60:2547–2556, 2000.

J. Fish and K. Shek. Computational plasticity and viscoplasticity for composite materials and structures. *Composites B*, 29:613–619, 1998.

J. Fish, K. Shek, M. Pandheeradi, and M.S. Shephard. Computational plasticity for composite structures based on mathematical homogenization: Theory and practice. *Comput.Meth.Appl.Mech.Engng.*, 148:53–73, 1997.

J. Fish, M.S. Shephard, and M.W. Beall. Automated multiscale fracture analysis. In H.A. Mang and F.G. Rammerstorfer, editors, *Discretization Methods in Structural Mechanics*, pages 249–256, Dordrecht, 1999. Kluwer.

C. Fond, A. Riccardi, R. Schirrer, and F. Montheillet. Mechanical interaction between spherical inhomogeneities: An assessment of a method based on the equivalent inclusion. *Eur.J.Mech. A/Solids*, 20:59–75, 2001.

F. Fritzen, T. Böhlke, and E. Schnack. Periodic three-dimensional mesh generation for crystalline aggregates based on Voronoi tessellations. *Comput.Mech.*, 43:701–713, 2009.

S.Y. Fu and B. Lauke. The elastic modulus of misaligned short-fiber-reinforced polymers. *Compos.Sci.Technol.*, 58:389–400, 1998.

H. Fukuda and T.W. Chou. A probabilistic theory of the strength of short-fibre composites with variable fibre length and orientation. *J.Mater.Sci.*, 17:1003–1007, 1982.

H. Fukuda and K. Kawata. Stress and strain fields in short fibre-reinforced composites. *Fibre Sci.Technol.*, 7:129–156, 1974.

M. Galli, J. Botsis, and J. Janczak-Rusch. An elastoplastic three-dimensional homogenization model for particle reinforced composites. *Comput.Mater.Sci.*, 41:312–321, 2008.

H.P. Gänser. *Large Strain Behavior of Two-Phase Materials*. Reihe 5, Nr. 528. VDI–Verlag, Düsseldorf, 1998.

H.P. Gänser, F.D. Fischer, and E.A. Werner. Large strain behaviour of two-phase materials with random inclusions. *Comput.Mater.Sci.*, 11:221–226, 1998.

H.P. Gänser, A.G. Atkins, O. Kolednik, F.D. Fischer, and O. Richard. Upsetting of cylinders: A comparison of two different damage indicators. *J.Engng.Mater.Technol.*, 123: 94–99, 2001.

M. Gărăjeu. *Contribution á l'étude du comportement non linéaire de milieux poreux avec ou sens renfort*. PhD thesis, Université de la Méditeranée, Marseille, France, 1995.

M. Gărăjeu, J.C. Michel, and P. Suquet. A micromechanical approach of damage in viscoplastic materials by evolution in size, shape and distribution of voids. *Comput.Meth.Appl.Mech.Engng.*, 183:223–246, 2000.

M.R. Garnich and G. Karami. Finite element micromechanics for stiffness and strength of wavy fiber composites,. *J.Compos.Mater.*, 38:273–292, 2004.

A.C. Gavazzi and D.C. Lagoudas. On the numerical evaluation of Eshelby's tensor and its application to elastoplastic fibrous composites. *Comput.Mech.*, 7:12–19, 1990.

M.G.D. Geers, R.A.B. Engelen, and R.J.M. Ubachs. On the numerical modelling of ductile damage with an implicit gradient-enhanced formulation. *Rev.Eur.Elem.Fin.*, 10:173–191, 2001a.

M.G.D. Geers, V.G. Kouznetsova, and W.A.M. Brekelmans. Gradient enhanced homogenization for the micro–macro scale transition. *J.Physique IV*, 11:145–152, 2001b.

M. Geni and M. Kikuchi. Void configuration under constrained deformation in ductile matrix materials. *Comput.Mater.Sci.*, 16:391–403, 1999.

S. Ghosh and S. Moorthy. Three dimensional Voronoi cell finite element model for microstructures with ellipsoidal heterogeneities. *Comput.Mech.*, 34:510–531, 2004.

S. Ghosh and S. Moorthy. Particle cracking simulation in non-uniform microstructures of metal-matrix composites. *Acta mater.*, 46:965–982, 1998.

S. Ghosh, K.H. Lee, and S. Moorthy. Two scale analysis of heterogeneous elastic-plastic materials with asymptotic homogenization and Voronoi cell finite element model. *Comput.Meth.Appl.Mech.Engng.*, 132:63–116, 1996.

S. Ghosh, K.H. Lee, and P. Raghavan. A multi-level computational model for multi-scale analysis in composite and porous materials. *Int.J.Sol.Struct.*, 38:2335–2385, 2001.

L.J. Gibson. The mechanical behavior of cancellous bone. *J.Biomech.*, 18:317–328, 1985.

L.J. Gibson and M.F. Ashby. *Cellular Solids: Structure and Properties*. Pergamon Press, Oxford, 1988.

P. Gilormini. Insuffisance de l'extension classique du modèle auto-cohérent au comportement non-linéaire. *C.R.Acad.Sci.Paris, série IIb*, 320:115–122, 1995.

A. Giraud, C. Gruescu, D.P. Do, F. Homand, and D. Kondo. Effective thermal conductivity of transversely isotropic media with arbitrary oriented ellipsoidal inhomogeneities. *Int.J.Sol.Struct.*, 44:2627–2647, 2007.

I.M. Gitman. *Representative Volumes and Multi-Scale Modelling of Quasi-Brittle Materials*. PhD thesis, Technische Universiteit te Delft, Delft, The Netherlands, 2006.

I.M. Gitman, H. Askes, and L.J. Sluys. Representative volume: Existence and size determination. *Engng.Fract.Mech.*, 74:2518–2534, 2007.

M. Gologanu, J.B. Leblond, G. Perrin, and J. Devaux. Recent extensions of Gurson's model for porous ductile materials. In P. Suquet, editor, *Continuum Micromechanics*, pages 61–130, Vienna, 1997. Springer–Verlag.

B. Gommers, I. Verpoest, and P. van Houtte. The Mori–Tanaka method applied to textile composite materials. *Acta mater.*, 46:2223–2235, 1998.

L. Gong, S. Kyriakides, and N. Triantafyllidis. On the stability of Kelvin cell foams under compressive loads. *J.Mech.Phys.Sol.*, 53:771–794, 2005.

C. González and J. LLorca. A self-consistent approach to the elasto-plastic behavior of two-phase materials including damage. *J.Mech.Phys.Sol.*, 48:675–692, 2000.

C. González and J. LLorca. Virtual fracture testing of composites: A computational micromechanics approach. *Engng.Fract.Mech.*, 74:1126–1138, 2007.

C. González and J. LLorca. Prediction of the tensile stress–strain curve and ductility in SiC/Al composites. *Scr.mater.*, 35:91–97, 1996.

J.L. Grenestedt. Influence of wavy imperfections in cell walls on elastic stiffness of cellular solids. *J. Mech. Phys. Sol.*, 46:29–50, 1998.

D. Gross and T. Seelig. *Bruchmechanik mit einer Einführung in die Mikromechanik*. Springer-Verlag, Berlin, 2001.

R.E. Guldberg, S.J. Hollister, and G.T. Charras. The accuracy of digital image-based finite element models. *J.Biomech.Engng.*, 120:289–295, 1998.

S.R. Gunawardena, S. Jansson, and F.A. Leckie. Transverse ductility of metal matrix composites. In K. Haritos, G. Newaz, and S. Mall, editors, *Failure Mechanisms in High Temperature Composite Materials*, pages 23–30, New York, NY, 1991. ASME.

S.R. Gunawardena, S. Jansson, and F.A. Leckie. Modeling of anisotropic behavior of weakly bonded fiber reinforced MMC's. *Acta metall.mater.*, 41:3147–3156, 1993.

G. Guo, J. Fitoussi, D. Baptiste, N. Sicot, and C. Wolff. Modelling of damage behavior of a short-fiber reinforced composite structure by the finite element analysis using a micro–macro law. *Int.J.Dam.Mech.*, 6:278–299, 1997.

A.L. Gurson. Continuum theory of ductile rupture by void nucleation and growth: Part I — Yield criteria and flow rules for porous ductile media. *J. Engng. Mater. Technol.*, 99: 2–15, 1977.

A.A. Gusev. Representative volume element size for elastic composites: A numerical study. *J.Mech.Phys.Sol.*, 45:1449–1459, 1997.

A.A. Gusev, P.J. Hine, and I.M. Ward. Fiber packing and elastic properties of a transversely random unidirectional glass/epoxy composite. *Compos.Sci.Technol.*, 60:535–541, 2000.

H. Haddadi and C. Téodosiu. 3D-analysis of the effect of interfacial debonding on the plastic behaviour of two-phase composites. *Comput.Mater.Sci.*, 16:315–322, 1999.

R.M. Haj-Ali. Cohesive micromechanics: A new approach for progressive damage modeling in laminated composites. *Int.J.Dam.Mech.*, 2009. in print, doi: 10.1177/1056789508096560.

J.C. Halpin and J.L. Kardos. The Halpin–Tsai equations: A review. *Polym.Engng.Sci.*, 16:344–351, 1976.

J.W. Hancock and A.C. Mackenzie. On the mechanisms of ductile failure in high-strength steels subjected to multi-axial stress-states. *J.Mech.Phys.Sol.*, 24:147–169, 1976.

R. Hashemi, R. Avazmohammadi, H.M. Shodja, and Weng G.J. Composites with supershperical inhomogenieties. *Phil.Mag.Lett.*, 89:439–451, 2009.

Z. Hashin. The elastic moduli of heterogeneous materials. *J.Appl.Mech.*, 29:143–150, 1962.

Z. Hashin. Viscoelastic behavior of heterogeneous media. *J.Appl.Mech.*, 32:630–636, 1965.

Z. Hashin. Complex moduli of viscoelastic composites: I. General theory and application to particulate composites. *Int.J.Sol.Struct.*, 6:539–552, 1970.

Z. Hashin. Theory of fiber reinforced materials. Technical Report NASA–CR–1974, NASA, Washington, DC, 1972.

Z. Hashin. Analysis of composite materials — A survey. *J.Appl.Mech.*, 50:481–505, 1983.

Z. Hashin. The differential scheme and its application to cracked materials. *J.Mech.Phys.Sol.*, 36:719–733, 1988.

Z. Hashin and B.W. Rosen. The elastic moduli of fiber-reinforced materials. *J.Appl.Mech.*, 31:223–232, 1964.

Z. Hashin and S. Shtrikman. Note on a variational approach to the theory of composite elastic materials. *J.Franklin Inst.*, 271:336–341, 1961.

Z. Hashin and S. Shtrikman. A variational approach to the theory of the elastic behavior of multiphase materials. *J.Mech.Phys.Sol.*, 11:127–140, 1963.

Z. Hashin and S. Shtrikman. On some variational principles in anisotropic and nonhomogeneous elasticity. *J.Mech.Phys.Sol.*, 10:335–342, 1962.

B. Hassani and E. Hinton. *Homogenization and Structural Topology Optimization.* Springer–Verlag. London, 1999.

D.P.H. Hasselman and L.F. Johnson. Effective thermal conductivity of composites with interfacial thermal barrier resistance. *J.Compos.Mater.*, 21:508–515, 1987.

H. Hatta and M. Taya. Equivalent inclusion method for steady state heat conduction in composites. *Int.J.Engng.Sci.*, 24:1159–1172, 1986.

S. Hazanov. Hill condition and overall properties of composites. *Arch. Appl. Mech.*, 68: 385–394, 1998.

S. Hazanov and M. Amieur. On overall properties of elastic bodies smaller than the representative volume. *Int. J. Engng. Sci.*, 33:1289–1301, 1995.

Q.C. He and A. Curnier. A more fundamental approach to damaged elastic stress–strain relations. *Int. J. Sol. Struct.*, 32:1433–1457, 1997.

G.L. Heness, B. Ben-Nissan, L.H. Gan, and Y.W. Mai. Development of a finite element micromodel for metal matrix composites. *Comput.Mater.Sci.*, 13:259–269, 1999.

E. Hervé and A. Zaoui. n-layered inclusion-based micromechanical modelling. *Int.J. Engng.Sci.*, 31:1–10, 1993.

E. Hervé, C. Stolz, and A. Zaoui. A propos de'l assemblage des sphères composites de Hashin. *C.R.Acad.Sci.Paris, série II*, 313:857–862, 1991.

R. Hill. A theory of the yielding and plastic flow of anisotropic metals. *Proc.Phys.Soc.London*, 193:281–297, 1948.

R. Hill. The elastic behavior of a crystalline aggregate. *Proc.Phys.Soc.London*, A65:349–354, 1952.

R. Hill. Elastic properties of reinforced solids: Some theoretical principles. *J.Mech.Phys. Sol.*, 11:357–372, 1963.

R. Hill. Theory of mechanical properties of fibre-strengthened materials: I. Elastic behaviour. *J.Mech.Phys.Sol.*, 12:199–212, 1964.

R. Hill. Continuum micro-mechanics of elastic-plastic polycrystals. *J.Mech.Phys.Sol.*, 13: 89–101, 1965a.

R. Hill. A self-consistent mechanics of composite materials. *J.Mech.Phys.Sol.*, 13:213–222, 1965b.

R. Hill. The essential structure of constitutive laws for metal composites and polycrystals. *J. Mech. Phys. Sol.*, 15:79–95, 1967.

S.J. Hollister, D.P. Fyhrie, K.J. Jepsen, and S.A. Goldstein. Application of homogenization theory to the study of trabecular bone mechanics. *J.Biomech.*, 24:825–839, 1991.

S.J. Hollister, J.M. Brennan, and N. Kikuchi. A homogenization sampling procedure for calculating trabecular bone effective stiffness and tissue level stress. *J.Biomech.*, 27: 433–444, 1994.

S. Holmberg, K. Persson, and H. Petersson. Nonlinear mechanical behaviour and analysis of wood and fibre materials. *Comput.Struct.*, 72:459–480, 1999.

C.L. Hom and R.M. McMeeking. Plastic flow in ductile materials containing a cubic array of rigid spheres. *Int.J.Plast.*, 7:255–274, 1991.

M.F. Horstemeyer, M.M. Matalanis, A.M. Sieber, and M.L. Botos. Micromechanical finite element calculations of of temperature and void configuration effects on void growth and coalescence. *Int.J.Plast.*, 16:979–1013, 2000.

C. Hu, S. Moorthy, and S. Ghosh. A Voronoi cell finite element for ductile damage in MMCs. In S. Ghosh, J.M. Castro, and J.K. Lee, editors, *Proceedings of NUMIFORM 2004*, pages 1893–1898, Melville, NY, 2004. American Institute of Physics.

C. Hu, J. Bai, and S. Ghosh. Micromechanical and macroscopic models of ductile fracture in particle reinforced metallic materials. *Modell.Simul.Mater.Sci.Engng.*, 15:S377–S392, 2007.

G.K. Hu. Composite plasticity based on matrix average second order stress moment. *Int.J.Sol.Struct.*, 34:1007–1015, 1997.

G.K. Hu and G.J. Weng. Some reflections on the Mori–Tanaka and Ponte Castañeda–Willis methods with randomly oriented ellipsoidal inclusions. *Acta Mech.*, 140:31–40, 2000.

G.K. Hu, G. Guo, and D. Baptiste. A micromechanical model of influence of particle fracture and particle cluster on mechanical properties of metal matrix composites. *Comput.Mater.Sci.*, 9:420–430, 1998.

G.K. Hu, X.N. Liu, and T.J. Lu. A variational method for nonlinear micropolar composites. *Mech.Mater.*, 37:407–425, 2005.

J.H. Huang. Some closed-form solutions for effective moduli of composites containing randomly oriented short fibers. *Mater.Sci.Engng. A*, 315:11–20, 2001.

J.H. Huang and J.S. Yu. Electroelastic Eshelby tensors for an ellipsoidal piezoelectric inclusion. *Compos.Engng.*, 4:1169–1182, 1994.

Y. Huang and K.X. Hu. A generalized self-consistent mechanics method for solids containing elliptical inclusions. *J.Appl.Mech.*, 62:566–572, 1995.

Z.M. Huang and S. Ramakrishna. Micromechanical modeling approaches for the stiffness and strength of knitted fabric composites: A review and comparative study. *Composites A*, 31:479–501, 2000.

C.O. Huber, M.H. Luxner, S. Kremmer, S. Nogales, H.J. Böhm, and H.E. Pettermann. Forming simulations of MMC components by a micromechanics based hierarchical FEM approach. In J.M.A.C. de Sá and A.D. Santos, editors, *Proc. NUMIFORM 2007*, pages 1351–1356, New York, NY, 2007. American Institute of Physics.

C. Huet. Application of variational concepts to size effects in elastic heterogeneous bodies. *J.Mech.Phys.Sol.*, 38:813–841, 1990.

C. Huet, P. Navi, and P.E. Roelfstra. A homogenization technique based on Hill's modification theorem. In G.A. Maugin, editor, *Continuum Models and Discrete Systems*, pages 135–143, Harlow, 1990. Longman.

J.W. Hutchinson. Plasticity on the micron scale. *Int.J.Sol.Struct.*, 37:225–238, 2000.

J.W. Hutchinson. Elastic-plastic behavior of polycrystalline metals and composites. *Proc. Roy.Soc.London*, A319:247–272, 1970.

A. Ibrahimbegović and D. Markovič. Strong coupling methods in multi-phase and multi-scale modeling of inelastic behavior of heterogeneous structures. *Comput.Meth.Appl.Mech.Engng.*, 192:3089–3107, 2003.

L. Iorga, Y. Pan, and A.A. Pelegri. Numerical characterization of material elastic properties for random fiber composites. *J.Mech.Mater.Struct.*, 3:1279–1298, 2008.

N. Ishikawa, D. Parks, S. Socrate, and M. Kurihara. Micromechanical modeling of ferrite–pearlite steels using finite element unit cell models. *ISIJ Int.*, 40:1170–1179, 2000.

H. Ismar and U. Reinert. Modelling and simulation of the macromechanical nonlinear behavior of fibre-reinforced ceramics on the basis of a micromechanical–statistical material description. *Acta Mech.*, 120:47–60, 1997.

H. Ismar and U. Schmitt. Simulation von Einspiel- und Rißildungsvorgängen in Faserverbundwerkstoffen mit metallischer Matrix. *Arch.Appl.Mech.*, 61:18–29, 1991.

H. Ismar and F. Schröter. Three-dimensional finite element analysis of the mechanical behavior of cross ply-reinforced aluminum. *Mech.Mater.*, 32:329–338, 2000.

T. Iung and M. Grange. Mechanical behavior of two-phase materials investigated by the finite element method: Necessity of three-dimensional modeling. *Mater.Sci.Engng.*, A201:8–L11, 1995.

S.K. Iyer, C.J. Lissenden, and S.M. Arnold. Local and overall flow in composites predicted by micromechanics. *Composites B*, 31:327–343, 2000.

N. Järvstråt. Homogenization and the mechanical behavior of metal composites. In H. Fujiwara, T. Abe, and K. Tanaka, editors, *Residual Stresses — III*, pages 70–75, London, 1992. Elsevier.

N. Järvstråt. An ellipsoidal unit cell for the calculation of micro-stresses in short fibre composites. *Comput.Mater.Sci.*, 1:203–212, 1993.

K. Jayaraman and M.T. Kortschot. Correction to the Fukuda–Kawata Young's modulus theory and the Fukuda–Chou strength theory for short fibre-reinforced composite materials. *J.Mater.Sci.*, 31:2059–2064, 1996.

D. Jeulin. Random structure models for homogenization and fracture statistics. In D. Jeulin and M. Ostoja-Starzewski, editors, *Mechanics of Random and Multiscale Microstructures*, pages 33–91, Vienna, 2001. Springer–Verlag, CISM Courses and Lectures Vol. 430.

M. Jiang, M. Ostoja-Starzewski, and I. Jasiuk. Scale-dependent bounds on effective elastoplastic response of random composites. *J.Mech.Phys.Sol.*, 49:655–673, 2001.

M. Jiang, I. Jasiuk, and M. Ostoja-Starzewski. Apparent thermal conductivity of periodic two-dimensional composites. *Comput. Mater. Sci.*, 25:329–338, 2002a.

M. Jirásek. Comparative study on finite elements with embedded discontinuities. *Comput.Meth.Appl.Mech.Engng.*, 188:307–330, 2000.

M. Jirásek and S. Rolshoven. Comparison of integral-type nonlocal plasticity models for strain softening materials. *Int.J.Engng.Sci.*, 41:1553–1602, 2003.

B. Johannesson and O.B. Pedersen. Analytical determination of the average Eshelby tensor for transversely isotropic fiber orientation distributions. *Acta mater.*, 46:3165–3173, 1998.

J.W. Ju and L.Z. Sun. Effective elastoplastic behavior of metal matrix composites containing randomly located aligned spheroidal inhomogeneities. Part I: Micromechanics-based formulation. *Int.J.Sol.Struct.*, 38:183–201, 2001.

J.W. Ju and L.Z. Sun. A novel formulation for the exterior point Eshelby's tensor of an ellipsoidal inclusion. *J.Appl.Mech.*, 66:570–574, 1999.

M. Kachanov and I. Sevostianov. On quantitative characterization of microstructures and effective properties. *Int.J.Sol.Struct.*, 42:309–336, 2005.

M. Kachanov, I. Tsukrov, and B. Shafiro. Effective moduli of solids with cavities of various shapes. *Appl.Mech.Rev.*, 47:151–S174, 1994.

M. Kailasam, N. Aravas, and P. Ponte Castañeda. Porous metals with developing anisotropy: Constitutive models, computational issues and applications to deformation processing. *Comput.Model.Engng.Sci.*, 1:105–118, 2000.

T. Kanit, S. Forest, I. Gallier, V. Mounoury, and D. Jeulin. Determination of the size of the representative volume element for random composites: Statistical and numerical approach. *Int.J.Sol.Struct.*, 40:3647–3679, 2003.

P. Kenesei, A. Borbély, and H. Biermann. Microstructure based three-dimensional finite element modeling of particulate reinforced metal matrix composites. *Mater.Sci. Engng.A*, 387:852–856, 2004.

Z.F. Khisaeva and M. Ostoja-Starzewski. On the size of RVE in finite elasticity of random composites. *J.Elast.*, 85:153–173, 2006.

J. Koplik and A. Needleman. Void growth and coalescence in porous plastic solids. *Int.J.Sol.Struct.*, 24:835–853, 1988.

V.G. Kouznetsova, M.G.D. Geers, and W.A.M. Brekelmans. Advanced constitutive modeling of heterogeneous materials with a gradient-enhanced computational homogenization scheme. *Int.J.Num.Meth.Engng.*, 54:1235–1260, 2002.

I. Krakovsky and V. Myroshnychenko. Modelling dielectric properties of composites by finite element method. *J.Appl.Phys.*, 92:6743–6748, 2002.

A.M. Kraynik and D.A. Reinelt. Elastic-plastic behavior of a Kelvin foam. In D. Weaire, editor, *The Kelvin Problem. Foam Structures of Minimal Surface Area*, pages 93–1085, London, 1996. Taylor & Francis.

W.S. Kreher. Residual stresses and stored elastic energy of composites and polycrystals. *J.Mech.Phys.Sol.*, 38:115–128, 1990.

E. Kröner. Self-consistent scheme and graded disorder in polycrystal elasticity. *J.Phys.F*, 8:2261–2267, 1978.

G.T. Kuster and M.N. Toksöz. Velocity and attenuation of seismic waves in two-phase media: I. Theoretical formulation. *Geophysics*, 39:587–606, 1974.

N. Lahellec and P. Suquet. Effective behavior of linear viscoelastic composites: A time-integration approach. *Int.J.Sol.Struct.*, 44:507–529, 2007.

H.K. Lee and S. Simunovic. Modeling of progressive damage in aligned and randomly oriented discontinuous fiber polymer matrix composites. *Composites B*, 31:77–86, 2000.

K.H. Lee and S. Ghosh. Small deformation multi-scale analysis of heterogeneous materials with the Voronoi cell finite element model and homogenization theory. *Comput.Mater.Sci.*, 7:131–146, 1996.

B.A. Lerch, M.E. Melis, and M. Tong. Experimental and analytical analysis of the stress–strain behavior in a $[90/0]_{2S}$ SiC/Ti-15-3 laminate. Technical Report NASA–TM–104470, NASA, 1991.

M. Lévesque, M.D. Gilchrist, N. Bouleau, K. Derrien, and D. Baptiste. Numerical inversion of the Laplace–Carson transform applied to homogenization of randomly reinforced linear viscoelastic media. *Comput.Mech.*, 10:771–789, 2007.

V.M. Levin. On the coefficients of thermal expansion of heterogeneous materials. *Mech.Sol.*, 2:58–61, 1967.

A. Levy and J.M. Papazian. Elastoplastic finite element analysis of short-fiber-reinforced SiC/Al composites: Effects of thermal treatment. *Acta metall.mater.*, 39:2255–2266, 1991.

D.S. Li and M.R. Wisnom. Unidirectional tensile stress–strain response of bp-sic fiber reinforced ti-6al-4v. *J.Compos.Technol.Res.*, 16:225–233, 1994.

M. Li, S. Ghosh, O. Richmond, H. Weiland, and T.N. Rouns. Three dimensional characterization and modeling of particle reinforced metal matrix composites, Part I: Quantitative description of microstructural morphology. *Mater.Sci.Engng. A*, 265:153–173, 1999.

S.G. Li and A. Wongsto. Unit cells for micromechanical analyses of particle-reinforced composites. *Mech.Mater.*, 36:543–572, 2004.

Y.Y. Li and J.Z. Cui. The multi-scale computational method for the mechanics parameters of the materials with random distribution of multi-scale grains. *Compos.Sci.Technol.*, 65:1447–1458, 2005.

H. Liebowitz, J.S. Sandhu, J.D. Lee, and F.C.M. Menandro. Computational fracture mechanics: Research and applications. *Engng.Fract.Mech.*, 50:653–670, 1995.

G. Lielens, P. Pirotte, A. Couniot, F. Dupret, and R. Keunings. Prediction of thermo-mechanical properties for compression-moulded composites. *Composites A*, 29:63–70, 1997.

D.S. Liu, C.Y. Chen, and D.Y. Chiou. 3-D modeling of a composite material reinforced with multiple thickly coated particles using the infinite element method. *Comput.Model.Engng.Sci.*, 9:179–192, 2005a.

L. Liu, R.D. James, and P.H. Leo. Periodic inclusion–matrix microstructures with constant field inclusions. *Metall.Mater.Trans.*, 38A:781–787, 2007.

Y.J. Liu, N. Nishimura, Y. Otani, T. Takahashi, X.L. Chen, and H. Munakata. A fast boundary element method for the analysis of fiber-reinforced composites based on rigid-inclusion model. *J.Appl.Mech.*, 72:115–128, 2005b.

J. LLorca. A numerical analysis of the damage mechanisms in metal-matrix composites under cyclic deformation. *Comput.Mater.Sci.*, 7:118–122, 1996.

S.V. Lomov, D.S. Ivanov, I. Verpoest, M. Zeko, T. Kurashiki, H. Nakai, and S. Hirosawa. Meso-FE modelling of textile composites: Road map, data flow and algorithms. *Compos.Sci.Technol.*, 67:1870–1891, 2006.

V.A. Lubarda and X. Markenscoff. On the absence of Eshelby property for non-ellipsoidal inclusions. *Int.J.Sol.Struct.*, 35:3405–3411, 1998.

H.R. Lusti, P.J. Hine, and A.A. Gusev. Direct numerical predictions for the elastic and thermoelastic properties of short fibre composites. *Compos.Sci.Technol.*, 62:1927–1934, 2002.

M.H. Luxner, J. Stampfl, and H.E. Pettermann. Finite element modeling concepts and linear analyses of 3D regular open cell structures. *J.Mater.Sci.*, 40:5859–5866, 2005.

J.M. Mahishi. An integrated micromechanical and macromechanical approach to fracture behavior of fiber-reinforced composites. *Engng.Fract.Mech.*, 25:197–228, 1986.

J.M. Mahishi and D.F. Adams. Micromechanical predictions of crack initiation, propagation and crack growth resistance in boron/aluminum composites. *J.Compos.Mater.*, 16: 457–469, 1982.

E. Maire, F. Wattebled, J.Y. Buffière, and G. Peix. Deformation of a metallic foam studied by X-ray computed tomography and finite element calculations. In T.W. Clyne and F. Simancik, editors, *Metal Matrix Composites and Metallic Foams*, pages 68–73, Weinheim, 2000. Wiley–VCH.

J. Mandel. Une généralisation de la théorie de la plasticité de W.T. Koiter. *Int.J.Sol.Struct.*, 1:273–295, 1965.

F. Marketz and F.D. Fischer. Micromechanical modelling of stress-assisted martensitic transformation. *Modell.Simul.Mater.Sci.Engng.*, 2:1017–1046, 1994.

K. Markov. Elementary micromechanics of heterogeneous media. In K. Markov and L. Preziosi, editors, *Heterogeneous Media: Micromechanics Modeling Methods and Simulations*, pages 1–162, Boston, 2000. Birkhäuser.

R. Masson, M. Bornert, P. Suquet, and A. Zaoui. An affine formulation for the prediction of the effective properties of nonlinear composites and polycrystals. *J.Mech.Phys.Sol.*, 48:1203–1227, 2000.

C.F. Matt and M.A.E. Cruz. Application of a multiscale finite-element approach to calculate the effective thermal conductivity of particulate media. *Comput.Appl.Math.*, 21: 429–460, 2002.

C.F. Matt and M.A.E. Cruz. Effective thermal conductivity of composite materials with 3-D microstructures and interfacial thermal resistance. *Numer.Heat Transf.*, A53:577–604, 2008.

N.M. Mawsouf. A micromechanical mechanism of fracture initiation in discontinuously reinforced metal matrix composite. *Mater.Charact.*, 44:321–327, 2000.

F.A. McClintock. A criterion for ductile failure by the growth of holes. *J.Appl.Mech.*, 35: 363–371, 1968.

D.L. McDowell. Modeling and experiments in plasticity. *Int.J.Sol.Struct.*, 37:293–310, 2000.

P.E. McHugh and P. Connolly. Modelling the thermo-mechanical behavior of an Al alloy-SiC_p composite. effects of particle shape and microscale failure. *Comput.Mater.Sci.*, 3: 199–206, 1994.

P.E. McHugh, R.J. Asaro, and C.F. Shih. Computational modeling of metal-matrix composite materials — I. Isothermal deformation patterns in ideal microstructures. *Acta metall.mater.*, 41:1461–1476, 1993.

R. McLaughlin. A study of the differential scheme for composite materials. *Int.J.Engng. Sci.*, 15:237–244, 1977.

R. McMeeking and C.L. Hom. Finite element analysis of void growth in elastic-plastic materials. *Int.J.Fract.*, 42:1–19, 1990.

J.C. Michel and P. Suquet. Computational analysis of nonlinear composite structures using the nonuniform transformation field analysis. *Comput.Meth.Appl.Mech.Engng.*, 193:5477–5502, 2004.

J.C. Michel and P. Suquet. An analytical and numerical study of the overall behaviour of metal-matrix composites. *Modell.Simul.Mater.Sci.Engng.*, 2:637–658, 1994.

J.C. Michel, H. Moulinec, and P. Suquet. Effective properties of composite materials with periodic microstructure: A computational approach. *Comput.Meth.Appl.Mech.Engng.*, 172:109–143, 1999.

J.C. Michel, H. Moulinec, and P. Suquet. Composites à microstructure périodique. In M. Bornert, T. Bretheau, and P. Gilormini, editors, *Homogénéisation en mécanique des matériaux 1. Matériaux aléatoires élastiques et milieux périodiques*, pages 57–94, Paris, 2001. Editions Hermès.

C.A. Miller and S. Torquato. Effective conductivity of hard sphere suspensions. *J.Appl.Phys.*, 68:5486–5493, 1990.

T. Miloh and Y. Benveniste. A generalized self-consistent method for the effective conductivity of composites with ellipsoidal inclusions and cracked bodies. *J.Appl.Phys.*, 63: 789–796, 1988.

G.W. Milton. *The Theory of Composites*. Cambridge University Press, Cambridge, 2002.

G.W. Milton. Bounds on the electromagnetic, elastic, and other properties of two-component composites. *Phys.Rev.Lett.*, 46:542–545, 1981.

A. Miserez, A. Rossoll, and A. Mortensen. Fracture of aluminium reinforced with densely packed ceramic particles: Link between the local and the total work of fracture. *Acta mater.*, 52:1337–1351, 2004.

L.L. Mishnaevsky. Three-dimensional numerical testing of microstructures of particle reinforced composites. *Acta mater.*, 52:4177–4188, 2004.

D. Missoum-Benziane, D. Ryckelynck, and F. Chinesta. A new fully coupled two-scales modelling for mechanical problems involving microstructure: The 95/5 technique. *Comput.Meth.Appl.Mech.Engng.*, 196:2325–2337, 2007.

B. Mlekusch. Thermoelastic properties of short-fibre-reinforced thermoplastics. *Compos. Sci.Technol.*, 59:911–923, 1999.

N. Moës, M. Cloirec, P. Cartraud, and J.F. Remacle. A computational approach to handle complex microstructure geometries. *Comput.Meth.Appl.Mech.Engng.*, 192:3163–3177, 2003.

A. Molinari, G.R. Canova, and S. Ahzi. A self-consistent approach for large deformation viscoplasticity. *Acta metall.*, 35:2983–2984, 1987.

J. Monaghan and D. Brazil. Modeling the sub-subsurface damage associated with the machining of a particle reinforced MMC. *Comput.Mater.Sci.*, 9:99–107, 1997.

I. Monetto and W.J. Drugan. A micromechanics-based nonlocal constitutive equation and minimum RVE size estimates for random elastic composites containing aligned spheroidal heterogeneities. *J.Mech.Phys.Sol.*, 57:1578–1595, 2009.

T. Mori and K. Tanaka. Average stress in the matrix and average elastic energy of materials with misfitting inclusions. *Acta metall.*, 21:571–574, 1973.

Z.A. Moschovidis and T. Mura. Two ellipsoidal inhomogeneities by the equivalent inclusion method. *J.Appl.Mech.*, 42:847–852, 1975.

V.V. Moshev and L.L. Kozhevnikova. Structural cell of particulate elastomeric composites under extension and compression. *Int.J.Sol.Struct.*, 39:449–465, 2002.

C. Motz, R. Pippan, A. Ableidinger, H.J. Böhm, and F.G. Rammerstorfer. Deformation and fracture behavior of ductile aluminium foams in the presence of notches under tensile loading. In J. Banhart, M.F. Ashby, and N.A. Fleck, editors, *Cellular Metals and Metal Foaming Technology*, pages 299–304, Bremen, 2001. Verlag MIT Publishing.

H. Moulinec and P. Suquet. A fast numerical method for computing the linear and nonlinear mechanical properties of composites. *C.R.Acad.Sci.Paris, série II*, 318:1417–1423, 1994.

H. Moulinec and P. Suquet. A numerical method for computing the overall response of nonlinear composites with complex microstructure. *Comput.Meth.Appl.Mech.Engng.*, 157:69–94, 1997.

W.H. Müller. Mathematical versus experimental stress analysis of inhomogeneities in solids. *J.Phys.IV*, 6:1–139–C1–148, 1996.

P. Mummery, B. Derby, and C.B. Scruby. Acoustic emission from particulate-reinforced metal matrix composites. *Act metall.mater.*, 41:1431–1445, 1993.

T. Mura. *Micromechanics of Defects in Solids*. Martinus Nijhoff, Dordrecht, 1987.

J.C. Nadeau and M. Ferrari. On optimal zeroth-order bounds with application to Hashin–Shtrikman bounds and anisotropy parameters. *Int.J.Sol.Struct.*, 38:7945–7965, 2001.

K. Nahshon and J.W. Hutchinson. Modification of the Gurson model for shear failure. *Eur.J.Mech. A/Solids*, 27:1–17, 2008.

T. Nakamura and S. Suresh. Effects of thermal residual stresses and fiber packing on deformation of metal-matrix composites. *Acta metall.mater.*, 41:1665–1681, 1993.

R. Narasimhan. A numerical study of fracture initiation in a ductile population of 2nd phase particles. I. Static loading. *Engng.Fract.Mech.*, 47:919–934, 1994.

A. Needleman. A continuum model for void nucleation by inclusion debonding. *J.Appl.Mech.*, 54:525–531, 1987.

A. Needleman, S.R. Nutt, S. Suresh, and V. Tvergaard. Matrix, reinforcement, and interfacial failure:. In S. Suresh, A. Mortensen, and A. Needleman, editors, *Fundamentals of Metal Matrix Composites*, pages 233–250, Boston, MA, 1993. Butterworth–Heinemann.

S. Nemat-Nasser. Averaging theorems in finite deformation plasticity. *Mech.Mater.*, 31: 493–523, 1999.

S. Nemat-Nasser and M. Hori. *Micromechanics: Overall Properties of Heterogeneous Solids*. North–Holland, Amsterdam, 1993.

G.L. Niebur, J.C. Yuen, A.C. Hsia, and T.M. Keaveny. Convergence behavior of high-resolution finite element models of trabecular bone. *J.Biomech.Engng.*, 121:629–635, 1999.

C.F. Niordson and V. Tvergaard. Nonlocal plasticity effects on the tensile properties of a metal matrix composite. *Eur.J.Mech. A/Solids*, 20:601–613, 2001.

S. Nogales. *Numerical Simulation of the Thermal and Thermomechanical Behavior of Metal Matrix Composites*. Reihe 18, Nr. 317. VDI–Verlag, Düsseldorf, 2008.

S. Nogales and H.J. Böhm. Modeling of the thermal conductivity and thermomechanical behavior of diamond reinforced composites. *Int.J.Engng.Sci.*, 46:606–619, 2008.

A.N. Norris. The isotropic material closest to a given anisotropic material. *J.Mech.Mater.Struct.*, 1:223–238, 2006.

A.N. Norris. A differential scheme for the effective moduli of composites. *Mech.Mater.*, 4: 1–16, 1985.

D. Nouailhas and G. Cailletaud. Finite element analysis of the mechanical behavior of two-phase single crystal superalloys. *Scr.mater.*, 34:565–571, 1996.

S.R. Nutt and A. Needleman. Void nucleation at fiber ends in Al–SiC composites. *Scr.metall.*, 21:705–710, 1987.

J.F. Nye. *Physical Properties of Crystals, Their Representation by Tensors and Matrices*. Clarendon, Oxford, 1957.

M. Nygårds. Number of grains necessary to homogenize elastic materials with cubic symmetry. *Mech.Mater.*, 35:1049–1057, 2003.

J.T. Oden and T.I. Zohdi. Analysis and adaptive modeling of highly heterogeneous elastic structures. *Comput.Meth.Appl.Mech.Engng.*, 148:367–391, 1997.

S. Onaka. Averaged Eshelby tensor and elastic strain energy of a superspherical inclusion with uniform eigenstrains. *Phil.Mag.Lett.*, 81:265–272, 2001.

P. Onck and E. van der Giessen. Microstructurally-based modelling of intergranular creep fracture using grain elements. *Mech.Mater.*, 26:109–126, 1997.

M. Ostoja-Starzewski. Material spatial randomness: From statistical to representative volume element. *Probab. Engng. Mech.*, 21:112–131, 2006.

M. Ostoja-Starzewski. Towards scale-dependent constitutive laws for plasticity and fracture of random heterogeneous materials. In A. Pineau and A. Zaoui, editors, *Micromechanics of Plasticity and Damage of Multiphase Materials*, pages 379–386, Dordrecht, 1996. Kluwer.

M. Oyane. Criteria of ductile fracture strain. *Bull.JSME*, 15:1507–1513, 1972.

D.H. Pahr and S.M. Arnold. The applicability of the generalized method of cells for analyzing discontinuously reinforced composites. *Composites B*, 33:153–170, 2002.

D.H. Pahr and H.J. Böhm. Assessment of mixed uniform boundary conditions for predicting the mechanical behavior of elastic and inelastic discontinuously reinforced composites. *Comput.Model.Engng.Sci.*, 34:117–136, 2008.

D.H. Pahr and F.G. Rammerstorfer. Buckling of honeycomb sandwiches: Periodic finite element considerations. *Comput.Model.Engng.Sci.*, 12:229–241, 2006.

D.H. Pahr and P.K. Zysset. Influence of boundary conditions on computed apparent elastic properties of cancellous bone. *Biomech. Model. Mechanobiol.*, 7:463–476, 2008.

R. Pandorf. *Ein Beitrag zur FE-Simulation des Kriechens partikelverstärkter metallischer Werkstoffe*. PhD thesis, Ruhr–Universität Bochum, Bochum, 2000.

S.D. Papka and S. Kyriakides. In-plane compressive response and crushing of honeycomb. *J.Mech.Phys.Sol.*, 42:1499–1532, 1994.

A. Paquin, H. Sabar, and M. Berveiller. Integral formulation and self consistent modelling of elastoviscoplastic behaviour of heterogeneous materials. *Arch.Appl.Mech.*, 69:14–35, 1999.

O.B. Pedersen. Thermoelasticity and plasticity of composites — I. Mean field theory. *Acta metall.*, 31:1795–1808, 1983.

O.B. Pedersen and P.J. Withers. Iterative estimates of internal stresses in short-fibre metal matrix composites. *Phil.Mag.*, A65:1217–1233, 1992.

H.E. Pettermann. *Derivation and Finite Element Implementation of Constitutive Material Laws for Multiphase Composites Based on Mori–Tanaka Approaches*. Reihe 18, Nr. 217. VDI–Verlag, Düsseldorf, 1997.

H.E. Pettermann and S. Suresh. A comprehensive unit cell model: A study of coupled effects in piezoelectric 1–3 composites. *Int.J.Sol.Struct.*, 37:5447–5464, 2000.

H.E. Pettermann, H.J. Böhm, and F.G. Rammerstorfer. Some direction dependent properties of matrix–inclusion type composites with given reinforcement orientation distributions. *Composites B*, 28:253–265, 1997.

N. Phan-Thien and G.W. Milton. New third-order bounds on the effective moduli of n-phase composites. *Quart.Appl.Math.*, 41:59–74, 1983.

O. Pierard, C. Friebel, and I. Doghri. Mean-field homogenization of multi-phase thermoelastic composites: A general framework and its validation. *Compos.Sci.Technol.*, 64: 1587–1603, 2004.

A.F. Plankensteiner. *Multiscale Treatment of Heterogeneous Nonlinear Solids and Structures*. Reihe 18, Nr. 248. VDI–Verlag, Düsseldorf, 2000.

A.F. Plankensteiner, H.J. Böhm, F.G. Rammerstorfer, V.A. Buryachenko, and G. Hackl. Modeling of layer-structured high speed steel. *Acta mater.*, 45:1875–1887, 1997.

P. Ponte Castañeda. The effective mechanical properties of nonlinear isotropic composites. *J.Mech.Phys.Sol.*, 39:45–71, 1991.

P. Ponte Castañeda. Bounds and estimates for the properties on nonlinear inhomogeneous systems. *Phil.Trans.Roy.Soc.*, A340:531–567, 1992.

P. Ponte Castañeda. Variational methods for estimating the effective behavior of nonlinear composite materials. In K.Z. Markov, editor, *Continuum Models and Discrete Systems*, pages 268–279, Singapore, 1996. World Scientific.

P. Ponte Castañeda and P. Suquet. Nonlinear composites. In E. van der Giessen and T.Y. Wu, editors, *Advances in Applied Mechanics 34*, pages 171–302, New York, NY, 1998. Academic Press.

P. Ponte Castañeda and J.R. Willis. The effect of spatial distribution on the effective behavior of composite materials and cracked media. *J.Mech.Phys.Sol.*, 43:1919–1951, 1995.

G.L. Povirk, S.R. Nutt, and A. Needleman. Analysis of creep in thermally cycled Al/SiC composites. *Scr.metall.mater.*, 26:461–66, 1992.

Y.P. Qiu and G.J. Weng. A theory of plasticity for porous materials and particle-reinforced composites. *J.Appl.Mech.*, 59:261–268, 1992.

J. Qu and M. Cherkaoui. *Fundamentals of Micromechanics of Solids*. John Wiley, New York, NY, 2006.

S. Quilici and G. Cailletaud. FE simulation of macro-, meso- and microscales in polycrystalline plasticity. *Comput.Mater.Sci.*, 16:383–390, 1999.

J.A. Quintanilla. Microstructure and properties of random heterogeneous materials: A review of theoretical results. *Polym.Engng.Sci.*, 39:559–585, 1999.

D. Raabe. *Computational Materials Science*. VCH, Weinheim, 1998.

P. Raghavan and S. Ghosh. Adaptive multi-scale modeling of composite materials. *Comput.Model.Engng.Sci.*, 5:151–170, 2004.

F.G. Rammerstorfer and H.J. Böhm. Finite element methods in micromechanics of composites and foam materials. In B.H.V. Topping, editor, *Computational Mechanics for the Twenty First Century*, pages 145–164, Edinburgh, 2000. Saxe–Coburg Publications.

C. Redenbach. Microstructure models for cellular materials. *Comput.Mater.Sci.*, 44:1397–1407, 2009.

T.J. Reiter, G.J. Dvorak, and V. Tvergaard. Micromechanical models for graded composite materials. *J.Mech.Phys.Sol.*, 45:1281–1302, 1997.

Z.Y. Ren and Q.S. Zheng. Effects of grain sizes, shapes, and distribution on minimum sizes of representative volume elements of cubic polycrystals. *Mech.Mater.*, 36:1217–1229, 2004.

A. Reuss. Berechnung der Fließgrenze von Mischkristallen auf Grund der Plastizitätsbedingung für Einkristalle. *ZAMM*, 9:49–58, 1929.

J.R. Rice and D.M. Tracey. On the ductile enlargement of voids in triaxial stress fields. *J.Mech.Phys.Sol.*, 17:201–217, 1969.

M. Rintoul and S. Torquato. Reconstruction of the structure of dispersions. *J. Colloid Interf. Sci.*, 186:467–476, 1997.

A.P. Roberts and E.J. Garboczi. Elastic moduli of model random three-dimensional closed-cell cellular solids. *Acta mater.*, 49:189–197, 2001.

A.P. Roberts and E.J. Garboczi. Elastic properties of a tungsten–silver composite by reconstruction and computation. *J.Mech.Phys.Sol.*, 47:2029–2055, 1999.

F. Robitaille, A.C. Long, I.A. Jones, and C.D. Rudd. Automatically generated geometric descriptions of textile and composite unit cells. *Composites A*, 34:303–312, 2003.

G.J. Rodin. The overall elastic response of materials containing spherical inhomogeneities. *Int.J.Sol.Struct.*, 30:1849–1863, 1993.

R. Roscoe. Isotropic composites with elastic or viscoelastic phases: General bounds for the moduli and solutions for special geometries. *Rheol.Acta*, 12:404–411, 1973.

G. Rousselier. Ductile fracture models and their potential in local approach of fracture. *Nucl.Engng.Design*, 105:97–111, 1987.

I. Saiki, K. Terada, K. Ikeda, and M. Hori. Appropriate number of unit cells in a representative volume element for micro-structural bifurcation encountered in a multi-scale modeling. *Comput.Meth.Appl.Mech.Engng.*, 191:2561–2585, 2002.

W. Sanders and L.J. Gibson. Mechanics of hollow sphere foams. *Mater.Sci.Engng.*, A347: 70–85, 2003.

A. Sangani and W. Lu. Elastic coefficients of composites containing spherical inclusions in a periodic array. *J.Mech.Phys.Sol.*, 35:1–21, 1987.

S.P. Santosa and T. Wierzbicki. On the modeling of crush behavior of a closed-cell aluminum foam structure. *J.Mech.Phys.Sol.*, 46:645–669, 1998.

M. Sautter, C. Dietrich, M.H. Poech, S. Schmauder, and H.F. Fischmeister. Finite element modelling of a transverse-loaded fibre composite: Effects of section size and net density. *Comput.Mater.Sci.*, 1:225–233, 1993.

R.A. Schapery. Approximate methods of transform inversion in viscoelastic stress analysis. In *Proceedings of the Fourth US National Congress on Applied Mechanics*, pages 1075–1085, New York, NY, 1962. ASME.

R.A. Schapery. Viscoelastic behavior and analysis of composite materials. In G.P. Sendeckyj, editor, *Mechanics of Composite Materials 2*, pages 84–168, New York, NY, 1974. Academic Press.

J. Schjødt-Thomsen and R. Pyrz. Influence of statistical cell description on the local strain and overall properties of cellular materials. In S. Ghosh, J.M. Castro, and J.K. Lee, editors, *Proceedings of NUMIFORM 2004*, pages 1630–1635, Melville, NY, 2004. American Institute of Physics.

S. Schmauder, J. Wulf, T. Steinkopff, and H. Fischmeister. Micromechanics of plasticity and damage in an Al/SiC metal matrix composite. In A. Pineau and A. Zaoui, editors, *Micromechanics of Plasticity and Damage of Multiphase Materials*, pages 255–262, Dordrecht, 1996. Kluwer.

B.A. Schrefler, M. Lefik, and U. Galvanetto. Correctors in a beam model for unidirectional composites. *Compos.Mater.Struct.*, 4:159–190, 1997.

B.A. Schrefler, U. Galvanetto, C. Pellegrino, and F. Ohmenhäuser. Global non-linear behavior of periodic composite materials. In H.A. Mang and F.G. Rammerstorfer, editors, *Discretization Methods in Structural Mechanics*, pages 265–272, Dordrecht, 1999. Kluwer.

F. Schwabe. *Einspieluntersuchungen von Verbundwerkstoffen mit periodischer Mikrostruktur*. PhD thesis, Rheinisch-Westfälische Technische Hochschule, Aachen, 2000.

J. Segurado, J. LLorca, and C. González. On the accuracy of mean-field approaches to simulate the plastic deformation of composites. *Scr.mater.*, 46:525–529, 2002a.

J. Segurado, E. Parteder, A. Plankensteiner, and H.J. Böhm. Micromechanical studies of the densification of porous molybdenum. *Mater. Sci. Engng.*, A333:270–278, 2002b.

J. Segurado, C. González, and J. LLorca. A numerical investigation of the effect of particle clustering on the mechanical properties of composites. *Acta mater.*, 51:2355–2369, 2003.

Z. Shan and A.M. Gokhale. Micromechanics of complex three-dimensional microstructures. *Acta mater.*, 49:2001–2015, 2001.

H. Shen and L.C. Brinson. A numerical investigation of the effect of boundary conditions and representative volume element size for porous titanium. *J.Mech.Mater.Struct.*, 1: 1179–1204, 2006.

H. Shen and C.J. Lissenden. 3D finite element analysis of particle-reinforced aluminum. *Mater.Sci.Engng.*, A338:271–281, 2002.

M.S. Shephard, M.W. Beall, R. Garimella, and R. Wentorf. Automatic construction of 3/D models in multiple scale analysis. *Comput.Mech.*, 17:196–207, 1995.

M. Sherburn. *Geometrical and Mechanical Modelling of Textiles*. PhD thesis, University of Nottingham, Nottingham, 2007.

J.A. Sherwood and H.M. Quimby. Micromechanical modeling of damage growth in titanium based metal-matrix composites. *Comput.Struct.*, 56:505–54, 1995.

V. Shulmeister, M.W.D. van der Burg, E. van der Giessen, and R. Marissen. A numerical study of large deformations of low-density elastomeric open-cell foams. *Mech.Mater.*, 30: 125–140, 1998.

T. Siegmund, F.D. Fischer, and E.A. Werner. Microstructure characterization and FE-modeling of plastic flow in a duplex steel. In R. Pyrz, editor, *Microstructure–Property Interactions in Composite Materials*, pages 349–360, Dordrecht, 1995. Kluwer Academic Publishers.

T. Siegmund, R. Cipra, J. Liakus, B. Wang, M. LaForest, and A. Fatz. Processing–microstructure–property relationships in short fiber reinforced carbon–carbon composite system. In H.J. Böhm, editor, *Mechanics of Microstructured Materials*, pages 235–258, Springer–Verlag, Vienna, 2004. CISM Courses and Lectures Vol. 464.

S. Sihn and A.K. Roy. Modeling and prediction of bulk properties of open-cell carbon foam. *J.Mech.Phys.Sol.*, 52:167–191, 2005.

V.V. Silberschmidt and E.A. Werner. Analyses of thermal stresses' evolution in ferritic–austenitic duplex steels. In Y. Tanigawa, R.B. Hetnarski, and N. Noda, editors, *Thermal Stresses 2001*, pages 327–330, Osaka, 2001. Osaka Prefecture University.

N. Silnutzer. *Effective Constants of Statistically Homogeneous Materials*. PhD thesis, University of Pennsylvania, Philadelphia, PA, 1972.

A.E. Simone and L.J. Gibson. Deformation characteristics of metal foams. *Acta mater.*, 46:2139–2150, 1998.

R.J.M. Smit, W.A.M. Brekelmans, and H.E.H. Meijer. Prediction of the mechanical behavior of non-linear heterogeneous systems by multi-level finite element modeling. *Comput.Meth.Appl.Mech.Engng.*, 155:181–192, 1998.

N.J. Sørensen. A planar type analysis for the elastic-plastic behaviour of continuous fibre-reinforced metal-matrix composites under longitudinal shearing and combined loading. *Int.J.Sol.Struct.*, 29:867–877, 1992.

N.J. Sørensen, S. Suresh, V. Tvergaard, and A. Needleman. Effects of reinforcement orientation on the tensile response of metal matrix composites. *Mater.Sci.Engng. A*, 197:1–10, 1995.

R. Spiegler, S. Schmauder, and H.F. Fischmeister. Simulation of discrete void formation in a WC–Co microstructure. In *Finite Elements in Engineering Applications 1990*, pages 21–42, Stuttgart, 1990. INTES GmbH.

T. Steinkopff, M. Sautter, and J. Wulf. Mehrphasige Finite Elemente in der Verformungs- und Versagensanalyse grob mehrphasiger Werkstoffe. *Arch.Appl.Mech.*, 65:496–506, 1995.

M. Stroeven, H. Askes, and L.J. Sluys. Numerical determination of representative volumes for granular materials. *Comput.Meth.Appl.Mech.Engng.*, 193:3221–3238, 2004.

N. Sukumar, D.L. Chopp, N. Moës, and T. Belytschko. Modeling holes and inclusions by level sets in the extended finite element method. *Comput.Meth.Appl.Mech.Engng.*, 190: 6183–6900, 2001.

L.Z. Sun, J.W. Ju, and H.T. Liu. Elastoplastic modeling of metal matrix composites with evolutionary particle debonding. *Mech.Mater.*, 35:559–569, 2003.

P. Suquet. Elements of homogenization for inelastic solid mechanics. In E. Sanchez-Palencia and A. Zaoui, editors, *Homogenization Techniques in Composite Media*, pages 194–278, Berlin, 1987. Springer–Verlag.

P. Suquet. Overall properties of nonlinear composites: A modified secant moduli theory and its link with Ponte Castañeda's nonlinear variational procedure. *C.R.Acad.Sci.Paris, série IIb*, 320:563–571, 1995.

P. Suquet. Effective properties of nonlinear composites. In P. Suquet, editor, *Continuum Micromechanics*, pages 197–264, Vienna, 1997. Springer–Verlag.

T. Suzuki and P.K.L. Yu. Complex elastic wave band structures in three-dimensional periodic elastic media. *J.Mech.Phys.Sol.*, 46:115–138, 1998.

S. Swaminathan and S. Ghosh. Statistically equivalent representative volume elements for unidirectional composite microstructures: Part II — With interfacial debonding. *J.Compos.Mater.*, 40:605–621, 2006.

E.B. Tadmor, R. Phillips, and M. Ortiz. Hierarchical modeling in the mechanics of materials. *Int.J.Sol.Struct.*, 37:379–390, 2000.

N. Takano, M. Zako, and T. Okazaki. Efficient modeling of microscopic heterogeneity and local crack in composite materials by finite element mesh superposition method. *JSME Int.J. Srs.A*, 44:602–609, 2001.

D.R.S. Talbot and J.R. Willis. Variational principles for inhomogeneous non-linear media. *J.Appl.Math.*, 35:39–54, 1985.

D.R.S. Talbot and J.R. Willis. Upper and lower bounds for the overall response of an elastoplastic composite. *Mech.Mater.*, 28:1–8, 1998.

G.P. Tandon and G.J. Weng. The effect of aspect ratio of inclusions on the elastic properties of unidirectionally aligned composites. *Polym.Compos.*, 5:327–333, 1984.

G.P. Tandon and G.J. Weng. A theory of particle-reinforced plasticity. *J.Appl.Mech.*, 55: 126–135, 1988.

T. Tang and W. Yu. A variational asymptotic micromechanics model for predicting conductivities of composite materials. *J.Mech.Mater.Struct.*, 2:1813–1830, 2007.

X. Tang and J.D. Whitcomb. General techniques for exploiting periodicity and symmetries in micromechanics analysis of textile composites. *J.Compos.Mater.*, 37:1167–1189, 2003.

M. Taya and T. Mori. Dislocations punched-out around a short fibre in MMC subjected to uniform temperature change. *Acta metall.*, 35:155–162, 1987.

M. Taya, W.D. Armstrong, M.L. Dunn, and T. Mori. Analytical study on dimensional changes in thermally cycled metal matrix composites. *Mater.Sci.Engng. A*, 143:143–154, 1991.

J.L. Teply and G.J. Dvorak. Bounds on overall instantaneous properties of elastic-plastic composites. *J.Mech.Phys.Sol.*, 36:29–58, 1988.

K. Terada and N. Kikuchi. Microstructural design of composites using the homogenization method and digital images. *Mater.Sci.Res.Int.*, 2:65–72, 1996.

K. Terada, T. Miura, and N. Kikuchi. Digital image-based modeling applied to the homogenization analysis of composite materials. *Comput.Mech.*, 20:331–346, 1997.

K. Terada, M. Hori, T. Kyoya, and N. Kikuchi. Simulation of the multi-scale convergence in computational homogenization approach. *Int.J.Sol.Struct.*, 37:2285–2311, 2000.

K. Terada, I. Saiki, K. Matsui, and Y. Yamakawa. Two-scale kinematics and linearization for simultaneous two-scale analysis of periodic heterogeneous solids at finite strain. *Comput.Meth.Appl.Mech.Engng.*, 192:3531–3563, 2003.

K. Tohgo and T.W. Chou. Incremental theory of particulate-reinforced composites including debonding damage. *JSME Int.J.Srs.A*, 39:389–397, 1996.

S. Toll. Interpolative aggregate model for short-fibre composite. *J.Compos.Mater.*, 26: 1767–1782, 1992.

Y. Tomita, Y. Higa, and T. Fujimoto. Modeling and estimation of deformation behavior of particle reinforced metal-matrix composite. *Int.J.Mech.Sci.*, 42:2249–2260, 2000.

S. Torquato. *Random Heterogeneous Media*. Springer–Verlag, New York, NY, 2002.

S. Torquato. Random heterogeneous media: Microstructure and improved bounds on effective properties. *Appl.Mech.Rev.*, 44:37–75, 1991.

S. Torquato. Morphology and effective properties of disordered heterogeneous media. *Int.J.Sol.Struct.*, 35:2385–2406, 1998.

S. Torquato and S. Hyun. Effective-medium approximation for composite media: Realizable single-scale dispersions. *J.Appl.Phys.*, 89:1725–1729, 2001.

S. Torquato and F. Lado. Improved bounds on the effective moduli of random arrays of cylinders. *J.Appl.Mech.*, 59:1–6, 1992.

S. Torquato, F. Lado, and P.A. Smith. Bulk properties of two-phase disordered media. IV. Mechanical properties of suspensions of penetrable spheres at nondilute concentrations. *J.Chem.Phys.*, 86:6388–6392, 1987.

D. Trias, J. Costa, A. Turon, and J.F. Hurtado. Determination of the critical size of a statistical representative volume element (SRVE) for carbon reinforced polymers. *Acta mater.*, 54:3471–3484, 2006.

S.W. Tsai and E.M. Wu. A general theory of strength for anisotropic materials. *J.Compos.Mater.*, 5:38–80, 1971.

T.K. Tsotsis and Y. Weitsman. Energy release rates for cracks caused by moisture absorption in graphite/epoxy composites. *J.Compos.Mater.*, 24:483–496, 1990.

T.C. Tszeng. The effects of particle clustering on the mechanical behavior of particle reinforced composites. *Composites B*, 29:299–308, 1998.

C.L. Tucker and E. Liang. Stiffness predictions for unidirectional short-fiber composites: Review and evaluation. *Compos.Sci.Technol.*, 59:655–671, 1999.

V. Tvergaard. Debonding of short fibres among particulates in a metal matrix composite. *Int.J.Sol.Struct.*, 40:6957–6967, 2003.

V. Tvergaard. Analysis of tensile properties for a whisker-reinforced metal-matrix composite. *Acta metall.mater.*, 38:185–194, 1990.

V. Tvergaard. Fibre debonding and breakage in a whisker-reinforced metal. *Mater.Sci. Engng. A*, 190:215–222, 1994.

V. Tvergaard. Effect of void size difference on growth and cavitation instabilities. *J.Mech.Phys.Sol.*, 44:1237–1253, 1996.

V. Tvergaard and A. Needleman. Analysis of the cup-cone fracture in a round tensile bar. *Acta metall.*, 32:157–169, 1984.

V. Tvergaard and A. Needleman. Effects of nonlocal damage in porous plastic solids. *Int.J.Sol.Struct.*, 32:1063–1077, 1995.

A.J. Urbański. Unified, finite element based approach to the problem of homogenisation of structural members with periodic microstructure. In W. Wunderlich, editor, *Solids, Structures and Coupled Problems in Engineering*, Munich, 1999. TU München.

S. Vajjhala, A.M. Kraynik, and L.J. Gibson. A cellular solid model for modulus reduction due to resorption of trabeculae in bone. *J.Biomech.Engng.*, 122:511–515, 2000.

E. van der Giessen and V. Tvergaard. Development of final creep failure in polycrystalline aggregates. *Acta metall.mater.*, 42:952–973, 1994.

B. van Rietbergen, R. Müller, D. Ulrich, P. Rüegsegger, and R. Huiskes. Tissue stresses and strain in trabeculae of a canine proximal femur can be quantified from computer reconstructions. *J.Biomech.*, 32:165–173, 1999.

K. Váradi, Z. Néder, K. Friedrich, and J. Flöck. Finite-element analysis of a polymer composite subjected to ball indentation. *Compos.Sci.Technol.*, 59:271–281, 1999.

N. Vejen and R. Pyrz. Transverse crack growth in glass/epoxy composites with exactly positioned long fibers. Part II: Numerical. *Composites B*, 33:279–290, 2002.

A.S. Viglin. A quantitative measure of the texture of a polycrystalline material–texture function. *Sov.Phys.Solid State*, 2:2195–2207, 1961.

W. Voigt. Über die Beziehung zwischen den beiden Elasticitäts-Constanten isotroper Körper. *Ann. Phys.*, 38:573–587, 1889.

W.K. Vonach. *A General Solution to the Wrinkling Problem of Sandwiches.* Reihe 18, Nr. 268. VDI–Verlag, Düsseldorf, 2001.

P.H.J. Vosbeek, P.F.M. Meurs, and P.J.G. Schreurs. Micro-mechanical constitutive models for composite materials with interfaces. In *Proc.1st Forum of Young European Researchers*, pages 223–228, Liége, Belgium, 1993. Université de Liége.

G.Z. Voyiadjis and P.I. Kattan, editors. *Advances in Damage Mechanics: Metals and Metal Matrix Composites.* Elsevier, Amsterdam, 1999.

K. Wakashima, H. Tsukamoto, and B.H. Choi. Elastic and thermoelastic properties of metal matrix composites with discontinuous fibers or particles: Theoretical guidelines toward materials tailoring. In *The Korea–Japan Metals Symposium on Composite Materials*, pages 102–115, Seoul, 1988. The Korean Institute of Metals.

K. Wallin, T. Saario, and K. Törrönen. Fracture of brittle particles in a ductile matrix. *Int.J.Fract.*, 32:201–209, 1987.

L.J. Walpole. On bounds for the overall elastic moduli of inhomogeneous systems — I. *J.Mech.Phys.Sol.*, 14:151–162, 1966.

M.E. Walter, G. Ravichandran, and M. Ortiz. Computational modeling of damage evolution in unidirectional fiber reinforced ceramic matrix composites. *Comput.Mech.*, 20: 192–198, 1997.

J. Wang, J.H. Andreasen, and B.L. Karihaloo. The solution of an inhomogeneity in a finite plane region and its application to composite materials. *Compos.Sci.Technol.*, 60:75–82, 2000.

Y.U. Wang, Y.M. Jin, and A.G. Khachaturyan. Phase field microelasticity theory and modelling of elastically and structurally inhomogeneous solid. *J.Appl.Phys.*, 92:1351–1360, 2002.

W.E. Warren and A.M. Kraynik. The nonlinear elastic properties of open-cell foams. *J.Appl.Mech.*, 58:376–381, 1991.

D.F. Watt, X.Q. Xu, and D.J. Lloyd. Effects of particle morphology and spacing on the strain fields in a plastically deforming matrix. *Acta mater.*, 44:789–799, 1996.

E. Weissenbek. *Finite Element Modelling of Discontinuously Reinforced Metal Matrix Composites*. Reihe 18, Nr. 164. VDI–Verlag, Düsseldorf, 1994.

E. Weissenbek, H.J. Böhm, and F.G. Rammerstorfer. Micromechanical investigations of arrangement effects in particle reinforced metal matrix composites. *Comput.Mater.Sci.*, 3:263–278, 1994.

E. Weissenbek, H.E. Pettermann, and S. Suresh. Numerical simulation of plastic deformation in compositionally graded metal–ceramic structures. *Acta mater.*, 45:3401–3417, 1997.

E.W. Weisstein. Sphere packing. `http://mathworld.wolfram.com/SpherePacking.html`, 2000.

G.J. Weng. The theoretical connection between Mori–Tanaka theory and the Hashin–Shtrikman–Walpole bounds. *Int.J.Engng.Sci.*, 28:1111–1120, 1990.

M.L. Wilkins. *Computer Simulation of Dynamic Phenomena*. Springer–Verlag, Berlin, 1999.

J.R. Willis. The overall response of nonlinear composite media. *Eur.J.Mech. A/Solids*, 19: 165–184, 2000.

J.R. Willis. Bounds and self-consistent estimates for the overall moduli of anisotropic composites. *J.Mech.Phys.Sol.*, 25:185–202, 1977.

P.J. Withers. The determination of the elastic field of an ellipsoidal inclusion in a transversely isotropic medium, and its relevance to composite materials. *Phil.Mag.*, A59: 759–781, 1989.

P.J. Withers, W.M. Stobbs, and O.B. Pedersen. The application of the Eshelby method of internal stress determination to short fibre metal matrix composites. *Acta metall.*, 37: 3061–3084, 1989.

L.A. Wittig and D.H. Allen. Modeling the effect of oxidation on damage in SiC/Ti-15-3 metal matrix composites. *J.Engng.Mater.Technol.*, 116:421–427, 1994.

T.T Wu. The effect of inclusion shape on the elastic moduli of a two-phase material. *Int.J.Sol.Struct.*, 2:1–8, 1966.

J. Wulf, T. Steinkopff, and H. Fischmeister. FE-simulation of crack paths in the real microstructure of an Al(6061)/SiC composite. *Acta mater.*, 44:1765–1779, 1996.

Z. Xia, Y. Zhang, and F. Ellyin. A unified periodical boundary conditions for representative volume elements of composites and applications. *Int.J.Sol.Struct.*, 40:1907–1921, 2003.

Z.H. Xia, W.A. Curtin, and P.W.M. Peters. Multiscale modeling of failure in metal matrix composites. *Acta mater.*, 49:273–287, 2001.

Q.S. Yang, L. Tang, and H.R. Chen. Self-consistent finite element method: A new method of predicting effective properties of inclusion media. *Fin.Elem.Anal.Design*, 17:247–257, 1994.

Y.M. Yi, S.H. Park, and S.K. Youn. Asymptotic homogenization of viscoelastic composites with periodic microstructures. *Int.J.Sol.Struct.*, 35:2039–2055, 1998.

S. Youssef, E. Maire, and R. Gaertner. Finite element modelling of the actual structure of cellular materials determined by X-ray tomography. *Acta mater.*, 53:719–730, 2005.

W. Yu and T. Tang. Variational asymptotic method for unit cell homogenization of periodically heterogeneous materials. *Int.J.Sol.Struct.*, 44:3738–3755, 2007.

A. Zaoui. Plasticité: Approches en champ moyen. In M. Bornert, T. Bretheau, and P. Gilormini, editors, *Homogénéisation en mécanique des matériaux 2. Comportements non linéaires et problèmes ouverts*, pages 17–44, Paris, 2001. Editions Hermès.

A. Zaoui. Continuum micromechanics: Survey. *J.Engng.Mech.*, 128:808–816, 2002.

J. Zeman. *Analysis of Composite Materials with Random Microstructure*. PhD thesis, Czech Technical University, Prague, Czech Republic, 2003.

J. Zeman and M. Šejnoha. Numerical evaluation of effective elastic properties of graphite fiber tow impregnated by polymer matrix. *J.Mech.Phys.Sol.*, 49:69–90, 2001.

J. Zeman and M. Šejnoha. From random microstructures to representative volume elements. *Modell.Simul.Mater.Sci.Engng.*, 15:325–S335, 2007.

Y.H. Zhao and G.J. Weng. A theory of inclusion debonding and its influence on the stress–strain relations of a ductile matrix composite. *Int.J.Dam.Mech.*, 4:196–211, 1995.

X.A. Zhong and W.G. Knauss. Effects of particle interaction and size variation on damage evolution in filled elastomers. *Mech.Compos.Mater.Struct.*, 7:35–53, 2000.

S.J. Zhou and W.A. Curtin. Failure of fiber composites: A lattice Green function approach. *Acta metall.mater.*, 43:3093–3104, 1995.

H.X. Zhu, J.F. Knott, and N.J. Mills. Analysis of the elastic properties of open-cell foams with tetrakaidecahedral cells. *J.Mech.Phys.Sol.*, 45:319–343, 1997.

R.W. Zimmerman. Hashin–Shtrikman bounds on the Poisson ratio of a composite material. *Mech.Res.Comm.*, 19:563–569, 1992.

T.I. Zohdi. Constrained inverse formulations in random material design. *Comput.Meth. Appl.Mech.Engng.*, 192:3179–3194, 2003.

T.I. Zohdi. A model for simulating the deterioration of structural-scale material responses of microheterogeneous solids. In D. Gross, F.D. Fischer, and E. van der Giessen, editors, *Euromech Colloqium 402 — Micromechanics of Fracture Processes*, pages 91–92, Darmstadt, 1999. TU Darmstadt.

T.I. Zohdi and P. Wriggers. A model for simulating the deterioration of structural-scale material responses of microheterogeneous solids. *Comput.Meth.Appl.Mech.Engng.*, 190: 2803–2823, 2001.

T.I. Zohdi, J.T. Oden, and G.J. Rodin. Hierarchical modeling of heterogeneous bodies. *Comput.Meth.Appl.Mech.Engng.*, 138:273–289, 1996.